

# **Complexation strategies for the design of novel nano-drug delivery systems to treat bacterial infections caused by superbugs.**

***Daniel Hassan***

*(MSc. Pharm. Sci. – University of Greenwich, United Kingdom)*

Submitted as a fulfilment of the requirements for the degree of Doctor of Philosophy in Pharmaceutics at the Discipline of Pharmaceutical Sciences of the School of Health Sciences at the University of KwaZulu-Natal



UNIVERSITY OF <sup>TM</sup>  
**KWAZULU-NATAL**

---

INYUVESI  
**YAKWAZULU-NATALI**

**Supervisor:** Professor Thirumala Govender

(PhD, University of Nottingham, United Kingdom)

**Date submitted: October 2019**

“If you can't fly then run, if you can't run then walk, if you can't walk then crawl, but whatever you do, you have to keep moving forward.”

*--Martin Luther King Jr--*

## **Dedication**

“This thesis is dedicated to God Almighty, my late sister Mrs Christiana Solomon Hassan, all struggling parents and all children struggling to acquire education. Do not lose hope. You can achieve every good thing in life by God’s help and hard work. Keep moving!”.

***--Daniel Hassan--***

## Declaration 1 – Plagiarism

I, Mr Daniel Hassan, declare that

1. The research data reported in this thesis, except where otherwise indicated are my original work.
2. This thesis has not been submitted for any degree or examination at any other university.
3. This thesis does not contain data, pictures, graphs, or other information belonging to other people unless specifically acknowledged as being sourced from other people.
4. This thesis does not contain any other persons' writing unless specifically acknowledged as being sourced from other researchers. Where other written sources have been quoted, then:
  - a. Their words have been rephrased, but the general information attributed to them has been referenced;
  - b. Where their exact words have been used, their writing has been placed inside quotation marks and referenced.
5. Where I have reproduced a publication of which I am an author, co-author, or editor, I have indicated in detail which part of the publication was written by myself alone and have fully referenced such publications.
6. This dissertation does not contain any graphics, text or tables copied from the internet unless specifically acknowledged, and the source being detailed in the reference sections of the dissertation.

Signed:

Date:

**28<sup>th</sup> October 2019**

I, Professor Thirumala Govender as supervisor of the PhD studies at this moment consent to the submission of this PhD thesis.

Signed:

Date:

**28<sup>th</sup> October 2019**



## Declaration 2 –Publications

**Mr. Hassan D.** performed the literature searches that contributed to the conceptualisation, design and execution of these projects. These involved the synthesis and structural elucidation of the synthesised novel materials using different techniques. The techniques includes Proton, and <sup>13</sup> Carbon nuclear magnetic resonance spectroscopy (<sup>1</sup>H NMR and <sup>13</sup>C NMR), Fourier-transform infrared (FT-IR) spectroscopy and High-resolution mass spectrometry (HR-MS) analysis. Mr Hassan contributed to the formulation and characterisation of the nano-based drug delivery system (nanoplexes, nanovesicles and quatsomes) from available polymers and synthesised materials. The nanosystems were characterised for physicochemical properties (particle size, polydispersity index (PDI), zeta potential (ZP), entrapment efficiency (EE%), drug loading capacity (DLC%), differential scanning calorimetry (DSC), surface morphology, *in vitro* drug release, electrical conductivity and DNA/protein quantification. Furthermore, Mr Hassan contributed towards the characterisation of the formulation in terms of *in vitro* and *in vivo* antimicrobial activity, the mathematical modelling in terms of *in vitro* release kinetics data, stability studies and Molecular dynamics (MD) simulations studies. Dr Calvin Omolo Andeve assisted with the conceptualisation, design of the project, solving any technical problems and supervision of the studies. Dr R. Gannimani and Dr A. Y. Waddad assisted in project problem solving. Prof. M.E. S. Soliman, Mr A. A. Elrashedy and Dr N. Agrawal assisted in Molecular dynamics (MD) simulations. Dr S. Rambharose assisted in performing the cytotoxicity and the *in vivo* antibacterial activity studies in the nanoplexes manuscript published. Dr C. Mocktar supervised the *in vitro* and *in vivo* antibacterial activity studies. Dr B. Nkambule supervised the *in vitro* flow cytometry studies. Prof. T. Govender served as supervisor and was responsible for project conceptualisation, problem-solving, editing of papers and abstracts as well as general supervision of all the studies.

### Research output from the dissertation

#### 1. First authored Publications

The following experimental papers were published and/or submitted from the results generated from the specific objectives in this study. These include:

#### **Delivery of novel vancomycin nanoplexes for combating methicillin-resistant *Staphylococcus aureus* (MRSA) infections**

- **Hassan. D.**, Omolo, C.A., Gannimani R., Waddad, A. Y., Mocktar, C., Rambharose, S., Agrawal, N., Govender, T. (2019). Delivery of novel vancomycin nanoplexes for combating methicillin-resistant *Staphylococcus aureus* (MRSA) infections. *International Journal of Pharmaceutics*, 558 (10) 143-156. (Impact factor: 3.862). DOI:10.1016/j.ijpharm.2019.01.010.

#### **Novel Chitosan-Based pH-responsive Lipid-Polymer Hybrid nanovesicles (OLO-LPHVs) for Delivery of Vancomycin against Methicillin-Resistant *Staphylococcus aureus* Infections**

- **Hassan. D.**, Omolo, C.A., Victoria Oluwaseun Fasiku, Nkambule B., Mocktar, C., Govender, T. (2019). Novel Chitosan-Based pH-responsive Lipid-Polymer Hybrid nanovesicles (OLO-LPHVs) for Delivery of Vancomycin against Methicillin-Resistant *Staphylococcus aureus* Infections. Submitted to *International Journal of Biological Macromolecules*. (Manuscript ID: IJBIOMA\_2019\_7211). Impact Factor 4.784.

#### **Quaternary Bicephalic surfactant (StBAclm) and Cholesterol pH-responsive Quatsomes for Enhanced activity of Antibiotics against Methicillin-resistant *Streptococcus aureus* (MRSA)**

- **Hassan. D.**, Omolo, C.A., Victoria Oluwaseun Fasiku, Elrashedy. A.A., Mocktar, C., Soliman. M.E. S., Govender, T. (2019). Quaternary Bicephalic surfactant (StBAclm) and Cholesterol pH-responsive Quatsomes for Enhanced activity of Antibiotics against Methicillin-resistant *Streptococcus aureus* (MRSA). Submitted to *Journal of Drug Targeting*. (Manuscript ID: JDT-2019-OR-0382). Impact factor 3.408.

## 2. Conference Presentations

### (a) International Conferences

- **Daniel Hassan**, Calvin A. Omolo, Chunderika Mocktar, Thirumala Govender. Quaternary Two-arm pH-responsive Quatsomes for Delivery and Enhancement of Vancomycin against Superbug Methicillin-resistance *Staphylococcus aureus* (MRSA). Controlled Released Society Annual Meeting & Exposition, 21<sup>st</sup> - 24<sup>th</sup> July 2019, Palacio De Congressos Valencia. Valencia, Spain (**Poster Presentation**).
- **Daniel Hassan**, Calvin A. Omolo, Chunderika Mocktar, Thirumala Govender. Novel Delivery of pH-responsive Vancomycin Nanovesicles against Superbug (MRSA) Infections. American Society for Microbiology, ASM Microbe 2019, June 20 - 24, San Francisco, California, USA (**Poster Presentation**).
- **Daniel Hassan**, Calvin A. Omolo, Chunderika Mocktar, Thirumala Govender. Novel pH-responsive zwitterionic vancomycin-chitosan nanovesicles: *in vitro* antimicrobial activity against *Staphylococcus aureus* (SA) and Methicillin Resistance *Staphylococcus Aureus* (MRSA). Australasian Pharmaceutical Science Association, December 1 - 5, Adelaide, Australia (**Poster Presentation**).
- **Daniel Hassan**, Omolo, Calvin Andeve, Gannimani Ramesh, Waddad, A. Y., Mocktar, C., Rambharose, S., Agrawal, N., Govender, T. (2019). Delivery of novel vancomycin nanoplexes for combating methicillin-resistant *Staphylococcus aureus* (MRSA) infections. American Society for Microbiology, ASM Microbe 2018, June 6 - 11, Atlanta, GA USA (**Poster Presentation**).

### (b) Local Conferences

- **Daniel Hassan**, Calvin A. Omolo, Chunderika Mocktar, Thirumala Govender. Novel Delivery of pH-responsive Vancomycin Nanovesicles against Superbug (MRSA) Infections. UKZN College of Health Sciences Research Symposium, 1<sup>st</sup> November 2019, Durban, South Africa (**Oral Presentation**).
- **Hassan, D.**, Omolo, A., Mocktar, C., Govender, T. Two arm Hydrophilic Quaternary pH-responsive Quatsomes for Delivery and Enhancement of Vancomycin against *Streptococcus aureus* (SA) and Methicillin Resistance *Streptococcus aureus* (MRSA). UKZN College of Health Sciences Research Symposium, 11<sup>th</sup> - 12<sup>th</sup> October 2018, Durban, South Africa (**Oral Presentation**).
- **Hassan. D.**, Omolo, C.A., Gannimani R., Waddad, A. Y., Mocktar, C., Rambharose, S., Agrawal, N., Govender, T. (2019). Delivery of novel vancomycin nanoplexes for combating methicillin-resistant *Staphylococcus aureus* (MRSA) infections. UKZN Nanotechnology Platform Symposium, 9<sup>th</sup> October 2018, Durban, South Africa (**Oral Presentation**).

The posters can be found in Appendix III, IV, V and VI.

## Abstract

The study broadly aimed to identify the potential of existing as well as newly designed novel advanced materials for the preparation of novel nano-drug delivery systems to combat MRSA infections. In this study, dextran sulfate was explored for the preparation of nanoplexes (VCM-DXT<sub>5</sub>). Two new materials (OLA and StBAclm) were also designed, synthesised and employed for the formulation of nano-drug delivery systems for efficient delivery of vancomycin (VCM) to treat MRSA infections. The materials were characterised by FTIR, <sup>1</sup>H NMR, <sup>13</sup>C NMR and HR-MS. The nanoplexes (VCM-DXT<sub>5</sub>), nanovesicles (VM-OLA-LPHVs1) and quatsomes (VCM-StBAclm-Q<sub>t1</sub>) were characterised for their physicochemical properties (Zetasizer), *in vitro* drug release (dialysis bag), morphology (HR-TEM), *in vitro* cell viability studies (flow cytometry), *in vitro* time killing assay (broth dilution), *in vitro* cytotoxicity (MTT assay), *in vitro* antibacterial activity (broth dilution method) and *in vivo* antibacterial activity (mice skin infection model).

In this study, high molecular weight dextran sulfate sodium salt was explored for the preparation of vancomycin nanoplexes (VCM-DXT<sub>5</sub>). The nanoplexes were found to be non-toxic against different mammalian cell lines adenocarcinoma human alveolar basal epithelial cells (A549), embryonic kidney cells (HEK-293) and liver hepatocellular carcinoma (Hep G2) tested and may confirm its biosafety. The size, polydispersity index (PDI), and zeta potential (ZP) of the optimized VCM nanoplexes were 84.6±4.248nm, 0.449±0.024 and -33.0±4.87mV respectively, with 90.4±0.77% complexation efficiency (CE%) and 62.3 ± 0.23% drug loading. The *in vitro* drug release studies demonstrated slower sustained release as compared to bare VCM. A 6.24-fold enhancement was observed for VCM nanoplexes via *in vitro* antibacterial studies and 67% effective killing from VCM nanoplexes compared to 32.98% from the bare vancomycin at the minimum inhibitory concentration (MIC) of 1.25µg/mL using flow-cytometric analysis. The *in vivo* studies using BALB/c mouse skin infection model revealed that nanoplexes reduced MRSA burden by 2.3-folds compared to bare VCM.

The novel zwitterionic pH-responsive lipid (OLA) was synthesised and its structure confirmed. The OLA and the chitosan-based pH-responsive lipid- polymer hybrid vancomycin nanovesicles (VM-OLA-LPHVs1) demonstrated biocompatibility of greater than 75% in three different cell lines adenocarcinoma human alveolar basal epithelial cells (A549), embryonic kidney cells (HEK-293), liver hepatocellular carcinoma (Hep G2) and liver hepatocellular carcinoma cell lines (MCF-7). The nano drug was evaluated for their hydrodynamic diameter ( $D_H$ ), PDI, zeta potential ( $\zeta$ ), entrapment efficiency (EE%), and drug loading capacity (DLC%),

surface morphology, drug release, *in vitro* and *in vivo* antibacterial activity. The VM-OLA-LPHVs had a ( $D_H$ ), PDI, EE%, DLC%, of  $198.0 \pm 14.04\text{nm}$ ,  $0.137 \pm 0.02$ ,  $45.61 \pm 0.54\%$  and  $8.92 \pm 2.34\%$  respectively at physiological pH (7.4) with negative surface-charged switching to positive at pH 6.0. The VM release from the VM-OLA-LPHVs was found to be faster and sustained at pH 6.0 with 97% VM release in 72 hours compared to physiological pH 7.4. The *in vitro* antibacterial activity demonstrated a lower MICs values at pH 6.0 of 52.9-fold enhancement compared to bare VM against MRSA, while the *in vitro* flow cytometry study of the VM-OLA-LPHVs revealed 7-fold effective MRSA cells dead compared to the treatment with bare VM. Additionally, higher fluorescence intensity indicated higher biofilm eradication by the VM-OLA-LPHVs. The *in vivo* studies in BALB/c mouse infected skin model revealed 1.83-fold reduction in MRSA burden (CFU) compared to treatment with bare VM. These findings suggest that OLA can be used as a novel material with significant potential for complexation with biodegradable moieties to form pH-responsive LPHVs to enhance antibiotic therapy and improve treatment of infections.

The novel quaternary bicephalic surfactant (StBAclm) was synthesised and its structure confirmed. The StBAclm demonstrated higher biocompatibility than 75% cells viability in three different cell lines adenocarcinoma human alveolar basal epithelial cells (A549), embryonic kidney cells (HEK-293), liver hepatocellular carcinoma (Hep G2) and liver hepatocellular carcinoma cell lines (MCF-7). The quatsomes prepared had a size, PDI and EE% of  $122.9 \pm 3.78\text{nm}$ ,  $0.169 \pm 0.02\text{mV}$  and  $45.61 \pm 0.539\%$  respectively, while the surface charge revealed a switching from negative to positive at physiological pH 7.4 and acidic environment pH 6.0, respectively. The *in vitro* drug release from the quatsomes was found to be higher at pH 6.0 compared to pH 7.4. The MICs against MRSA revealed 32-folds in pH 6.0 as compared to the bare VCM. The higher electrical conductivity and decreases in protein and deoxyribonucleic acid (DNA) concentration, confirmed greater MRSA membrane damage with VCM-StBAclm-Qt<sub>1</sub> quatsomes compared to bare VCM. The *in vitro* flow cytometry study of the quatsomes confirmed higher MRSA dead cells when using the VCM-StBAclm-Qt<sub>1</sub> compared to the bare VCM at quatsomes MIC value with higher fluorescence enhancement in the biofilm. The *in vivo* studies with the VCM-StBAclm-Qt<sub>1</sub> quatsomes revealed a 1.83-fold decreased in MRSA CFUs compared to the corresponding bare VCM.

In summary, the high molecular weight dextran, OLA and StBAclm were shown to be biosafe and demonstrate the potential for developing novel nano drug delivery systems of antibiotics with superior efficacy against bacterial infections.

## **Acknowledgements**

I appreciate God Almighty for the gift of life and the privilege to see this long-awaited dream come through today. I also extend my gratitude to those who so generously contributed to the work presented in this research findings leading to the completion of this project presented in this thesis. My sincere appreciation goes to my supervisor, Professor Thirumala Govender. You have been a pillar of excellent guidance, motivation, compassion and steering me in the right direction. You will always be remembered. My thanks goes to Dr Chunderika Mocktar for her encouragement, support, advice, creative criticism, and approachable nature that has allowed me to learn valuable lab techniques.

My special gratitude goes to my colleagues in the laboratory; Dr Calvin A. Omolo, Dr. Ayman Waddad, Dr. Ramesh Ganimani, Dr. Sanjeev Rambharose, Dr. Ruma Maji, Dr. Andile Mbuso Faya, Ms., Nawras Abdelmoniem, Ms. Victoria Fasiku, Danford Mhule, Sifiso Makhatini, Dr Pavan Walvekar, Abdeen Mohamed, Melissa Ramtahal and Leslie Murugan for all their support, technical assistance in the laboratory and life-long friendship. My sincere thanks go to all the organisations that gave me indispensable generous resources, including the National Research Foundation (NRF), UKZN Nanotechnology Platform and the College of Health Sciences at UKZN. Without their support and financial help, it would not have been possible for me to pursue and to complete this thesis successfully. My appreciation goes to Ms Carrin Martin for editorial assistance, the Electron Microscope Unit (MMU), and Biomedical Resource Unit (BRU) at UKZN for their technical support. My thanks goes to my wife (Blessing), daughter (Christiana), parents, brother and sisters for support and motivation throughout my studies. Thank you all for always praying, pushing and believing for greatness.

## **Table of Contents**

Declaration 1 - Plagiarism .....	i
Declaration 2 - Publications.....	ii
Research output from the Dissertation.....	ii
Abstract.....	vi
Acknowledgements.....	vi
<b>CHAPTER ONE: INTRODUCTION</b>	
1.1 Introduction.....	1
1.2 Background .....	1
1.3 Problem Statement.....	7
1.4 Aims and Objectives of this Study .....	8
1.5 Novelty of the Study .....	10
1.6 Significance of the Study.....	11
1.7 Overview of Dissertation.....	13
1.8 References.....	15
<b>CHAPTER TWO: EXPERIMENTAL PAPER ONE</b>	
2.1 Introduction.....	25
2.2 Graphical Abstract.....	26
2.3 Published Manuscript.....	27
2.4 Abstract .....	28
2.5 Materials, Instrumentation and Methods.....	30
2.6 Results and Discussion .....	36
2.7 Conclusions.....	52
2.8 References.....	54
<b>CHAPTER THREE: EXPERIMENTAL PAPER TWO</b>	
3.1 Introduction.....	61
3.2 Graphical Abstract.....	62
3.3 Submitted Manuscript.....	63
3.4 Abstract .....	66
3.6 Materials and Methods.....	69
3.7 Results and Discussion.....	77
3.8 Conclusion .....	91

3.9 References.....	93
<b>CHAPTER FOUR: EXPERIMENTAL PAPER THREE</b>	
4.1 Introduction.....	105
4.2 Graphical Abstract.....	106
4.3 Submitted Manuscript.....	107
4.4 Abstract .....	110
4.6 Materials and Methods.....	113
4.7 Results and Discussion.....	122
4.8 Conclusion .....	138
4.9 References.....	140
<b>CHAPTER FIVE: CONCLUSION</b>	
5.1 General Conclusions.....	149
5.2 Significance of the Findings in the Study .....	153
5.3 Recommendations for Future Studies .....	155
5.4 Conclusion .....	157
Appendix I.....	158
Appendix II.....	172
Appendix III.....	173
Appendix IV.....	174
Appendix V.....	175
Appendix VI.....	176
Appendix VII.....	177
Appendix VIII.....	178
Appendix IX.....	180
Appendix X.....	182
Appendix XI.....	183
Appendix XII.....	186
Appendix XIII.....	189

**List of Abbreviations (add abbreviations for all Chapters)**

A-549	Adenocarcinoma Human Alveolar Epithelial	ALZ	After lyophilisation
ATP	Adenosine triphosphatase	BCA	Bicinchoninic acid
BLZ	Before Lyophilisation	CDC	Centers for Disease Control and Prevention
CE	Complexation Efficiency	CHol	Cholesterol
CFUs	Colony Forming Units	CHs	Chitosan
<sup>13</sup> C NMR	Carbon 13 nuclear magnetic resonance	COM	Centre of Mass
CTAB	Cationic hexadecyltrimethylammonium bromide	DCM	Dichloromethane
DEE	Drug encapsulation efficiency	$D_H$	Hydrodynamic diameter
DL	Drug Loading	DLS	Dynamic Light Scattering
DLC	Drug loading capacity	DMSO	Dimethyl sulfoxide
DNA	Deoxyribonucleic acids	DSC	Differential Scanning Calorimetry
DXT	Dextran Sulfate Sodium salt	EE	Encapsulation efficiency
FACS	Fluorescence-activated Cell Sorting	FT-IR	Fourier Transform-Infrared
HEK-293	Human Embryonic Kidney Cells	Hep-G2	Human Liver Hepatocellular Carcinoma Cell
H&E	Hematoxylin and Eosin	HR-MS	High-resolution mass spectrometry
<sup>1</sup> H NMR	Proton nuclear magnetic resonance	<sup>1</sup> H NMR	Proton nuclear magnetic resonance
MHA	Mueller-Hinton Agar	MCF-7	Liver hepatocellular carcinoma cell lines
MHB	Mueller-Hinton Broth	MIC	Minimum Inhibitory Concentration
MRSA	Methicillin-Resistant <i>staphylococcus aureus</i>	MTT	3-(4,5-dimethylthiazole-2-yl)-2,5-diphenyltetrazolium bromide
MHD	Mean hydrodynamic diameter	MI	Methyl iodide
MDT	Mean dissolution time		



NCP	No cryoprotectant	NPT	Isobaric-isothermic ensemble
NVT	Canonical Ensemble	NB	Nutrient Broth
NaOH	Sodium hydroxide	OD	Optical density
OLM	Oleylamine	PBS	Phosphate Buffers Saline
PDI	Poly Dispersity Index	PI	Propidium Iodide
PME	Particle Mesh Ewald	PS	Particles Size
PY	Percentage Yield	pDNA	Plasmid Deoxyribonucleic Acid
R <sup>2</sup>	Correlation coefficient	RMSE	Root mean square error
R <sub>(VCM/DXT)</sub>	Charge ratio of vancomycin to dextran sulfate sodium salt	siRNA	Small interfering ribonucleic acid
TEM	Transmission Electron Microscope	tBA	<i>Tert</i> -butyl acrylate
TFA	Trifluoroacetic acid	TIPs	Triisopropylsilane
TPP	Sodium tripolyphosphate	UFF	Universal Force Field
UV/Vis-Spectroscopy	Ultraviolet–Visible Spectrophotometer	VCM	Vancomycin
XRD	X-ray Powder Diffractometry	ZP	Zeta Potential

### List of Figures and Tables

NUMBER	TITLE	PAGE
<b>CHAPTER ONE: Introduction (Figures)</b>		
<b>Figure 1</b>	History of antibiotics and resistance	<b>2</b>
<b>Figure 2</b>	Novel FDA-approved antibacterial and non-bacterial drugs in the last 15 years	<b>2</b>
<b>Figure 3</b>	Expected global antimicrobial resistance death rates to occur every year by 2050.	<b>4</b>
<b>CHAPTER TWO: Experimental Paper (Figures)</b>		
<b>Figure</b>	Graphical abstract	<b>26</b>
<b>Figure 1</b>	Structure of A) VCM and B) DXT used in the present study	<b>34</b>
<b>Figure 2</b>	Effect of charge ratio on particle sizes and zeta potential of VCM-DXT. Values are expressed as mean $\pm$ SD (n=3).	<b>37</b>
<b>Figure 3</b>	Morphology of VCM-DXT <sub>5</sub> nanoplexes	<b>40</b>
<b>Figure 4</b>	DSC profiles of (A) DXT, (B) VCM, (C) Physical mixture of VCM and DXT, and (D) VCM-DXT <sub>5</sub> nanoplexes.	<b>41</b>
<b>Figure 5</b>	Diffractograms of (A) DXT, (B) VCM, (C) Physical mixture (DXT and VCM) and (D) VCM-DXT <sub>5</sub> nanoplexes.	<b>42</b>
<b>Figure 6</b>	FT-IR spectra for (A) DXT, (B) VCM, (C) Physical mixture of VCM and DXT, and (D) VCM-DXT <sub>5</sub> nanoplexes.	<b>43</b>
<b>Figure 7</b>	The drug release profile of bare VCM, VCM-DXT <sub>5</sub> and VCM-DXT <sub>5</sub> nanoplexes. The values are expressed as mean $\pm$ SD, n = 3.	<b>44</b>
<b>Figure 8</b>	Percentage cell viabilities of A-549, HEK-293 and HEP-G2 cells, after being exposed to different concentration of VCM-DXT <sub>5</sub> nanoplexes. Results are presented as mean $\pm$ SD (n = 6).	<b>46</b>
<b>Figure 9</b>	A) Shows time evolution of COM distance between VCM and DXT; B) Shows time evolution of interaction energy between VCM and DXT; C) Shows two representative images from the simulations at two different time points in the presence of 12 Na <sup>+</sup> and 12 Cl <sup>-</sup> .	<b>47</b>

<b>Figure 10</b>	A) Shows time evolution of COM distance between VCM and DXT; B) Shows time evolution of interaction energy between VCM and DXT; C) Shows two representative images from the simulations at two different time points in the presence of 24 Na <sup>+</sup> and 24 Cl <sup>-</sup> .	<b>48</b>
<b>Figure 11</b>	<i>In vitro</i> antibacterial activity of MRSA cells determined by flow cytometry analysis. A) Cell fluorescence of untreated MRSA; B) Overlay of fluorescence of treated MRSA cells with bare VCM at its MIC; C) Overlay of fluorescence of MRSA cells treated with bare VCM at the MIC value of VCM-DXT <sub>5</sub> nanoplexes; D) Overlay of percentage fluorescence of MRSA cells treated with VCM-DXT <sub>5</sub> at its MIC values.	<b>50</b>
<b>Figure 12</b>	MRSA CFUs quantification post 48-hours of treatment, the data represent the mean ± SD (n = 3). *** denotes significant differences when compared untreated with VCM-DXT <sub>5</sub> nanoplexes. ** denotes untreated when compared to bare VCM, and * denotes significant difference between the bare VCM and VCM-DXT <sub>5</sub> nanoplexes.	<b>51</b>
<b>Figure 13</b>	Photomicrographs of the skin lesions at the site of injection; A) control and B) treated mice. Histomorphology of controls and treated (Scale bar = 500µm): C) control/untreated, D) Bare VCM treated, E) VCM-DXT <sub>5</sub> nanoplexes treated.	<b>52</b>
<b>CHAPTER TWO: Experimental Paper (Tables)</b>		
<b>Table 1</b>	Effect of charge ratios on sizes, PDI, ZP and CE% of nanoplexes (n = 3).	<b>38</b>
<b>Table 2</b>	Effects of cryoprotectant on sizes, PDI and ZP of VCM-DXT <sub>5</sub> nanoplexes before and after lyophilisation (n = 3).	<b>39</b>
<b>Table 3</b>	Effect of storage conditions on physicochemical characteristics of VCM-DXT <sub>5</sub> nanoplexes. The values are expressed as mean ± SD, n = 3	<b>45</b>
<b>Table 4</b>	<i>In vitro</i> antibacterial activity of the formulations (VCM-DXT <sub>5</sub> ) and (VCM-DXT <sub>1</sub> ) against MRSA at PBS pH 7.4. The values are expressed as mean ± SD, n = 3	<b>49</b>
<b>CHAPTER THREE: Experimental Paper (Figures)</b>		
<b>Figure</b>	Graphical abstract	<b>62</b>

<b>Scheme 1</b>	Synthesis and characterisation: Dichloromethane (DCM), stirring at room temperature 24-hours, b). <b>Compound 3</b> dissolved DCM with the addition of trifluoroacetic acid/triisopropylsilane (TFA/TIPs) under constant stirring for 8-hours at room temperature.	<b>70</b>
<b>Figure 1</b>	A) Percentage cell viability of different concentrations of OLA on A-549, HEK-293, Hep-G2 and MCF-7 cell lines; B) VM-OLA-LPHVs1 on A-549, HEK-293, Hep-G2 and MCF-7 cell lines. All results are presented as mean $\pm$ SD (n = 6).	<b>78</b>
<b>Figure 2</b>	TEM images of VM-loaded (VM-OLA-LPHVs1)	<b>79</b>
<b>Figure 3</b>	A) Thermal profile of (i) VM, (ii) OLA (iii) CHs (iv) physical mixture (VM, OLA and CHs) and (v) lyophilized VM-OLA-LPHVs1 and B) <i>In vitro</i> drug release profile of bare VM and VM-OLA-LPHVs1 in pH 7.4 and pH 6.0 (n = 3).	<b>81</b>
<b>Figure 4</b>	A) The killing kinetics of MRSA exposed to 5x MIC of VM-OLA-LPHVs1, bare VM and sterile water (control) B) HR-TEM images of MRSA after incubation with VM-OLA-LPHVs1. (i) Initial intact structure of MRSA before treatment; (ii) After 1-hour of treatment and incubation; (iii) Formation of pores on the bacterial membrane after 2-hours of treatment; and (iv) Complete loss, disruption and deformation of MRSA membrane after 4-hours.	<b>83</b>
<b>Figure 5</b>	The <i>in vitro</i> antibacterial mechanism of bare VM and VM-OLA-LPHVs1: A) Histogram representation of electrical conductivity of bare VM and VM-OLA-LPHVs1; B) Representation of protein quantification of bare VM and VM-OLA-LPHVs1 at Optical Density at 405nm and C) Histogram representation of DNA concentration of bare VM and VM-OLA-LPHVs1.	<b>85</b>
<b>Figure 6</b>	Flow cytometric analysis of MRSA cells after incubation with VM and VM-OLA-LPHVs1 A) Untreated, B) MRSA treated with VM at its MIC (31.25 $\mu$ g/mL), C) MRSA treated with VM-OLA-LPHVs1 at its MIC (2.390 $\mu$ g/mL).	<b>86</b>
<b>Figure 7</b>	Fluorescence microscopy images of A) Untreated biofilms; B) MRSA biofilms treated with bare VM and C) MRSA biofilms treated with VM-OLA-LPHVs1 showing biofilms disruption and internalisation by the VM-OLA-LPHVs1. Scale bars: 500 $\mu$ m.	<b>88</b>

<b>Figure 8</b>	MRSA CFUs quantification post 48-hours treatment. Data represent mean $\pm$ SD (n=3). ** represents a significant difference between the bare VM and VM-OLA-LPHVs1, *** represents a significant difference between the untreated and bare VM and **** represents a significant difference between untreated and VM-OLA-LPHVs1.	<b>90</b>
<b>CHAPTER THREE: Experimental Paper (Tables)</b>		
<b>Table 1</b>	Effect of storage condition (4°C and ambient temperature 25°C) and time (days) on D <sub>H</sub> , PDI, $\zeta$ and EE% of VM-OLA-LPHVs1	<b>82</b>
<b>Table 2</b>	The <i>in vitro</i> antibacterial activity of bare VM, CHs, OLA, OLA-LPHVs and VM-OLA-LPHVs1 showing MICs against MRSA at pH 6.0 and pH 7.4.	<b>82</b>
<b>Table 3</b>	<b>Table 3:</b> The analysis of MRSA cell membrane permeability after VM-OLA-LPHVs1 treatment.	<b>85</b>
<b>CHAPTER FOUR: Experimental Paper (Figures)</b>		
<b>Figure</b>	Graphical abstract	<b>95</b>
<b>Scheme</b>	Synthesis and characterisation: A). Dichloromethane (DCM), reflux with constant stirring at 80°C, 24-hours, B). DCM, room temperature, 8-hours and c). DCM, room temperature, 12-hours.	<b>106</b>
<b>Figure 1</b>	A) Percentage cell viability of StBAclm on different cell lines A-549; HEK-293; Hep-G2 and MCF-7; B) Percentage cell viability of VCM-StBAclm-Qt <sub>1</sub> quatsomes on different cell lines A-549, HEK-293; Hep-G2 and MCF-7.	<b>123</b>
<b>Figure 2</b>	A) Morphology of VCM-StBAclm-Qt <sub>1</sub> quatsomes Scale bar: 200nm; B) size distribution of VCM-StBAclm-Qt <sub>1</sub> quatsomes measured using Dynamic Light Scattering (DLS).	<b>124</b>
<b>Figure 3</b>	Preliminary, optimised characterization of quatsomes. A) Effect of novel surfactant (StBAclm) concentration on size at different pHs; B) Effect of $\zeta$ at different pH; demonstrated a notable switch from negative to positive charge with decrease in pH; C) Effect of sonication time at different pHs; D) Effect of sonication time on DEE%. (n = 3 for all observations).	<b>125</b>

<b>Figure 4</b>	Self-assembly simulation at a different time point (a-d). Where purple is VCM, green is CHol and sky blue is StBAclm.	<b>126</b>
<b>Figure 5</b>	Drug release profiles of bare VCM and VCM-StBAclm-Qt <sub>1</sub> quatsomes in different (pH 7.4 and pH 6.0). (Mean ± SD, n = 3).	<b>127</b>
<b>Figure 6</b>	A) Killing kinetics of MRSA exposed to 5 x MIC of VCM-StBAclm-Qt <sub>1</sub> quatsomes, VCM, bacterial in PBS 7.4 (positive control) and sterile water (negative control) at different time intervals (n = 3); B) HR-TEM images of MRSA treated with VCM-StBAclm-Qt <sub>1</sub> quatsomes (5× MICs) showing the membrane disruption that occurred after 1-hour incubation, pores on bacterial membrane after treatment and total loss of MRSA cell membrane after 4-hours of VCM-StBAclm-Qt <sub>1</sub> quatsomes treatment. These arrows shows the damaged cytoplasmic membrane exposure to VCM-StBAclm-Qt <sub>1</sub> quatsomes.	<b>129</b>
<b>Figure 7</b>	Red colour represents the gate for alive MRSA cells while the Green colour represents the gate for dead cells in the population. Flow cytometry PI emission intensity plot) A) Histogram plot of the control group showing live MRSA cells; B) Histogram plots percentage uptake of dead MRSA cells when treated with bare VCM; C) Histogram plot showing percentage uptake of dead MRSA cells when treated VCM-StBAclm-Qt <sub>1</sub> quatsomes.	<b>131</b>
<b>Figure 8</b>	Fluorescence microscopy images of MRSA biofilm: A) Untreated biofilms stained with Syto9; B) Untreated biofilms stained with Syto9 and Propidium Iodide; C) VCM treated and D) VCM-StBAclm-Qt <sub>1</sub> quatsomes treated showing internalisation in the biofilms. (scale bar = 500µm).	<b>133</b>
<b>Figure 9</b>	A) Electrical conductivity of bare VCM and VCM-StBAclm-Qt <sub>1</sub> quatsomes. ** denote statistical significance of bare VCM compared to MRSA (control): **** denotes statistical significance of bare VCM compared to VCM-StBAclm-Qt <sub>1</sub> quatsomes, and # denoted when VCM-StBAclm-Qt <sub>1</sub> quatsomes was compared to MRSA (control); B) Reduction of DNA quantification of bare VCM and VCM-StBAclm-Qt <sub>1</sub> quatsomes. **** denote statistical significance of bare VCM compared to MRSA (control): *** denotes statistical significance of bare VCM compared to VCM-StBAclm-Qt <sub>1</sub> quatsomes, and # denoted when VCM-StBAclm-Qt <sub>1</sub> quatsomes was compared to MRSA (control); C) Reduction of	<b>135</b>

	protein quantification bare VCM and VCM-StBAclm-Qt <sub>1</sub> quatsomes. **** denote statistical significance of bare VCM compared to MRSA (control): *** denotes statistical significance of bare VCM compared to VCM-StBAclm-Qt <sub>1</sub> quatsomes.	
<b>Figure 10</b>	MRSA CFU evaluation post 48-hour of treatment (mean $\pm$ SD) (n = 3). *** denotes the significant difference between the bare VCM vs VCM-StBAclm-Qt <sub>1</sub> quatsomes and VCM vs Untreated groups. **** denotes the significant difference between VCM-StBAclm-Qt <sub>1</sub> quatsomes vs Untreated groups.	<b>137</b>
<b>CHAPTER FOUR: Experimental Paper (Tables)</b>		
<b>Table 1</b>	The binding energies (Kcal/mol) for the VCM-CHol-StBAclm computed from the MD trajectories:	<b>125</b>
<b>Table 2</b>	Stability observation on MHD, PDI, $\zeta$ and DEE% of VCM-StBAclm-Qt <sub>1</sub> quatsomes after twelve weeks of storage.	<b>127</b>
<b>Table 3</b>	MICs values of bare VCM, StBAclm-Qt <sub>1</sub> and VCM-StBAclm-Qt <sub>1</sub> quatsomes against MRSA at pH 6.0 and pH 7.4.	<b>128</b>
<b>Table 4</b>	The analysis of MRSA cell membrane permeability after treatment with bare VCM and VCM-StBAclm-Qt <sub>1</sub> quatsomes.	<b>134</b>

# CHAPTER ONE

## INTRODUCTION

### 1.1 Introduction

This chapter consists of a brief background to the study indicating the status of infectious diseases and the various challenges of antibiotics therapy. The chapter further provides details on several strategies used to improve antibiotic therapy. It also highlights the aims, objectives, novelty of the study and structure of the thesis.

### 1.2 Background

Since the discovery of penicillin by Alexander Fleming in 1928, the development of antibiotics in the 20th century has decreased with an increase in antibiotic resistance as shown in **Figure 1**. After the discovery, it was believed that bacterial diseases would be effortlessly controlled. However, since the 1950's, physicians are faced with newly emerging infectious diseases (EIDs) that have led to significant economic and public health challenges [1, 2]. Infectious diseases continue to be at the forefront concern for health workers globally [3] and are considered to be responsible for high morbidity and mortality rates in both developed and developing countries [4]. Generally, infectious diseases are caused by pathogenic microorganisms, including viruses, bacteria, parasites, and fungi. Compared to other diseases, infectious diseases can be exponentially transmitted among populations in a relatively short period, thus threatening the general public health sector and potentially causing massive economic cost [5]. It is estimated that over half of the world's population are at risk of infectious diseases, causing a disproportionately high disease burden [6]. The World Health Organization (WHO) estimated that by 2050, antibiotic resistance would result in approximately 300 million deaths causing nearly \$100 trillion in global economic loss. These concerns have generated a search for innovative strategies in antimicrobial therapies [7, 8]. In recent years, the challenges of developing new antibiotics for bacterial infection treatment have become a massive problem, especially in the 21<sup>st</sup> century as shown in **Figure 2**. These figures demonstrate that only a few classes of antibiotics have reached patients in the last four decades, and the appearance of multidrug-resistant bacteria has worsened the scenario [9]. Thus, there is an urgent call for new ways to prevent, treat and control infectious diseases.



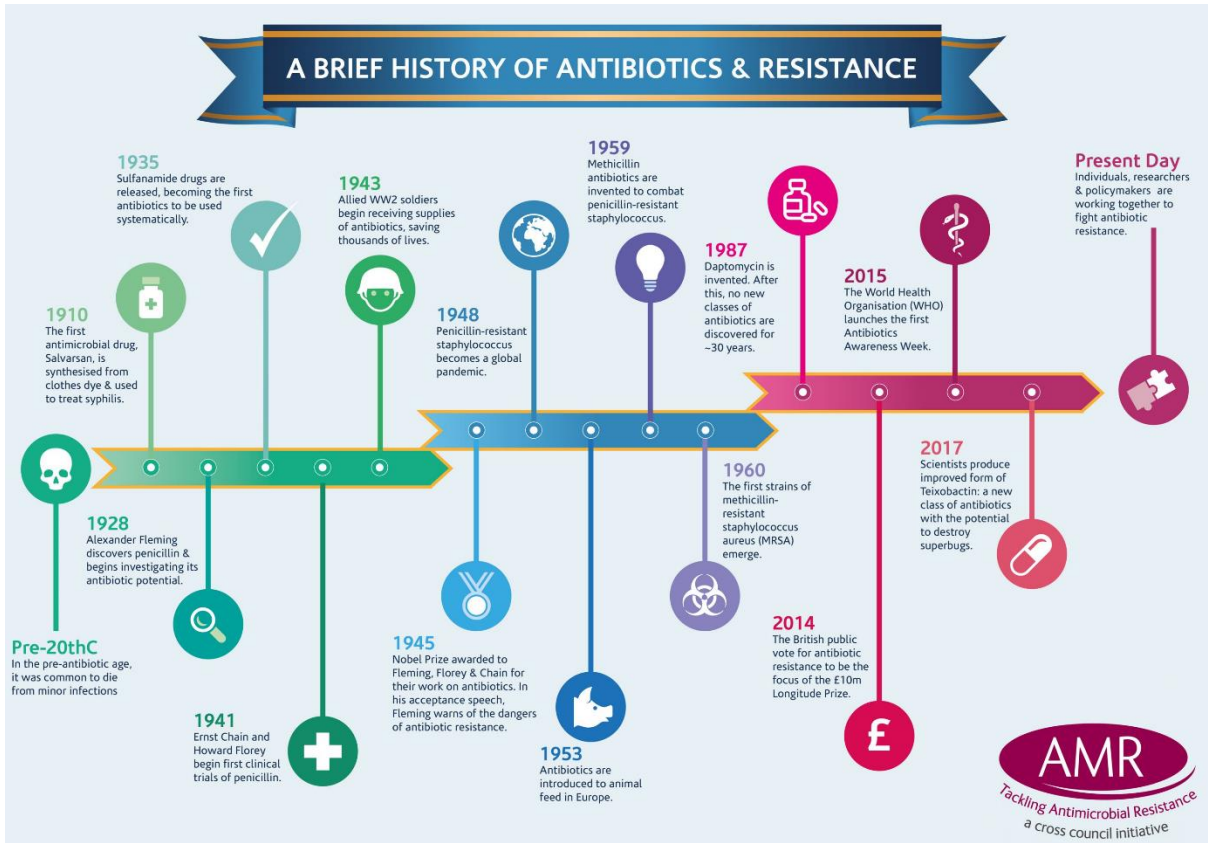


Figure 1: History of antibiotics and resistance [10]

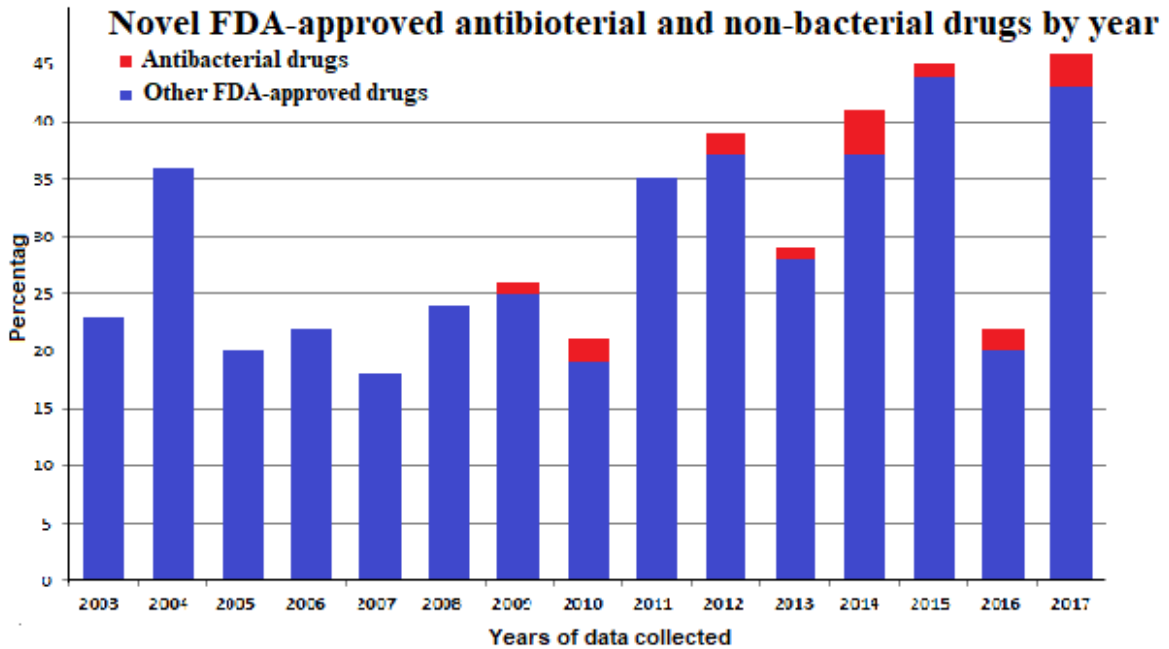
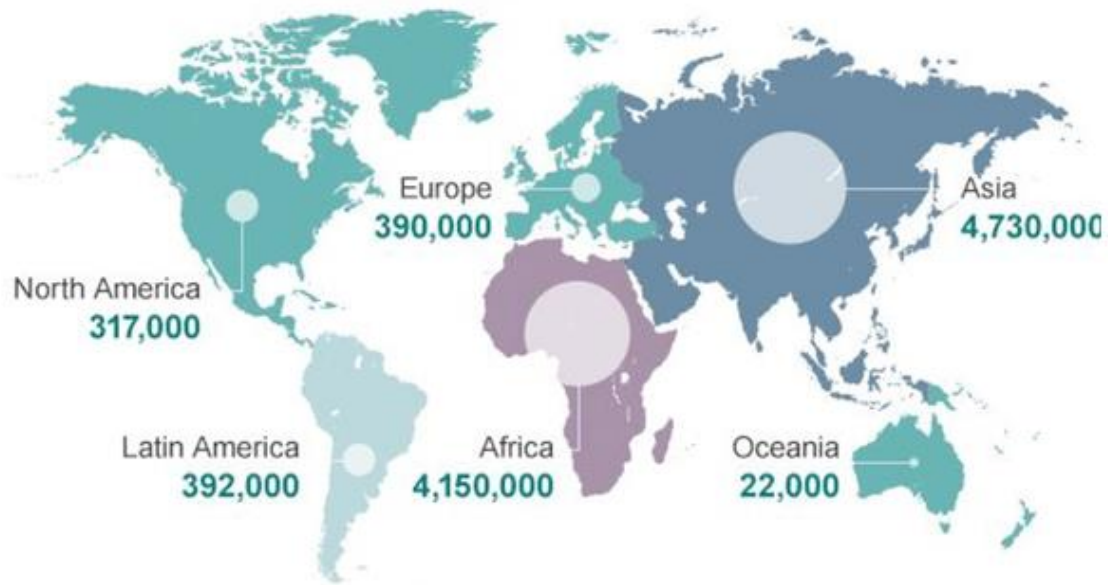


Figure 2: Novel FDA-approved antibacterial and non-bacterial drugs in the last 15 years [9].

Antimicrobial resistance is known to be one of the greatest threats to human health globally [11] and several antibiotics are compromised for infectious diseases treatment due to resistance [12]. Since Alexander Fleming discovered penicillin in 1928, hundreds of antibacterial drugs have been introduced into clinical use to combat infectious diseases [13]. However, extensive misuse and underuse of antibiotics have led to the development of resistance which limit their therapeutic effect to combat infectious diseases caused by MRSA bacteria [13]. O'Neill in 2016 reported that 10 million deaths would be recorded globally due to antimicrobial resistance by 2025 [14] and MRSA resistance will affect greater than 2 million persons every year [15].

Methicillin-resistant *Staphylococcus aureus* (MRSA) considered as a superbug is reported to be resistant to many drugs, including the last-resort antibiotic vancomycin for bacteria treatment leading to vancomycin-resistant strains problems [16, 17]. This problem will continue to rise unless multidimensional global research attention is adopted towards antimicrobial chemotherapy to combat and target the deadly bacteria [18]. According to the Centers for Disease Control and Prevention (CDC), globally nearly 80,641 severe MRSA infections occur every year, leading to nearly 11,285 deaths [19]. Similarly, study by Wozniak *et al.* suggested that the global economic cost output of antimicrobial resistance (AMR) infections is estimated to be around \$100 trillion by 2050. Wozniak *et al.* reported that Australian hospitals spent nearly AUD\$5.5 million per year treating MRSA patients [20]. The European Union Member States reported about 5,400 deaths with increased economic loss of US\$672 [21]. While the European Centre for Disease Prevention and Control (ECDC), estimated nearly 33,000 people die each year in Europe due to infections caused by antibiotic-resistant bacteria (MRSA). Furthermore, in the United States and Africa, death rate are expected to reach nearly 19,000 [11] and 4,150,000 [22] respectively, from infectious diseases caused by MRSA as shown in **Figure 3**. An in-depth review by Iqbal *et al.* in the United Kingdom (UK) revealed that MRSA is one of the main health care problems. The studies revealed that, the UK government and the health care organisation had taken significant measure to reduce MRSA bacteremia by setting targets in the hospitals. The target was set by the UK government health care organization in the hospitals instructed to use universal MRSA screening exercised for admitted patients in the hospital which replaced the targeted screening policy based on risk factors [21].

### Deaths attributable to antimicrobial resistance every year by 2050



**Figure 3:** Expected global antimicrobial resistance death rates to occur every year by 2050 [23].

Antibiotics are a class of secondary metabolites produced by microorganisms, which are synthesised or semi-synthesised analogous compounds that can inhibit the growth and survival of microorganisms [24]. The discovery of antibiotics have saved millions of lives over the past decades [10, 25] by preventing and treating bacterial infections [10] due to their cost-effectiveness and powerful outcomes since the Second World War giving substantial benefits in public health [26]. However, several studies have provided direct evidence that the widespread use of antibiotics has led to the emergence of multidrug-resistant bacterial strains [27]. Several factors such as overuse of antibiotics for systemic infections, improper dosing regimens, misuse of antibiotics for nonbacterial infections and inadequate drug concentrations at the infection sites [28, 29] have contributed to antibiotics resistance developments [30, 31]. Furthermore, faster drug degradation leading to quick elimination in the bloodstream [32] and extended duration of therapy poor patients compliance due to side effects [33, 34], exposure of healthy cells to antibiotics [35] and poor adherence to prescribed regimens demanding for frequent administration prolonged drug usage have contributed to antibiotics resistance [30, 36]. These factors have left a large gap between the introduction of antibiotics and resistance development. The need to develop additional bactericidal nano-drugs have significantly increased due to the growing concern regarding multidrug-resistant bacterial strains associated with infections [37]. The use of cutting-edge nanotechnologies in drug delivery are critical

alternative needed to facilitate the enhancement of conventional antibiotics against infectious disease [11].

Novel nano-drug delivery systems using nanotechnology provide solutions to several modern conventional drugs challenges in the treatment of infectious diseases [38, 39]. These involve the manipulation of matters on atomic, molecular and supramolecular scales to fabricate products macroscopically for drug use beyond regular materials capacity [40]. Nano-sized drug delivery systems offer greater versatility due to size, composition, stimuli-responsiveness [39], biocompatibility, biodegradability, decreased side effects [41, 42] and decreased exposure of antibiotics to healthy sites [43]. Additionally, drug nanosystems enhance antibacterial activities [37, 44-46], cellular internalization [47-50], drug solubility [51], protect drug against degradation [52], prevent exposure of drug molecules to healthy sites, ensure controlled and sustained release and improved cellular internalization [53]. In recent years, billions of dollars was invested in the nanoparticles global market for life sciences, especially in drug delivery systems accounting to nearly 76% of nanotechnology research publications in 2014 [54]. Since the development of the first drug carrier systems, a large number of nanosystems such as polymeric nanoparticles [55], micelles [56], lipid nanovesicles [57], solid lipid nanoparticles (SLN) [58] and liposomes [59, 60] have been developed for targeted delivery of antibiotics [61] revealing less toxicity [62], improve biological activities [63] and enable drug controlled release [64]. Therefore, for biomedical application, nanotechnology is considered as a “responsible benchtop to the bedside” [38] to address conventional dosage forms of antibiotics limitations and decrease bacterial resistance.

The urgency to formulate novel nano-antibiotics systems with suitable properties to target infectious disease for prolonged delivery and enhance antibacterial activity are needed. In this study, three novel approaches for designing nanosystem was explored: i) nanoplexes synthesized with high molecular weight dextran sulfate sodium salt, ii) chitosan-based pH-responsive lipid-polymer hybrid nanovesicles (OLA-LPHVs), iii) quaternary bicephalic surfactant (StBAclm) and cholesterol pH-responsive quatsomes to efficiently enhance vancomycin activity against Methicillin-resistant *Staphylococcus aureus* (MRSA) and infections.

Nanoplexes are drug- nanoparticles complexed with an oppositely charged polyelectrolyte with an excellent alternative to conventional dosage forms antibiotics [65]. These novel nanosystems offer several advantages which include high complexation efficiency (CE%),

higher drug loading capacities (DLC%), solvent-free conditions, feasibility in scale-up, minimal energy expenses and drug wastage [65, 66]. Several studies have reported different advantages of nanoplexes such as minimal energy requirement during nanoplexes preparation [66, 67], decrease frequent drug administration, drug protection from the chemical environment [68] and increase drug molecule targetability [69-71]. Recently, antibiotics nanoplexes of several drugs such as streptomycin [72], gentamicin [73], ciprofloxacin [74], ofloxacin and levofloxacin [75], itraconazole [76], curcumin [77, 78] complexed with polymers such as chitosan, and dextran sulfate sodium salt are employed for combating bacterial resistance. These nanoplexes have demonstrated higher and enhanced antibacterial activity leading to reductions in infections burden reduction.

The zwitterionic pH-responsive lipid (OLA) and the quaternary bicephalic surfactant (StBAclm) nanosystems were efficient for drug delivery and antibacterial enhancement [79, 80]. Additionally, the ability to functionalize the oleylamine and stearylamine terminal groups makes them useful to enhance antibacterial activity [81, 82], biodegradable [83, 84], and ideal for sustained drug release [85]. Although several reports are available for pH-responsive LPHVs [86-88] and zwitterionic lipid [89-91], these are the only reports on pH-responsive LPHVs synthesised from oleylamine and quaternary bicephalic surfactant pH-responsive quatsomes for antibiotics delivery. This highlights the feasibility and importance of developing LPHVs and quatsomes for antibiotics delivery. Nano drug delivery systems are designed to respond to several disease conditions for targeted delivery.

Nano-antibiotic systems have demonstrated the ability to overcome several conventional antibiotics challenges. These are achieved by increasing localised drug concentration at the sites of infection and decrease drug exposure to healthy sites leading to improved infectious disease treatment with minimum side effects and improved patients' compliance. Lipid-polymer hybrid nanovesicles (LPHVs) are core-shell nanoparticle structures comprising of polymer cores and lipid shells, which exhibit complementary characteristics of both polymeric nanoparticles and liposomes, in terms of their physical structure and stability [61]. This nanosystems demonstrated pH-sensitive linkages [92, 93], biocompatibility, higher EE%, drug loading capacity (DLC%) and good stability.

Quatsomes are composed of sterols/cholesterol and quaternary ammonium materials that self-assemble into bilayers nanovesicles [94, 95]. Several quaternary materials such as cationic hexadecyltrimethylammonium bromide (CTAB) [96-98] and myristalkonium chloride (MKC)

[99-101] has been used for quatsomes formulation. They are confirmed to be stable with uniform reproducible, lamellarity [97, 99, 102-104], and revealed enhanced antimicrobial activity against *S. aureus* [105-107]. Furthermore, quatsomes have shown to protect drugs against premature degradation to improve intracellular penetration [108], and ideal for membrane functionalization for drug delivery and targetability [109-111]. The nanosystems ability to encapsulate drug, protect from degradation and enhance their therapeutic efficacy makes them important candidates for drug delivery [112]. Therefore, designing a pH-responsive quaternary bicephalic surfactant (StBAclm) quatsomes to enhance the activity of antibiotics against MRSA, disrupt bacterial membrane to eradicate infectious disease are urgently needed.

To achieve the proposed nano-drug delivery systems, particularly nanoplexes, nanovesicles and quatsomes for vancomycin, is urgently needed. Vancomycin a glycopeptide antibiotic act by inhibiting the biosynthesis of peptidoglycan layer by disrupting the assembly of *N*-acetyl muramic acid and *N*-acetyl glucosamine (NAM-NAG)-polypeptide [113]. It is presently used for the prevention, treatment and prophylaxis of Gram-positive bacteria such as the community-acquired Methicillin-resistant *Staphylococcus aureus* (MRSA), Methicillin-susceptible *Staphylococcus aureus* (MSSA), and Vancomycin-Resistant Enterococci (VRE) [114]. With the increasing occurrence of MRSA, MSSA, and VRE, the potential ability of vancomycin to treat life-threatening infections are becoming difficult due to resistance thus, demand for new treatment approach [115-117]. Therefore, these studies aimed to enhance antibacterial activity and performance of vancomycin (VCM) against MRSA using high molecular weight dextran sulfate sodium salt (DXT), zwitterionic lipid (OLA) and quaternary bicephalic surfactant (StBAclm) derived from nanoplexes, pH-responsive lipid polymer-hybrid nanovesicles (LPHVs), and quaternary bicephalic pH-responsive quatsomes, respectively, against MRSA. Chapters two, three and four represent the first efforts undertaken on the development of new nanosystem to efficiently deliver vancomycin against Methicillin-resistant *Staphylococcus aureus* (MRSA).

### **1.3 Problem Statement**

Infectious diseases, including bacterial infections, continue to be a significant cause of high morbidity and mortality rates globally. Regrettably, conventional dosage forms (CDFs) have demonstrated several limitations, including inadequate drug concentration at infection sites, exposure to beneficial flora to healthy side, fast degradation and quick elimination of the drug in the bloodstream, frequency of drug administration, severe side effects and poor patient

compliance. These limitations have contributed to suboptimal therapeutic outcomes and the current global antimicrobial resistance crisis. Nano-drug delivery systems are showing significant potential for overcoming challenges associated with conventional antibiotics dosage form. The identification of novel nano-based strategies to enhance antibacterial activity and therapy, and to target infection sites, therefore, contribute to the enhancement of patient disease treatments. The design and synthesis of advanced materials for nano-based strategies for developing novel nano-formulations are urgently needed to improve the antibacterial activity of current conventional antibiotics.

#### **1.4 Aims and Objectives of this Study**

The study broadly aimed to design novel, advanced materials and explore their potential for the preparations of nano-based drug delivery systems to treat infectious disease caused by Methicillin-resistant *Staphylococcus aureus* (MRSA) infections. The research aims and objectives of the three developed nanosystems in this study are highlighted below.

##### **Aim 1**

This study aimed to explore the potential of higher molecular weight dextran sulfate sodium salt for complexation with vancomycin into stable nanoplexes formulation and explore its potential for delivering antimicrobials *via* nanoplexes. To achieve this aim, the objectives of the study were to:

1. Screen different concentrations of conventional antibiotic vancomycin to identify a suitable size for stable nanoplexes.
2. Determine the *in vitro* cytotoxicity of the synthesised VCM-DXT<sub>5</sub> nanoplexes to confirm its safety in three different cell lines [adenocarcinoma human alveolar basal epithelial cells (A-549), human embryonic kidney cells (HEK-293) and human liver hepatocellular carcinoma cell (HepG-2)].
3. Perform molecular dynamics simulation between VCM and DXT in order to understand the mechanism behind the nanoplexes formation with salts.
4. Perform and evaluate the formulated nanoplexes in terms of size, PDI, zeta potential, complexation efficiency, drug loading, morphology, *in vitro* drug release, flow cytometry *in vitro* and *in vivo* antibacterial activity.

##### **Aim 2**

This study aimed to synthesise a novel zwitterionic pH-responsive lipid (OLA) from oleylamine and explore its potential to formulate chitosan-based pH-responsive vancomycin-

loaded lipid polymer-hybrid nanovesicles (VM-OLA-LPHVs) through a modified ionic gelation method for VM delivery and antibacterial activity enhancement. To achieve this aim, the objectives of the study were to:

1. Synthesise novel zwitterionic pH-responsive lipid (OLA) and confirm its structure using  $^1\text{H}$  NMR,  $^{13}\text{C}$  NMR, FT-IR, HR-MS.
2. Determine the *in vitro* biocompatibility of the synthesised zwitterionic pH-responsive lipid (OLA) and the chitosan-based pH-responsive vancomycin-loaded lipid polymer-hybrid nanovesicles (VM-OLA-LPHVs) to study its safety margin on different cell-lines [adenocarcinoma human alveolar basal epithelial cells (A-549), liver hepatocellular carcinoma cell lines (MCF-7), human embryonic kidney cells (HEK-293) and human liver hepatocellular carcinoma cells (HepG-2)].
3. Formulate the novel chitosan-based pH-responsive vancomycin-loaded lipid-polymer hybrid nanovesicles (VM-OLA-LPHVs) and evaluate their physicochemical properties in terms of hydrodynamic diameter ( $D_H$ ), polydispersity index (PDI), zeta potential (ZP), entrapment efficiency (EE %), drug-loading capacity (DLC), surface morphology, *in vitro* drug release, *in vitro* and *in vivo* antibacterial activities.
4. Perform quantification analysis using electrical conductivity, deoxyribonucleic acid (DNA) and protein concentration using the VM-OLA-LPHVs nanovesicles to increase electrical conductivity and decrease DNA and protein concentration, respectively towards MRSA infections.
5. Perform bactericidal assay, MRSA membrane disruption and cell wall disruption and observe the rate of bacterial death per hour.
6. Perform quantitative analysis of bacteria cell viability and biofilms reduction after exposure to VM-OLA-LPHVs nanovesicles using flow cytometry and fluorescence microscopy respectively to quantify the percentage of MRSA eliminated and determine MRSA biofilms disruption.

### **Aim 3**

This study aimed to synthesise a novel quaternary bicephalic surfactant (StBAclm) from stearylamine and formulate quaternary bicephalic pH-responsive vancomycin quatsomes (VCM-StBAclm-Qt) to deliver and enhance VCM antibacterial activity against MRSA. To achieve this aim, the objectives of the study were to:

1. Synthesise novel quaternary bicephalic surfactant (StBAclm) and confirm its structure using  $^1\text{H}$  NMR,  $^{13}\text{C}$  NMR, FT-IR and HR-MS.



2. Determine the *in vitro* biocompatibility of the synthesised quaternary bicephalic surfactant (StBAclm) and the quaternary bicephalic pH-responsive vancomycin quatsomes (VCM-StBAclm-Qt) in adenocarcinoma human alveolar basal epithelial cells (A-549), liver hepatocellular carcinoma cell lines (MCF-7), human embryonic kidney cells (HEK-293) and human liver hepatocellular carcinoma cell (HepG-2) to confirm its use in biological systems.
3. Formulate quaternary bicephalic pH-responsive vancomycin-loaded quatsomes and evaluate their physiochemical properties in terms of mean hydrodynamic diameter (MHD), polydispersity index (PDI), zeta potential (ZP), entrapment efficiency (EE %), drug-loading capacity (DLC %), surface morphology, *in vitro* drug release, *in vitro* and *in vivo* antibacterial activity.
4. Perform quantification analysis in terms of electrical conductivity, deoxyribonucleic acid (DNA) and protein concentration to quantify electrical conductivity, DNA and protein concentration in MRSA using the VCM-StBAclm-Qt quatsomes.
5. Perform bactericidal assay, MRSA membrane disruption and cell wall disruption and observe the rate of bacterial death per hour.
6. Perform quantitative analysis of cell viability and biofilms reduction after the exposure of VM-StBAclm-Qt quatsomes to MRSA and MRSA biofilm using flow cytometry and fluorescence microscopy and percentage of MRSA dead cells, MRSA membrane disruption, and elimination of biofilms revealed by the VM-StBAclm-Qt quatsomes.

### 1.5 Novelty of the study

The novelty of the research undertaken is described below.

#### Aim 1

The experimental research in **Chapter two** performed in this study is to the best of our knowledge novel due to the following reasons:

- It is the first antibiotic nanoplex formulation comprising of a polysaccharide based architecture using dextran sulphate.
- It is the first formulated VCM nanoplex formulation.
- It is the first reported antibiotic nanoplex formulation with smaller sizes and high complexation efficiencies than those reported so far.

- It is the first antibiotic nanoplex formulation confirming bactericidal efficacy against MRSA.

### **Aim 2**

The experimental research in **Chapter three** performed in this study is to the best of our knowledge novel due to the following reasons:

- The synthesis of OLA as a novel zwitterionic pH-responsive lipid is reported for the first time.
- This is the first reported pH-responsive nanovesicles (VM-OLA-LPHVs1) formulated using the novel synthesised zwitterionic pH-responsive lipid (OLA) for any class of drug.
- This is the first reported study using electrostatic complexation to form pH-responsive nanovesicles for targeted delivery of antibiotics.
- This is the first report of bactericidal assay and biofilm eradication studies with pH-responsive nanovesicles for bacterial infections.

### **Aim 3**

The experimental research in **Chapter four** performed in this study is to the best of our knowledge novel due to the following reasons:

- The synthesis of (StBAclm) as a quaternary bicephalic surfactant is reported for the first time.
- This is the first reported pH-responsive quatsomes (VCM-StBAclm-Qt<sub>1</sub>) formulated using the novel synthesised quaternary bicephalic surfactant (StBAclm).
- This study reports the first antibiotic quatsomes formulation.

### **1.6 Significance of the study**

The nanosystems drug delivery approaches established in this studies are novel and can contribute to the overwhelming antibiotics, bacterial resistance problems and limitations associated with conventional dosage forms (CFD). The significance of this study is highlighted, as shown below:

***New pharmaceutical products:*** The proposed VCM-DXT<sub>5</sub>, VM-OLA-LPHVs, and VCM-StBAclm-Qt are new pharmaceutical products which have not been reported and can inspire the local pharmaceutical industries to manufacture cost-effective and superior medicines.

***Improved patient therapy and disease treatment:*** All the novel proposed formulations can improve patient therapy; treatment of various diseases associated with bacterial infections and reduce hospital stay by patients. These are advantageous due to enhance antibacterial performance, minimising doses, lowering side effects and improving patient compliance. Therefore, contribute to the enhancement of patient quality of life.

***Creation of new knowledge to the scientific community:*** The studies proposed can lead to new knowledge being produced in Pharmaceutical Sciences. These can include the following:

- Synthesis schemes for new materials, preparation procedures for the novel drug delivery systems and their properties *in vitro*, *in silico*, and *in vivo* can contribute to the creation of new scientific knowledge.
- The extensive *in vivo* testing of these novel systems on infected mice models can offer knowledge for *in vivo* correlations in human.

***Stimulation of new research:*** The proposed VCM-DXT<sub>5</sub>, VM-OLA-LPHVs, and VCM-StBAclm-Qt nanosystems can generate new potential research ideas which include the following:

- The newly proposed VCM-DXT<sub>5</sub>, VM-OLA-LPHVs, and VCM-StBAclm-Qt nanosystems could be used for delivery of other classes of drugs to treat various disease conditions.
- The newly designed and formulated VCM-DXT<sub>5</sub>, VM-OLA-LPHVs and VCM-StBAclm-Qt could stimulate intensive research in the development and manufacturing of nanosuspensions in the pharmaceutical industry to develop novel dosage forms that can decrease major challenges associated with conventional dosage forms.
- The elimination of intracellular MRSA with the novel VM-OLA-LPHVs nanovesicles and VCM-StBAclm-Qt quatsomes will stimulate research in the elimination of other bacteria that hide intracellularly acting as reservoirs and sources of chronic infections and resistant strains.
- The *in vitro* evaluation of electrical conductivity, deoxyribonucleic acid (DNA) and protein concentration quantification in the MRSA using the novel VM-OLA-LPHVs and

VCM-StBAclm-Qt nanosystems will drastically demonstrate a massive reduction of the higher DNA and protein concentration in MRSA.

### **1.7 Overview of dissertation**

The research work performed during these studies presented in this thesis is in a publication format, according to the University of KwaZulu-Natal, College of Health Sciences guidelines. It specifies the inclusion of a brief introductory chapter, published papers and a closing chapter on the conclusions. A PhD degree requires at least three first-authored papers, two of which must be experimental.

**CHAPTER TWO: EXPERIMENTAL PAPER ONE:** This chapter addresses Aim 1, Objectives 1 - 4 and is a first-authored experimental article published in an ISI International Journal: International Journal of Pharmaceutics (Impact Factor = 3.862). This article highlights the formulation of the novel nanoplexes, the *in vitro* toxicity evaluation, formulation of the ultra-small vesicles (VCM-DXT<sub>5</sub>) to deliver VCM, molecular dynamics simulation of the self-assembly of nanoplexes, characterisation of its physical properties and *in vitro* and *in vivo* antibacterial properties.

**CHAPTER THREE: EXPERIMENTAL PAPER TWO:** This chapter addresses Aim 2, Objectives 1 - 6 and is a first-authored experimental article communicated to the International Journal of Biological Macromolecules (Impact Factor 4.784) an ISI International Journal (Manuscript ID: IJBIOMA\_2019\_7211). This article highlights the synthesis of a novel OLA<sub>t</sub>BAC lipid from oleylamine, the *in vitro* toxicity evaluation, hemolytic study, formulation of the pH-responsive nanovesicles (VM-OLA-LPHVs) for targeted delivery of VM, characterisation of its physical and antibacterial properties both *in vitro* and *in vivo* activity and the quantification of DNA and protein concentration.

**CHAPTER FOUR: EXPERIMENTAL PAPER THREE:** This chapter addresses Aim 3, Objectives 1 - 6 and is a first-authored experimental article communicated to the European International Journal of Pharmaceutics (Impact Factor = 3.408) with an ISI International Journal (Manuscript ID: JDT-2019-OR-0382). This article highlights the synthesis of a novel quaternary bicephalic surfactant (StBAclm), *in vitro* toxicity evaluation, hemolytic study, formulation of the quaternary bicephalic pH-responsive quatsomes (VCM-StBAclm-Qt) for targeted delivery of VCM. The formulation was characterised for its physicochemical properties, *in vitro* DNA and protein quantification, *in vitro* time killing assay, membrane

disruption, *in vitro*, and *in vivo* antibacterial properties of the drug-loaded quatsomes against Methicillin-resistant *Staphylococcus aureus* (MRSA).

**CHAPTER FIVE: CONCLUSION:** This chapter includes the overall conclusions from research findings in the study which, provides information on the potential significance of the findings and makes recommendations for future research work in the field of strategic solutions to combat bacterial resistance of antibiotics.

## 1.8 References

- [1] M. Vouga, G. Greub, Emerging bacterial pathogens: the past and beyond, *Clinical Microbiology and Infection* 22 (2016) 12-21.
- [2] D.B. McArthur, Emerging Infectious Diseases, *Nursing Clinics* (2019).
- [3] S. Zhang, H. Guo, Global analysis of age-structured multi-stage epidemic models for infectious diseases, *Applied Mathematics and Computation* 337 (2018) 214-233.
- [4] A. Dube, J.L. Reynolds, W.C. Law, C.C. Maponga, P.N. Prasad, G.D. Morse, Multimodal nanoparticles that provide immunomodulation and intracellular drug delivery for infectious diseases, *Nanomedicine: Nanotechnology, Biology and Medicine* 10 (2014) 831-838.
- [5] N. Madhav, B. Oppenheim, M. Gallivan, P. Mulembakani, E. Rubin, N. Wolfe, Chapter 17. Pandemics: risks, impacts, and mitigation, *Disease control priorities* 9 (2017).
- [6] H. Chen, K. Liu, Z. Li, P. Wang, Point of care testing for infectious diseases, *Clinica Chimica Acta* (2019).
- [7] Y. Yang, A. Chawla, J. Zhang, A. Esa, H.L. Jang, A. Khademhosseini, Applications of Nanotechnology for Regenerative Medicine; Healing Tissues at the Nanoscale, *Principles of Regenerative Medicine*, Elsevier 2019, pp. 485-504.
- [8] Q. Pan, F. Luo, M. Liu, X.-L. Zhang, Oligonucleotide aptamers: Promising and powerful diagnostic and therapeutic tools for infectious diseases, *Journal of Infection* 77(2) (2018) 83-98.
- [9] S. Andrei, L. Valeanu, R. Chirvasuta, M.G. Stefan, New FDA approved antibacterial drugs: 2015-2017, *Discoveries* 6 (2018) e81.
- [10] U.R.a. Innovation, Tackling antimicrobial resistance, (2019).
- [11] I.D.S.o. America, Combating antimicrobial resistance: policy recommendations to save lives, *Clinical Infectious Diseases* 52 (2011) S397-S428.
- [12] B. Li, T.J. Webster, Bacteria antibiotic resistance: New challenges and opportunities for implant-associated orthopedic infections, *Journal of Orthopaedic Research* 36 (2018) 22-32.
- [13] P. Gao, X. Nie, M. Zou, Y. Shi, G. Cheng, Recent advances in materials for extended-release antibiotic delivery system, *The Journal of Antibiotics* 64 (2011) 625.
- [14] J. O'Neill, No antibiotics without a test, says report on rising antimicrobial resistance, (2016).
- [15] L. Lin, X. Mao, Y. Sun, H. Cui, Antibacterial mechanism of artemisinin/beta-cyclodextrins against Methicillin-resistant *Staphylococcus aureus* (MRSA), *Micro. Path.* 118 (2018) 66-73.

- [16] R.J. Fair, Y. Tor, Antibiotics and bacterial resistance in the 21st century, *Perspectives in Medicinal Chemistry* 6 (2014) PMC. S14459.
- [17] J. Davies, D. Davies, Origins and evolution of antibiotic resistance, *Microbiol. Mol. Biol. Rev.* 74(3) (2010) 417-433.
- [18] N.I.f.H.a. Welfare, Around the World antibiotic-resistant bacteria are causing increased numbers of serious infections, but in Finland the situation is still relatively good, (2019).
- [19] N. Andreatos, F. Shehadeh, E.E. Pliakos, E. Mylonakis, The impact of antibiotic prescription rates on the incidence of MRSA bloodstream infections: a county-level, US-wide analysis, *International journal of antimicrobial agents* (2018).
- [20] T.M. Wozniak, E.J. Bailey, N. Graves, Health and economic burden of antimicrobial-resistant infections in Australian hospitals: a population-based model, *Infection Control & Hospital Epidemiology* 40(3) (2019) 320-327.
- [21] H. Iqbal, N. Ponniah, S. Long, N. Rath, M. Kent, Review of MRSA screening and antibiotics prophylaxis in orthopaedic trauma patients; The risk of surgical site infection with inadequate antibiotic prophylaxis in patients colonized with MRSA, *Injury*. 48 (2017) 1382-1387.
- [22] K. Govender, S. Sharma, W. Jessee, K. Nagaraju, N.J. Pearse, P. Chhetri, E.M. Bodenstab, P. Yu, S.C. Srinivas, Leadership and Task Shifting to Address the Challenges of Antimicrobial Resistance in South Africa, *Asian Journal of Pharmaceutical Research and Health Care* 10(1) (2018) 10-20.
- [23] J. Myers, Future of Health and Healthcare-This is how many people antibiotic resistance could kill every year by 2050 if nothing is done. 2016).
- [24] Y. Ben, C. Fu, M. Hu, L. Liu, M.H. Wong, C. Zheng, Human health risk assessment of antibiotic resistance associated with antibiotic residues in the environment: A review, *Environmental Research* (2018).
- [25] J.M. Tiedje, W. Fang, C.M. MANAIA, M. Virta, H. Sheng, M. Liping, T. Zhang, T. Edward, Antibiotic Resistance Genes in the Human-Impacted Environment: A One Health Perspective, *Pedosphere* 29(3) (2019) 273-282.
- [26] (!!! INVALID CITATION !!! [12, 25-27]).
- [27] (!!! INVALID CITATION !!! [26-28]).
- [28] M. Taubert, M. Zoller, B. Maier, S. Frechen, C. Scharf, L.-M. Holdt, L. Frey, M. Vogeser, U. Fuhr, J. Zander, Predictors of inadequate linezolid concentrations after standard dosing in critically ill patients, *Antimicrobial agents and chemotherapy* 60(9) (2016) 5254-5261.

- [29] L. Wang, C. Hu, L. Shao, The antimicrobial activity of nanoparticles: present situation and prospects for the future, *International journal of nanomedicine* 12 (2017) 1227.
- [30] P. Karpecki, M.R. Paterno, T.L. Comstock, Limitations of current antibiotics for the treatment of bacterial conjunctivitis, *Optometry and Vision Science* 87(11) (2010) 908-919.
- [31] S. Tong, J. Pan, S. Lu, J. Tang, Patient compliance with antimicrobial drugs: A Chinese survey, *American journal of infection control* 46(4) (2018) e25-e29.
- [32] M. Baym, L.K. Stone, R. Kishony, Multidrug evolutionary strategies to reverse antibiotic resistance, *Science* 351(6268) (2016) aad3292.
- [33] W.H. Organization, Adherence to long-term therapies: evidence for action, (2003).
- [34] D.T. Gold, B. McClung, Approaches to patient education: emphasizing the long-term value of compliance and persistence, *The American journal of medicine* 119(4) (2006) S32-S37.
- [35] R. Poveda Roda, J.V. Bagán, J.M. Sanchis Bielsa, E. Carbonell Pastor, Antibiotic use in dental practice: A review, *Medicina Oral, Patología Oral y Cirugía Bucal (Internet)* 12(3) (2007) 186-192.
- [36] H.M. Nguyen, C.J. Graber, Limitations of antibiotic options for invasive infections caused by methicillin-resistant *Staphylococcus aureus*: is combination therapy the answer?, *Journal of Antimicrobial Chemotherapy* 65 (2009) 24-36.
- [37] N. Beyth, Y. Houry-Haddad, A. Domb, W. Khan, R. Hazan, Alternative antimicrobial approach: nano-antimicrobial materials, *Evidence-based complementary and alternative medicine* 2015 (2015).
- [38] V. Leso, L. Fontana, I. Iavicoli, Biomedical nanotechnology: Occupational views, *Nano Today* 24 (2019) 10-14.
- [39] S. Ramanavičius, R. Žalneravičius, G. Niaura, A. Drabavičius, A. Jagminas, Shell-dependent antimicrobial efficiency of cobalt ferrite nanoparticles, *Nano. Stru. Nano Obj.* 15 (2018) 40-47.
- [40] R. Olawoyin, Nanotechnology: The future of fire safety, *Safety science* 110 (2018) 214-221.
- [41] X. Jiang, J. Li, M. Ding, H. Tan, Q. Ling, Y. Zhong, Q. Fu, Synthesis and degradation of nontoxic biodegradable waterborne polyurethanes elastomer with poly ( $\epsilon$ -caprolactone) and poly (ethylene glycol) as soft segment, *Eur. Polymer J.* 43(5) (2007) 1838-1846.
- [42] Y. Wen, S. Pan, X. Luo, X. Zhang, W. Zhang, M. Feng, A biodegradable low molecular weight polyethylenimine derivative as low toxicity and efficient gene vector, *Biocon. Chem.* 20(2) (2009) 322-332.



- [43] S. Honary, P. Ebrahimi, R. Hadianamrei, Optimization of particle size and encapsulation efficiency of vancomycin nanoparticles by response surface methodology, *Pharmaceutical Development and Technology* 19(8) (2014) 987-998.
- [44] A. Oloffs, C. Grosse-Siestrup, S. Bisson, M. Rinck, R. Rudolph, U. Gross, Biocompatibility of silver-coated polyurethane catheters and silvercoated Dacron® material, *Biomaterials* 15(10) (1994) 753-758.
- [45] M. Flores, N. Colón, O. Rivera, N. Villalba, Y. Baez, D. Quispitupa, J. Avalos, O. Perales, A study of the growth curves of *C. xerosis* and *E. coli* bacteria in mediums containing cobalt ferrite nanoparticles, *MRS Online Proceedings Library Archive* 820 (2004).
- [46] D.N. Williams, S.H. Ehrman, T.R.P. Holoman, Evaluation of the microbial growth response to inorganic nanoparticles, *Journal of Nanobiotechnology* 4(1) (2006) 3.
- [47] Y. Zhao, Y. Tian, Y. Cui, W. Liu, W. Ma, X. Jiang, Small molecule-capped gold nanoparticles as potent antibacterial agents that target gram-negative bacteria, *Journal of the American Chemical Society* 132(35) (2010) 12349-12356.
- [48] E. Lima, R. Guerra, V. Lara, A. Guzmán, Gold nanoparticles as efficient antimicrobial agents for *Escherichia coli* and *Salmonella typhi*, *Chemistry Central Journal* 7(1) (2013) 11.
- [49] X. Li, S.M. Robinson, A. Gupta, K. Saha, Z. Jiang, D.F. Moyano, A. Sahar, M.A. Riley, V.M. Rotello, Functional gold nanoparticles as potent antimicrobial agents against multi-drug-resistant bacteria, *ACS nano* 8(10) (2014) 10682-10686.
- [50] S. Muzammil, S. Hayat, M. Fakhar-E-Alam, B. Aslam, M. Siddique, M. Nisar, M. Saqalein, M. Atif, A. Sarwar, A. Khurshid, Nanoantibiotics: Future nanotechnologies to combat antibiotic resistance, *Front Biosci (Elite Ed)* 10 (2018) 352-74.
- [51] D. Jones, S. Caballero, G. Davidov-Pardo, Bioavailability of nanotechnology-based bioactives and nutraceuticals, (2019).
- [52] A.C. Santos, I. Pereira, M. Pereira-Silva, L. Ferreira, M. Caldas, M. Collado-González, M. Magalhães, A. Figueiras, A.J. Ribeiro, F. Veiga, Nanotechnology-based formulations for resveratrol delivery: effects on resveratrol in vivo bioavailability and bioactivity, *Colloids and Surfaces B: Biointerfaces* (2019).
- [53] S.H. Hussein-Al-Ali, M.E. El Zowalaty, M.Z. Hussein, B.M. Geilich, T.J. Webster, Synthesis, characterization, and antimicrobial activity of an ampicillin-conjugated magnetic nanoantibiotic for medical applications, *International journal of nanomedicine* 9 (2014) 3801.
- [54] H. Zazo, C.I. Colino, J.M. Lanao, Current applications of nanoparticles in infectious diseases, *Journal of controlled release* 224 (2016) 86-102.

- [55] M.L. Knetsch, L.H. Koole, New strategies in the development of antimicrobial coatings: the example of increasing usage of silver and silver nanoparticles, *Polymers* 3(1) (2011) 340-366.
- [56] M. Hasan, G.B. Messaoud, F. Michaux, A. Tamayol, C. Kahn, N. Belhaj, M. Linder, E. Arab-Tehrany, Chitosan-coated liposomes encapsulating curcumin: study of lipid–polysaccharide interactions and nanovesicle behavior, *RSC Advances* 6(51) (2016) 45290-45304.
- [57] A. Dwivedi, A. Mazumder, N. Nasongkla, Layer-by-layer nanocoating of antibacterial niosome on orthopedic implant, *International journal of pharmaceutics* (2018).
- [58] M.S. Baig, A. Ahad, M. Aslam, S.S. Imam, M. Aqil, A. Ali, Application of Box–Behnken design for preparation of levofloxacin-loaded stearic acid solid lipid nanoparticles for ocular delivery: Optimization, in vitro release, ocular tolerance, and antibacterial activity, *International journal of biological macromolecules* 85 (2016) 258-270.
- [59] A.C. Santos, F. Veiga, A.J. Ribeiro, New delivery systems to improve the bioavailability of resveratrol, *Expert opinion on drug delivery* 8(8) (2011) 973-990.
- [60] Y.O. Jeon, J.-S. Lee, H.G. Lee, Improving solubility, stability, and cellular uptake of resveratrol by nanoencapsulation with chitosan and  $\gamma$ -poly (glutamic acid), *Colloids and Surfaces B: Biointerfaces* 147 (2016) 224-233.
- [61] K. Hadinoto, A. Sundaresan, W.S. Cheow, Lipid–polymer hybrid nanoparticles as a new generation therapeutic delivery platform: a review, *European journal of pharmaceutics and biopharmaceutics* 85(3) (2013) 427-443.
- [62] P.F. Bonventre, G. Gregoriadis, Killing of intraphagocytic *Staphylococcus aureus* by dihydrostreptomycin entrapped within liposomes, *Antimicrobial agents and chemotherapy* 13(6) (1978) 1049.
- [63] F.-F. Zhang, L.-L. Gan, C.-H. Zhou, Synthesis, antibacterial and antifungal activities of some carbazole derivatives, *Bioorganic & medicinal chemistry letters* 20(6) (2010) 1881-1884.
- [64] S.H. Lee, J.E. Lee, W.Y. Baek, J.O. Lim, Regional delivery of vancomycin using pluronic F-127 to inhibit methicillin resistant *Staphylococcus aureus* (MRSA) growth in chronic otitis media in vitro and in vivo, *Journal of controlled release* 96(1) (2004) 1-7.
- [65] D. Hassan, C.A. Omolo, R. Gannimani, A.Y. Waddad, C. Mocktar, S. Rambharose, N. Agrawal, T. Govender, Delivery of novel vancomycin nanoplexes for combating methicillin resistant *Staphylococcus aureus* (MRSA) infections, *International journal of pharmaceutics* 558 (2019) 143-156.

- [66] W.S. Cheow, T.Y. Kiew, K. Hadinoto, Amorphous nanodrugs prepared by complexation with polysaccharides: Carrageenan versus dextran sulfate, *Carbohydrate Polymers* 117 (2015) 549-558.
- [67] C.L.-N. Vo, C. Park, B.-J. Lee, Current trends and future perspectives of solid dispersions containing poorly water-soluble drugs, *European Journal of Pharmaceutics and Biopharmaceutics* 85(3) (2013) 799-813.
- [68] A.J. Huh, Y.J. Kwon, "Nanoantibiotics": a new paradigm for treating infectious diseases using nanomaterials in the antibiotics resistant era, *Journal of controlled release* 156(2) (2011) 128-145.
- [69] S.D. Mahajan, R. Aalinkeel, J.L. Reynolds, B. Nair, D.E. Sykes, W.-C. Law, H. Ding, E.J. Bergey, P.N. Prasad, S.A. Schwartz, Nanotherapeutics using an HIV-1 poly A and transactivator of the HIV-1 LTR-(TAR-) specific siRNA, *Pathology research international* 2011 (2011).
- [70] S.D. Mahajan, R. Aalinkeel, J.L. Reynolds, B. Nair, D.E. Sykes, A. Bonoiu, I. Roy, K.-T. Yong, W.-C. Law, E.J. Bergey, Suppression of MMP-9 expression in brain microvascular endothelial cells (BMVEC) using a gold nanorod (GNR)-siRNA nanoplex, *Immunological investigations* 41(4) (2012) 337-355.
- [71] A. Bonoiu, S.D. Mahajan, L. Ye, R. Kumar, H. Ding, K.-T. Yong, I. Roy, R. Aalinkeel, B. Nair, J.L. Reynolds, MMP-9 gene silencing by a quantum dot-siRNA nanoplex delivery to maintain the integrity of the blood brain barrier, *Brain research* 1282 (2009) 142-155.
- [72] M.N. Seleem, N. Jain, N. Pothayee, A. Ranjan, J. Riffle, N. Sriranganathan, Targeting *Brucella melitensis* with polymeric nanoparticles containing streptomycin and doxycycline, *FEMS Microbiology Letters* 294(1) (2009) 24-31.
- [73] A. Ranjan, N. Pothayee, M. Seleem, N. Jain, N. Sriranganathan, J. Riffle, R. Kasimanickam, Drug delivery using novel nanoplexes against a *Salmonella* mouse infection model, *Journal of Nanoparticle Research* 12(3) (2010) 905-914.
- [74] W.S. Cheow, K. Hadinoto, Self-assembled amorphous drug-polyelectrolyte nanoparticle complex with enhanced dissolution rate and saturation solubility, *Journal of Colloid and Interface Science* 367(1) (2012) 518-526.
- [75] W.S. Cheow, K. Hadinoto, Green preparation of antibiotic nanoparticle complex as potential anti-biofilm therapeutics via self-assembly amphiphile-polyelectrolyte complexation with dextran sulfate, *Colloids and Surfaces B: Biointerfaces* 92 (2012) 55-63.

- [76] W.S. Cheow, T.Y. Kiew, Y. Yang, K. Hadinoto, Amorphization strategy affects the stability and supersaturation profile of amorphous drug nanoparticles, *Molecular Pharmaceutics* 11(5) (2014) 1611-1620.
- [77] H. Yu, T.-T. Tran, J. Teo, K. Hadinoto, Dry powder aerosols of curcumin-chitosan nanoparticle complex prepared by spray freeze drying and their antimicrobial efficacy against common respiratory bacterial pathogens, *Colloids and Surfaces A: Physicochemical and Engineering Aspects* 504 (2016) 34-42.
- [78] H. Yu, M.-H. Nguyen, W.S. Cheow, K. Hadinoto, A new bioavailability enhancement strategy of curcumin via self-assembly nano-complexation of curcumin and bovine serum albumin, *Materials Science and Engineering: C* 75 (2017) 25-33.
- [79] J. Zhao, X. Zhang, X. Sun, M. Zhao, C. Yu, R.J. Lee, F. Sun, Y. Zhou, Y. Li, L. Teng, Dual-functional lipid polymeric hybrid pH-responsive nanoparticles decorated with cell penetrating peptide and folate for therapy against rheumatoid arthritis, *European Journal of Pharmaceutics and Biopharmaceutics* 130 (2018) 39-47.
- [80] W. Gao, J.M. Chan, O.C. Farokhzad, pH-responsive nanoparticles for drug delivery, *Molecular pharmaceutics* 7(6) (2010) 1913-1920.
- [81] P.S. Pramod, N.U. Deshpande, M. Jayakannan, Real-time drug release analysis of enzyme and pH responsive polysaccharide nanovesicles, *The Journal of Physical Chemistry B* 119(33) (2015) 10511-10523.
- [82] E. Gallon, T. Matini, L. Sasso, G. Mantovani, A. Armiñan de Benito, J. Sanchis, P. Caliceti, C. Alexander, M.J. Vicent, S. Salmaso, Triblock copolymer nanovesicles for pH-responsive targeted delivery and controlled release of siRNA to cancer cells, *Biomacromolecules* 16(7) (2015) 1924-1937.
- [83] J. Dai, S. Lin, D. Cheng, S. Zou, X. Shuai, Interlayer-crosslinked micelle with partially hydrated core showing reduction and pH dual sensitivity for pinpointed intracellular drug release, *Angewandte Chemie International Edition* 50(40) (2011) 9404-9408.
- [84] Y. Zhao, Z. Luo, M. Li, Q. Qu, X. Ma, S.H. Yu, Y. Zhao, A Preloaded Amorphous Calcium Carbonate/Doxorubicin@ Silica Nanoreactor for pH-Responsive Delivery of an Anticancer Drug, *Angewandte Chemie International Edition* 54(3) (2015) 919-922.
- [85] C. Fan, T. Bian, L. Shang, R. Shi, L.-Z. Wu, C.-H. Tung, T. Zhang, pH-Responsive reversible self-assembly of gold nanoparticles into nanovesicles, *Nanoscale* 8(7) (2016) 3923-3925.

- [86] J. Shi, Z. Xiao, A.R. Votruba, C. Vilos, O.C. Farokhzad, Differentially charged hollow core/shell lipid–polymer–lipid hybrid nanoparticles for small interfering RNA delivery, *Angewandte Chemie International Edition* 50(31) (2011) 7027-7031.
- [87] A. Najer, D. Wu, D. Vasquez, C.G. Palivan, W. Meier, Polymer nanocompartments in broad-spectrum medical applications, *Nanomedicine* 8(3) (2013) 425-447.
- [88] L. Zhang, J.M. Chan, F.X. Gu, J.W. Rhee, A.Z. Wang, A.F. Radovic Moreno, F. Alexis, R. Langer, O.C. Farokhzad, Self-assembled lipid polymer hybrid nanoparticles: A robust drug delivery platform, *ACS Nano* 2 (2008) 1696-1702.
- [89] Y. Obata, S. Tajima, S. Takeoka, Evaluation of pH-responsive liposomes containing amino acid-based zwitterionic lipids for improving intracellular drug delivery in vitro and in vivo, *Journal of Controlled Release* 142(2) (2010) 267-276.
- [90] C.L. Walsh, J. Nguyen, F.C. Szoka, Synthesis and characterization of novel zwitterionic lipids with pH-responsive biophysical properties, *Chemical communications* 48(45) (2012) 5575-5577.
- [91] A.J. Mason, A. Martinez, C. Glaubitz, O. Danos, A. Kichler, B. Bechinger, The antibiotic and DNA-transfecting peptide LAH4 selectively associates with, and disorders, anionic lipids in mixed membranes, *The FASEB journal* 20(2) (2006) 320-322.
- [92] G. Xu, P. Liu, D. Pranantyo, K.-G. Neoh, E.-T. Kang, Dextran-and Chitosan-Based Antifouling, Antimicrobial Adhesion, and Self-Polishing Multilayer Coatings from pH-Responsive Linkages-Enabled Layer-by-Layer Assembly, *ACS Sustainable Chemistry & Engineering* 6(3) (2018) 3916-3926.
- [93] A. Roointan, J. Farzanfar, S. Mohammadi-Samani, A. Behzad-Behbahani, F. Farjadian, Smart pH responsive drug delivery system based on poly (HEMA-co-DMAEMA) nanohydrogel, *International journal of pharmaceutics* 552(1-2) (2018) 301-311.
- [94] L. Ferrer-Tasies, E. Moreno-Calvo, M. Cano-Sarabia, M. Aguilera-Arzo, A. Angelova, S. Lesieur, S. Ricart, J. Faraudo, N. Ventosa, J. Veciana, Quatsomes: vesicles formed by self-assembly of sterols and quaternary ammonium surfactants, *Langmuir* 29(22) (2013) 6519-6528.
- [95] E. Elizondo, J. Veciana, N. Ventosa, Nanostructuring molecular materials as particles and vesicles for drug delivery, using compressed and supercritical fluids, *Nanomedicine* 7(9) (2012) 1391-1408.
- [96] S. Ganta, H. Devalapally, A. Shahiwala, M. Amiji, A review of stimuli-responsive nanocarriers for drug and gene delivery, *Journal of controlled release* 126(3) (2008) 187-204.

- [97] I. Cabrera, E. Elizondo, O. Esteban, J.L. Corchero, M. Melgarejo, D. Pulido, A. Córdoba, E. Moreno, U. Unzueta, E. Vazquez, Multifunctional nanovesicle-bioactive conjugates prepared by a one-step scalable method using CO<sub>2</sub>-expanded solvents, *Nano letters* 13(8) (2013) 3766-3774.
- [98] G. McDonnell, A.D. Russell, Antiseptics and disinfectants: activity, action, and resistance, *Clinical microbiology reviews* 12(1) (1999) 147-179.
- [99] N. Grimaldi, F. Andrade, N. Segovia, L. Ferrer-Tasies, S. Sala, J. Veciana, N. Ventosa, Lipid-based nanovesicles for nanomedicine, *Chemical Society Reviews* 45(23) (2016) 6520-6545.
- [100] X. Liu, A. Ardizzone, B. Sui, M. Anzola, N. Ventosa, T. Liu, J. Veciana, K.D. Belfield, Fluorenyl-Loaded Quatsome Nanostructured Fluorescent Probes, *ACS Omega* 2(8) (2017) 4112-4122.
- [101] D.A. Silbaugh, L. Ferrer-Tasies, J. Faraudo, J. Veciana, N. Ventosa, B.A. Korgel, Highly Fluorescent Silicon Nanocrystals Stabilized in Water Using Quatsomes, *Langmuir* 33(50) (2017) 14366-14377.
- [102] E. Elizondo, J. Larsen, N.S. Hatzakis, I. Cabrera, T. Bjørnholm, J. Veciana, D. Stamou, N. Ventosa, Influence of the preparation route on the supramolecular organization of lipids in a vesicular system, *Journal of the American Chemical Society* 134(4) (2012) 1918-1921.
- [103] M. Cano-Sarabia, N. Ventosa, S. Sala, C. Patino, R. Arranz, J. Veciana, Preparation of uniform rich cholesterol unilamellar nanovesicles using CO<sub>2</sub>-expanded solvents, *Langmuir* 24(6) (2008) 2433-2437.
- [104] B. Kronberg, B. Lindman, *Surfactants and polymers in aqueous solution*, John Wiley & Sons Ltd., Chichester 2003.
- [105] N. Thomas, D. Dong, K. Richter, M. Ramezanpour, S. Vreugde, B. Thierry, P.J. Wormald, C.A. Prestidge, Quatsomes for the treatment of *Staphylococcus aureus* biofilm, *J. Mat. Chem. B* 3 (2015) 2770-2777.
- [106] N. Cottenye, Z.-K. Cui, K.J. Wilkinson, J. Barbeau, M. Lafleur, Interactions between non-phospholipid liposomes containing cetylpyridinium chloride and biofilms of *Streptococcus mutans*: modulation of the adhesion and of the biodistribution, *Biofouling* 29(7) (2013) 817-827.
- [107] Q. Pan, F. Luo, M. Liu, X.-L. Zhang, Oligonucleotide aptamers: promising and powerful diagnostic and therapeutic tools for infectious diseases, *Journal of Infection* (2018).

- [108] N. Ventosa, I. Cabrera, J. Veciana, H. Santana, E. Martinez, J. Berlanga, Vesicles comprising epidermal growth factor and compositions that contain them, Cuban Patent Appl. CU 112 (2012) 2012.
- [109] S. Azarmi, W.H. Roa, R. Löbenberg, Targeted delivery of nanoparticles for the treatment of lung diseases, *Advanced drug delivery reviews* 60(8) (2008) 863-875.
- [110] T. Kubo, T. Sugita, S. Shimose, Y. Nitta, Y. Ikuta, T. Murakami, Targeted delivery of anticancer drugs with intravenously administered magnetic liposomes in osteosarcoma-bearing hamsters, *International journal of oncology* 17(2) (2000) 309-324.
- [111] R.R. Sawant, V.P. Torchilin, Liposomes as 'smart' pharmaceutical nanocarriers, *Soft Matter* 6(17) (2010) 4026-4044.
- [112] A.E. Nadimi, S.Y. Ebrahimipour, E.G. Afshar, S.K. Falahati-Pour, Z. Ahmadi, R. Mohammadinejad, M. Mohamadi, Nano-scale drug delivery systems for antiarrhythmic agents, *European journal of medicinal chemistry* (2018).
- [113] S.P. Chakraborty, S.K. Sahu, P. Pramanik, S. Roy, In vitro antimicrobial activity of nanoconjugated vancomycin against drug resistant *Staphylococcus aureus*, *International journal of pharmaceutics* 436(1-2) (2012) 659-676.
- [114] C. Vazquez-Guillamet, M.H. Kollef, Treatment of gram-positive infections in critically ill patients, *BMC infectious diseases* 14(1) (2014) 92.
- [115] P.S. Loomba, J. Taneja, B. Mishra, Methicillin and vancomycin resistant *S. aureus* in hospitalized patients, *Journal of global infectious diseases* 2(3) (2010) 275.
- [116] B. Tarai, P. Das, D. Kumar, Recurrent challenges for clinicians: emergence of methicillin-resistant *Staphylococcus aureus*, vancomycin resistance, and current treatment options, *Journal of laboratory physicians* 5(2) (2013) 71.
- [117] P.W. Ament, N. Jamshed, J.P. Horne, Linezolid: Its Role in the Treatment of Gram-Positive, Drug-Resistance Bacterial Infections, *American family physician* 65(4) (2002).

## CHAPTER TWO: EXPERIMENTAL PAPER ONE

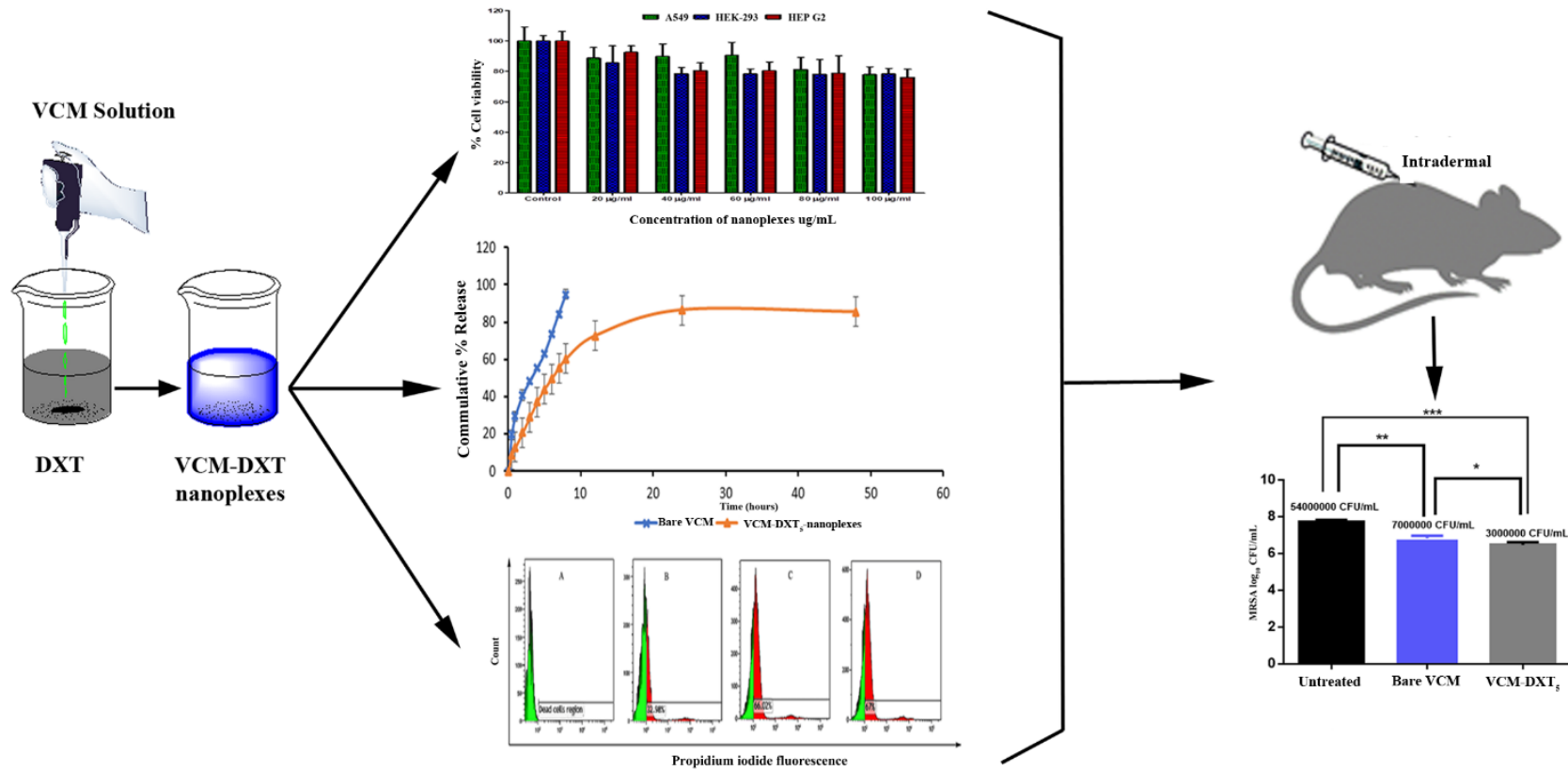
### 2.1 Introduction

This chapter addresses **Aim 1** and **Objectives 1 - 6**. It is a first authored experimental article published highlights the formulation and characterisation of vancomycin nanoplexes (VCM-DXT<sub>5</sub>) from high molecular weight dextran sulfate sodium salt. The nanoplexes was evaluated for *in vitro* toxicity, physicochemical properties, *in-silico* study, *in vitro* and *in vivo* antibacterial properties.

The ethical approval is attached in Appendix I.



## 2.2 Graphical abstract



### **2.3 Published manuscript**

#### **Delivery of Novel Vancomycin Nanoplexes for Combating Methicillin Resistant *staphylococcus aureus* (MRSA) Infections**

**Daniel Hassan<sup>1</sup>, Calvin A. Omolo<sup>1</sup>, Ramesh Gannamani<sup>1</sup>, Ayman Y. Waddad<sup>1</sup>, Chunderika Mocktar<sup>1</sup>, Sanjeev Rambharose<sup>1,2</sup>, Nikhil Agrawal<sup>1</sup>, Thirumala Govender<sup>\*1</sup>**

1. Discipline of Pharmaceutical Sciences, College of Health Sciences, University of KwaZulu-Natal, Private Bag X54001, Durban, South Africa.
2. Division of Emergency Medicine, Department of Surgery, University of Cape Town, Cape Town, South Africa.

\*Corresponding author.

Email address: govenderth@ukzn.ac.za

## 2.4 Abstract

The development of novel antibiotic systems is needed to address the methicillin-resistant *Staphylococcus aureus* (MRSA) infections. The aim of the study was to explore the novel nanoplex delivery method for vancomycin (VCM) against MRSA using dextran sulfate sodium salt (DXT) as a polyelectrolyte complexing agent. Nanoplexes were formulated by the self-assembling amphiphile polyelectrolyte complexation method and characterized. The size, PDI, and ZP of the optimized VCM nanoplexes were  $84.6 \pm 4.248$  nm,  $0.449 \pm 0.024$  and  $-33.0 \pm 4.87$  mV respectively, with  $90.4 \pm 0.77$  % complexation efficiency (CE %) and  $62.3 \pm 0.23$  % drug loading. The *in vitro* MTT studies of the nanoplexes using different cell lines showed VCM nanoplexes to be non-cytotoxic and demonstrated sustained delay release. The *in-silico* study confirmed the spontaneous interaction of VCM with DXT in presence of sodium chloride. A 6.24-fold enhancement was observed for VCM nanoplexes in *in vitro* antibacterial studies. Flow-cytometric analysis showed effective cell killing of 67 % from VCM nanoplexes compared to 32.98 % from the bare vancomycin at the MIC of  $1.25 \mu\text{g/mL}$ . The *in vivo* studies using BALB/c mouse skin infection model revealed that nanoplexes reduced MRSA burden by 2.3-folds compared to bare VCM. The novel nanoplexes show the potential to be a promising delivery system to combat MRSA infections for improved treatment of bacterial infections.

**Keywords:** Vancomycin, dextran sulfate sodium salt (DXT), nanoplexes, antibacterial, methicillin-resistant *Staphylococcus aureus*.

## 2.5 Introduction

Infectious diseases caused by methicillin-resistant *Staphylococcus aureus* (MRSA) continues to be a major concern globally. Statistics by the United State Center for Disease Control and Prevention specifically reported approximately 80 000 invasive MRSA infections and 11 285 associated deaths in 2017 [118]. The effectiveness of conventional antibiotics, such as  $\beta$ -lactam antibiotics (penicillins and cephalosporins) and trimethoprim against MRSA, is compromised due to antibiotic resistance [119]. Currently, vancomycin (VCM), a tricyclic glycopeptide, is one of the main drugs widely used to combat MRSA infections [120, 121]. However, its frequent use and misuse as well as limitations of current dosage forms such as inadequate drug concentration at disease site [122], increased exposure of healthy sites to the drug, higher doses required and side effects, increased frequency of administration, poor patient adherence leads to poor disease treatment outcomes and development of resistance [123-125]. Furthermore, vancomycin suffers from several major drawbacks, such as inducement of nephrotoxicity, on prolonged and persistent usage [126].

Nano-antibiotic delivery systems can help to overcome the problems associated with vancomycin treatment and reduce MRSA infections by offering several advantages, such as increased localized concentration at the infection sites, decreased exposure of the drug to healthy sites, resulting in improved infection treatment, minimized side effects and improved patient compliance [43]. Vancomycin encapsulation in liposomes [127, 128], solid lipid nanoparticles [129], nanostructured lipid carriers [130], polymersomes [131] and polymeric nano carriers [132] has been reported to be an effective method to increase drug accumulation at the site of infection with reduced toxicity and side effects. However, some of these formulations are less feasible due to a number of limitations, such as poor scalability, use of toxic solvents and expensive materials, and high material wastage during preparation [66, 67]. Amorphous VCM–nanoplexes, which involve drug nanoparticles complexed with an oppositely charged polyelectrolyte, can be a good alternate to conventional solid dosage forms and the afore-mentioned nano-formulation strategies [66]. The advantages of nanoplexes include easy preparation methods with high drug loading capacities, solvent free conditions, feasibility in scale-up, minimal energy expenses and drug loss or wastage. Recently, Sikwal *et al* reported VCM polyacrylic acid nanoplexes, with size ranges of  $229.7 \pm 47.76$  nm and complexation efficiency up to 75 %, using the anionic polymer polyacrylic acid sodium and VCM hydrochloride [133]. To the best of our knowledge, this is the only nanoplexes formulation of VCM reported in the literature and hence, there is a need to identify other complexing agents to widen their applicability. While other nanoplexes for drugs, such as

curcumin [134], ciprofloxacin [135], streptomycin [72], ofloxacin, levofloxacin [75], ibuprofen [75], gentamicin [73] and doxorubicin [136], have been reported, there is no data on VCM-dextran sulfate sodium salt (DXT) nanoplexes. Herein we extend the investigation of VCM nanoplexes to a different anionic polysaccharide polymer dextran sulfate sodium salt (DXT) for improved preparation efficiencies.

Dextran sulfate sodium salt (DXT) is widely used in pharmaceutical formulation applications, due to its biodegradable and biocompatible properties [137-139]. The anionic electrostatic interaction, arising from sulfate-groups, enables dextran sulfate sodium salt to readily undergo electrostatic complexation with oppositely charged drug molecules, while hydrophobic interaction from glucoside rings plays an important role in the formation of nanoplexes with small molecule drugs [140]. Dextran sulfate sodium salt (DXT) has been reported to be a useful agent in nanoplexes preparation and for delivering nucleic acids, antibacterial and anticancer drug molecules [66, 137-141]. The use of natural polysaccharides-based polyelectrolyte architectures could offer VCM nanoplexes desirable pharmaceutical properties for commercial applications.

The aim of this study was to explore the potential of dextran sulfate sodium salt for complexation with vancomycin into a stable nanoplexes formulation. In this study, VCM-DXT binary nanoplexes were successfully formulated and characterized for their physicochemical properties, followed by *in-silico*, *in vitro* and *in vivo* antibacterial activity to assess their potential in VCM delivery.

## **2. Materials and Methods**

### **2.1. Materials**

VCM hydrochloride (VCM) was obtained from Sinobright Import and Export Co. Ltd. (China), Dextran sulfate sodium salt (MW = 500,000) was purchased from Millipore/Calbiochem® (Japan). Dialysis tubing of MWCO 14,000 Da (Sigma-Aldrich, USA) was employed for drug release studies and 3-(4, 5-dimethylthiazole-2-yl)-2, 5-diphenyltetrazolium bromide (MTT) used in cytotoxicity study was obtained from Merck Chemicals (Germany). Mueller-Hinton Agar (MHA), Mueller-Hinton Broth (MHB) and Nutrient Broth used for antibacterial assay were Biolab (South Africa) products. The bacteria culture used were MRSA (Rosenbach ATCC BAA 1683), while propidium iodide (PI) and Syto9 cell were obtained from Thermofisher Scientific (USA).

## **2.2. Preparation of VCM-DXT nanoplexes**

VCM-DXT nanoplexes were prepared by a previously reported self-assembling amphiphile polyelectrolyte complexation method, with minor modifications [142]. Briefly, 0.45 % (w/v) of DXT in 0.1 M sodium chloride solution and 1 % (w/v) VCM solution in milli-Q water were prepared separately. Varying amounts of VCM solution of 2.5, 5, 10, 15 and 20 mL were added drop wise to 5 mL of DXT solution (0.45 % w/v) under gentle and constant stirring at ambient condition. The mixture was left for one hour under ambient stirring conditions for the formation of VCM-DXT nanoplexes.

The effect of the VCM concentrations on the nanoplexes formation were explored at an initial DXT concentration of 4.5 mg/mL. The VCM concentration in the formulation varied from 3.3 mg/mL to 8 mg/mL, resulting in the VCM-DXT nanoplexes formation with charge ratios ( $R_{\text{VCM/DXT}}$ ) ranges from 0.31 - 2.49. The charge ratios were calculated from the molecular weights of VCM and DXT and the number of charged groups per molecule for both VCM and DXT (**Supplementary material**). The 24-OSO<sub>3</sub><sup>-</sup> groups per DXT molecule, that contribute to charge density of  $4.8 \times 10^{-6}$  mol.charge/mg for DXT [76] and two amine groups (-NH<sub>3</sub><sup>+</sup>) per VCM molecule, resulting in  $1.3 \times 10^{-6}$  mol.charge/mg for VCM [133] (**Supplementary materials**).

## **2.3. Physical characterizations of VCM-DXT nanoplexes**

### **2.3.1. Particle size, polydispersity index, zeta potential and morphology**

The VCM-DXT nanoplexes, before and after lyophilization were analysed for particles size (PS), polydispersity index (PDI) and zeta potential (ZP) using a zeta sizer (Nano ZS, Malvern Instruments Corp, UK) at 25 °C after diluting the dispersion to an appropriate volume with deionized water. All measurement was done in triplicate. The morphology of VCM-DXT nanoplexes was observed using transmission electron microscope (TEM, Jeol, JEM-1000) at an accelerated voltage of 100 Kv. Samples for TEM analysis were prepared by loading a small amount of nanoplex dispersion onto a carbon coated grid and dried for approximately three minutes to ensure the adherence of sample to grid, with the excess dispersion being removed by filter paper.

### **2.3.2. Complexation efficiency CE %**

The complexation efficiency (CE) is characterized as the mass percentage of drug that forms nanoplexes relative to the initial amount of drug added [75]. Untrapped drug from the VCM-DXT formulations was separated after centrifuging (Beckman Coulter Optima™ MAX XP Centrifuge) at 1300 x g for 30 min at 4 °C. The free drug from the supernatant was collected

and estimated using UV spectrophotometry (Shimadzu UV 1601, Japan) at 280 nm. The complexation efficiency percentage (CE %) was calculated based on **Equation 1**.

$$CE \% = \frac{(Total\ amount\ of\ VCM - amount\ of\ VCM\ in\ supernatant)}{Total\ amount\ of\ VCM} \times 100 \text{ --- Eq. 1}$$

### 2.3.3. Drug loading (DL)

Drug loading was determined by measuring the amount of drug released when a known amount of nanoplexes was completely dissolved in PBS [75]. The freeze dried VCM-DXT nanoplexes concentration was calculated after re-dispersion in the deionized water. The drug percentage loading was determined using UV spectrophotometry (Shimadzu UV 1601, Japan) at 280 nm using **Equation 2**.

$$DL = \frac{Weight\ of\ VCM\ in\ nanoplexes}{Weight\ of\ nanoplexes} \times 100 \text{ --- Eq. 2}$$

### 2.3.4. Percentage yield

A previously reported method was employed to determine the percentage yield of the total nanoplexes mass produced [75, 143]. The VCM-DXT nanoplexes was centrifuged following three washing cycles to remove un-complexed VCM and DXT. The obtained nanoplex dispersion was freeze dried. The resulted amount of nanoplex was weighed, and the percentage yield calculated using **Equation 3**.

$$Percentage\ yield = \frac{weight\ of\ nanoplexes\ obtained\ after\ freeze\ drying}{Total\ weight\ of\ VCM\ and\ DXT\ added} \times 100 \text{ --- Eq. 3}$$

### 2.3.5. Solid state characterisation of nanoplexes

The melting and crystallization behaviour of DXT, VCM, physical mixtures (DXT and VCM) and lyophilized VCM-DXT nanoplexes was determined using differential scanning calorimetry (DSC) [133]. The powder X-ray diffraction (XRD) patterns of DXT, VCM, physical mixture (DXT and VCM) and nanoplexes VCM-DXT were recorded on a Bruker D8 Advance instrument that was equipped with an Anton-Paar XRK 900 reaction chamber and a Cu radiation source with a wavelength of 1.5406 Å at ambient temperature. Fourier Transform Infrared Spectroscopy (FT-IR) was adopted to investigate the structural changes in the VCM-DXT nanoplexes compared to the VCM and DXT using a Bruker Alfa Spectrophotometer (Germany). The spectrum of all samples was recorded within the wave number range of 550-3700 cm<sup>-1</sup> at an average of 16 scans and resolution of 4 cm<sup>-1</sup>.

#### **2.4. *In vitro* drug release**

An *in vitro* release study was performed to understand the release pattern by applying sink conditions [144]. Briefly, a dialysis bag of approximately 10 mm (MWCO 14,000 Da) was filled with 1 mL of nanoplexes dispersion. The dialysis bag was tied at both ends and immersed into 40 mL bottle filled with phosphate buffers saline (PBS) pH 7.4 and placed in a mechanical shaker at 37 °C and 100 rpm. At designated time intervals (0.5, 1, 2, 3, 4, 5, 6, 7, 8, 12, 24, and 48 h), 3 mL of sample solution was withdrawn and substituted with fresh PBS (pH 7.4) solution that had been kept at the same temperature. The VCM concentration from the triplicate samples was quantified at 280 nm using a UV Spectrophotometer using appropriate blanks [145]. Thus obtained release data of the bare VCM and VCM-DXT nanoplexes were kinetically studied using several mathematical models, with the correlation coefficient ( $R^2$ ), root mean square error (RMSE) and mean dissolution time (MDT) being calculated using excel add-in DDSolver program (China) [146].

#### **2.5. *Molecular modelling***

In order to investigate the interaction between VCM and DXT at different ion concentrations, MD simulations were performed. The structure of Vancomycin (**Figure 1A**) was taken from PDB id: 1QD8 [147], and the DXT structure was extracted from PDB id: 5OCA [148]. The obtained DXT structure contained two units, which were replicated to four units using the VMD software [149] (**Figure 1B**), with universal Force Field (UFF) [150] parameters being used for VCM and DXT. The UFF parameters were generated using the OBGMX server [151], and the VCM and DXT simulations were performed at two different ion concentrations (12 Na<sup>+</sup> and 12 Cl<sup>-</sup>, 24 Na<sup>+</sup> and 24 Cl<sup>-</sup>). The SPC water model was used for solvation, and the system with 12 Na<sup>+</sup> and 12 Cl<sup>-</sup> contained 3982 water molecules, while the 24 Na<sup>+</sup> and 24 Cl<sup>-</sup> system contained 3958 water molecules. VCM and DXT were placed at ~ 30.00 Å centre of mass distance (COM) in the systems, both of which were first energy minimized using the 5000 steps of steepest descent method [152]. Two short equilibration simulations were performed using canonical ensemble (NVT), followed by an isobaric-isothermic ensemble (NPT) for 100 ps, each. The production run for both systems was performed using the NPT ensemble for 1 ns each (total 2 ns), at 323 K temperature with a velocity-rescale thermostat [153] at 1 atm pressure using the Parrinello-Rahman pressure coupling method [154]. The pressure coupling time was 2.0 ps while that of the temperature was 0.1 ps. The particle Mesh Ewald (PME) method [155] was used for long-range electrostatic interactions, and for both the short-range coulombic and VdW interactions, a 10 Å cut-off was used. The simulations were performed



using GROMACS [156], and the COM were calculated between VCM and DXT using in-house Tcl script, while the interaction energies were calculated using a rerun option of the “MDRUN” package of GROMACS.

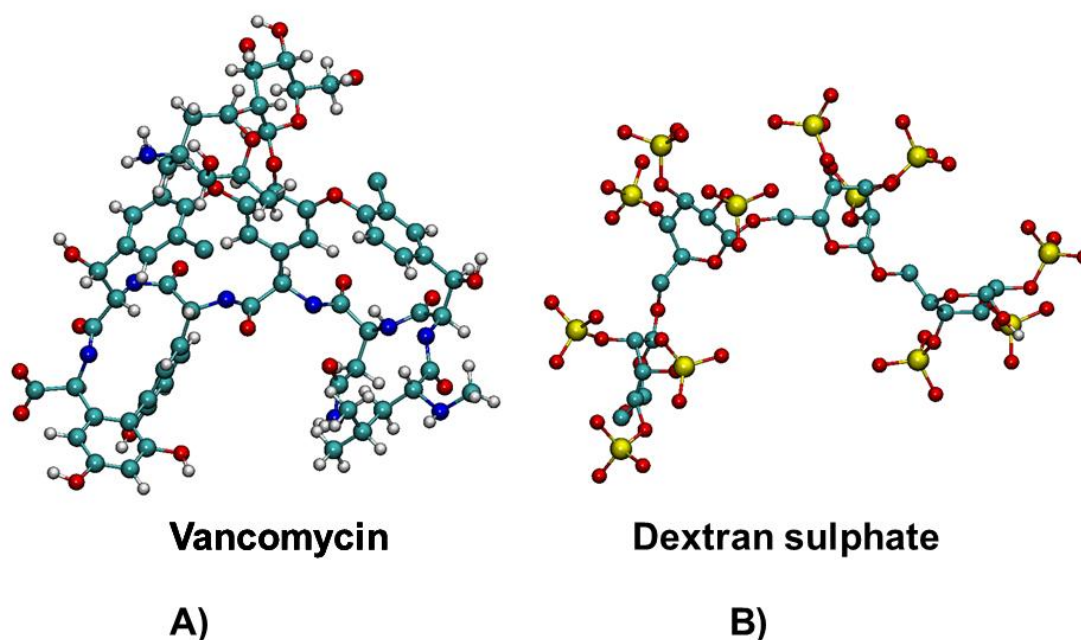


**Figure 1:** Structure of A) VCM and B) DXT used in present study.

### **2.6. Stability**

The short-term physical stability of the VCM-DXT nanoplexes was evaluated at 4 °C and at room temperature (RT) for 90 days. The evaluation of the formulations physical appearance, particle sizes, PDI and ZP was performed at the end of 30, 60 and 90 days. This study was performed in triplicate, and the effects of cryoprotectant at 5 % was explored on their sizes, PDI and ZP.

### **2.7. In vitro cytotoxicity**

The MTT assay was employed to determine the cytotoxicity of the bare VCM and the VCM-DXT nanoplexes using adenocarcinoma human alveolar basal epithelial cells (A549), embryonic kidney cells (HEK-293) and liver hepatocellular carcinoma (Hep G2) cell lines. The cells were cultured and seeded as per previously reported procedure (n = 6) [157]. The different concentration of bare VCM and VCM-DXT nanoplexes (20, 40, 60, 80 and 100 µg/mL) were introduced into the wells seeded with cells [133]. The positive control wells (with culture medium containing cells only) and the negative control (with culture medium without cells) were also included. The sample were incubated for 48 h, there after sample-laden medium was replaced with 100 µL of fresh culture medium and 20 µL of MTT solution (5

mg/mL in PBS) in each well. Cell viability was determined at absorbance wavelength of 540 nm (Spectrostar Nano, Germany) and the percentage cell viability was calculated using Equation 4.

$$\% \text{ Cell Viability} = \frac{(\text{A540 nm treated cells})}{(\text{A540 nm untreated cells})} \times 100 \text{ ---Eq. 4}$$

### **2.8. *In vitro* antibacterial activity**

The minimum inhibitory concentration (MIC) of the VCM-DXT nanoplexes and bare VCM were evaluated against Methicillin resistant *Staphylococcus aureus* Rosenbach ATCC®BAA-1683 (MRSA) using the broth dilution technique [131]. The bacterial cultures were grown in Nutrient Broth (Biolab, South Africa) at 37 °C for 18 h in a shaking incubator set at 100 rpm. The bacterial cultures were adjusted with sterile distilled water to achieve a concentration equivalent to 0.5 McFarland Standard using a DEN-1B McFarland densitometer (Latvia). The bacterial cultures were further diluted 1:150 with sterile distilled water to obtain a final concentration of  $5 \times 10^5$  colony forming units (CFU)/mL. Serial dilutions of the VCM-DXT nanoplexes and VCM were prepared in Mueller-Hinton Broth 2 (MHB) (Sigma-Aldrich, USA) using 96 well plates. These were then inoculated with the diluted bacterial cultures and incubated at 37 °C for 18 h in a shaking incubator set at 100 rpm. After incubation, 10  $\mu$ L of the VCM-DXT nanoplex and bare VCM were spotted onto the Mueller-Hinton Agar (MHA) (Biolab, South Africa) plates and incubated for a further 18 h at 37 °C. This procedure was repeated daily for three days, and all MIC studies were carried out in triplicate. The blank formulation of dextran was used as a negative control the while bare VCM served as a positive control.

### **2.9. *Bacterial cell viability assay***

Cell viability studies on the MRSA cells were performed using a flow cytometry method a previously reported procedure [158-160]. The processing of the bacteria and percentage cell viability was determined after six hours of incubation of the bacteria with VCM and VCM-DXT following our previously reported procedure [161]. The VCM and VCM-DXT broths (50  $\mu$ L) were added to the flow cytometry tubes, each containing 350  $\mu$ L of the sheath fluid, and vortexed for 5 min [161, 162]. The mixture was incubated for 30 min with 5  $\mu$ L of the non-cell wall permeant Propidium iodide (PI) and the Syto9 cell permeant dye. Thereafter, study and analysis was performed on BD FACSCANTO II (Becton Dickinson, CA, USA) following our previously reported protocol [157].

### **2.10. *In vivo* antibacterial activity and histological evaluation**

A mouse skin infection model was used to determine the *in vivo* antibacterial activity of the VCM-DXT nanoplex [131] with ethical clearance from the University of KwaZulu-Natal's Animal Research Ethics Committee (Approval number: AREC/104/015PD). The guidelines of the AREC of UKZN and the South African National Standard SANS 10386:2008 were followed for humane care and animal use. BALB/c mice weighing 18 - 20 g obtained and housed in Biomedical Research Unit, University of KwaZulu-Natal. A day preceding the study, the mice back hair was shaved, and the shaven area disinfected 70 % ethanol. On the following day, the mice were intradermally infected with 50  $\mu$ L MRSA of  $1.5 \times 10^8$  CFU/mL then divided into three groups, (negative control, positive control and treatment) (n = 4). 30 min post-infection, 50  $\mu$ L of bare VCM, DXT and VCM-DXT nanoplexes were injected at the same site of infection to all the three groups. The mice were kept under observation for 48 h with normal 12 h light and dark condition at 19 – 23 °C, and  $55 \pm 10$  % relative humidity with adequate ventilation.

The mice were euthanized, and the infected skin was harvested and processed to prepare tissue homogenates [131]. The obtained homogenates were spotted (20  $\mu$ L) on nutrient agar plates, incubated at 37 °C for 24 h, before being analysed for number of colonies forming units (CFU). For histological investigations the skin samples were processed and stained following reported procedure [131], then sections were examined and captured with a Leica Microscope DM 500 that was fitted with a Leica ICC50 HD camera (Leica Biosystems, Germany).

### **2.11. *Statistical analysis***

Statistical analysis of data was performed using one-way analysis of variance (ANOVA), followed by Bonferroni's multiple comparison test using GraphPad Prism<sup>®</sup> 6 (GraphPad Software Inc., USA). Statistical significance was based on a *P value* < 0.05, and the data was expressed as mean  $\pm$  standard deviation (SD).

## **3. *Results and Discussion***

### **3.1. *Preparation of VCM-DXT nanoplexes***

Preparation of the VCM-DXT nanoplexes was evaluated as a function of charge ratios  $R_{(VCM/DXT)}$  (0.31, 0.62, 1.24, 1.86 and 2.49) using a solution of DXT in 0.1 M NaCl. For all the tested charge ratios, a complexation efficiency of higher than 90 % of the VCM were observed, and the particle size varied with varying concentrations of VCM. The different charge ratios  $R_{(VCM/DXT)}$  of 0.31, 0.62, 1.24, 1.86, and 2.49, which correspond to the varying concentration of VCM, resulted in nanoplexes with particle sizes of  $84.6 \pm 4.24$ ,  $247.7 \pm 28.0$ ,  $404.0 \pm 13.24$ ,

429.4 ± 40.24 and 500.6 ± 0.33 respectively (**Table 1**). The ZP was proportional to the concentration of VCM and changed from  $-33.0 \pm 4.87$  to  $-23.1 \pm 4.71$  mV as the VCM concentration varied. The negative ZP was an indication of the colloidal stability in the aqueous suspension formed, as shown in **Figure 2**. The above studies showed that the VCM-DXT could be successfully prepared at different charge ratios.

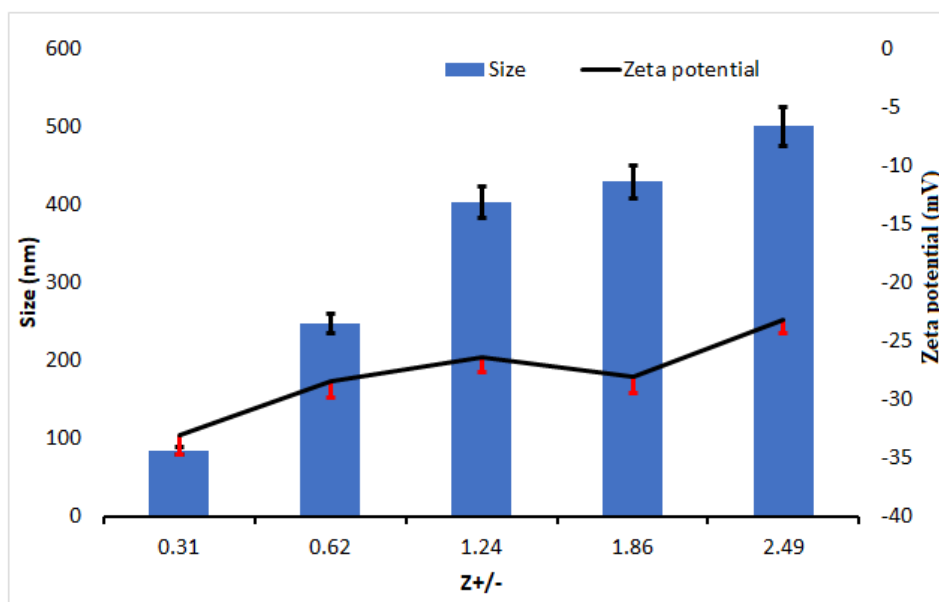


**Figure 2:** Effect of charge ratio on particle sizes and zeta potential of VCM-DXT. Values are expressed as mean ± SD (n=3).

The percentage of CEs at the different charge ratio  $R_{(VCM/DXT)}$  were found to be in the range of 90 – 98 % (**Table 1**). The CE % increased when charge ratio varied from  $R_{(VCM/DXT)}$  of 0.31 to 1.24, after which, as the charge ratio increased, a slight reduction in CE % was observed. At a higher charge ratio the sizes of the VCM-DXT nanoplexes obtained were similar to other studies, where ciprofloxacin was complexed with DXT [66, 142]. At higher charge ratio, the amount of DXT being completely utilised in complexation process, does not favour the aggregation of excess VCM added and hence decreasing CE % at higher concentration VCM [75]. Thus, the ratio of  $R_{(VCM/DXT)}$  had a significant influence on CE % and ZP. The higher complexation efficiency of the VCM in VCM-DXT nanoplexes was attributed to the higher charge density of the DXT [75]. However, the particle sizes were different for various charge ratios, with an increase in the particle sizes being observed with an increase in charge ratio (**Table 1**).

**Table 1:** Effect of charge ratios on sizes, PDI, ZP and CE % of nanoplexes (n = 3).

Formulation	R <sub>(VCM/DXT)</sub>	Size (nm)	PDI	ZP (mV)	CE %
VCM-DXT <sub>1</sub>	2.49	500.6 ± 0.33	0.29 ± 0.07	-23.1 ± 4.71	95.26 ± 0.18
VCM-DXT <sub>2</sub>	1.86	429.4 ± 40.28	0.24 ± 0.03	-28.0 ± 3.75	96.86 ± 0.29
VCM-DXT <sub>3</sub>	1.24	404.0 ± 13.23	0.22 ± 0.02	-26.3 ± 3.40	98.67 ± 0.14
VCM-DXT <sub>4</sub>	0.62	247.7 ± 28.0	0.45 ± 0.08	-28.4 ± 4.40	95.87 ± 0.20
VCM-DXT <sub>5</sub>	0.31	84.6 ± 4.240	0.45 ± 0.02	-33.0 ± 4.87	90.40 ± 0.77

### 3.2. Characterization of the optimized VCM-DXT<sub>5</sub> nanoplexes formulation

From the **Table 1**, the addition of 2.5 mL of the VCM solution (1 % w/v) to 5 mL DXT (0.45 % w/v) under magnetic stirring for 1 h, was concluded as optimal nanoplexes preparation method. Thus obtained, VCM-DXT<sub>5</sub> nanoplexes formulation, with particle size of 84.55 ± 4.24 nm, PDI 0.45 ± 0.02, and ZP of - 33.0 ± 4.87 mV at the lowest charge ratio R<sub>(VCM/DXT)</sub> of 0.31, was therefore considered as the optimized formulation due to its lower sizes, higher ZP value and CE %. In other studies, where polyacrylic acid sodium was complexed with VCM, a sizes greater than 220 nm with only ~74 CE % were observed [133]. Thus, the VCM nanoplexes obtained in this study with DXT were found to have better size, stability and CE % compared to previous reports. Similar CE % for other drugs, such as ofloxacin, levofloxacin and ciprofloxacin, using DXT as a polyelectrolyte [75], indicating that DXT could be a suitable complexing agent for antibiotics, with further studies therefore being performed on the optimized formulation.

To prevent aggregation of the VCM-DXT<sub>5</sub> nanoplexes, the formulation was lyophilized in presence of different cryoprotectants i.e 0.5 % of mannitol, sucrose, D(+) glucose and D(-) glucose [133, 163]. The effect of lyophilisation on its stability of nanoplexes was determined in terms of size, PDI and ZP, after dispersing 10 mg of the freeze-dried formulation in 10 mL of distilled water, with the results being depicted in **Table 2**. Interestingly, lyophilisation in the presence of cryoprotectant improved the PDI values of nanoplexes formulation, while there were no significant changes in ZP indicating their stability in the dry form. The VCM-DXT<sub>5</sub> nanoplexes in dry form can be a great advantage for its pharmaceutical applications as lyophilized solid nano drug delivery systems have been found to be more stable than those is liquid dosage forms [75, 164].

**Table 2:** Effects of cryoprotectant on sizes, PDI and ZP of VCM-DXT<sub>5</sub> nanoplexes before and after lyophilization (n=3).

Parameters	BLZ	ALZ (Mannitol)	ALZ (Sucrose)	ALZ (D+ glucose)	ALZ (D-glucose)	ALZ NCP
Size (nm)	84.55± 4.24	91.33± 4.62	91.44± 6.08	93.17± 13.13	104.8± 17.14	97.37± 8.10
PDI	0.450± 0.02	0.330± 0.09	0.320± 0.09	0.240± 0.16	0.380± 0.15	0.220± 0.07
ZP (mV)	-33.0± 4.87	-34.6 ± 3.13	-33.4± 1.36	-33.9± 0.46	-33.3± 1.23	-32.4± 4.26

*BLZ=before lyophilisation, ALZ=after lyophilisation, NCP= No cryoprotectant.*

### 3.2.2. Drug loading (DL)

Drug loading calculated was  $62.27 \pm 0.23$  %, which was relatively higher than that obtained using polyacrylic acid sodium (PAA) in a previous study [133]. Higher drug loading in the VCM-DXT<sub>5</sub> indicates a stronger affinity between the positively charged amines in the VCM and the negatively charged sulfate groups in the DXT, leading to a stable polyelectrolyte complexation.

### 3.2.3. Percentage yield

The percentage yield of VCM-DXT<sub>5</sub> calculated was found to be  $84.52 \pm 0.31$  %, this result was similar to other studies where DXT was employed as a polyelectrolyte further indicating mass efficiency of the technique [74, 76].

### 3.2.4. Morphology

The morphological analysis of the VCM-DXT<sub>5</sub> nanoplexes was performed using TEM. TEM images showed that the VCM-DXT<sub>5</sub> nanoplexes were discrete and homogeneous, with an almost spherical shape (**Figure 3**). The images were similar in previous studies [66, 76, 142]. The sizes were also comparable to that observed in dynamic light scattering studies.

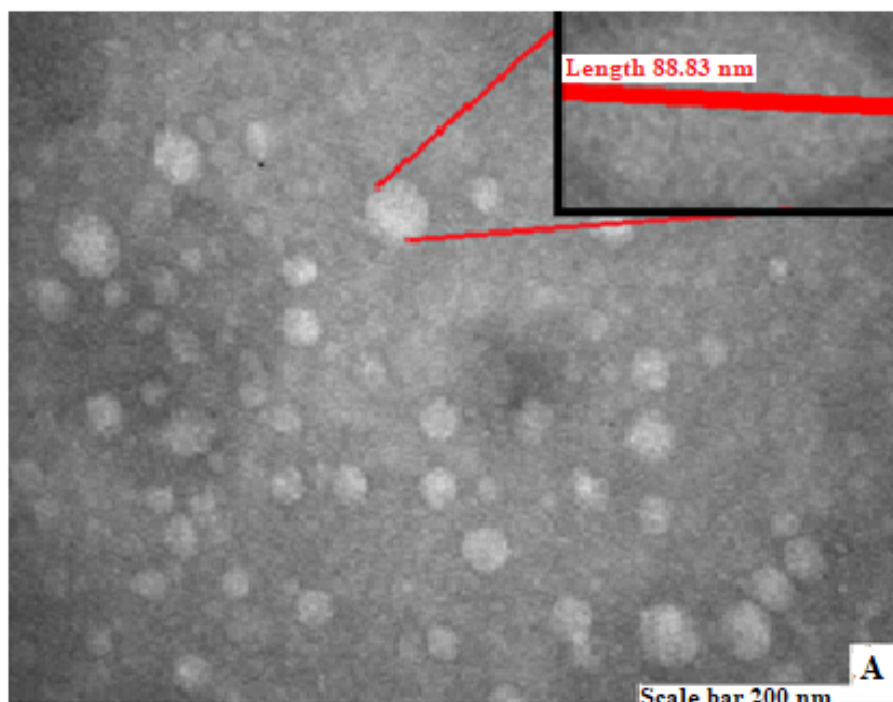


**Figure 3:** Morphology of VCM-DXT<sub>5</sub> nanoplexes

### 3.2.5. Differential scanning calorimetry (DSC)

An overview of the DSC thermograms of DXT, VCM, physical mixture (VCM and DXT) and nanoplexes (VCM-DXT<sub>5</sub>) is shown in **Figure 4**. The DSC thermograms of the VCM and DXT contained characteristics peak at 106 °C and 239 °C respectively, with Cevher *et al.* (2006) observing a similar VCM thermogram profile [165]. The profile of the physical mixture revealed no major shifts in the thermal peaks of the DXT, while the VCM did not show any theta values. In contrast, no sharp thermal events were observed for the lyophilized nanoplexes, indicating its conversion from crystalline form into amorphous form upon complexation with DXT.

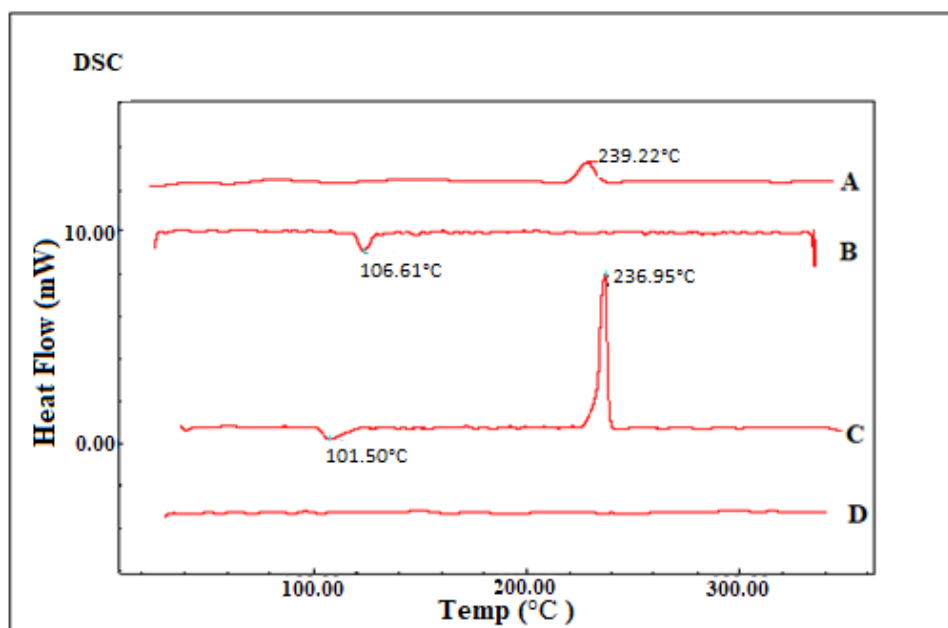


**Figure 4:** DSC profiles of (A) DXT, (B) VCM, (C) Physical mixture of VCM and DXT, and (D) VCM-DXT<sub>5</sub> nanoplexes.

### 3.2.6. X-ray diffraction (XRD)

The inter- and intra-molecular interactions involved during the formation of the nanoplexes, effects the crystal properties of both the VCM and DXT, which can be studied by changes in the diffraction pattern. **Figure 5** represents the comparative diffraction pattern of the DXT, VCM, their physical mixture and the nanoplexes. The powder XRD pattern of the DXT contained several sharp peaks indicating its crystalline nature, while the bare VCM did not show any sharp peaks similar phenomenon has also been reported in other literatures [166, 167] due to its transformation from crystalline states into amorphous states after complexation in the nanoplexes. The physical mixture of the DXT and VCM contained sharp peaks, indicating that the simple mixing did not result in nanoplexes formation. In liquid state the crystalline of the ingredients are broken and free ions are available for complexation unlike in the solid state where there are no charges to induce electrostatic interactions [168-170]. In contrast, the freeze dried VCM-DXT<sub>5</sub> nanoplexes did not show any noticeable peaks in the spectra, confirming the nanoplexes formation. This is in good agreement with the DSC results, and can be attributed to the amorphous nature of VCM in the VCM-DXT<sub>5</sub>.



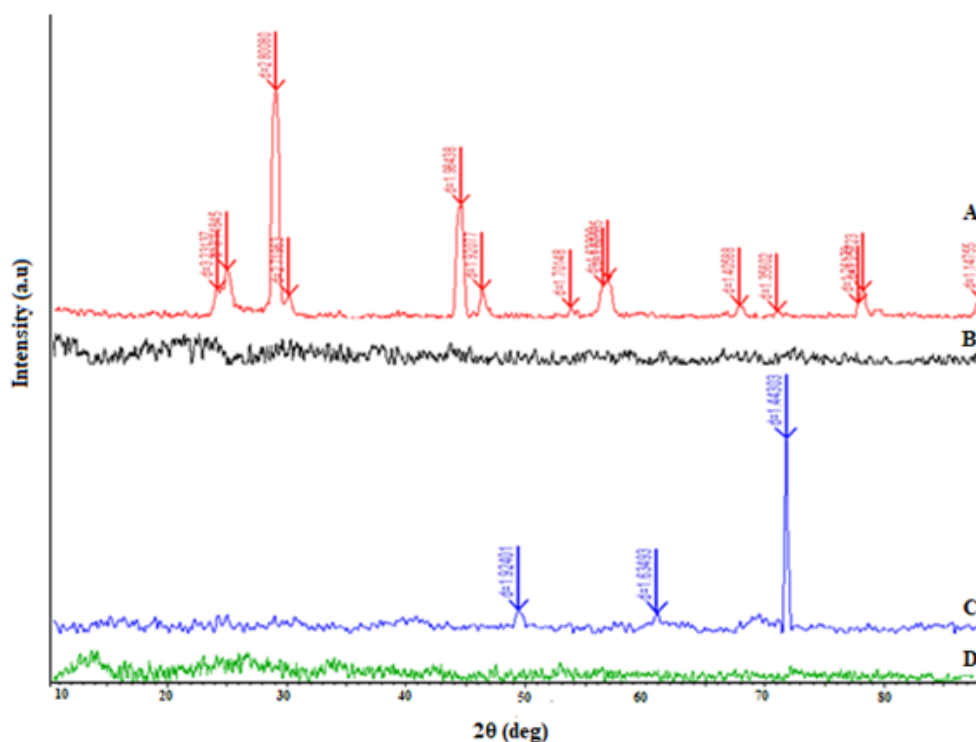


**Figure 5:** Diffractograms of (A) DXT, (B) VCM, (C) Physical mixture (DXT and VCM) and (D) VCM-DXT<sub>5</sub> nanoplexes.

### 3.2.7. Fourier transform-infrared (FT-IR) analysis

The FT-IR spectroscopy analysis was performed to confirm the presence of VCM in the nanoplexes formulation and its complexation with DXT, the comparative infrared (IR) spectra being presented in **Figure 6**. The IR spectra of dextran sulfate sodium salt contained peaks at 1219, 980, 798 and 574  $\text{cm}^{-1}$ , arising due to the vibrations of S=O and O-S-O chemical bonds [171]. These bands shifted to 1229, 1017, 695 and 578  $\text{cm}^{-1}$  respectively in the nanoplexes, indicating that the sulfate group interacted with the oppositely charged VCM molecules. In addition, the peak at 1585  $\text{cm}^{-1}$  (aromatic C=C) for VCM shifted to 1587  $\text{cm}^{-1}$ , which could be due to the  $\pi$ - $\pi$  stacking interaction between the aromatic rings of VCM during the self-assembly process. These changes in IR frequencies confirmed the formation of nanoplexes in a polyelectrolyte directed self-assembly process.

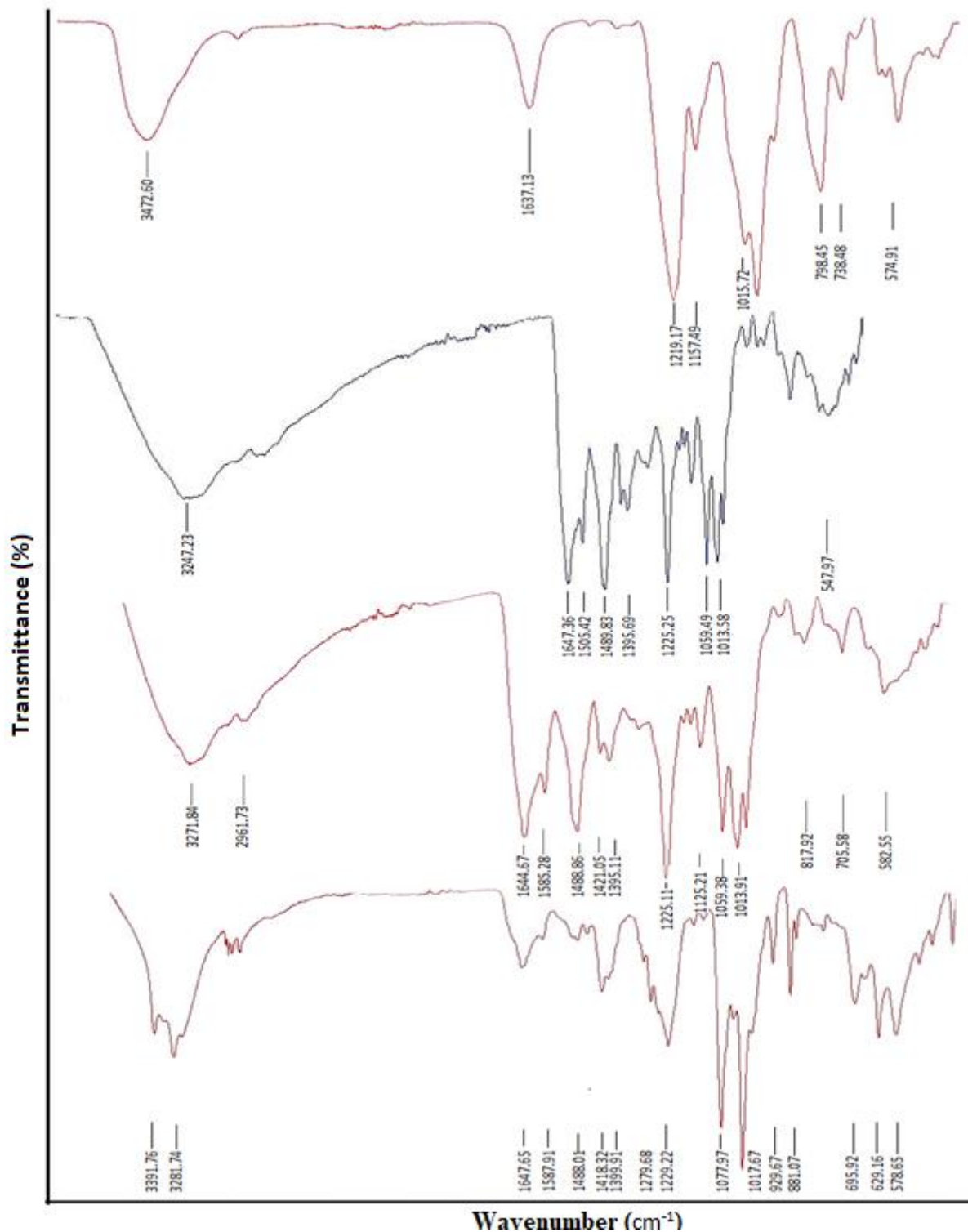


**Figure 6:** FT-IR spectra for (A) DXT, (B) VCM, (C) Physical mixture of VCM and DXT, and (D) VCM-DXT<sub>5</sub> nanoplexes.

### 3.3. *In vitro* drug release

The *in vitro* release of VCM from the optimized nanoplexes and the nanoplex with high charge ratio which resulted to high particles (VCM-DXT<sub>1</sub>) was studied in PBS pH 7.4 over 48 h at 37

°C and are shown in **Figure 7**. At the end of the first two hours, the cumulative percentage of bare VCM released was  $40.9 \pm 2.77$  %, whereas for VCM-DXT<sub>5</sub> it was  $20.7 \pm 1.9$  % and  $20.63 \pm 1.54$  % for VCM-DXT<sub>1</sub>. The bare VCM reached nearly  $94.9 \pm 2.59$  % release at the end of eight hours, while only  $60.4 \pm 1.70$  % was achieved from the optimized VCM-DXT<sub>5</sub> and  $20.63 \pm 1.54$  % for the nanoplex with higher charge ratio. By the end of the 48 h, approximately 86 % and  $39.76 \pm 0.10$  % of the VCM was released from the VCM-DXT<sub>5</sub>, and VCM-DXT<sub>1</sub> respectively indicating slower release pattern from the nanoplexes compared to the bare drug. This slower release profile could be beneficial for reducing the dosage frequency of VCM-DXT<sub>5</sub> nanoplexes formulation.

Additionally, the erodibility of DXT, owing to its biodegradability properties, possibly contributed to the release of VCM from VCM-DXT<sub>5</sub> nanoplexes. The high molecular weight of VCM could be an obstacle to its passage through the DXT matrix, while the unique properties of DXT to swell and erode provided the sustained release pattern of the VCM-DXT<sub>5</sub> nanoplexes over the 48 h compared to 12 h and 15 min in similar studies [133, 142]. The slower release profile displayed by the VCM-DXT<sub>5</sub> nanoplexes compared to the bare drug could provide an effective drug delivery system that, reduces the frequency of administration and increases patient adherence, which could lead to better patient treatment outcomes.

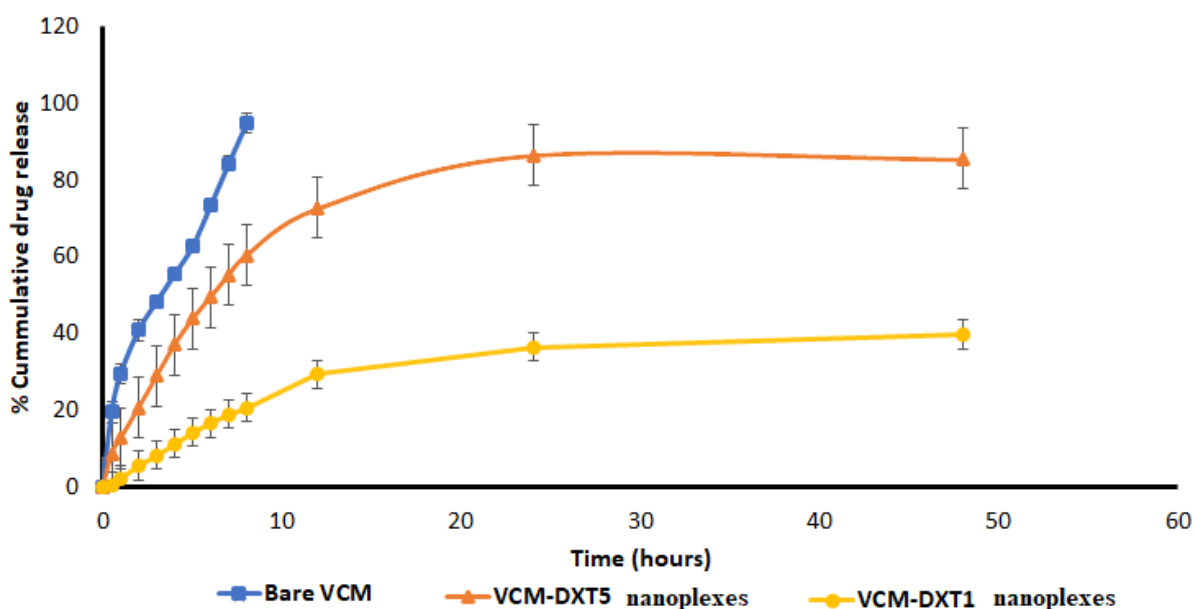


**Figure 7:** Drug release profile of bare VCM, VCM-DXT<sub>5</sub> and VCM-DXT<sub>5</sub> nanoplexes. The values are expressed as mean  $\pm$  SD, n = 3.

### 3.4. Stability study

The novel VCM-DXT<sub>5</sub> nanoplexes formulation was studied for its stability for three months at both room temperature (RT) and 4 °C. The stability of the formulation was assessed in terms of the PS, PDI and ZP, with the results being presented in **Table 3**. The VCM-DXT<sub>5</sub> were stable for the period of three months at 4 °C (*P value* > 0.05), as no change in physical appearance of the formulation was observed. At room temperature (RT), change in size and zeta potential was observed after the second month of the study (*P value* < 0.05), indicating that the physical stability was achieved only for the first month. The instability of the VCM-DXT<sub>5</sub> nanoplexes at room temperature could be associated with the non-fickian release mechanism, which may have caused the structural changes and relaxation behaviour of the DXT due to the swelling process in the aqueous medium [172].

**Table 3:** Effect of storage conditions on physicochemical characteristics of VCM-DXT<sub>5</sub> nanoplexes. The values are expressed as mean ± SD, n = 3

Time (days)	Particle sizes		PDI		ZP	
	4 °C	RT	4 °C	RT	4 °C	RT
0	84.53 ± 4.24	84.55 ± 4.24	0.449 ± 0.02	0.449 ± 0.02	-33.0 ± 4.87	-33.0 ± 4.87
30	84.90 ± 6.01	88.13 ± 6.23	0.448 ± 0.03	0.456 ± 0.08	-29.0 ± 3.19	-23.9 ± 2.34
60	87.33 ± 1.77	89.51 ± 2.30	0.433 ± 0.09	0.459 ± 0.01	-22.0 ± 3.47	-22.2 ± 6.27
90	88.92 ± 1.46	90.20 ± 1.43	0.457 ± 0.01	0.455 ± 0.01	-35.2 ± 1.52	-22.21 ± 2.2

### 3.5. In vitro cytotoxicity

Biosafety being an essential criteria to establish the nontoxic dosages of formulation for biomedical applications, MTT assay based cytotoxicity study was employed to evaluate and quantify the cytotoxicity of the bare VCM and newly derived nanoplexes formulation [173]. The viability of cells after exposure to the bare VCM and the VCM-DXT<sub>5</sub> nanoplexes were assessed by quantifying crystalline blue formazan formation [51]. **Figure 8** shows the bar chart breakdown of the cytotoxicity assay of the VCM-DXT<sub>5</sub> against the A549, HEK 293 and HEP G2 cells. The bare VCM demonstrate cell viability from 77.05 - 93.71 % for A549, 77.31 - 95.18 % for HEK-293 and 76.37 - 91.48 % for HEP G2 cell across all concentration (**Supplementary Material 2: Figure S1**). The results indicate a high percentage of cell viability, from 77.9 to 90.6 % for A549 cells, 78.1 to 85.6 % for HEK 293, and 76.0 to 92.6 % for HEP G2 cell for all concentrations of nanoplexes tested. The results indicating the non-cytotoxic nature of the VCM-DXT<sub>5</sub> nanoplexes, with greater than 75 % cell viabilities

indicating nontoxicity of the material to the mammalian cells [133]. Based on these results, the VCM-DXT<sub>5</sub> can therefore be considered as a nontoxic and safe drug delivery system.

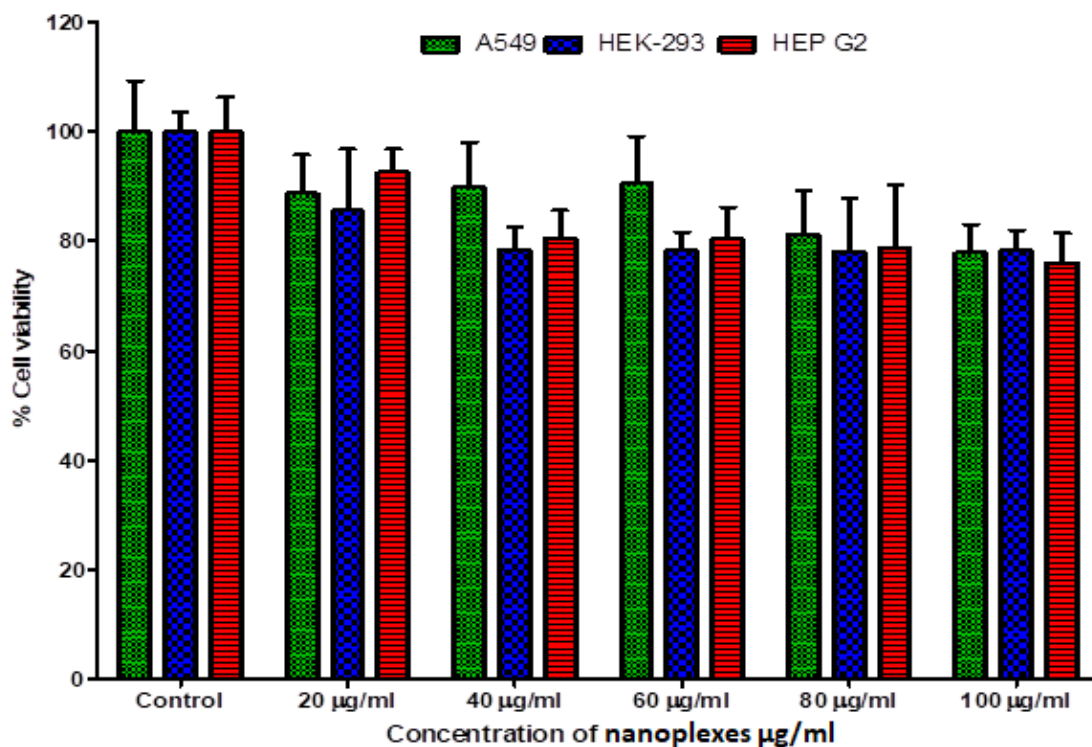


**Figure 8:** Percentage cell viabilities of A549, HEK-293 and HEP G2 cells, after being exposed to different concentration of VCM-DXT<sub>5</sub> nanoplexes. Results are presented as mean  $\pm$  SD (n = 6).

### 3.6. Molecular modelling (Spontaneous interaction between VCM and DXT)

In the experiments, conducted as shown in **Figure 1**, it was observed that spontaneous interaction between the VCM and DXT to form nanoplexes occurred only in the presence of a higher concentration of ions. To investigate the interaction between VCM and DXT at different ion concentrations MD simulations were performed. In the system with 12Na<sup>+</sup> and 12 Cl<sup>-</sup> ions, there was no noticeable interaction between the VCM and the DXT unit at the end of the simulations (**Figure: 9**). However, in the system with 24 Na<sup>+</sup> and 24 Cl<sup>-</sup> ions, the VCM and DXT formed a spontaneous interaction during equilibration simulation, which was further strengthened during the production run, with both molecules remained bound to each other until the end of the simulation time (**Figure: 10A and 10C**). The interaction energy between VCM and DXT was  $\sim$ 80 kJ/mol in the presence of 24 Na<sup>+</sup> and 24 Cl<sup>-</sup> ions (**Figure: 10B**). Thus, the simulations data corroborated to the experimental data.

Previous *in silico* studies indicated that VCM complexation could have been through the  $\pi$ - $\pi$  stacking and alkyl-alkyl hydrophobic interactions [133]. A balance between the attractive and

repulsive forces could be the reason for the salt-induced spontaneous interaction between VCM and DXT. The  $^-OSO_4$  functional group of DXT being negatively charged in presence of sodium salt, might have complexed with ammonium groups ( $NH_3^+$ ) positively charge groups of VCM [174]. Thus, the anionic DXT might have neutralized the positive charge on the VCM molecules and reducing the repulsive forces between them [66]. The ionic concentration could have enhanced the mutual inter molecular interaction between the hydrophobic VCM counter ions by reducing their aqueous solubility [175], and thus supporting antibiotic formation of the nanoplexes with polyelectrolyte DXT. The electrostatic charge shielding function of the sodium salt also might have helped to reduce the inter-molecular repulsions between the like-charges of the DXT chains, and promoting the conformational arrangements to the favoured nanoplexes formation [74, 174]. Thus, a series of salt driven mechanism might have led to nanoplexes formation.

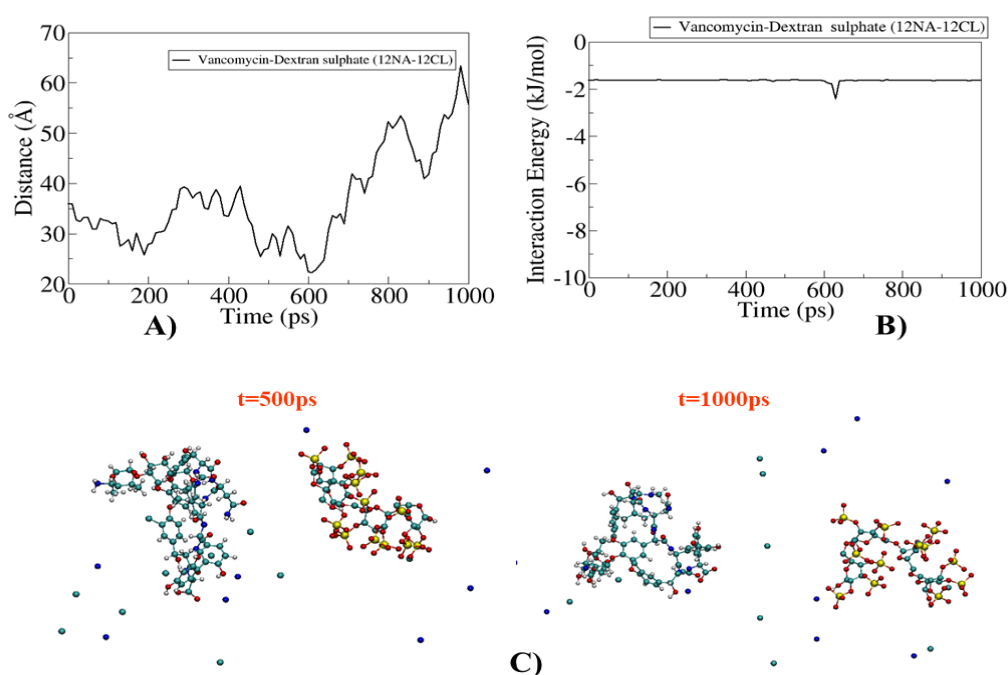


**Figure 9:** A) Shows time evolution of COM distance between VCM and DXT; B) Shows time evolution of interaction energy between VCM and DXT; C) Shows two representative images from the simulations at two different time points in presence of 12  $Na^+$  and 12  $Cl^-$ .

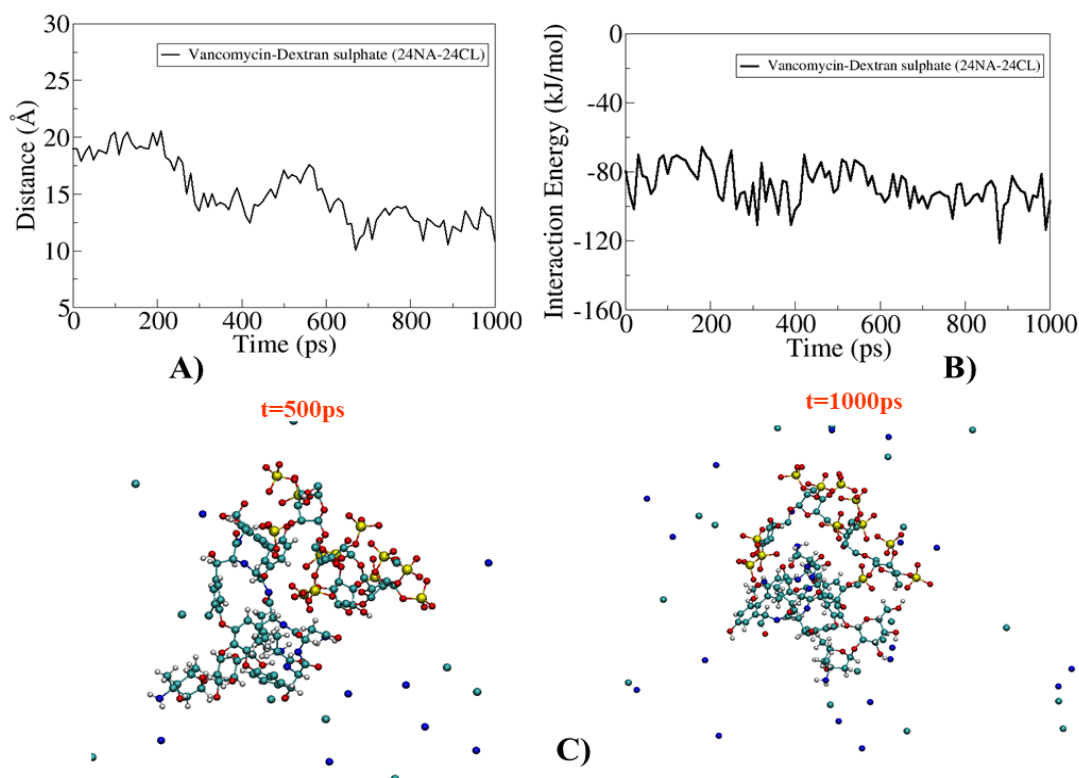


**Figure 10:** A) Shows time evolution of COM distance between VCM and DXT; B) Shows time evolution of interaction energy between VCM and DXT; C) Shows two representative images from the simulations at two different time points in presence of 24 Na<sup>+</sup> and 24 Cl<sup>-</sup>.

### 3.7. *In vitro* antibacterial activity

The *in vitro* antibacterial activity of the bare VCM, the DXT, VCM-DXT<sub>1</sub> and the VCM-DXT<sub>5</sub> was determined by using the 96 well plate-broth dilution technique to confirm and compare the potency and enhancement of VCM upon its transformation into a nanoplexes formation (**Table 4**). The DXT alone did not show any activity, even at the highest concentration tested. After 24 hrs, the MIC values for bare VCM, VCM-DXT<sub>1</sub> and VCM-DXT<sub>5</sub> against MRSA at physiological pH 7.4 were 7.8 µg/mL, 62.5 µg/mL and 1.25 µg/mL respectively, indicating 0.14-fold and 6.24-fold increase in activity of VCM-DXT<sub>1</sub> and VCM-DXT<sub>5</sub> when compared to the bare VCM. Although, VCM-DXT<sub>1</sub> demonstrated slower sustained release compared to VCM-DXT<sub>5</sub>, its MIC was shown to be higher. We couldn't fully explain this result however, this could be attributed to very slow release of the drug limiting the amount of drug available to kill the bacteria due to retarded release however, more studies are needed to explain this phenomenon. The complexation of the VCM with DXT therefore did not adversely affect the antimicrobial activity of the VCM. The results were in good agreement with previous studies, which reported no adverse changes in the antibacterial activity of ofloxacin and levofloxacin

after complexation with DXT [66, 75]. For the VCM nanoplexes derived from the polyacrylic acid sodium (PAA) [133], and for those involving other antibiotics (ofloxacin and ciprofloxacin) with DXT [66, 75], the activity remained the same as for the free drug, with no enhancement. Interestingly, an enhancement by 6.24-folds was observed for VCM-DXT nanoplexes, which could be attributed to a smaller size, high CE % sustained release resulting in the continuous delivery of lethal concentration of the antibiotics to the bacteria for long periods of time thus resulting to complete elimination of the bacteria [176]. The improved activity could also be attributed to the small sizes of VCM-DXT<sub>5</sub> that lead to an increase in the surface area volumes ratio, drug adsorption efficiency that lead higher penetration and uptake. Thus, the *in vitro* studies confirmed the ability of the VCM-DXT<sub>5</sub> to enhance the activity of VCM against MRSA upon its complexation with DXT.

**Table 4:** *In vitro* antibacterial activity of the formulations (VCM-DXT<sub>5</sub>) and (VCM-DXT<sub>1</sub>) against MRSA at PBS pH 7.4. The values are expressed as mean  $\pm$  SD, n = 3

	(MIC $\mu$ g/mL) after 24 hrs.	(MIC $\mu$ g/mL) after 48 hrs.	(MIC $\mu$ g/mL) after 72 hrs.
Bare VCM	7.8	7.8	7.8
DXT	NA	NA	NA
VCM-DXT <sub>5</sub> nanoplexes	1.25	1.25	1.25
VCM-DXT <sub>1</sub> nanoplexes	62.5	62.5	62.5

NA = No activity.

### 3.8. Bacterial cell viability assay

The percentage bacterial cell deaths after exposure to the bare VCM and VCM-DXT<sub>5</sub> nanoplexes at their respective MICs (7.8  $\mu$ g/mL and 1.25  $\mu$ g/mL VCM concentrations respectively) were quantified as shown in **Figure 11**. The results showed that the bare VCM and VCM-DXT<sub>5</sub> nanoplexes at the MIC of formulation 1.25  $\mu$ g/mL had a killing percentage of  $32.98 \pm 1.49$  % (**Figure 11C**) and  $66.24 \pm 0.56$  % (**Figure 11D**) respectively. This indicates a 2-fold higher killing activity of VCM-DXT<sub>5</sub> compared to bare VCM at similar concentrations. When the MRSA cells were incubated with the VCM-DXT<sub>5</sub> nanoplex and bare VCM at their respective MIC of 1.25  $\mu$ g/mL and 7.8  $\mu$ g/mL, they showed similar results of  $66.24 \pm 0.56$  % (**Figure 11D**) and  $65.27 \pm 1.3$  % (**Figure 11B**). Although the VCM concentration in the VCM-DXT<sub>5</sub> (MIC of 1.25  $\mu$ g/mL) was 6.24-folds lower than that of the bare VCM treatment, it was still able to achieve a similar killing percent as that of the bare VCM (MIC of 7.8  $\mu$ g/mL). This



result indicated that the VCM-DXT<sub>5</sub> nanoplexes can be used at lower drug concentrations for treatment without affecting the desired therapeutic outcomes. Moreover, lower doses of treatment that could be achieved using the VCM-DXT<sub>5</sub> nanoplexes could lead to an avoidance of a dose dependent nephrotoxicity of VCM [177]. This further confirmed the ability of the VCM-DXT<sub>5</sub> nanoplexes to retain their potency and enhance the antibacterial activity of VCM.

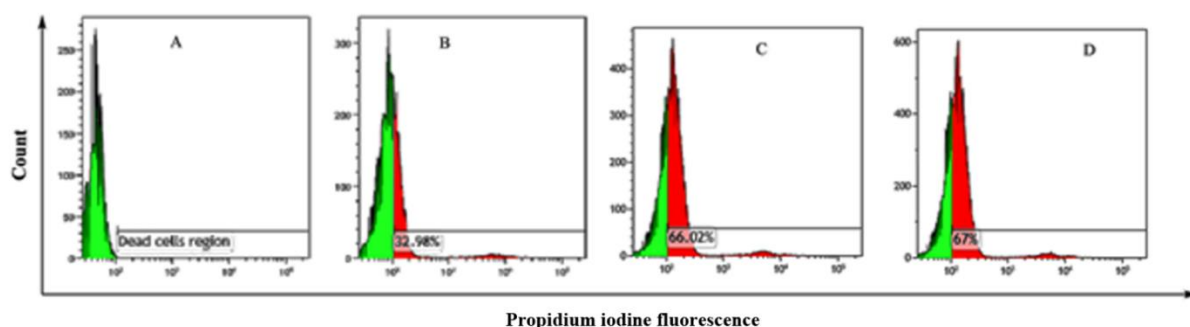


**Figure 11:** *In vitro* antibacterial activity of MRSA cells determined by flow cytometry analysis. A) Cell fluorescence of untreated MRSA; B) Overlay of fluorescence of treated MRSA cells with bare VCM at its MIC; C) Overlay of fluorescence of MRSA cells treated with bare VCM at the MIC value of VCM-DXT<sub>5</sub> nanoplexes; D) Overlay of percentage fluorescence of MRSA cells treated with VCM-DXT<sub>5</sub> at its MIC values.

### 3.9. *In vivo* antibacterial activity

The *in vivo* studies were determined using a BALB/c mice skin infection model to confirm the antimicrobial activity of VCM-DXT<sub>5</sub> nanoplexes. The number of colony-forming units (CFUs) from each treatment group were quantified and represented as log<sub>10</sub>, shown in **Figure 12**. The mean MRSA load (log<sub>10</sub> CFU) retrieved from the VCM-DXT<sub>5</sub> and bare VCM treatments, and untreated skin samples were  $6.46 \pm 0.15$  (3,000,000 CFU/mL),  $6.83 \pm 0.13$  (7,000,000 CFU/mL) and  $7.72 \pm 0.11$  (54,000,000 CFU/mL) respectively. The results showed that the bare VCM had a 7.7-fold lower CFUs when compared to the untreated group. However, when VCM-DXT<sub>5</sub> nanoplexes treatment group was compared to the untreated group, the VCM-DXT<sub>5</sub> nanoplexes had an 18-fold reduction in CFUs with  $P = 0.001$ . When CFUs from the bare VCM treatment group were compared to the VCM-DXT<sub>5</sub> nanoplexes, the latter had lowered CFUs of up to 2.3-fold, with a  $P$  value = 0.0324.

The one-way ANOVA showed significant differences in CFUs, with a  $P$  value = 0.001 among all the groups. The groups treated with VCM-DXT<sub>5</sub> nanoplexes significantly decreased the MRSA load in the skin samples by 2.5-fold compared to the bare VCM treated groups. This

result was in agreement with other *in vivo* results, for example: streptomycin, doxycycline and gentamicin nanoplexes against bacterial infections [72, 73]. As the DXT on its own does not demonstrate antibacterial activity, the experiment showcased the degree of VCM binding to the DXT, with the subsequent improved targeting by nanoplexes possibly having led to the enhanced activities [178]. Therefore, the VCM-DXT<sub>5</sub> nanoplexes formulated in this study demonstrated the potential for combating MRSA infections.

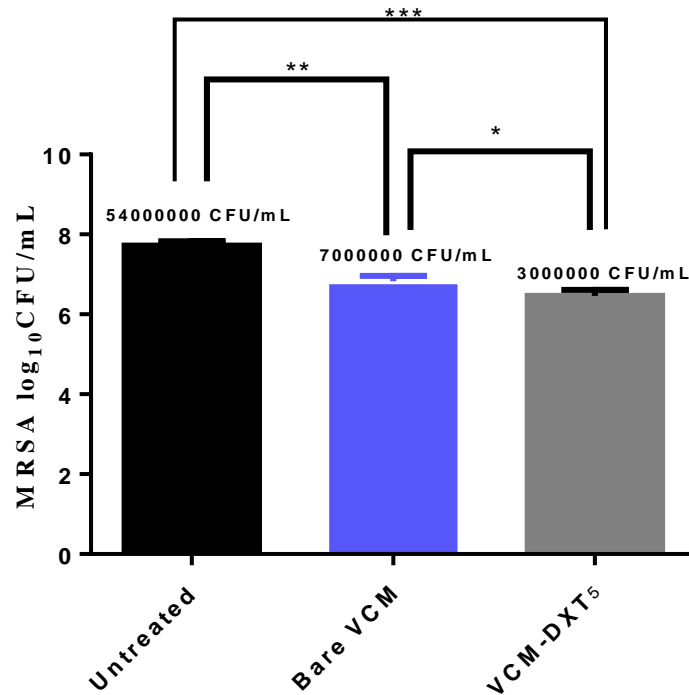


**Figure 12:** MRSA CFUs quantification post 48 h of treatment, the data represent the mean  $\pm$  SD (n=3). \*\*\* denotes significant differences when compared untreated with VCM-DXT<sub>5</sub> nanoplexes. \*\* denotes untreated when compared to bare VCM, and \* denotes significant difference between the bare VCM and VCM-DXT<sub>5</sub> nanoplexes.

The skin samples collected from all the groups were assessed for histomorphological changes that occurred on the experimental groups after infection and treatment, with the samples being stained with H&E and observed under a light microscope. The results indicated that the untreated skin samples showed tissue inflammation and abscess formation, as shown in **Figure 13A**. The signs of swelling and abscess formation were observed for bare VCM treated group (**Figure 13B**), but to a lesser extent than the untreated group (**Figure 13A**). However, the VCM-DXT<sub>5</sub> nanoplexes displayed minimal signs of tissue inflammation and abscess formation (**Figure 13C**). The extensive quantities of white blood cells (WBC) at the infection site were

present for the untreated and bare VCM groups. Nevertheless, lower WBCs were displayed for the group treated with VCM-DXT<sub>5</sub> nanoplexes, as shown in **Figure 13C**. The histomorphology analysis was found to correlate with the CFU/mL calculated in the *in vivo* antibacterial study. The absence of abscess formation and reduced immune response mechanisms (lesser extent of inflammation and reduced number of white blood cells) at infection site for the skin samples of VCM-DXT<sub>5</sub> treated group, when compared to that of untreated and VCM treated group, confirm the antimicrobial potency of the VCM-DXT<sub>5</sub> nanoplexes.

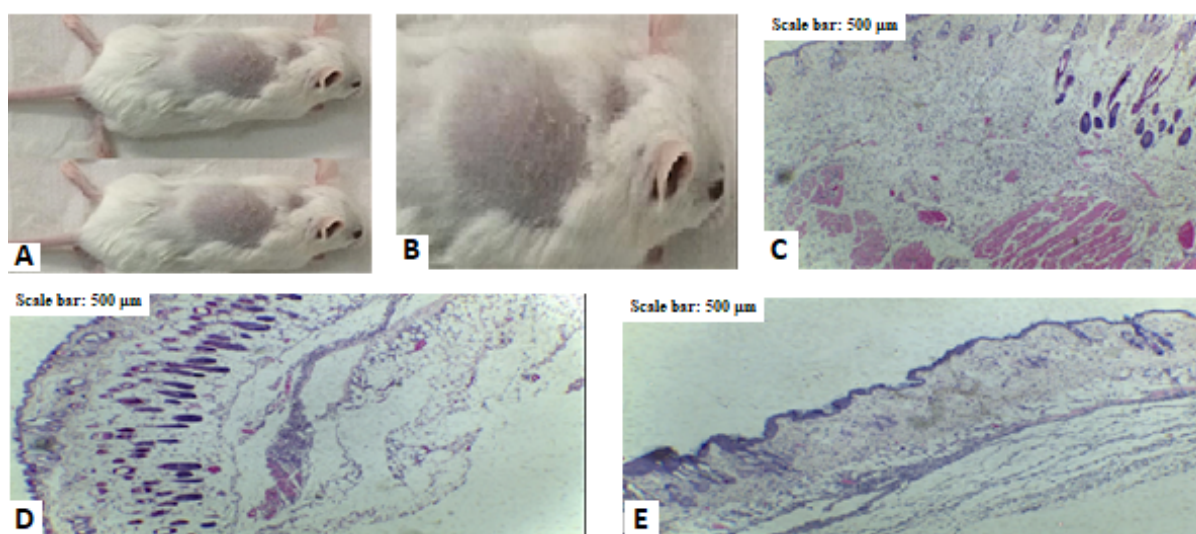


**Figure 13:** Photomicrographs of the skin lesions at the site of injection; A) control and B) treated mice. Histomorphology of controls and treated (Scale bar = 500 μm): C) control/untreated, D) Bare VCM treated, E) VCM-DXT<sub>5</sub> nanoplexes treated.

#### 4. Conclusion

With increasing rates of antimicrobial resistance, novel drug delivery systems, such as nanoplexes, which protect and enhance current antibiotics in the market are required. In this study, a novel VCM-DXT nanoplex was successfully formulated by polyelectrolyte complexation of VCM and DXT for the bio-safe delivery of vancomycin against MRSA. Complexation efficiency of greater than 90 % was achieved for the drug VCM, with the drug releases from nanoplexes occurring in a sustained manner. The molecular modelling studies proved that the presence of salt concentration is a prerequisite for nanoplex formation. *In vitro* antibacterial studies of the nanoplexes against MRSA showed enhanced activity for nanoplexes over bare VCM. The results were further confirmed by flow cytometry, where the VCM-DXT<sub>5</sub>-nanoplexes had a better percentage killing compared to the bare VCM at similar applied concentrations. The *in vivo* BALB/c mouse, skin infection model revealed that treatment with

the VCM-DXT<sub>5</sub>-nanoplexes significantly reduced the MRSA burden compared to the bare VCM. The superior antimicrobial activity and nontoxicity/biosafety of the VCM-DXT nanoplexes formulation upholds its applicability as a promising novel nano-carrier for antibiotic delivery.

***Conflict of interest***

The authors declare no conflict of interest.

***Acknowledgement***

The authors acknowledge the College of Health Sciences, University of KwaZulu-Natal (UKZN), UKZN Nanotechnology Platform, National Research Foundation of South Africa (Grant No. 87790 and 88453) for financial support. The Microscopy and Microanalysis Unit, Biomedical Resource Unit, Department of Human Physiology and Flow Cytometry Research Laboratory at UKZN, CHPC (Cape Town) for supercomputing resources are acknowledged.

***Data availability***

The raw/ processed data if required to reproduce these findings can be shared at any time.

## References

- Abraham, M.J., Murtola, T., Schulz, R., Páll, S., Smith, J.C., Hess, B., Lindahl, E., 2015. GROMACS: High performance molecular simulations through multi-level parallelism from laptops to supercomputers. *SoftwareX* 1, 19-25.
- Ahmed, S., Vepuri, S.B., Jadhav, M., Kalhapure, R.S., Govender, T., 2018. Identifying the interaction of vancomycin with novel pH-responsive lipids as antibacterial biomaterials via accelerated molecular dynamics and binding free energy calculations. *Cell biochemistry and biophysics* 76, 147-159.
- Arndt-Jovin, D.J., Jovin, T.M., 1989. Fluorescence labeling and microscopy of DNA. *Methods in Cell Biology* 30, 417-448.
- Baelo, A., Levato, R., Julián, E., Crespo, A., Astola, J., Gavaldà, J., Engel, E., Mateos-Timoneda, M.A., Torrents, E., 2015. Disassembling bacterial extracellular matrix with DNase-coated nanoparticles to enhance antibiotic delivery in biofilm infections. *Journal of Controlled Release* 209, 150-158.
- Bal, A., David, M., Garau, J., Gottlieb, T., Mazzei, T., Scaglione, F., Tattevin, P., Gould, I., 2017. Future trends in the treatment of methicillin-resistant *Staphylococcus aureus* (MRSA) infection: An in-depth review of newer antibiotics active against an enduring pathogen. *Journal of Global Antimicrobial Resistance* 10, 295-303.
- Begum, G., Reddy, T.N., Kumar, K.P., Dhevendar, K., Singh, S., Amarnath, M., Misra, S., Rangari, V.K., Rana, R.K., 2016. *In situ* strategy to encapsulate antibiotics in a bioinspired CaCO<sub>3</sub> structure enabling pH-sensitive drug release Apt for therapeutic and imaging applications. *ACS Applied Materials & Interfaces* 8, 22056-22063.
- Bexfield, A., Bond, A.E., Roberts, E.C., Dudley, E., Nigam, Y., Thomas, S., Newton, R.P., Ratcliffe, N.A., 2008. The antibacterial activity against MRSA strains and other bacteria of a < 500Da fraction from maggot excretions/secretions of *Lucilia sericata* (Diptera: Calliphoridae). *Microbes and Infection* 10, 325-333.
- Bixon, M., Lifson, S., 1967. Potential functions and conformations in cycloalkanes. *Tetrahedron* 23, 769-784.
- Burygin, G., Khlebtsov, B., Shantrokha, A., Dykman, L., Bogatyrev, V., Khlebtsov, N., 2009. On the enhanced antibacterial activity of antibiotics mixed with gold nanoparticles. *Nanoscale Research Letters* 4, 794.
- Bussi, G., Donadio, D., Parrinello, M., 2007. Canonical sampling through velocity rescaling. *The Journal of Chemical Physics* 126, 014101.

Cakić, M., Nikolić, G., Ilić, L., Stanković, S., 2005. Synthesis and FTIR characterization of some dextran sulphates. *Chemical Industry and Chemical Engineering Quarterly* 11, 74-78.

Caram-Lelham, N., Hed, F., Sundelöf, L.O., 1997. Adsorption of charged amphiphiles to oppositely charged polysaccharides—a study of the influence of polysaccharide structure and hydrophobicity of the amphiphile molecule. *Biopolymers* 41, 765-772.

Cevher, E., Orhan, Z., Mülazımoğlu, L., Şensoy, D., Alper, M., Yıldız, A., Özsoy, Y., 2006. Characterization of biodegradable chitosan microspheres containing vancomycin and treatment of experimental osteomyelitis caused by methicillin-resistant *Staphylococcus aureus* with prepared microspheres. *International Journal of Pharmaceutics* 317, 127-135.

Chang, S., Sievert, D.M., Hageman, J.C., Boulton, M.L., Tenover, F.C., Downes, F.P., Shah, S., Rudrik, J.T., Pupp, G.R., Brown, W.J., 2003. Infection with vancomycin-resistant *Staphylococcus aureus* containing the vanA resistance gene. *New England Journal of Medicine* 348, 1342-1347.

Chen, C.-H., Lin, Y.-S., Wu, S.-J., Mi, F.-L., 2018. Multifunctional nanoparticles prepared from arginine-modified chitosan and thiolated fucoidan for oral delivery of hydrophobic and hydrophilic drugs. *Carbohydrate polymers* 193, 163-172.

Cheow, W.S., Chang, M.W., Hadinoto, K., 2011. The roles of lipid in anti-biofilm efficacy of lipid-polymer hybrid nanoparticles encapsulating antibiotics. *Colloids and Surfaces A: Physicochemical and Engineering Aspects* 389, 158-165.

Cheow, W.S., Hadinoto, K., 2012a. Green preparation of antibiotic nanoparticle complex as potential anti-biofilm therapeutics via self-assembly amphiphile-polyelectrolyte complexation with dextran sulfate. *Colloids and Surfaces B: Biointerfaces* 92, 55-63.

Cheow, W.S., Hadinoto, K., 2012b. Self-assembled amorphous drug-polyelectrolyte nanoparticle complex with enhanced dissolution rate and saturation solubility. *Journal of Colloid and Interface Science* 367, 518-526.

Cheow, W.S., Kiew, T.Y., Hadinoto, K., 2015. Amorphous nanodrugs prepared by complexation with polysaccharides: Carrageenan versus dextran sulfate. *Carbohydrate Polymers* 117, 549-558.

Cheow, W.S., Kiew, T.Y., Yang, Y., Hadinoto, K., 2014. Amorphization strategy affects the stability and supersaturation profile of amorphous drug nanoparticles. *Molecular Pharmaceutics* 11, 1611-1620.

Darden, T., York, D., Pedersen, L., 1993. Particle mesh Ewald: An  $N \cdot \log(N)$  method for Ewald sums in large systems. *The Journal of Chemical Physics* 98, 10089-10092.

Deurenberg, R., Vink, C., Kalenic, S., Friedrich, A., Bruggeman, C., Stobberingh, E., 2007. The molecular evolution of methicillin-resistant *Staphylococcus aureus*. *Clinical Microbiology and Infection* 13, 222-235.

Florence, A.T., Attwood, D., 1988. *Physicochemical Principles of Pharmacy*, 2nd ed. Chapman and Hall, New York, NY.

Garberoglio, G., 2012. OBGMX: A web-based generator of GROMACS topologies for molecular and periodic systems using the universal force field. *Journal of Computational Chemistry* 33, 2204-2208.

Ghosh, N., Chavada, R., Maley, M., van Hal, S., 2014. Impact of source of infection and vancomycin AUC<sub>0-24</sub>/MICBMD targets on treatment failure in patients with methicillin-resistant *Staphylococcus aureus* bacteraemia. *Clinical Microbiology and Infection* 20, O1098-O1105.

Gustafsen, C., Olsen, D., Vilstrup, J., Lund, S., Reinhardt, A., Wellner, N., Larsen, T., Andersen, C.B., Weyer, K., Li, J.-p., 2017. Heparan sulfate proteoglycans present PCSK9 to the LDL receptor. *Nature Communications* 8, 503.

Heo, R., You, D.G., Um, W., Choi, K.Y., Jeon, S., Park, J.-S., Choi, Y., Kwon, S., Kim, K., Kwon, I.C., 2017. Dextran sulfate nanoparticles as a theranostic nanomedicine for rheumatoid arthritis. *Biomaterials* 131, 15-26.

Honary, S., Ebrahimi, P., Hadianamrei, R., 2014. Optimization of particle size and encapsulation efficiency of vancomycin nanoparticles by response surface methodology. *Pharmaceutical Development and Technology* 19, 987-998.

Humphrey, W., Dalke, A., Schulten, K., 1996. VMD: visual molecular dynamics. *Journal of Molecular Graphics* 14, 33-38.

Ingram, P.R., Lye, D.C., Tambyah, P.A., Goh, W.P., Tam, V.H., Fisher, D.A., 2008. Risk factors for nephrotoxicity associated with continuous vancomycin infusion in outpatient parenteral antibiotic therapy. *Journal of Antimicrobial Chemotherapy* 62, 168-171.

Ionita, D., Bajenaru-Georgescu, D., Totea, G., Mazare, A., Schmuki, P., Demetrescu, I., 2017. Activity of vancomycin release from bioinspired coatings of hydroxyapatite or TiO<sub>2</sub> nanotubes. *International Journal of Pharmaceutics* 517, 296-302.

Jain, N., Jain, G.K., Javed, S., Iqbal, Z., Talegaonkar, S., Ahmad, F.J., Khar, R.K., 2008. Recent approaches for the treatment of periodontitis. *Drug Discovery Today* 13, 932-943.

Kiew, T.Y., Cheow, W.S., Hadinoto, K., 2015. Preserving the supersaturation generation capability of amorphous drug-polysaccharide nanoparticle complex after freeze drying. *International Journal of Pharmaceutics* 484, 115-123.

Kutscher, M., Cheow, W.S., Werner, V., Lorenz, U., Ohlsen, K., Meinel, L., Hadinoto, K., Germershaus, O., 2015. Influence of salt type and ionic strength on self-assembly of dextran sulfate-ciprofloxacin nanoplexes. *International Journal of Pharmaceutics* 486, 21-29.

Lazzarini, L., Lipsky, B.A., Mader, J.T., 2005. Antibiotic treatment of osteomyelitis: what have we learned from 30 years of clinical trials? *International Journal of Infectious Diseases* 9, 127-138.

Lewies, A., Wentzel, J.F., Jordaan, A., Bezuidenhout, C., Du Plessis, L.H., 2017. Interactions of the antimicrobial peptide nisin Z with conventional antibiotics and the use of nanostructured lipid carriers to enhance antimicrobial activity. *International Journal of Pharmaceutics* 526, 244-253.

Liu, J., Wang, Z., Li, F., Gao, J., Wang, L., Huang, G., 2015. Liposomes for systematic delivery of vancomycin hydrochloride to decrease nephrotoxicity: Characterization and evaluation. *Asian Journal of Pharmaceutical Sciences* 10, 212-222.

Lodise, T., Miller, C., Graves, J., Evans, A., Graffunder, E., Helmecke, M., Stellrecht, K., 2008. Predictors of high vancomycin MIC values among patients with methicillin-resistant *Staphylococcus aureus* bacteraemia. *Journal of Antimicrobial Chemotherapy* 62, 1138-1141.

Loll, P.J., Kaplan, J., Selinsky, B.S., Axelsen, P.H., 1999. Vancomycin binding to low-affinity ligands: Delineating a minimum set of interactions necessary for high-affinity binding. *Journal of Medicinal Chemistry* 42, 4714-4719.

Michael, Z., Ian, M., 2017. Recently approved antibacterials for MRSA and other gram-positive pathogens: the shock of the new. *International Journal of Antimicrobial Agents*.

Nguyen, M.-H., Tran, T.-T., Hadinoto, K., 2016. Controlling the burst release of amorphous drug-polysaccharide nanoparticle complex via crosslinking of the polysaccharide chains. *European Journal of Pharmaceutics and Biopharmaceutics* 104, 156-163.

Nguyen, M.H., Yu, H., Kiew, T.Y., Hadinoto, K., 2015. Cost-effective alternative to nano-encapsulation: Amorphous curcumin-chitosan nanoparticle complex exhibiting high payload and supersaturation generation. *European Journal of Pharmaceutics and Biopharmaceutics* 96, 1-10.

Nimesh, S., Kumar, R., Chandra, R., 2006. Novel polyallylamine-dextran sulfate-DNA nanoplexes: highly efficient non-viral vector for gene delivery. *International Journal of Pharmaceutics* 320, 143-149.

Niu, X., Zhang, Z., Zhong, Y., 2017. Hydrogel loaded with self-assembled dextran sulfate-doxorubicin complexes as a delivery system for chemotherapy. *Materials Science and Engineering: C* 77, 888-894.



O'Brien-Simpson, N.M., Pantarat, N., Attard, T.J., Walsh, K.A., Reynolds, E.C., 2016. A Rapid and quantitative flow cytometry method for the analysis of membrane disruptive antimicrobial activity. *PloS one* 11, e0151694.

Omolo, C.A., Kalhapure, R.S., Agrawal, N., Rambharose, S., Mocktar, C., Govender, T., 2018. Formulation and Molecular Dynamics Simulations of a Fusidic Acid Nanosuspension for Simultaneously Enhancing Solubility and Antibacterial Activity. *Molecular Pharmaceutics*.

Omolo, C.A., Kalhapure, R.S., Jadhav, M., Rambharose, S., Mocktar, C., Ndesendo, V.M., Govender, T., 2017. Pegylated oleic acid: A promising amphiphilic polymer for nano-antibiotic delivery. *European Journal of Pharmaceutics and Biopharmaceutics* 112, 96-108.

Ozbas, B., Kretsinger, J., Rajagopal, K., Schneider, J.P., Pochan, D.J., 2004. Salt-triggered peptide folding and consequent self-assembly into hydrogels with tunable modulus. *Macromolecules* 37, 7331-7337.

Parrinello, M., Rahman, A., 1981. Polymorphic transitions in single crystals: A new molecular dynamics method. *Journal of Applied Physics* 52, 7182-7190.

Ranjan, A., Pothayee, N., Seleem, M., Jain, N., Sriranganathan, N., Riffle, J., Kasimanickam, R., 2010. Drug delivery using novel nanoplexes against a Salmonella mouse infection model. *Journal of Nanoparticle Research* 12, 905-914.

Rappé, A.K., Casewit, C.J., Colwell, K., Goddard Iii, W., Skiff, W., 1992. UFF, a full periodic table force field for molecular mechanics and molecular dynamics simulations. *Journal of the American Chemical Society* 114, 10024-10035.

Rüger, M., Bensch, G., Tüngler, R., Reichl, U., 2012. A flow cytometric method for viability assessment of *Staphylococcus aureus* and *Burkholderia cepacia* in mixed culture. *Cytometry Part A* 81, 1055-1066.

Saidykhan, L., Bakar, M.Z.B.A., Rukayadi, Y., Kura, A.U., Latifah, S.Y., 2016. Development of nanoantibiotic delivery system using cockle shell-derived aragonite nanoparticles for treatment of osteomyelitis. *International journal of nanomedicine* 11, 661.

Seleem, M.N., Jain, N., Pothayee, N., Ranjan, A., Riffle, J., Sriranganathan, N., 2009. Targeting *Brucella melitensis* with polymeric nanoparticles containing streptomycin and doxycycline. *FEMS Microbiology Letters* 294, 24-31.

Shrestha, N.K., Scalera, N.M., Wilson, D.A., Procop, G.W., 2011. Rapid differentiation of methicillin-resistant and methicillin-susceptible *Staphylococcus aureus* by flow cytometry after brief antibiotic exposure. *Journal of Clinical Microbiology* 49, 2116-2120.

Sikwal, D.R., Kalhapure, R.S., Rambharose, S., Vepuri, S., Soliman, M., Mocktar, C., Govender, T., 2016. Polyelectrolyte complex of vancomycin as a nanoantibiotic: Preparation, in vitro and in silico studies. *Materials Science and Engineering: C* 63, 489-498.

Sonawane, S.J., Kalhapure, R.S., Jadhav, M., Rambharose, S., Mocktar, C., Govender, T., 2015. Transforming linoleic acid into a nanoemulsion for enhanced activity against methicillin susceptible and resistant *Staphylococcus aureus*. *RSC Advances* 5, 90482-90492.

Tiyaboonchai, W., Woiszwilllo, J., Middaugh, C.R., 2003. Formulation and characterization of DNA–polyethylenimine–dextran sulfate nanoparticles. *European Journal of Pharmaceutical Sciences* 19, 191-202.

Vo, C.L.-N., Park, C., Lee, B.-J., 2013. Current trends and future perspectives of solid dispersions containing poorly water-soluble drugs. *European Journal of Pharmaceutics and Biopharmaceutics* 85, 799-813.

Waltho, J.P., Williams, D.H., 2007. The natural design of vancomycin family antibiotics to bind their target peptides, *Ciba Foundation Symposium 158-Host-Guest Molecular Interactions: From Chemistry to Biology: Host-Guest Molecular Interactions: From Chemistry to Biology: Ciba Foundation Symposium 158*. Wiley Online Library, pp. 73-97.

Wijesiri, N., Ozkaya-Ahmadov, T., Wang, P., Zhang, J., Tang, H., Yu, X., Ayres, N., Zhang, P., 2017. Photodynamic inactivation of multidrug-resistant *Staphylococcus aureus* using hybrid photosensitizers based on mmphiphilic block copolymer-functionalized gold nanoparticles. *ACS Omega* 2, 5364-5369.

Xu, J., Xu, B., Shou, D., Xia, X., Hu, Y., 2015. Preparation and evaluation of vancomycin-loaded N-trimethyl chitosan nanoparticles. *Polymers* 7, 1850-1870.

Yang, Z., Liu, J., Gao, J., Chen, S., Huang, G., 2015. Chitosan coated vancomycin hydrochloride liposomes: characterizations and evaluation. *International journal of pharmaceutics* 495, 508-515.

Yousefpour, P., Atyabi, F., Farahani, E.V., Sakhtianchi, R., Dinarvand, R., 2011. Polyanionic carbohydrate doxorubicin–dextran nanocomplex as a delivery system for anticancer drugs: in vitro analysis and evaluations. *International journal of nanomedicine* 6, 1487.

Yousry, C., Fahmy, R.H., Essam, T., El-Laithy, H.M., Elkhesheh, S.A., 2016. Nanoparticles as tool for enhanced ophthalmic delivery of vancomycin: a multidistrict-based microbiological study, solid lipid nanoparticles formulation and evaluation. *Drug development and industrial pharmacy* 42, 1752-1762.

Yu, H., Hadinoto, K., 2017. Impacts of dextran sulfate's chain length on the characteristics of its self-assembled colloidal complex formed with amphiphilic small-molecule drug. *International journal of biological macromolecules* 103, 493-500.

Yu, H., Teo, J., Chew, J.W., Hadinoto, K., 2016. Dry powder inhaler formulation of high-payload antibiotic nanoparticle complex intended for bronchiectasis therapy: Spray drying versus spray freeze drying preparation. *International journal of pharmaceutics* 499, 38-46.

Zarif, M., Afidah, A., Abdullah, J., Shariza, A., 2012. Physicochemical characterization of vancomycin and its complexes with $\beta$ -cyclodextrin. *Biomedical Research* 23.

Zhang, Y., Huo, M., Zhou, J., Zou, A., Li, W., Yao, C., Xie, S., 2010. DDSolver: an add-in program for modeling and comparison of drug dissolution profiles. *The AAPS Journal* 12, 263-271.

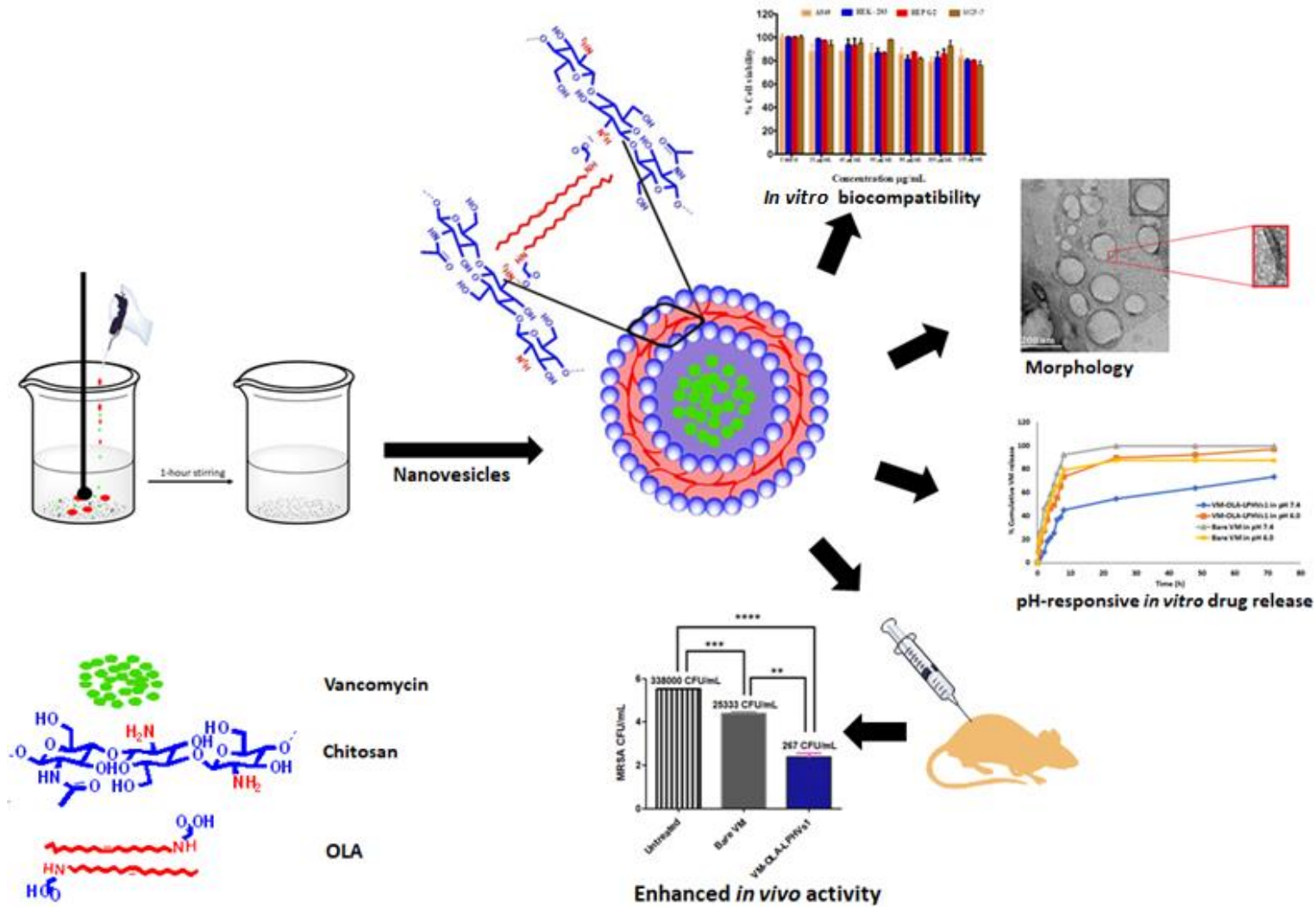
## CHAPTER THREE: EXPERIMENTAL PAPER TWO

### 3.1 Introduction

This chapter addresses **Aim 2** and **Objectives 1 – 6**. It is a first authored experimental article submitted and highlights the formulation and characterisation of chitosan-based pH-responsive lipid-polymer hybrid nanovesicles (VM-OLA-LPHVs) from the novel zwitterionic lipid (OLA). The nanovesicles was evaluated for *in vitro* toxicity, physicochemical properties, morphology, *in vitro* electrical conductivity, protein/DNA concentration quantification, membrane damage, time killing assay, membrane disruption, bacteria-killing percentage, biofilm eradication, *in vitro* and *in vivo* antibacterial properties.

The ethical approval is attached in Appendix II.

### 3.2 Graphical Abstract



### **3.3 Submitted Manuscript**

**Novel Chitosan-Based pH-responsive Lipid-Polymer Hybrid Nanovesicles (OLA-LPHVs) for Delivery of Vancomycin against Methicillin-Resistant *Staphylococcus aureus* Infections.**

**Daniel Hassan<sup>1</sup>, Calvin A. Omolo<sup>1, 2#</sup>, Victoria Oluwaseun Fasiku<sup>1</sup>, Chunderika Mocktar<sup>1</sup>, Thirumala Govender<sup>1#</sup>**

<sup>1</sup>Discipline of Pharmaceutical Sciences, College of Health Sciences, University of KwaZulu-Natal, Private Bag X54001, Durban, South Africa.

<sup>2</sup>United States International University-Africa, School of Pharmacy and Health Sciences, Department of Pharmaceutics, P. O. Box 14634-00800, Nairobi, Kenya.

Tel: +27 31 260 7357/8, Fax: +27 31 260 7792

#Corresponding authors.

Email address: govenderth@ukzn.ac.za; comolo@usiu.ac.ke

## Highlights

- A novel zwitterionic lipid (OLA) was synthesized and characterized to confirm its structure.
- The novel OLA was used to formulate a chitosan-based pH-responsive VM-loaded lipid-polymer hybrid nanovesicles (VM-OLA-LPHVs1).
- The biosafety of the OLA and VM-OLA-LPHVs1 was confirmed with four cell lines.
- There was a higher VM release from VM-OLA-LPHVs1 at pH 6.0 compared to pH 7.4.
- The VM-OLA-LPHVs1 showed an enhanced *in vitro* and *in vivo* antibacterial activity against MRSA compared to bare VM.

## Abbreviation

A-549	Adenocarcinoma human alveolar basal epithelial cells
BCA	Bicinchoninic acid
CHs	Chitosan
CDC	Centers for Disease Control and Prevention
CFU	<i>Colony-forming unit</i>
DLC	Drug loading capacity
DLS	Dynamic Light Scattering
DCM	Dichloromethane
DSC	Differential scanning calorimetry
DNA	Deoxyribonucleic acids
$D_H$	Hydrodynamic diameter
EE	Encapsulation efficiency
FT-IT	Fourier transform infrared
HEK-293	Human embryonic kidney cells
HepG-2	Human liver hepatocellular carcinoma cell
MICs	Minimum inhibitory concentrations
MCF-7	Liver hepatocellular carcinoma cell lines
MRSA	Methicillin-resistance <i>Staphylococcus aureus</i>
MTT	3-(4,5-dimethylthiazol-2-yl)-2,5-diphenyltetrazolium bromide
MHB	Mueller-Hinton Broth
MHA	Mueller-Hinton agar
MDT	Mean dissolution time
MHA	Mueller–Hinton agar
NaOH	Sodium hydroxide
NB	Nutrient Broth
OLM	Oleylamine
PBS	Phosphate buffer saline
pDNA	Plasmid deoxyribonucleic acid
PDI	Polydispersity index
PI	Propidium iodide
$R^2$	Correlation coefficient
RMSE	Root mean square error
siRNA	Small interfering ribonucleic acid
tBA	<i>Tert</i> -butyl acrylate
TIPs	Triisopropylsilane
TFA	Trifluoroacetic acid
TPP	Sodium tripolyphosphate
UVis-Spec	UV Spectrophotometer
VM	Vancomycin
$^1\text{H}$ NMR	Proton nuclear magnetic resonance
$^{13}\text{C}$ NMR	Carbon 13 nuclear magnetic resonance
$\zeta$	Zeta potential



## Abstract

The development of novel materials is necessary for adequate delivery of drugs to combat the Methicillin-resistant *Staphylococcus aureus* (MRSA) burden due to the limitations of conventional methods and challenges associated with antimicrobial resistance. Hence, this study aimed to synthesise a novel oleylamine based zwitterionic lipid (OLA) and explore its potential to formulate chitosan-based pH-responsive lipid-polymer hybrid nanovesicles (VM-OLA-LPHVs1) to deliver VM against MRSA. The OLA was synthesised, and the structure characterised by  $^1\text{H}$  NMR,  $^{13}\text{C}$  NMR, FT-IR and HR-MS. The preliminary biocompatibility of OLA and VM-OLA-LPHVs1 was evaluated on HEK-293, A-549, MCF-7 and HepG-2 cell lines using *in vitro* cytotoxicity assay. The VM-OLA-LPHVs1 were formulated by ionic gelation method and characterized in order to determine the hydrodynamic diameter ( $D_H$ ), morphology *in vitro* and *in vivo* antibacterial efficacy. The result of the *in vitro* cytotoxicity study revealed cell viability of above 75% in all cell lines when exposed to OLA and VM-OLA-LPHVs1, thus indicating their biosafety. The VM-OLA-LPHVs1 had a  $D_H$ , polydispersity index (PDI), and EE% of  $198.0 \pm 14.04\text{nm}$ ,  $0.137 \pm 0.02$ , and  $45.61 \pm 0.54\%$  respectively at physiological pH, with surface-charge ( $\zeta$ ) switching from negative at pH 7.4 to positive at pH 6.0. The VM release from the VM-OLA-LPHVs1 was faster at pH 6.0 compared to physiological pH, with 97% release after 72-hour. The VM-OLA-LPHVs1 had a lower minimum inhibitory concentration (MIC) value of  $0.59\mu\text{g/mL}$  at pH 6.0 compared to  $2.39\mu\text{g/mL}$  at pH 7.4, against MRSA with 52.9-fold antibacterial enhancement. The flow cytometry study revealed that VM-OLA-LPHVs1 had similar bactericidal efficacy on MRSA compared to bare VM, despite an 8-fold lower VM concentration in the nanovesicles. Additionally, fluorescence microscopy study showed the ability of the VM-OLA-LPHVs1 to eliminate biofilms. The electrical conductivity, and protein/DNA concentration, increased and decreased respectively, as compared to bare VM which indicated greater MRSA membrane damage. The *in vivo* studies in a BALB/c mouse-infected skin model treated with VM-OLA-LPHVs1 revealed 95-fold lower MRSA burden compared to the group treated with bare VM. These findings suggest that OLA can be used as an effective novel material for complexation with biodegradable polymer chitosan (CHs) to form pH-responsive VM-OLA-LPHVs1 nanovesicles which show greater potential for enhancement and improvement of treatment of bacterial infections.

**Keywords:** Antibacterial, Methicillin-resistant *Staphylococcus aureus* (MRSA), Lipid-Polymer Hybrid Nanovesicles, Vancomycin

## 1.0 Introduction

Infectious diseases caused by Methicillin-Resistant *Staphylococcus aureus* (MRSA) pose a serious global health challenge that affects more than two million people every year [179, 180], resulting in increased morbidity and mortality rates [181, 182]. The Centers for Disease Control and Prevention (CDC) reported that nearly 80,461 severe infections are caused by MRSA every year, leading to 11,285 deaths [183], and costing approximately \$34,657 to manage each person's case [184]. In Europe, MRSA infections have led to longer hospital stays and have caused 5,400 deaths at an estimated cost of \$700 million [21]. In Africa, by 2050, around 4,150,000 deaths are expected from antimicrobial resistance, with higher figures likely if proper measures are not taken by researchers and industries [185]. Therefore, proper and urgent measures are currently needed to develop a novel strategy to confront the emergence of antibiotic bacterial strains which are resistant to the existing conventional antibiotics [186].

Currently, antibiotics such as arylthiazoles [187], tetracycline, ofloxacin, penicillin [188], chloramphenicol [189] and linezolid used against MRSA are ineffective due to resistance thereby leaving vancomycin (VM) as one of the last-resort drugs [190-192] to use against MRSA [193-195]. Frequent misuse and the limitations of conventional dosage methods, such as inadequate concentration at the infection sites [122, 196]; rapid decrease of plasma concentration levels [197]; increased frequency of administration; higher dose requirements leading to side effects [123-125]; and prolonged treatment regimens [126] are factors that have significantly contributed to antibiotic resistance to these drugs. Thus, calls for immediate and better strategies for protecting and potentiating current antibiotics are being highlighted in the literature.

Novel strategies using nano-delivery systems are being explored to tackle the antimicrobial resistance problem and have shown the potential to address the limitations of conventional dosage forms such as increased localised drug concentration at infection sites; decreased exposure of drugs to healthy sites; and protection of the drug from premature enzymatic degradation [43]. The use of different nanosystems such as micelles [198], solid lipid nanoparticles [199], liposomes, nanoemulsions, and nanovesicles [200-202] has been reported for antibiotic delivery. Specifically, nanovesicles are showing the potential to efficiently deliver drugs and enhance their biological activity [203]. Such lipid-based nanovesicles have been formulated from phospholipids to form liposomes and successfully encapsulated both hydrophobic and hydrophilic drugs [204-206]. In the late 1990s, amphiphilic block polymers were found to self-assemble into vesicular structures that were referred to as polymersomes

[206-208]. The discovery of polymersomes greatly impacted the field of drug delivery due to their toughness, permeability and surface functionality [209, 210]. This has helped to overcome limitations such as instabilities and osmotic shocks associated with liposomes [211, 212]. The formulation of vesicles that can encompass the positive attributes of both polymersomes and liposomes, known as the lipid-polymer hybrid system, has been proposed [213]. The polymersomes are reported to demonstrate better drug release properties [214, 215]. The lipid increases drug loading efficiency and membrane permeability [216, 217].

One of the main objectives of designing such lipid-polymer hybrid vesicles (LPHVs) is the ability of the bio-functionalisation of their membrane properties to introduce targeted drug delivery. Stimuli-responsiveness of nanosystems can potentiate targeting by responding to the unique conditions at disease sites and increasing drug release and binding activity. Depending on the polymer and lipid chains and functional groups, various stimuli-responsive systems such as pH-responsiveness have been reported [218] for targeted drug delivery for various diseases such as chronic obstructive pulmonary disease (COPD) [219], metastatic breast cancer therapy [88], and memory disorders [220]. However, there is limited research involving the delivery of antibiotics. Thus, there is a need to identify new materials to formulate pH-responsive LPHVs in the delivery of drugs for the treatment of bacterial infection.

In this study, we propose a novel drug delivery system derived from Chitosan (CHs) and zwitterionic pH-responsive lipid (OLA) to formulate chitosan-based lipid-polymer hybrid nanovesicles (VM-OLA-LPHVs) for the efficient delivery of VM and the targeting of bacterial infection. CHs is a natural polysaccharide biopolymer [221, 222] which is widely employed in pharmaceutical research [223] due to its biocompatibility; biodegradability; antimicrobial activity [224-226]; mucoadhesive properties [221, 227]; and low immunogenicity [228, 229]. Oleylamine (OLM), a long-chain primary alkylamine, is reported in drug delivery due to enhanced antimicrobial activity [230-232]. However, due to its cationic properties, OLM shows dose-dependent toxicity [233, 234]. Modifying the lipid could result in forming a zwitterionic pH-responsive biomaterial with improved biosafety [235]. The application of zwitterionic lipids has been previously reported [235], with lipids such as phosphatidylethanolamine [236] and glycerophospholipids [237] indicating feasibility in drug delivery. Based on the literature survey, there are no reports of the application of this novel oleylamine based zwitterionic lipid (OLA) in the formulation of OLA-LPHVs for delivery of any class of drug [238].

Therefore, this study aimed to synthesise a novel oleylamine based zwitterionic lipid (OLA) and formulate pH-responsive VM-OLA-LPHVs nanovesicles by polyelectrolyte complexing for the delivery of VM [239, 240]. This complex will result in a polyelectrolyte vesicles and we envisage the free hydroxyl groups and the amine group of CHs to be at the surface, while a carboxylic group of OLA will be electrostatically bonded to the VM [88, 241] and CHs. To the best of our knowledge, there is no report of the synthesis of this novel oleylamine based zwitterionic lipid and its formulation into a chitosan-based pH-responsive VM-OLA-LPHVs for the delivery of VM or any class of drug. This strategy could contribute to the alleviation of the current global antimicrobial resistance crisis and widen the pool of available novel pH-responsive platforms for the delivery of antibiotics for the treatment of different diseases. The data resulting from the synthesis of the lipid, and the formulation of chitosan-based pH-responsive LPHVs optimisation, *in vitro*, *in vivo* and in molecular antimicrobial studies, are herein reported.

## **2.0 Materials and methods**

### **2.1 Materials**

Oleylamine (OLM); *tert*-butyl acrylate; dichloromethane (DCM); trifluoroacetic acid (TFA); triisopropylsilane (TIPs) silica gel; chitosan (CHs) (low mol. wt; 75-85% deacetylated; viscosity 200-300 cp) with an average molecular weight of 250 kDa; sodium tripolyphosphate (TPP); and sodium hydroxide (NaOH) were purchased from Sigma-Aldrich (USA). Vancomycin (VM) and 3-(4,5-dimethylthiazol-2-yl)-2,5-diphenyltetrazolium bromide (MTT) were purchased from Sinobright Import and Export Co., Ltd. (China), and Merck Chemicals (Germany), respectively. All other chemicals and solvents used were of analytical grade. NB, MHB and MHA were obtained from Biolab (South Africa). Propidium iodide and Syto9 dyes were purchased from Thermofisher (USA). The bacterial culture used was Methicillin-resistant *Staphylococcus aureus* (MRSA) (*S. aureus* ATCC 700669). Bacteria deoxyribonucleic acid (DNA) and bicinchoninic acid (BCA) kits were purchased from Zymo Research California, (USA) and Wako Chemicals, Virginia (USA), respectively. Sheep blood was obtained from Polychem Handelsges, South Africa. Purified water used during the study was produced in the laboratory with a Milli-Q water purification system (Millipore corp., USA).

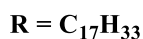
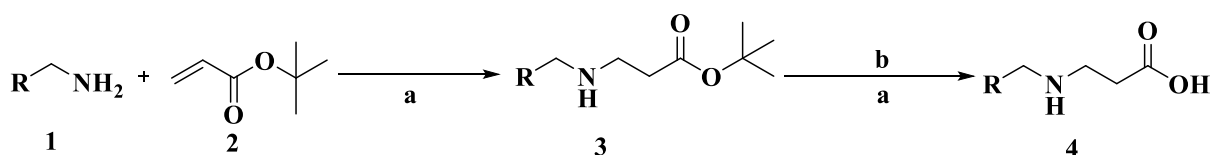
### **2.2 Instrumentation (FT-IR, <sup>1</sup>H NMR, <sup>13</sup>C NMR and HR-MS spectra)**

FT-IR spectra of all the major components involved in the synthesis of the compound (OLA) and structural changes of the all components were recorded on a Bruker Alpha-p spectrometer with a diamond ATR (Germany). The spectrum was recorded within the wavelength of 500-

3500  $\text{cm}^{-1}$  at a mean of 16 scans and resolution of 4  $\text{cm}^{-1}$ .  $^1\text{H}$  NMR and  $^{13}\text{C}$  NMR measurements were performed on a Bruker 400 Ultra shield™ (United Kingdom) NMR spectrometer. Finally, high-resolution mass spectrometry (HR-MS) was performed on a Bruker Micro-TOF QII mass spectrometer (Bruker Daltonics, Bremen, Germany) fitted with an electrospray ionisation source and coupled to an Agilent 1100 series high-pressure liquid chromatography (Agilent Technologies, Japan).

### 2.3 Synthesis and characterisation of the pH-responsive oleylamine based zwitterionic lipid (OLA).

The lipid was synthesised as per **Scheme 1**. The synthesis and characterisation of the lipid are described in **Supplementary Materials 1**.



**Scheme 1.** a). Dichloromethane (DCM), stirring at room temperature 24-hours, b). **Compound 3** dissolved DCM with the addition of trifluoroacetic acid/triisopropylsilane (TFA/TIPs) under constant stirring for 8-hours at room temperature.

### 2.4 *In vitro* preliminary biocompatibility assay

The biocompatibility of OLA and VM-OLA-LPHVs1 was evaluated using MTT assay as described in previously reported methods [242, 243] on four different cell lines. These included human embryonic kidney cells, liver hepatocellular carcinoma cell lines, adenocarcinoma human alveolar basal epithelial cells, and human liver hepatocellular carcinoma cells (HEK-293, MCF-7, A-549, and HepG-2 respectively). Briefly, the cell lines of  $5.0 \times 10^3$  /mL were grown exponentially for 24-hours at 37°C in a humidified atmosphere of 5% carbon dioxide ( $\text{CO}_2$ ), trypsinised when confluent, and seeded into 96-well plates. The samples OLA and VM-OLA-LPHVs1 were prepared, respectively, by diluting with sterilised deionised water. A broad range of concentrations from 20, 40, 60, 80, 100 and 120  $\mu\text{g}/\text{mL}$  was obtained [242]. All the cell lines were treated with 100  $\mu\text{L}$  of these various concentrations and the control group was exposed to the culture media only. All groups were incubated for 48-hours and the solutions (treatments and media respectively) were decanted and replaced with 100  $\mu\text{L}$  of fresh culture medium and MTT solution (5mg/mL in PBS). After 4-hours of incubation, both the culture medium and MTT assay solutions were immediately removed. This was followed by the

solubilisation of the MTT formazan by adding 100  $\mu$ L of dimethyl sulfoxide. The optical density was measured at a wavelength of 540 nm using a microplate spectrophotometer (Spectrostar Nano, Germany). All experiments were repeated six times and the cell viability percentage calculated using equation 1 below:

$$\text{Cell viability \%} = \left( \frac{\text{A540 nm treated cells}}{\text{A540 nm untreated cells}} \right) \times 100 \dots \dots \dots \text{Equation 1}$$

## 2.5 Formulation of the pH-responsive VM-OLA-LPHVs

The VM-OLA-LPHVs were prepared using a slightly modified version of an ionic complexation technique [244]. TPP was employed to ionically complex CHs and the novel zwitterionic pH-responsive lipid to form blank formulation LPHVs and the VM-loaded LPHVs (VM-OLA-LPHVs). Preliminary studies with different ratios of the excipients and the drug were performed before arriving at an optimal formulation. The optimal blank formulation contained CHs: TPP: OLA in a ratio of 5:1:0.5 (w/w), while for the VM-loaded formulation 1mg/mL of VM was added. Briefly, CHs (0.1% w/v) was dissolved in acetic acid (1% v/v) and the pH was adjusted to 5.5 using 1 M NaOH [245]. The mixture of TPP, OLA and VM (for drug loading) was then dropwisely added to the solution of CHs in acetic acid under stirring, and the process of complexation was allowed to occur for one-hour under constant magnetic stirring at 500rpm.

## 2.6 Characterisation of the novel zwitterionic pH-responsive VM-OLA-LPHVs

### 2.6.1 Hydrodynamic diameter size ( $D_H$ ), polydispersity index (PDI), zeta potential ( $\zeta$ ) and morphology

The hydrodynamic diameter size ( $D_H$ ), PDI and  $\zeta$  of the novel VM-OLA-LPHVs were determined by DLS using a Zetasizer Nano ZS90 (Malvern Instruments Ltd., UK) [246]. The surface morphology of the VM-OLA-LPHVs was examined using a High-resolution Transmission Electron Microscope, JEOL, HR-TEM-2100 (Japan), in a liquid nitrogen atmosphere and an accelerated voltage of 200kV. Briefly, to acquire HR-TEM images, a drop of appropriately 10 $\mu$ L of VM-OLA-LPHVs solution was placed on the 3mM coated carbon grid (300 mesh) and the excess removed using clean filter paper. The grids were allowed to dry for about 5-minutes, followed by negative staining with 2% uranyl acetate (UA) solution [247].

### 2.6.2 Entrapment efficiency (EE%) and drug loading capacity (DLC%)

The prepared VM-OLA-LPHVs formulation was further characterised for entrapment efficiency (EE%) and drug loading capacity (DLC%) using an ultrafiltration method [248]. The VM-OLA-LPHVs formulation of 3mL was loaded in Amicon® Ultra-4 centrifugal filter tubes

(Millipore Corp., USA) with 10kDa pore size and centrifuged at 3000rpm (25°C) for 30-minutes. The amount of untrapped VM in the filtrate was determined spectrophotometrically at 280nm using a UV Spectrophotometer Shimadzu UV 1601 (Japan). The regression equation of  $Y = 0.003X + 0.0031$ , with a linear regression coefficient ( $R^2$ ) of 0.9998, was used to obtain the unknown drug concentration values. The experiment was conducted thrice; the supernatant containing the untrapped VM was calculated; and the EE% and DLC% were calculated using the following equations 2 and 3 respectively, as previously reported [249].

$$EE\% = \left( \frac{\text{VM weight in the VM - OLA - LPHVs}}{\text{VM added during VM - OLA - LPHVs preparation}} \right) \times 100 \dots \dots \dots \text{Equation 2}$$

$$DLC\% = \left( \frac{\text{Complete weight of VM in VM - OLA - LPHVs}}{\text{Complete weight of VM - OLA - LPHVs}} \right) \times 100 \dots \dots \dots \text{Equation 3}$$

### 2.6.3 Differential scanning calorimetry (DSC)

Differential scanning calorimetry (DSC) Shimadzu DSC-60, (Japan) was used to determine the thermal profile of the bare VM, OLA, CHs, the physical combination (bare VM, OLA and CHs), and the lyophilised drug loaded LPHVs (VM-OLA-LPHVs). Briefly, approximately 2mg of each sample was placed in an aluminium pan and sealed, followed by heating to 300 °C at a constant rate of 10°C/minute under a constant nitrogen flow of 20mL/minute using an empty pan as a reference [250]. All samples were allowed to equilibrate at 25°C in a DSC chamber and were then exposed to a temperature run up of 25-300°C at a heating rate of 10°C/minute under a nitrogen atmosphere.

### 2.6.4 *In vitro* drug release of the VM-OLA-LPHVs

The *in vitro* drug release study was employed to provide the release profile mechanism of the encapsulated VM from the VM-OLA-LPHVs. Drug release of VM was performed using the diffusion dialysis bag method, as in formerly reported methods [251, 252]. Two mL of the bare VM, the corresponding blank formulation (OLA-LPHVs) and drug-loaded formulation (VM-OLA-LPHVs) were loaded into dialysis bags with a porosity size of 8,000-14,400Da. The dialysis bag was placed in a 40mL PBS (pH 6.0 and pH 7.4) receiver compartment at 37°C in a shaking incubator at 100rpm. During sampling, exactly 3mL was drawn at time intervals of 0.5, 1, 2, 3, 4, 5, 6, 7, 8, 24, 48 and 72-hours from the receiver solution and replaced with an equal amount of fresh PBS to keep a constant volume of the compartment. The amount of VM released from the dialysis bags in the receiver compartment was measured

spectrophotometrically using Shimadzu UV 1601 (Japan), at the VM wavelength of 280nm with a regression equation  $Y = 0.003X + 0.0031$  and a linear regression coefficient ( $R^2$ ) using OLA-LPHVs as the reference. During the study, experiments were done in triplicate, with the release fraction of VM from VM-OLA-LPHVs calculated using the following equation 4:

$$\text{Drug cumulative release \%} = \left( \frac{Q_t}{Q_v} \right) \times 100\% \dots \dots \dots \text{Equation 4}$$

where  $Q_t$  is the quantity of VM released from the VM-OLA-LPHVs at time  $t$ , and  $Q_v$  the quantity of VM previously-loaded in the VM-OLA-LPHVs.

## 2.7 Stability studies

The physical stability of drug-loaded-LPHVs was investigated by keeping the VM-OLA-LPHVs in 4°C and 25°C environments for 90 days, and the physicochemical stability (size, PDI,  $\zeta$ ) and EE% were evaluated and measured at the end of 30, 60 and 90 days. These results were further analysed using one-way ANOVA.

## 2.8 Bacterial characterisation of the VM-OLA-LPHVs

### 2.8.1 Determination of the minimum inhibitory concentration (MIC)

The *in vitro* antibacterial activity study was carried out in order to determine the MIC. This was done using the broth microdilution method, as previously described [253, 254]. Briefly, the bacteria culture was grown in MBH, with MHB-suitable dilutions being made to achieve colony forming units per mL (CFU/mL) of  $5 \times 10^5$ . The tested samples (bare VM, CHs, OLA, OLA-LPHVs and VM-OLA-LPHVs) were serially diluted in the MHB broth and then incubated with bacterial cultures containing  $5 \times 10^5$  colony-forming units per mL (CFU/mL) for 24-hours in a shaking incubator at 37°C and 100 rpm. Afterwards, 10 $\mu$ L of the serially diluted solutions was spotted on Mueller–Hinton Agar (MHA) plates and incubated for another 24-hours. The spot with no visible bacterial growth was regarded as the MIC for all tested samples.

### 2.8.2 Time-killing analysis (plate colony count) against MRSA

The time-killing assay of the VM-OLA-LPHVs was performed using the plate colony counting method, as a previously reported method [15]. The MRSA was placed in a shaking incubator and cultured for 48-hours at 37°C in nutrient broth (NB), followed by diluting the bacteria in sterile PBS to concentrations of  $10^5$ - $10^6$  CFU/mL [25]. Subsequently, the prepared bare VM and VM-OLA-LPHVs were added to the PBS containing MRSA at a concentration of  $5 \times \text{MIC}$ . The PBS containing the same concentration bacteria ( $10^5$ - $10^6$  CFU/mL) was employed as a control. The samples were shaken at 37°C. Thereafter, periodically, 0.1mL of each suspension





### **2.9.3 MRSA cell viability using flow cytometry**

Flow cytometry was employed to determine and separate the viable and non-viable bacteria after exposure to antibiotics [256]. The *in vitro* bacterial cell viability assay of MRSA after exposure to VM and VM-OLA-LPHVs at their respective MIC was studied using a previously reported flow cytometric method [158-160]. Nutrient Broth was used to grow the pure culture of MRSA overnight at 37°C in a shaking incubator (Labcon, USA) at 100rpm. Dilutions were made to achieve final bacterial concentration similar to the employed concentration in the *in vitro* antibacterial activity studies. Subsequently, 15µL of the bacterial suspension was added to a 96-well plate containing 135µL of bare VM (31.6µg/mL) and VM-OLA-LPHVs (2.39µg/mL) and then incubated at 37°C in a shaking incubator at 100rpm for 8-hours. The untreated MRSA cells were used as a negative control [161]. The bare VM and VM-OLA-LPHVs broths (50µL) were added to the flow cytometry tubes, each containing 350µL of the sheath fluid, and vortexed for 5-minutes. [161, 162]. The mixture was incubated again for 30 minutes with 5µL of the non-cell permeate dye Propidium iodide (PI) and the Syto9. The PI fluorescence was excited by a 455nm laser and collected through a 636nm bandpass filter, while the Syto9 excitation laser was set at 485nm laser and collected through a 498nm bandpass filter [158-160]. The BD FACSCANTO II (Becton Dickinson, CA, USA) instrument used to perform this experiment was set at a sheath fluid flow rate of 16mL/minute and a sample flow rate of 0.1mL/minute and the data was collected using a flow cytometer (BD FACSDIVA V8.0.1 software [USA]). The voltage settings used for the fluorescence-activated cell sorting (FACS) analysis were: 731 (forward scatter [FSC]); 538 (side scatter [SSC]); 451 (Syto9); and 444 for PI. The bacteria were at first gated using forward scatter. Afterwards, the cells were then gated with at least 10,000 cells being collected (n = 3). Then the position of the 'live' and 'dead' cells gates was determined. To avoid background signals from the particles smaller than the bacteria, the detection threshold was set to 1,000 in the SSC analysis [257]. The data captured from the flow machine (flow cytometer) was analysed using Kaluza-1.5.20 (Beckman Coulter USA) flow cytometer software [159, 258].

### **2.9.4 Reduction of MRSA biofilm by VM-OLA-LPHVs using fluorescence microscopy**

The eradication of MRSA biofilms by VM-OLA-LPHVs was determined by fluorescence microscopy [259]. Briefly, coverslips were placed at the bottom of a 6-well plate. This was followed by the addition of 2mL of MRSA ( $1.5 \times 10^8$  CFU/mL) suspensions in NB and incubated for 4-days at 37°C to form a fully mature biofilm. Before treatment, the media was sucked out of the wells with a sterilised Pasteur pipette, and the wells were washed 4-times to

remove the non-adhered bacteria. Exactly 1mL of bare VM solution and the VM-OLA-LPHVs formulation containing 125µg/mL of VM were added to the wells and incubated for an additional 12-hours at 37°C. The wells were then washed with PBS to remove the treatments and the non-adhered MRSA cells. While still in the wells, the coverslips were stained with a solution of Syto9 and Propidium iodide (PI) containing 30µL of each in 1mL of sterilised distilled water for 30-minutes in total darkness. The 6-wells plates were further washed to remove excess dyes, then inverted on a microscope glass slide and the coverslips were carefully glued at the edges on the glass slides. The elimination of formed biofilm by bare VM and VM-OLA-LPHVs were viewed on the Fluorescence microscope (Nikon Eclipse 80i FM Japan). Microscopic observations were performed in quadruplicate in an independent experiment.

### 2.10 Intradermal *in vivo* antibacterial activity in BALB/c mice

The *in vivo* antibacterial activity of the VM-OLA-LPHVs was evaluated against MRSA skin infection model mice. The BALB/c mice were obtained following the protocol approved by the University of KwaZulu-Natal's (UKZN) Animal Research Ethics Committee (Approval number: AREC/104/015PD) [235, 260]. The humane welfare/endpoint and the use of the animals were according to the protocol of the AREC of UKZN and the South African National Standard SANS 10386:2008. Male BALB/c mice weighing approximately 18-20g were collected from the Biomedical Research Unit (BRU) of UKZN. A day before the experiment, back hair of the mice was shaved and the exposed skin disinfected using 70% ethanol. The male BALB/c mice were separated into treatment, positive and negative control groups, with four mice in each group. On the day of the experiment, 50µL of MRSA ( $1.5 \times 10^8$ CFU/mL) in saline was injected intradermally into the mice. Approximately 30-minutes after infecting with the bacteria, 50µL of VM-OLA-LPHVs and free VM were injected into the mice in the various groups *via* the same spot. Afterwards, the mice were kept under observation for 48-hours in 12-hours of light and dark conditions at 19-23°C and  $55 \pm 10\%$  relative humidity, with adequate ventilation. Immediately after the 48-hours, the mice were euthanised with halothane, and the infected areas of the mice skin were harvested and homogenized in 5mL PBS (pH 7.4). Finally, the homogenised tissues were serially diluted in PBS (pH 7.4), 50µL was spotted on nutrient agar plates and incubated at 37°C for 24-hours. The colony-forming units (CFU/mL) were counted and calculated using equation 5.

$$\frac{\text{CFU}}{\text{mL}} = \frac{\text{Number of colonies} \times \text{dilution factor}}{\text{Volume of a culture plate}} \dots \dots \dots \text{Equation 6}$$

## 2.11 Statistical analysis

All experiments were performed in triplicate and results summarised as mean values of the standard deviation. Data obtained from  $D_H$ , PDI,  $\zeta$ , EE%, and *in vitro* drug release were subjected to one-way ANOVA with a level of significance kept at  $P$  value > 0.05.

## 3.0 Results and discussion

### 3.1 Synthesis and characterisation

The oleylamine based zwitterionic lipid (OLA) was synthesised in two steps as per **Scheme 1**. The first step involved Michael's addition reaction, as described in **Scheme 1**. **Compound 3** was synthesised through the addition of *tert*-butyl acrylic acid (**Compound 2**) to **Compound 1** and the spectra was confirmed by  $^1\text{H}$  NMR,  $^{13}\text{C}$  NMR and HR-MS. The appearance of a strong multiplet at  $\delta$  1.37 ppm integrating for 18 protons in  $^1\text{H}$  NMR represents isobutyl protons, and the appearance of carbon peaks at  $\delta$  28, 35, 80 and 172 in  $^{13}\text{C}$  NMR, representing,  $-\text{CH}_2\text{C}=\text{O}-$ ,  $\text{C}(\text{CH}_3)_3-\text{COO}-$  and  $\text{C}=\text{O}$ , confirms the formation of **Compound 3**. The second step involved the cleaving of the *tert*butyl protection on the carboxylic group. TFA/TIPs were added to **Compound 3** to obtain **Compound 4**. The tertiary butyl esters of **Compound 3** were cleaved to form OLA, using TFA and TIIPs as scavengers to avoid any possible side reactions. The product was confirmed by the appearance of aliphatic peaks at  $\delta$  0.808 (multiplet),  $\delta$  1.18 (multiplet) and  $\delta$  1.53 (multiplet) and the disappearance of **isobutyl** peaks at 1.4ppm on  $^1\text{H}$  NMR and at 28ppm in  $^{13}\text{C}$  NMR and HR-MS.

### 3.2 *In vitro* biocompatibility study (cytotoxicity)

Non-toxicity is an essential prerequisite for any novel material used in pharmaceutical and biomedical applications [261]. The cytotoxicity associated with the OLA and VM-OLA-LPHVs1 was determined using a 3-(4,5-Dimethylthiazol-2-yl)-2,5-diphenyltetrazolium bromide (MTT) cell viability assay. This study was performed on HEK-293, MCF-7, A-549 and Hep-G2 and the results are presented in **Figure 1**. The results showed that OLA maintained over 75% cell viability. According to the results, the percentage cell viability range obtained for the individual cell lines was 80.61- 96.03% for HEK-293; 77.62 - 86.74% for A-549; 80.43 - 85.60% for HEP-G2; and 75.47-83.56% for MCF-7 across all concentrations, as shown in **Figure 1A**. The Two-way ANOVA analysis demonstrated that the OLA and VM-OLA-LPHVs1 groups did not differ significantly ( $P>0.5$ ). Furthermore, these revealed that there is no significant cytotoxicity effect on all the cell lines; thus, indicating it to be safe for biomedical application in the nano-drug delivery system.

The MTT assay results in **Figure 1B** indicated a high percentage of cell viability in all the cell lines exposed to VM-OLA-LPHVs1. The cell viabilities were from 78.60 to 87.85% for A-549 cells; 79.85 to 98.20% for HEK-293; 79.85 to 96.98 % for HEP-G2; 75.89 to 97.95% for MCF-7. The results indicated the non-cytotoxic nature of the VM-OLA-LPHVs1, as shown in a cell viability of more than 75% of the mammalian cells. This percentage of viability demonstrated by OLA and VM-OLA-LPHVs1 was above the minimum levels required for biocompatibility for synthesised biomaterial material [262-264]. Conclusively, the drug-loaded formulation showed no significant decrease in the number of viable cells, indicating suitability for biomedical applications.

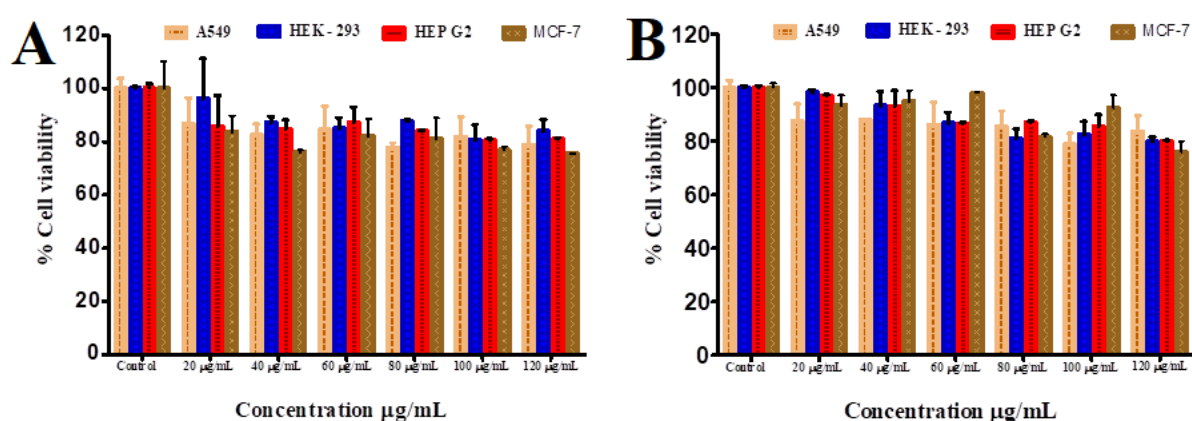


**Figure 1:** A) Percentage cell viability of different concentrations of OLA on A-549, HEK-293, Hep-G2 and MCF-7 cell lines; B) VM-OLA-LPHVs1 on A-549, HEK-293, Hep-G2 and MCF-7 cell lines. All results are presented as mean  $\pm$  SD (n = 6).

### 3.3 Preparation, characterisation of VM-OLA-LPHVs

The VM-OLA-LPHVs1 were formulated by a slightly modified ionic complexation method, as previously reported [265]. Preliminary studies were performed to obtain an optimal formulation (**Supplementary Material Table S1 and Figure S9**). The optimum formulation has  $D_H$ , PDI and  $\zeta$ , of  $198.0 \pm 14.04$ nm,  $0.137 \pm 0.02$  and  $-6.95 \pm 6.50$ mV, respectively, at pH 7.4; while at pH 6.0,  $D_H$ , PDI and  $\zeta$  were  $207.0 \pm 6.69$ nm,  $0.182 \pm 0.03$  and  $+13.3 \pm 1.75$ mv respectively, as shown in (**Supplementary Material Table S2**). In addition, the surface-charge switched from negative pH 7.4 (at the physiological pH 7.4) to positive pH 6.0 (at acidic pH 6.0). The negative  $\zeta$  observed in physiological pH 7.4 could be due to the free hydroxyl groups on CHs, and the deprotonation of carboxylic acid group (COOH) in OLA, which might bond electrostatically with the amine group of CHs, thereby neutralising its cationic effect [266]. The positive charge of the VM-OLA-LPHVs1 at acidic pH could be advantageous for adhesion

to the negatively charged biological membranes of bacteria. Furthermore, OLA consists of a secondary amine which protonates in acidic media; this might have contributed to the positive charge of the system in the acidic medium [267-270]. The results suggest that the VM-OLA-LPHVs could be successfully and effectively employed to deliver drugs to acidic infection sites. The EE% and DLC% of the optimised formulation were  $44.62 \pm 0.34\%$  and  $18.92 \pm 2.34\%$  w/w, respectively. This encapsulation was comparable to other VM-loaded nanovesicles [271-273]. The morphology of the VM-OLA-LPHVs1 was further observed with TEM and the image obtained was spherically shaped, and discrete indicating vesicle formation with a similar to that size obtained using the DLS techniques (**Figure 2**). DSC studies showed that the lyophilised VM-OLA-LPHVs formulation showed the disappearance of the VM thermal peak, which confirms the successful encapsulation of VM. On the other hand, the physical mixture of the excipients and the VM did not reveal the disappearance of the VM thermal peak (**Figure 3A**).

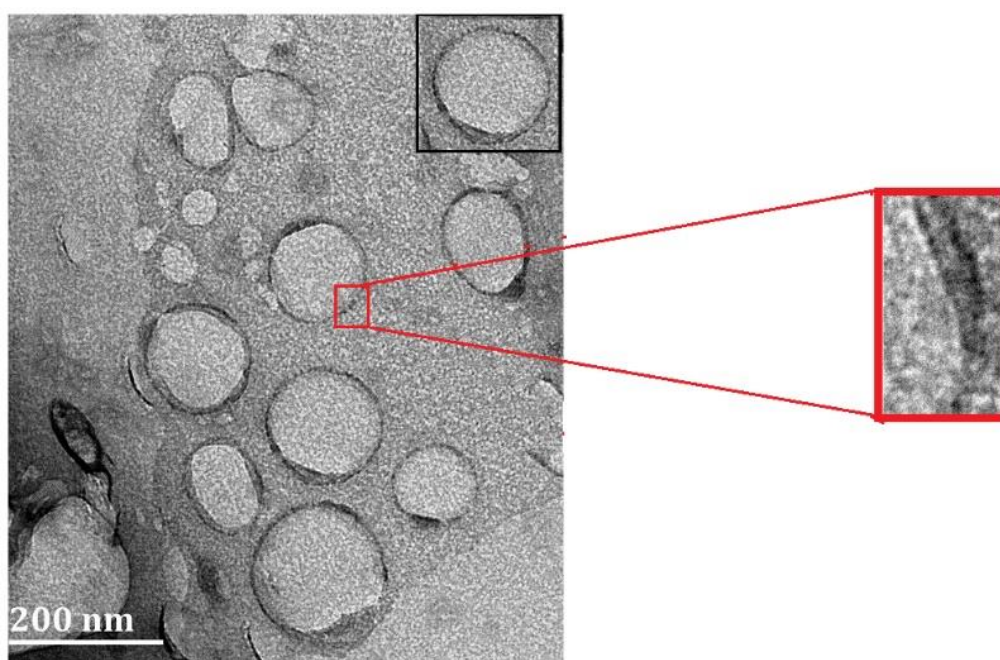


**Figure 2:** TEM images of VM-loaded (VM-OLA-LPHVs1)

### 3.4 *In vitro* drug release behaviour

Having considered the physicochemical studies performed previously, VM-OLA-LPHVs1 was used for *in vitro* drug release. The cumulative amounts of VM released from the VM-OLA-LPHVs1 at pH 6.0 and 7.4 are shown in **Figure 3B**. The cumulative amount of VM released from the VM-OLA-LPHVs1 nanovesicles occurred faster at pH 6.0, compared to pH 7.4 with  $12.61 \pm 3.55\%$  and  $4.33 \pm 1.40\%$ , respectively, after the initial 30-minutes. The VM release

from VM-OLA-LPHVs1 at the end of 8, 24, 48 and 72-hours at pH 6.0 was  $73.42 \pm 0.12\%$ ,  $89.45 \pm 0.21\%$ ,  $92.12 \pm 1.10\%$  and  $97.12 \pm 0.11\%$ , respectively; while at pH 7.4, it was  $45.11 \pm 0.05\%$ ,  $54.41 \pm 0.12\%$ ,  $63.80 \pm 0.01\%$  and  $73.22 \pm 0.02\%$ , respectively. As is clearly shown in **Figure 3B**, approximately 97% of the overall dose of VM was released in 72-hours, indicating an initial burst followed by the sustained release [274]. The initial burst release might be attributed to the diffusion of VM molecules that are localised at the surface of the VM-OLA-LPHVs1 [272, 275, 276]; while the increased drug release at pH 6.0 could be due to the pH-responsiveness of the VM-OLA-LPHVs1 *via* the protonation of nitrogen atoms in the amine group of OLA and CHs. Thus, at acidic pH there is a repulsion of the electrostatically bonded functional groups of the lipid and CHs, resulting in/from the disturbance and breakdown of the system. It is also possible that at acidic pH there is increased hydrophilicity of the formulation due to the protonation of the amines, promoting faster drug release. This study indicates that VM releases from VM-OLA-LPHVs1 was pH dependent.

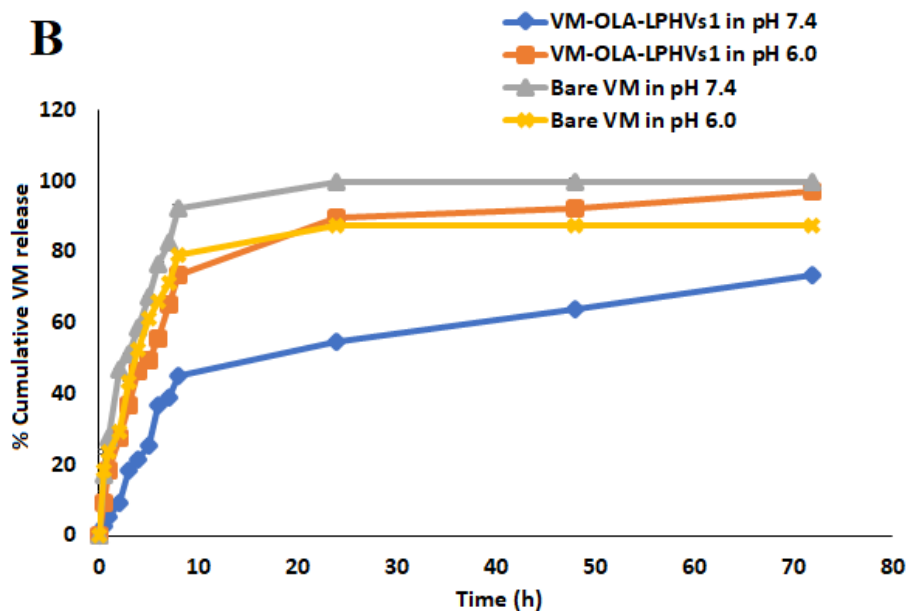
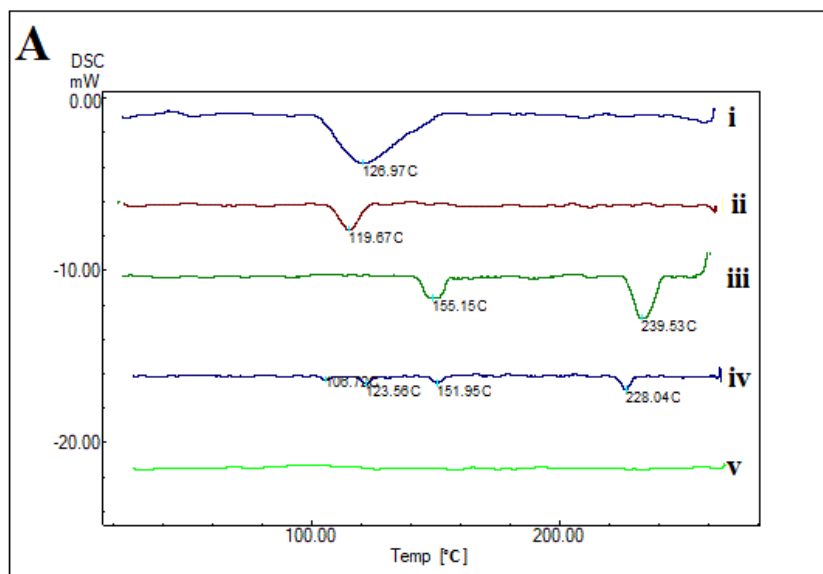


**Figure 3:** **A)** Thermal profile of (i) VM, (ii) OLA (iii) CHs (iv) physical mixture (VM, OLA and CHs) and (v) lyophilized VM-OLA-LPHVs1 and **B)** *In vitro* drug release profile of bare VM and VM-OLA-LPHVs1 in pH 7.4 and pH 6.0 (n = 3).

### 3.5 Stability studies

The physical colloidal stability of the VM-OLA-LPHVs1 was tested using DLS and a UV spectrophotometer [277, 278]. The  $D_H$ ,  $\zeta$  and EE of VM-OLA-LPHVs1 remained stable for 90 days with no significant changes. The experimental results indicated no significant increase in the  $D_H$ ,  $\zeta$  and EE of the VM-OLA-LPHVs1 throughout the 90 days of storage, both at 4°C and room temperature, as shown in **Table 1**.



**Table 1:** Effect of storage condition (4°C and ambient temperature 25°C) and time (days) on  $D_H$ , PDI,  $\zeta$  and EE% of VM-OLA-LPHVs1

Time (days)	4°C				Room temperature 25°C			
	$D_H$ (nm)	PDI	$\zeta$ (mV)	EE%	$D_H$ (nm)	PDI	$\zeta$ (mV)	EE%
0	207.0±6.69	0.137±0.02	-6.95±6.50	45.61±0.54	207.0±6.69	0.14±0.02	-6.95±6.50	45.6 ± 0.54
30	199.0±3.04	0.123±0.02	-3.23±2.42	45.32±0.12	199.5±1.10	0.17±0.02	-3.17±2.56	44.6 ± 1.03
60	198.4±0.40	0.132±0.41	-3.42±1.24	45.12±0.11	210.2±9.25	0.18±0.12	-4.74±4.26	44.0 ± 0.11
90	203.6 ±8.32	0.142 ±1.32	-4.57± 1.52	44.25 ±1.34	214.1 ±5.22	0.26±1.33	-5.28 ± 3.21	42.9 ± 1.12

### 3.6 Antibacterial activity

#### 3.6.1 MICs of the VM-OLA-LPHVs1

A microbroth dilution method was used to determine the MIC of the VM-OLA-LPHVs1 nanovesicles. The MICs values for bare VM against MRSA at both pH values (7.4 and 6.0) were 31.25µg/mL; while VM-OLA-LPHVs1 showed MICs values of 0.59 and 2.39µg/mL at pH 6.0 and 7.4, respectively (**Table 2**). The VM-OLA-LPHVs1 demonstrated 52.96-fold and 13.07-fold antimicrobial enhancement activity at pH 6.0 and pH 7.4, respectively, when compared to bare VM. This could be due to the increase in the binding of VM-OLA-LPHVs1 on the negative bacteria membrane. Overall, the increase in antibacterial activity of the systems is also attributed to the enhanced antimicrobial activity of CHs and OLA acting on the different sites of the bacterial membrane [279]. These results were in line with other drug-loaded CHs nanoparticles that have been reported to show enhanced antibacterial activity [280-282]. The obtained results suggested the potential relevance of VM-OLA-LPHVs1 in applications that target drugs to the acidic sites of infections due to the greater antibacterial activity observed in the acidic pH compared to the physiological pH.

**Table 2:** The *in vitro* antibacterial activity of bare VM, CHs, OLA, OLA-LPHVs and VM-OLA-LPHVs1 showing MICs against MRSA at pH 6.0 and pH 7.4.

Time (h)	pH 6.0			pH 7.4		
	24	48	72	24	48	72
	MIC µg/mL			MIC µg/mL		
Bare VM	31.25	31.25	31.25	31.25	31.25	31.25
CHs	1000	1000	1000	1000	1000	1000
OLA	62.50	62.50	62.50	125.0	125.0	125.0
OLA-LPHVs	62.50	62.50	125.0	250.0	250.0	250.0
VM-OLA-LPHVs1	0.590	0.590	1.190	2.390	4.780	4.780

*All experimental result values are expressed as mean ± SD (n=3)*

### 3.6.2 Time-killing analysis of VM-OLA-LPHVs1

The results of the *in vitro* time bactericidal studies of bare VM and VM-OLA-LPHVs1 at 5× MIC against MRSA are displayed in **Figure 4A**. The VM-OLA-LPHVs1 demonstrated spontaneous bacterial elimination with nearly 97.4% clearance of MRSA in less than 8-hours, despite having a 13-fold lower concentration of VM when compared to the bare drug. This suggests that VM-OLA-LPHVs1 could effectively treat MRSA infections faster, even at a lower dose, with quick elimination of the bacterial infection and reduced treatment duration.

### 3.7 Mechanistic and molecular studies

#### 3.7.1 Bacterial membrane disruption

After determining that VM-OLA-LPHVs1 had superior activity to the bare drug, the effect of VM-OLA-LPHVs1 on the membrane of MRSA was determined by incubating bacteria separately and bacteria with VM-OLA-LPHVs1 for 4-hours. At the initial stages of incubation, intact bacterial membranes were observed, but there was a loss of bacteria membrane after 1-hour of incubation. This was followed by the subsequent loss and disruption of more bacteria membrane after 4-hours of incubation. These observations are shown in **Figure 4B** (i), (ii), (iii) and (iv). These results showed that VM-OLA-LPHVs1 had caused irrecoverable damage to the cell wall of the bacteria, causing permanent death, even at a low concentration of VM in the formulation.

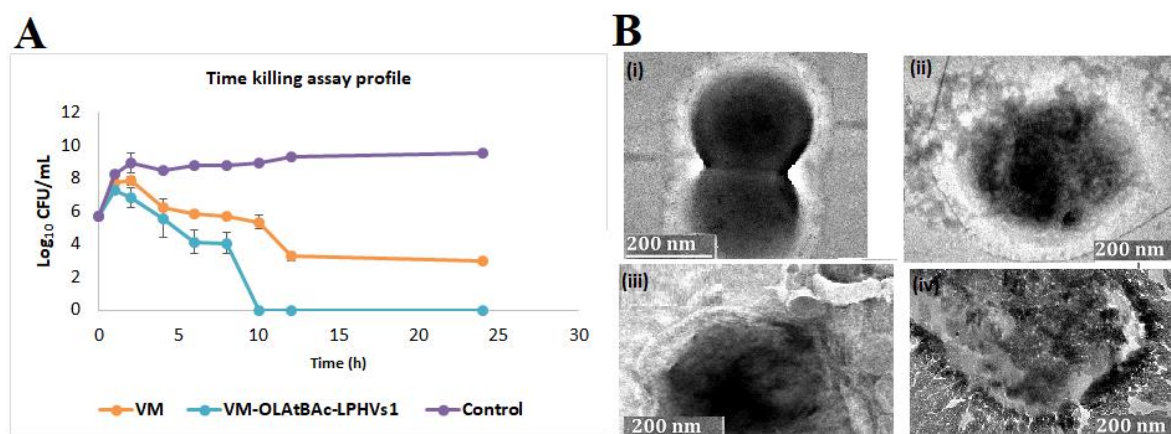


**Figure 4:** **A)** The killing kinetics of MRSA exposed to 5x MIC of VM-OLA-LPHVs1, bare VM and sterile water (control) **B)** HR-TEM images of MRSA after incubation with VM-OLA-LPHVs1. (i) Initial intact structure of MRSA before treatment; (ii) After 1-hour of treatment and incubation; (iii) Formation of pores on the bacterial membrane after 2-hours of treatment; and (iv) Complete loss, disruption and deformation of MRSA membrane after 4-hours.

### 3.7.2 Evaluation of electrical conductivity, DNA leakage and protein quantification

The effect of treating bacteria with VM-OLA-LPHVs1 on the membrane integrity, electrical conductivity and intracellular components leakage was investigated. The results revealed that the negative control (MRSA in NB) and the bare VM had an electrical conductivity of  $0.323 \pm 0.01 \text{ mScm}^{-1}$  and  $0.357 \pm 0.02 \text{ mS cm}^{-1}$ , respectively; while VM-OLA-LPHVs1 displayed an increase in electrical conductivity ( $0.567 \pm 0.03 \text{ mS cm}^{-1}$ ) compared to the negative control and the treatment with bare VM, as shown in **Figure 5A**. The rise in the electrical conductivity could be due to the greater ability of the VM-OLA-LPHVs1 to destroy bacterial membrane when compared to VM. This could be due to leakage of the intracellular electrolytes and displacement of the bacteria cell membrane by the nanovesicles [283-286]. The protein concentration was also quantified at an absorbance of 562nm using the bicinchoninic acid method (BCA). The protein quantity in MRSA drastically decreased from  $158.58 \pm 8.54 \mu\text{g}\cdot\text{mL}^{-1}$  to  $106.94 \pm 11.14 \mu\text{g}\cdot\text{mL}^{-1}$  for bare VM and from  $158.58 \pm 8.54 \mu\text{g}\cdot\text{mL}^{-1}$  to  $82.29 \pm 3.63 \mu\text{g}\cdot\text{mL}^{-1}$  for VM-OLA-LPHVs1. This corresponds to  $24.68 \pm 0.19\%$  and  $69.20 \pm 0.12\%$  of protein concentration reduction for bare VM and VM-OLA-LPHVs1, respectively, when compared to the control (**Figure 5B**). The VM-OLA-LPHVs1 demonstrated a nearly 2-fold reduction compared to bare VM. These results could be due to the disruption of bacteria cell membrane causing cellular substance of DNA leakage [287].

The quantity of DNA in the MRSA after exposure to bare VM and VM-OLA-LPHVs1 was significantly reduced by 54.61% and 48.53%, respectively, as compared to the control (**Figure 5C**). The loss of DNA and protein is attributed to the cell membrane disruption, which led to the leakage of DNA and protein into the external environment [15, 288]. This study demonstrated that the destruction of the MRSA cell membrane by VM-OLA-LPHVs1 led to an increase in the electrical conductivity [15] and leakage of the cellular substances within the bacteria subsequently led to cell death [283, 289]. The studies further showed the superiority of the VM-OLA-LPHVs1 when compared to the bare drug.

**Table 3:** The analysis of MRSA cell membrane permeability after VM-OLA-LPHVs1 treatment.

Parameter	Control	Bare VM	VM-OLA-LPHVs1
DNA concentration ( $\mu\text{g}\cdot\text{mL}^{-1}$ )	$17.53 \pm 0.49$	$4.43 \pm 0.22$	$2.73 \pm 0.41$
Protein concentration ( $\mu\text{g}\cdot\text{mL}^{-1}$ )	$158.58 \pm 8.54$	$106.94 \pm 11.14$	$82.29 \pm 3.63$
Electrical conductivity ( $\text{mS}\cdot\text{cm}^{-1}$ )	$0.323 \pm 0.01$	$0.357 \pm 0.02$	$0.567 \pm 0.03$
<i>Values are expressed as mean <math>\pm</math> SD</i>			

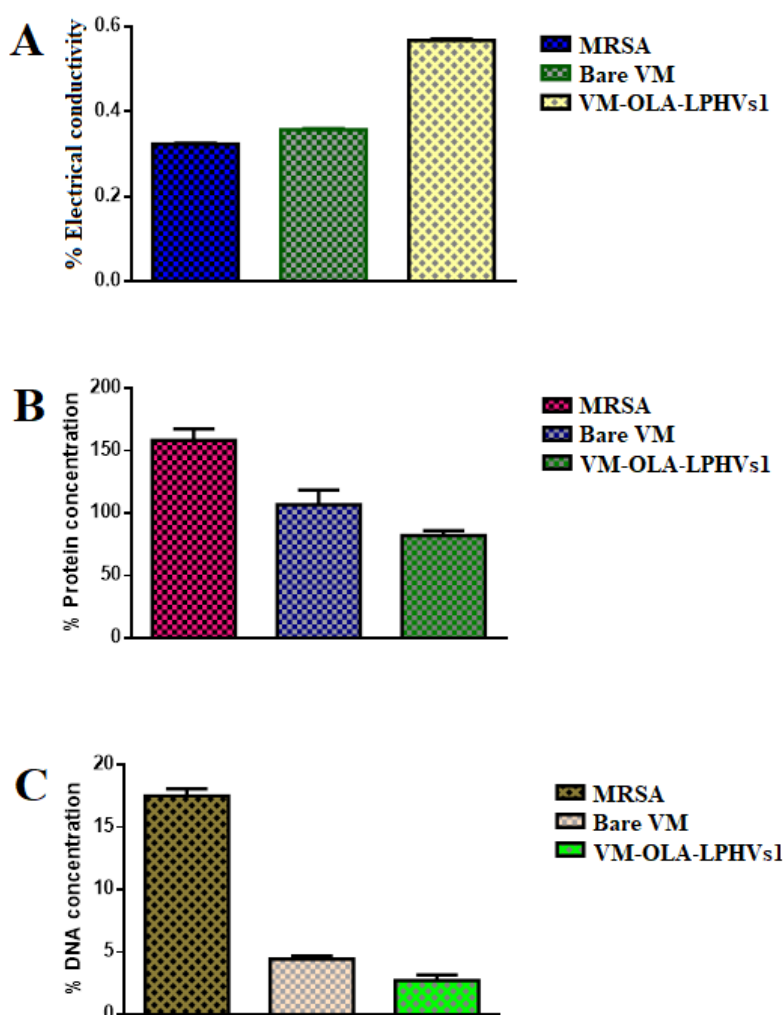


**Figure 5:** The *in vitro* antibacterial mechanism of bare VM and VM-OLA-LPHVs1: **A)** Histogram representation of electrical conductivity of bare VM and VM-OLA-LPHVs1; **B)** Representation of protein quantification of bare VM and VM-OLA-LPHVs1 at Optical Density at 405 nm and **C)** Histogram representation of DNA concentration of bare VM and VM-OLA-LPHVs1.

### 3.8 *In vitro* cell viability of MRSA using Fluorescence-activated cell sorting (FACS)

Under environmental stress conditions, several pathogens enter into a viable, but not cultivable, state [290, 291]. Therefore, there is a need for sensitive studies that detect irreversibly damaged bacterial cells from the viable but non-cultivable colonies [292]. In this study, cell viability after the treatment of MRSA with VM and VM-OLA-LPHVs1 was investigated using FACS [161]. Two dyes, PI and SYTO 9, were employed to separate the dead cells from live cells. PI is a non-permeant dye that only penetrates cells that have lost membrane after the cell membrane loses its integrity; while SYTO 9 unselectively penetrates all membranes. Once in the cell, the dyes intercalate with DNA and their fluorescence intensity can be recorded. In this study, the percentage of PI penetration into the cell membrane of MRSA after exposure to bare VM and VM-OLA-LPHVs1 is shown in **Figure 6**. Data captured from flow cytometry were analysed using Kaluza-1.5.20 (Beckman Coulter USA) flow cytometer software [159, 258]. The results showed that bare VM and VM-OLA-LPHVs1 at MICs of 31.25 $\mu$ g/mL and 2.39 $\mu$ g/mL, respectively, had similar bacteria killing ability of above 90% (**Figure 6B and C**). Interestingly, the VM-OLA-LPHVs1 contained a 13-fold lower VM concentration. This demonstrated that VM-OLA-LPHVs1 could achieve an antibacterial effect similar to the higher doses of bare VM. This could help prevent dose-dependent toxicities, such as nephrotoxicity associated with the administration of bare VM [177].

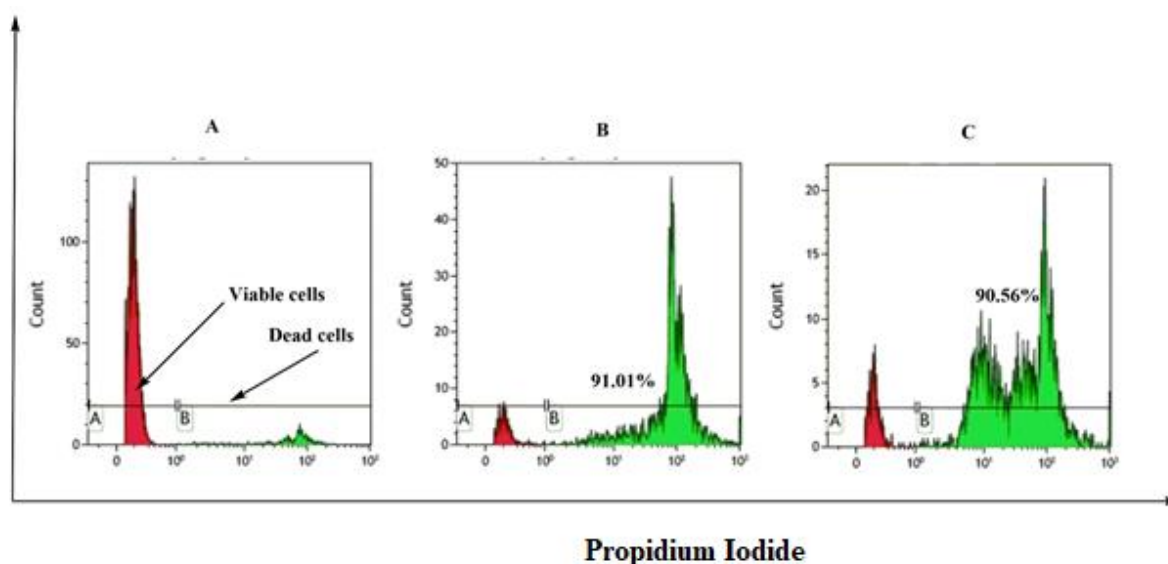


**Figure 6:** Flow cytometric analysis of MRSA cells after incubation with VM and VM-OLA-LPHVs1 **A)** Untreated, **B)** MRSA treated with VM at its MIC (31.25 $\mu$ g/mL), **C)** MRSA treated with VM-OLA-LPHVs1 at its MIC (2.390 $\mu$ g/mL).

### 3.9 MRSA biofilm eradication

In addition to the dead cell quantification using fluorescence-activated cell sorting, the ability of VM-OLA-LPHVs1 to eliminate biofilms was further investigated using fluorescence microscopy. Following a 4-days incubation of MRSA, matured biofilms were formed. These were treated with bare VM and VM-OLA-LPHVs1 and visualised using a fluorescence microscopy technique. The mature biofilms were grown on coverslips, stained with a solution containing 30 $\mu$ L of Propidium iodide (PI) and Syto9 in 1mL sterilised, deionised water and kept in the darkroom to be incubated for approximately 30-minutes. This was followed by washing the excess dyes, and the coverslips were inverted on glass slides for image capturing (**Figure 7A**). The untreated biofilms demonstrated high Syto9 fluorescence due to the ability of the dye to permeate the cell membrane of intact bacteria [282, 283]. PI, being a non-permeating dye, revealed no high fluorescence intensity in untreated MRSA cells (**Figure 7A**). However, compared to the control, a slight decrease in biofilm was observed for biofilms treated with bare VM, demonstrating the substantial antibacterial ability of VM (**Figure 7B**). Interestingly, a larger decrease in biofilms treated with VM-OLA-LPHVs1 was observed, as revealed in the decrease of Syto9 fluorescence intensity, when compared to the bare VM-treated group and the untreated biofilms (**Figure 7C**). These demonstrated higher cell membrane penetration by PI due to the destruction of the exopolymeric matrix polysaccharide (biofilms) cover by VM-OLA-LPHVs1. This result demonstrated that VM-OLA-LPHVs1 could be a good system for eradicating the biofilms that contribute to chronic infections in patients using implants and catheters.

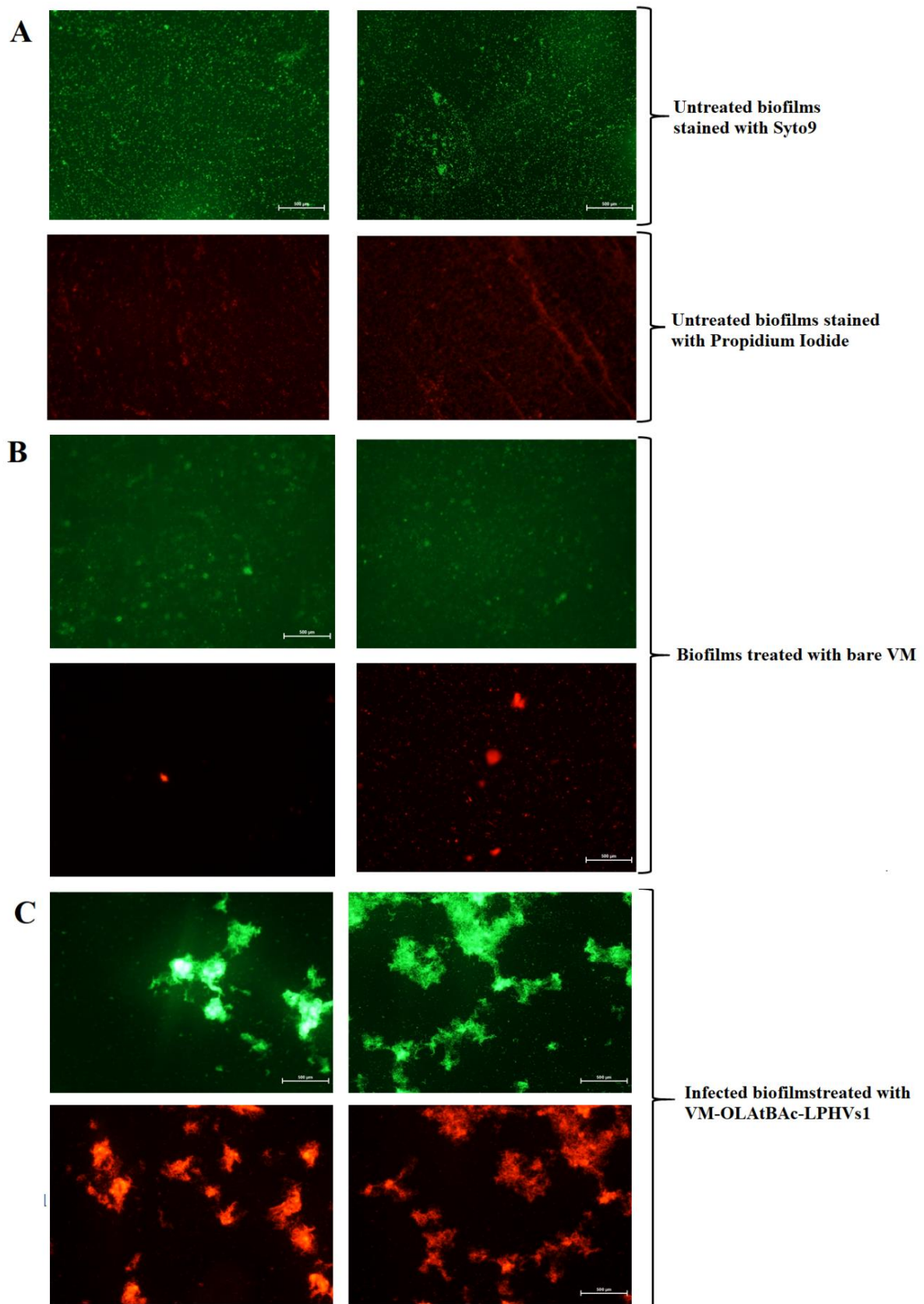


**Figure 7:** Fluorescence microscopy images of **A)** Untreated biofilms; **B)** MRSA biofilms treated with bare VM and **C)** MRSA biofilms treated with VM-OLA-LPHVs1 showing biofilms disruption and internalisation by the VM-OLA-LPHVs1. Scale bars: 500  $\mu$ m.

### 3.10 Intradermal *in vivo* antibacterial activity

For proof of the efficacy of VM-OLA-LPHVs1 in animal models, a mice skin infection *in vivo* study was performed. The bare VM and VM-OLA-LPHVs1 were subcutaneously administered intradermally to BALB/c mice previously infected with MRSA. Mice treated with bare VM showed limited MRSA eradication, while the mice treated with VM-OLA-LPHVs1 revealed greater MRSA elimination, as demonstrated in **Figure 8**. The colony-forming units (CFUs) of all groups were quantitatively measured and plotted in  $\log_{10}$  as shown in **Figure 8**. The MRSA mean load ( $\log_{10}$  CFU) calculated for bare VM, VM-OLA-LPHVs1 and the untreated samples from the mice skin were  $4.40 \pm 0.05$  (25333 CFU/mL),  $2.40 \pm 0.17$  (266 CFU/mL) and  $5.52 \pm 0.014$  (338000 CFU/mL), respectively. The mice skins treated with VM-OLA-LPHVs1 revealed a 95-fold higher reduction in MRSA burden (CFU) compared to the bare VM-treated groups. The one-way ANOVA showed statistically significant differences in CFUs among all the groups with a *P value* = 0.0001. The ability of VM-OLA-LPHVs1 to bind, disrupt and deform the MRSA membrane may be responsible for the enhanced antibacterial activities [293, 294]. These results were in agreement with an *in vivo* study that emplaned other nanovesicles against a superbug [295]. This study revealed the potential of VM-OLA-LPHVs1 in eradicating and eliminating MRSA infections.



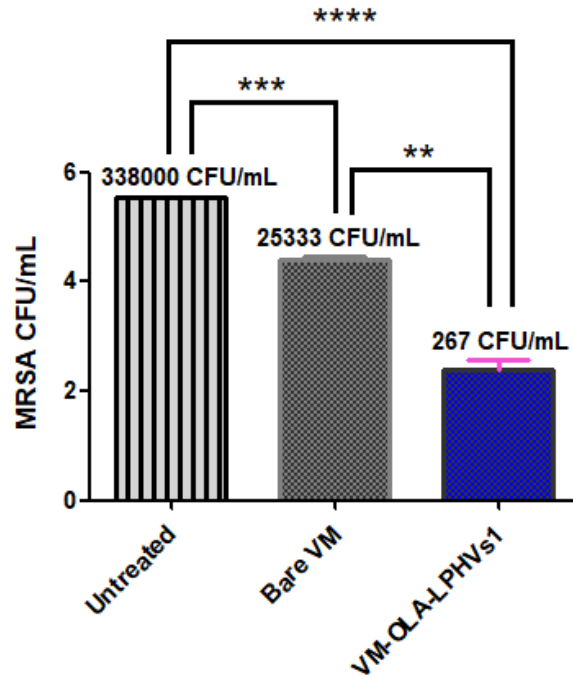


**Figure 8:** MRSA CFUs quantification post 48-hours treatment. Data represent mean  $\pm$  SD (n=3). \*\* represents a significant difference between the bare VM and VM-OLA-LPHVs1, \*\*\* represents a significant difference between the untreated and bare VM and \*\*\*\* represents a significant difference between untreated and VM-OLA-LPHVs1.

#### 4.0 Conclusions

A novel lipid OLA was successfully synthesised by Michael's addition reaction and deprotection. Its potential to prepare a novel chitosan-based VM-loaded pH-responsive nanovesicle (VM-OLA-LPHVs1) was explored. Biocompatibility studies showed that OLA and VM-OLA-LPHVs1 were non-cytotoxic to different cell lines. A stable VM-OLA-LPHVs1 was successfully formulated with a smaller  $D_H$  and higher EE%, and DLC%. The release of VM from VM-OLA-LPHVs1 was higher at pH 6.0 compared to physiological pH 7.4. The *in vitro* antibacterial activity of the VM-OLA-LPHVs1 against MRSA at pH 6.0 revealed an enhanced antibacterial effect compared to VM-OLA-LPHVs1 nanovesicles at pH 7.4 and bare VM. The increased electrical conductivity and decreased protein/DNA concentrations when treated with VM-OLA-LPHVs1, compared to bare VM, indicated that VM-OLA-LPHVs1 caused greater membrane damage on bacteria. The time killing assay and membrane disruption studies VM-OLA-LPHVs1 showed 97.64% bacterial elimination and loss of MRSA membrane with maximum effective damage, respectively. These results were further confirmed by flow cytometry and fluorescence microscopy techniques and the VM-OLA-LPHVs1 displayed a significantly higher percentage of bacteria-killing and biofilm eradication, respectively, when compared to bare VM. The *in vivo* findings obtained by treating BALB/c skin infection revealed the ability of VM-OLA-LPHVs1 to decrease and eradicate the MRSA burden by 95-fold, when compared to bare VM treatment. Our findings suggests that VM-OLA-LPHVs1 can potentially be effective in delivering drugs to the site of infection with low pH and effectively eradicate the incriminating pathogens infectious disease.

**Conflict of interest**

The authors declare no conflict of interest.

**Acknowledgement**

The authors acknowledge the College of Health Sciences, University of KwaZulu-Natal (UKZN), UKZN Nanotechnology Platform, National Research Foundation of South Africa (Grant No. 87790 and 88453) for financial support. The Microscopy and Microanalysis Unit, Biomedical Resource Unit and Department of Human Physiology and Flow Cytometry Research Laboratory at UKZN for supercomputing resources are acknowledged.

## References

- [1] D. Medina Cruz, G. Mi, T.J. Webster, Synthesis and characterization of biogenic selenium nanoparticles with antimicrobial properties made by *Staphylococcus aureus*, methicillin-resistant *Staphylococcus aureus* (MRSA), *Escherichia coli*, and *Pseudomonas aeruginosa*, *J. Bio. Mat. Res. Part A* 106 (2018) 1400-1412.
- [2] C.P. Harkins, B. Pichon, M. Doumith, J. Parkhill, H. Westh, A. Tomasz, H. D. Lencastre, S.D. Bentley, A.M. Kearns, M.T. Holden, Methicillin-resistant *Staphylococcus aureus* emerged long before the introduction of methicillin into clinical practice, *Gen. Bio.* 18 (2017) 130-140.
- [3] D. Harada, H. Nakaminami, E. Miyajima, T. Sugiyama, N. Sasai, Y. Kitamura, T. Tamura, T. Kawakubo, N. Noguchi, Change in genotype of methicillin-resistant *Staphylococcus aureus* (MRSA) affects the antibiogram of hospital-acquired MRSA, *J. Inf. Chemo.* 24(7) (2018) 563-569.
- [4] A.C. Uhlemann, M. Otto, F.D. Lowy, F.R. DeLeo, Evolution of community-and healthcare associated methicillin-resistant *Staphylococcus aureus*, *Infec. Gene. Evol.* 21 (2014) 563-574.
- [5] N. Andreatos, F. Shehadeh, E.E. Pliakos, E. Mylonakis, The impact of antibiotic prescription rates on the incidence of MRSA bloodstream infections: A county-level, US-wide analysis, *Inter. J. Ant. Agents.* 52 (2018) 195-200.
- [6] G.A. Filice, J.A. Nyman, C. Lexau, C.H. Lees, L.A. Bockstedt, K. Como-Sabeti, L.J. Leshner, R. Lynfield, Excess costs and utilization associated with methicillin resistance for patients with *Staphylococcus aureus* infection, *Infec. Cont. Hosp. Epid.* 31(4) (2010) 365-373.
- [7] H. Iqbal, N. Ponniah, S. Long, N. Rath, M. Kent, Review of MRSA screening and antibiotics prophylaxis in orthopaedic trauma patients; The risk of surgical site infection with inadequate antibiotic prophylaxis in patients colonized with MRSA, *Injury.* 48 (2017) 1382-1387.
- [8] K. Govender, S. Sharma, W. Jessee, K. Nagaraju, N.J. Pearse, P. Chhetri, E.M. Bodenstab, P. Yu, S.C. Srinivas, Leadership and Task Shifting to Address the Challenges of Antimicrobial Resistance in South Africa, *Asian J. Pharm. Res. Health Care.* 10 (2018) 10-20.
- [9] R. Xie, X.D. Zhang, Q. Zhao, B. Peng, J. Zheng, Analysis of global prevalence of antibiotic resistance in *Acinetobacter baumannii* infections disclosed a faster increase in OECD countries, *Emerg. Microbes Infe.* 7(1) (2018) 1-10.
- [10] I. Eid, M.M. Elsebaei, H. Mohammad, M. Hagrass, C.E. Peters, Y.A. Hegazy, B. Cooper, J. Pogliano, K. Pogliano, H.S. Abulkhair, Arylthiazole antibiotics targeting intracellular

methicillin-resistant *Staphylococcus aureus* (MRSA) that interfere with bacterial cell wall synthesis, *Eur. J. Med. Chem.* 139 (2017) 665-673.

[11] S.Y. Lee, O.Y. Kim, S.Y. Yoon, S.J. Hur, Changes in resistance to and antimicrobial activity of antibiotics during *in vitro* human digestion, *J. Global Ant. Res.* 15 (2018) 277-282.

[12] C.Y. Hsu, S.C. Yang, C.T. Sung, Y.H. Weng, J.Y. Fang, Anti-MRSA malleable liposomes carrying chloramphenicol for ameliorating hair follicle targeting, *Int. J. Nano.* 12 (2017) 8227.

[13] X. Meng, F. Li, F. Li, Y. Xiong, H. Xu, Vancomycin modified PEGylated-magnetic nanoparticles combined with PCR for efficient enrichment and detection of *Listeria monocytogenes*, *Sen. Act. B: Chem.* 247 (2017) 546-555.

[14] A. Kaur, D. Goyal, R. Kumar, Surfactant mediated interaction of vancomycin with silver nanoparticles, *Appl. Surf. Sci.* 449 (2018) 23-30.

[15] P. Le Thi, Y. Lee, T.T.H. Thi, K.M. Park, K.D. Park, Catechol-rich gelatin hydrogels *in situ* hybridizations with silver nanoparticle for enhanced antibacterial activity, *Mat. Sci. Eng.: C* 92 (2018) 52-60.

[16] J.B. Okado, J.S. Avaca-Crusca, A.L. Oliveira, A.N.G. Dabul, D.C. Camargo, I.L. Baratella, Daptomycin and vancomycin heteroresistance revealed among CC5-SCCmecII MRSA clone and *in vitro* evaluation of treatment alternatives, *J. Glo. Ant. Res.* 14 (2018) 209-216.

[17] D. Martirosov, M. Bidell, M. Pai, M. Scheetz, S. Rosenkranz, T. Lodise, Relationship between vancomycin exposure and outcomes among patients with MRSA bloodstream infections with vancomycin Etest® MIC values of 1.5 mg/L: A pilot study, *Diag. Micro. Infec. Dis.* 88(3) (2017) 259-263.

[18] Z. Yang, Y. Wang, D. Zhang, A novel multifunctional electrochemical platform for simultaneous detection, elimination, and inactivation of pathogenic bacteria based on the vancomycin-functionalised AgNPs/3D-ZnO nanorod arrays, *Bios. Bioelec.* 98 (2017) 248-253.

[19] N. Jain, G.K. Jain, S. Javed, Z. Iqbal, S. Talegaonkar, F.J. Ahmad, R.K. Khar, Recent approaches for the treatment of periodontitis, *Drug Dis. Today* 13(21-22) (2008) 932-943.

[20] K. Hiramatsu, Y. Kayayama, M. Matsuo, Y. Aiba, M. Saito, T. Hishinuma, A. Iwamoto, Vancomycin-intermediate resistance in *Staphylococcus aureus*, *J. Glo. Anti. Res.* 2(4) (2014) 213-224.

[21] K.A. Gates, H. Grad, P. Birek, P.I. Lee, A new bioerodible polymer insert for the controlled release of metronidazole, *Pharm. Res.* 11(11) (1994) 1605-1609.

[22] S. Chang, D.M. Sievert, J.C. Hageman, M.L. Boulton, F.C. Tenover, F.P. Downes, S. Shah, J.T. Rudrik, G.R. Pupp, W.J. Brown, Infection with vancomycin-resistant

*Staphylococcus aureus* containing the vanA resistance gene, New Eng. J. Med. 348(14) (2003) 1342-1347.

[23] T. Lodise, C. Miller, J. Graves, A. Evans, E. Graffunder, M. Helmecke, K. Stellrecht, Predictors of high vancomycin MIC values among patients with methicillin-resistant *Staphylococcus aureus* bacteraemia, J. Anti. Chem. 62(5) (2008) 1138-1141.

[24] R. Deurenberg, C. Vink, S. Kalenic, A. Friedrich, C. Bruggeman, E. Stobberingh, The molecular evolution of methicillin-resistant *Staphylococcus aureus*, Cli. Micro. Inf. 13(3) (2007) 222-235.

[25] Z. Michael, M. Ian, Recently approved antibacterials for MRSA and other gram-positive pathogens: The shock of the new, Inter. J. Anti. Agents (2017).

[26] S. Honary, P. Ebrahimi, R. Hadianamrei, Optimization of particle size and encapsulation efficiency of vancomycin nanoparticles by response surface methodology, Pharm. Devel. Tech. 19 (2014) 987-998.

[27] M. Hasan, G.B. Messaoud, F. Michaux, A. Tamayol, C. Kahn, N. Belhaj, M. Linder, E. ArabTehrany, Chitosan-coated liposomes encapsulating curcumin: Study of lipid-polysaccharide interactions and nanovesicle behavior, RSC Adv. 6 (2016) 45290-45304.

[28] M.S. Baig, A. Ahad, M. Aslam, S.S. Imam, M. Aqil, A. Ali, Application of Box–Behnken design for preparation of levofloxacin-loaded stearic acid solid lipid nanoparticles for ocular delivery: Optimization, *in vitro* release, ocular tolerance, and antibacterial activity, Int. J. Bio. Macromol. 85 (2016) 258-270.

[29] A.C. Santos, F. Veiga, A.J. Ribeiro, New delivery systems to improve the bioavailability of resveratrol, Exp. Opi. Drug Del. 8 (2011) 973-990.

[30] Y.O. Jeon, J.S. Lee, H.G. Lee, Improving solubility, stability, and cellular uptake of resveratrol by nanoencapsulation with chitosan and  $\gamma$ -poly (glutamic acid), Coll. Surf. B: Biointer. 147 (2016) 224-233.

[31] A. Dwivedi, A. Mazumder, N. Nasongkla, Layer-by-layer nanocoating of antibacterial niosome on orthopedic implant, Int. J. Pharm. 547 (2018) 235-243.

[32] F.F. Zhang, L.L. Gan, C.H. Zhou, Synthesis, antibacterial and antifungal activities of some carbazole derivatives, Bioorg. Med. Chem. Lett. 20 (2010) 1881-1884.

[33] O.Y. Kim, S.J. Choi, S.C. Jang, K.S. Park, S.R. Kim, J.P. Choi, J.H. Lim, S.W. Lee, J. Park, D. Di Vizio, Bacterial protoplast-derived nanovesicles as vaccine delivery system against bacterial infection, Nano Lett. 15 (2014) 266-274.

- [34] Y. Chen, X. Li, H. Xiao, J. Xiao, B. Li, X. Chen, Y. Wang, D. Cheng, X. Shuai, Reduction and pH dual-sensitive nanovesicles co-delivering doxorubicin and gefitinib for effective tumor therapy, *RSC Adv.* 8 (2018) 2082-2091.
- [35] J.F. Le Meins, C. Schatz, S. Lecommandoux, O. Sandre, Hybrid polymer/lipid vesicles: State of the art and future perspectives, *Mat. Today* 16 (2013) 397-402.
- [36] S.S. Kulthe, Y.M. Choudhari, N.N. Inamdar, V. Mourya, Polymeric micelles: Authoritative aspects for drug delivery, *Desig. Monomers Polymers* 15 (2012) 465-521.
- [37] J. Prakash Jain, W. Yenet Ayen, N. Kumar, Self assembling polymers as polymersomes for drug delivery, *Cur. Pharm. Design.* 17 (2011) 65-79.
- [38] B.M. Discher, Y.Y. Won, D.S. Ege, J.C. Lee, F.S. Bates, D.E. Discher, D.A. Hammer, Polymersomes: tough vesicles made from diblock copolymers, *Sci.* 284 (1999) 1143-1146.
- [39] L. Klermund, S.T. Poschenrieder, K. Castiglione, Simple surface functionalization of polymersomes using non-antibacterial peptide anchors, *J. Nanobiotech.* 14 (2016) 48-60.
- [40] Y. Zhao, X. Li, X. Zhao, Y. Yang, H. Li, X. Zhou, W. Yuan, Asymmetrical polymer vesicles for drug delivery and other applications, *Front. Pharm.* 8 (2017) 374-383.
- [41] H.E. Colley, V. Hearnden, M. Avila-Olias, D. Cecchin, I. Canton, J. Madsen, S. MacNeil, N. Warren, K. Hu, J.A. McKeating, Polymersome-mediated delivery of combination anticancer therapy to head and neck cancer cells: 2D and 3D *in vitro* evaluation, *Mol. Pharm.* 11 (2014) 1176-1188.
- [42] R. Salva, J.F. Le Meins, O. Sandre, A. Brûlet, M. Schmutz, P. Guenoun, S. Lecommandoux, Polymersome shape transformation at the nanoscale, *ACS Nano* 7 (2013) 9298-9311.
- [43] A. Kumari, S.K. Yadav, S.C. Yadav, Biodegradable polymeric nanoparticles based drug delivery systems, *Coll. Surf. B: Biointer.* 75 (2010) 1-18.
- [44] H.K. Makadia, S.J. Siegel, Poly lactic-co-glycolic acid (PLGA) as biodegradable controlled drug delivery carrier, *Polymers* 3 (2011) 1377-1397.
- [45] N. Dos Santos, K.A. Cox, C.A. McKenzie, F. van Baarda, R.C. Gallagher, G. Karlsson, K. Edwards, L.D. Mayer, C. Allen, M.B. Bally, pH gradient loading of anthracyclines into cholesterol-free liposomes: Enhancing drug loading rates through use of ethanol, *Bioch. Biophys. Acta Biom.* 1661 (2004) 47-60.
- [46] B. Chaize, J.P. Colletier, M. Winterhalter, D. Fournier, Encapsulation of enzymes in liposomes: High encapsulation efficiency and control of substrate permeability, *Artif. Cells, Blood Sub. Biotech.* 32 (2004) 67-75.

- [47] T.T. Dao, F. Fernandes, M. Er-Rafik, R. Salva, M. Schmutz, A. Brûlet, M. Prieto, O. Sandre, J.F. Le Meins, Phase separation and nanodomain formation in hybrid polymer/lipid vesicles, *ACS Macro Lett.* 4 (2015) 182-186.
- [48] W.S. Cheow, K. Hadinoto, Lipid-polymer hybrid nanoparticles with rhamnolipid-triggered release capabilities as anti-biofilm drug delivery vehicles, *Particuology.* 10 (2012) 327-333.
- [49] L. Zhang, J.M. Chan, F.X. Gu, J.W. Rhee, A.Z. Wang, A.F. Radovic Moreno, F. Alexis, R. Langer, O.C. Farokhzad, Self-assembled lipid polymer hybrid nanoparticles: A robust drug delivery platform, *ACS Nano* 2 (2008) 1696-1702.
- [50] R.H. Fang, S. Aryal, C.M.J. Hu, L. Zhang, Quick synthesis of lipid-polymer hybrid nanoparticles with low polydispersity using a single step sonication method, *Lang.* 26 (2010) 16958-16962.
- [51] L. Sun, Y. Du, L. Fan, X. Chen, J. Yang, Preparation, characterization and antimicrobial activity of quaternized carboxymethyl chitosan and application as pulp-cap, *Polymer* 47 (2006) 1796-1804.
- [52] P. Mukhopadhyay, K. Sarkar, S. Soam, P. Kundu, Formulation of pH-responsive carboxymethyl chitosan and alginate beads for the oral delivery of insulin, *J. Appl. Polymer Sci.* 129 (2013) 835-845.
- [53] I.M. Da Silva, J.F. Boelter, N.P. Da Silveira, A. Brandelli, Phosphatidylcholine nanovesicles coated with chitosan or chondroitin sulfate as novel devices for bacteriocin delivery, *J. Nanopart. Res.* 16 (2014) 2479.
- [54] M.I. Lionzo, G.C. Lorenzini, J. Tomedi, P. Pranke, N.P. Silveira, Effects of the composite nanovesicles on the physical properties and cellular adhesion of chitosan films, *J. Biomed. Nanotech.* 8 (2012) 337-344.
- [55] O. Mertins, M. Sebben, A.R. Pohlmann, N.P. Da Silveira, Production of soybean phosphatidylcholine-chitosan nanovesicles by reverse phase evaporation: A step by step study, *Chem. Physics Lipids* 138 (2005) 29-37.
- [56] K. Blecher, A. Nasir, A. Friedman, The growing role of nanotechnology in combating infectious disease, *Virulence* 2 (2011) 395-401.
- [57] I.A. Sogias, A.C. Williams, V.V. Khutoryanskiy, Why is chitosan mucoadhesive?, *Biomacromolecules.* 9 (2008) 1837-1842.
- [58] J. You, S. Xie, J. Cao, H. Ge, M. Xu, L. Zhang, J. Zhou, Quaternized chitosan/poly (acrylic acid) polyelectrolyte complex hydrogels with tough, self-recovery, and tunable mechanical properties, *Macromolecules* 49 (2016) 1049-1059.



- [59] Z.S. Sheikholeslami, H. Salimi-Kenari, M. Imani, M. Atai, A. Nodehi, Exploring the effect of formulation parameters on the particle size of carboxymethyl chitosan nanoparticles prepared via reverse micellar crosslinking, *J. Microencapsul.* 34 (2017) 270-279.
- [60] S. Mourdikoudis, L.M. Liz-Marzan, Oleylamine in nanoparticle synthesis, *Chem. Mat.* 25 (2013) 1465-1476.
- [61] R. Xing, A.A. Bhirde, S. Wang, X. Sun, G. Liu, Y. Hou, X. Chen, Hollow iron oxide nanoparticles as multidrug resistant drug delivery and imaging vehicles, *Nano Res.* 6 (2013) 1-9.
- [62] D.H. Kim, D.E. Nikles, D.T. Johnson, C.S. Brazel, Heat generation of aqueously dispersed  $\text{CoFe}_2\text{O}_4$  nanoparticles as heating agents for magnetically activated drug delivery and hyperthermia, *J. Mag. Magnetic Mat.* 320 (2008) 2390-2396.
- [63] G. Sharma, S. Beg, K. Thanki, O. Katare, S. Jain, K. Kohli, B. Singh, Systematic development of novel cationic self-nanoemulsifying drug delivery systems of candesartan cilexetil with enhanced biopharmaceutical performance, *RSC Adv.* 5 (2015) 71500-71513.
- [64] S. Simovic, H. Hui, Y. Song, A.K. Davey, T. Rades, C.A. Prestidge, An oral delivery system for indomethacin engineered from cationic lipid emulsions and silica nanoparticles, *J. Control. Rel.* 143 (2010) 367-373.
- [65] R.S. Kalhapure, M. Jadhav, S. Rambharose, C. Mocktar, S. Singh, J. Renukuntla, T. Govender, pH-responsive chitosan nanoparticles from a novel twin-chain anionic amphiphile for controlled and targeted delivery of vancomycin, *Coll. Surf. B: Biointer.* 158 (2017) 650-657.
- [66] C.I. Von Deuster, V. Knecht, Antimicrobial selectivity based on zwitterionic lipids and underlying balance of interactions, *Bioch. Biophys. Acta Biomembranes.* 1818 (2012) 2192-2201.
- [67] A. Velikonja, Š. Perutkova, E. Gongadze, P. Kramar, A. Polak, A. Maček Lebar, A. Iglič, Monovalent ions and water dipoles in contact with dipolar zwitterionic lipid headgroups-theory and MD simulations, *Inter. J. Mol. Sci.* 14 (2013) 2846-2861.
- [68] W.E. Rudzinski, T.M. Aminabhavi, Chitosan as a carrier for targeted delivery of small interfering RNA, *Inter. J. Pharm.* 399 (2010) 1-11.
- [69] K. Sarkar, P. Kundu, Preparation of low molecular weight N-maleated chitosan-graft-PAMAM copolymer for enhanced DNA complexation, *Inter. J. Biol. Macromol.* 51 (2012) 859-867.

- [70] P. Mukhopadhyay, K. Sarkar, M. Chakraborty, S. Bhattacharya, R. Mishra, P. Kundu, Oral insulin delivery by self-assembled chitosan nanoparticles: *In vitro* and *in vivo* studies in diabetic animal model, *Mat. Sci. Eng.: C* 33 (2013) 376-382.
- [71] J.P. Quiñones, H. Peniche, C. Peniche, Chitosan based self-assembled nanoparticles in drug delivery, *Polymers*. 10 (2018) 235.
- [72] C.A. Omolo, R.S. Kalhapure, M. Jadhav, S. Rambharose, C. Mocktar, V.M. Ndesendo, T. Govender, Pegylated oleic acid: A promising amphiphilic polymer for nano-antibiotic delivery, *Euro. J. Pharm. Biopharm.* 112 (2017) 96-108.
- [73] D. Hassan, C.A. Omolo, R. Gannimani, A.Y. Waddad, C. Mocktar, S. Rambharose, N. Agrawal, T. Govender, Delivery of novel vancomycin nanoplexes for combating methicillin-resistant *Staphylococcus aureus* (MRSA) Infections, *Inter. J. Pharm.* (2019).
- [74] D.R. Nogueira, L. Tavano, M. Mitjans, L. Pérez, M.R. Infante, M.P. Vinardell, *In vitro* antitumor activity of methotrexate via pH-sensitive chitosan nanoparticles, *Biomaterials*. 34 (2013) 2758-2772.
- [75] Q. Gan, T. Wang, C. Cochrane, P. McCarron, Modulation of surface charge, particle size and morphological properties of chitosan-TPP nanoparticles intended for gene delivery, *Coll. Surf. B: Biointer.* 44 (2005) 65-73.
- [76] L.Y. Gao, X.Y. Liu, C.J. Chen, J.C. Wang, Q. Feng, M.Z. Yu, X.F. Ma, X.W. Pei, Y.J. Niu, C. Qiu, Core-shell type lipid/rPAA-Chol polymer hybrid nanoparticles for *in vivo* siRNA delivery, *Biomaterials* 35 (2014) 2066-2078.
- [77] E. Sánchez López, M. Egea, A. Cano, M. Espina, A. Calpena, M. Ettcheto, A. Camins, E.B. Souto, A.M. Silva, M.L. García, PEGylated PLGA nanospheres optimized by design of experiments for ocular administration of dexibuprofen *in vitro*, *ex vivo* and *in vivo* characterization, *Coll. Surf. B: Biointer.* 145 (2016) 241-250.
- [78] Q. Wang, H. Jiang, Y. Li, W. Chen, H. Li, K. Peng, Z. Zhang, X. Sun, Targeting NF- $\kappa$ B signaling with polymeric hybrid micelles that co-deliver siRNA and dexamethasone for arthritis therapy, *Biomat.* 122 (2017) 10-22.
- [79] N. Liu, J. Han, X. Zhang, Y. Yang, Y. Liu, Y. Wang, G. Wu, pH-responsive zwitterionic polypeptide as a platform for anti-tumor drug delivery, *Coll. Surf. B: Biointer.* 145 (2016) 401-409.
- [80] M.A. Sallam, M.T.M. Boscá, Mechanistic analysis of human skin distribution and follicular targeting of adapalene-loaded biodegradable Nanospheres with an insight into hydrogel matrix influence, *in vitro* skin irritation, and *in vivo* tolerability, *J. Pharm. Sci.* 106 (2017) 3140-3149.

- [81] X. Cheng, H. Yan, X. Jia, Z. Zhang, Preparation and *in vivo/in vitro* evaluation of formononetin phospholipid/vitamin E TPGS micelles, *J. Drug Target.* 24 (2016) 161-168.
- [82] S.J. Sonawane, R.S. Kalhapure, S. Rambharose, C. Mocktar, S.B. Vepuri, M. Soliman, T. Govender, Ultra-small lipid-dendrimer hybrid nanoparticles as a promising strategy for antibiotic delivery: *In vitro* and *in silico* studies, *Inter. J. Pharm.* 504 (2016) 1-10.
- [83] J.H. Jorgensen, J.D. Turnidge, Susceptibility test methods: Dilution and disk diffusion methods, *Manual Clinical Microbiology*, Eleventh Edition, Ame. Soc. Microbio.2015, pp. 1253-1273.
- [84] A. AbdelKhalek, N.S. Abutaleb, H. Mohammad, M.N. Seleem, Antibacterial and antivirulence activities of auranofin against *Clostridium difficile*, *Intern. J. Antimicro. Agents* 53 (2019) 54-62.
- [85] L. Lin, X. Mao, Y. Sun, H. Cui, Antibacterial mechanism of artemisinin/beta-cyclodextrins against Methicillin-resistant *Staphylococcus aureus* (MRSA), *Micro. Path.* 118 (2018) 66-73.
- [86] N. Chauhan, A.K. Tyagi, P. Kumar, A. Malik, Antibacterial potential of jatropa curcas synthesized silver nanoparticles against food borne pathogens, *Front. Microbio.* 7 (2016) 1748-1761.
- [87] E. Van Andel, I. De Bus, E.J. Tijhaar, M.M. Smulders, H.F. Savelkoul, H. Zuilhof, Highly specific binding on antifouling zwitterionic polymer-coated microbeads as measured by flow cytometry, *ACS Appl. Mat. Interf.* 9 (2017) 38211-38221.
- [88] A. Bexfield, A.E. Bond, E.C. Roberts, E. Dudley, Y. Nigam, S. Thomas, R.P. Newton, N.A. Ratcliffe, The antibacterial activity against MRSA strains and other bacteria of a < 500Da fraction from maggot excretions/secretions of *Lucilia sericata* (Diptera: Calliphoridae), *Microbes Infec.* 10 (2008) 325-333.
- [89] N.K. Shrestha, N.M. Scalera, D.A. Wilson, G.W. Procop, Rapid differentiation of methicillin-resistant and methicillin-susceptible *Staphylococcus aureus* by flow cytometry after brief antibiotic exposure, *J. Cli. Microbio.* 49 (2011) 2116-2120.
- [90] D.J. Arndt-Jovin, T.M. Jovin, Fluorescence labeling and microscopy of DNA, *Methods Cell Bio.* 30 (1989) 417-448.
- [91] N.M. O'Brien-Simpson, N. Pantarat, T.J. Attard, K.A. Walsh, E.C. Reynolds, A rapid and quantitative flow cytometry method for the analysis of membrane disruptive antimicrobial activity, *PloS One* 11 (2016) e0151694.

- [92] M. Rüger, G. Bensch, R. Tüngler, U. Reichl, A flow cytometric method for viability assessment of *Staphylococcus aureus* and *Burkholderia cepacia* in mixed culture, *Cytomet. Part A* 81 (2012) 1055-1066.
- [93] S. Renggli, W. Keck, U. Jenal, D. Ritz, Role of autofluorescence in flow cytometric analysis of *Escherichia coli* treated with bactericidal antibiotics, *J. Bacter.* 195 (2013) 4067-4073.
- [94] M. Fittipaldi, A. Nocker, F. Codony, Progress in understanding preferential detection of live cells using viability dyes in combination with DNA amplification, *J. Microbio. Methods.* 91 (2012) 276-289.
- [95] F. Berlutti, A. Frioni, T. Natalizi, F. Pantanella, P. Valenti, Influence of sub-inhibitory antibiotics and flow condition on *Staphylococcus aureus* ATCC 6538 biofilm development and biofilm growth rate: Bio timer assay as a study model, *J. Antibiotics* 67 (2014) 763.
- [96] E. Kugelberg, T. Norström, T.K. Petersen, T. Duvold, D.I. Andersson, D. Hughes, Establishment of a superficial skin infection model in mice by using *Staphylococcus aureus* and *Streptococcus pyogenes*, *Anti. Agents Chemoth.* 49 (2005) 3435-3441.
- [97] K.Y. Lee, D.J. Mooney, Alginate: Properties and biomedical applications, *Prog. Polymer Sci.* 37 (2012) 106-126.
- [98] T.L. Riss, R.A. Moravec, A.L. Niles, S. Duellman, H.A. Benink, T.J. Worzella, L. Minor, Cell viability assays, *Assay Guidance Manual*, Eli Lilly & Company and the National Center for Advancing Translational Sciences 2016.
- [99] R. Hamid, Y. Rotshteyn, L. Rabadi, R. Parikh, P. Bullock, Comparison of alamar blue and MTT assays for high through-put screening, *Tox. in vitro* 18 (2004) 703-710.
- [100] T. Mosmann, Rapid colorimetric assay for cellular growth and survival: Application to proliferation and cytotoxicity assays, *J. Immu. Methods.* 65 (1983) 55-63.
- [101] S. Taabache, A. Bertin, Vesicles from amphiphilic dumbbells and janus dendrimers: Bioinspired self-assembled structures for biomedical applications, *Polymers.* 9 (2017) 280.
- [102] V. Uskoković, T.A. Desai, *In vitro* analysis of nanoparticulate hydroxyapatite/chitosan composites as potential drug delivery platforms for the sustained release of antibiotics in the treatment of osteomyelitis, *J. Pharm. Sci.* 103 (2014) 567-579.
- [103] O. Mertins, P.H. Schneider, A.R. Pohlmann, N.P. Da Silveira, Interaction between phospholipids bilayer and chitosan in liposomes investigated by <sup>31</sup>P NMR spectroscopy, *Coll. Surf. B: Biointer.* 75 (2010) 294-299.

- [104] Y. Wang, C. Yang, R. Hu, H.T. Toh, X. Liu, G. Lin, F. Yin, H.S. Yoon, K.T. Yong, Assembling Mn: ZnSe quantum dots-siRNA nanoplexes for gene silencing in tumor cells, *Biomater. Sci.* 3 (2015) 192-202.
- [105] O. Mertins, M.B. Cardoso, A.R. Pohlmann, N.P. da Silveira, Structural evaluation of phospholipidic nanovesicles containing small amounts of chitosan, *J. Nanosci. Nanotech.* 6 (2006) 2425-2431.
- [106] M. Gumustas, C.T. Sengel-Turk, A. Gumustas, S.A. Ozkan, B. Uslu, Effect of Polymer-Based Nanoparticles on the Assay of Antimicrobial Drug Delivery Systems, *Multifunctional Systems for Combined Delivery, Biosensing and Diagnostics*, Elsevier 2017, pp. 67-108.
- [107] T. Cerchiara, A. Abruzzo, R.A.Ñ. Palomino, B. Vitali, R. De Rose, G. Chidichimo, L. Ceseracciu, A. Athanassiou, B. Saladini, F. Dalena, Spanish Broom (*Spartium junceum* L.) fibers impregnated with vancomycin-loaded chitosan nanoparticles as new antibacterial wound dressing: Preparation, characterization and antibacterial activity, *Eur. J. Pharm. Sci.* 99 (2017) 105-112.
- [108] J.M. Unagolla, A.C. Jayasuriya, Drug transport mechanisms and *in vitro* release kinetics of vancomycin encapsulated chitosan-alginate polyelectrolyte microparticles as a controlled drug delivery system, *Eur. J. Pharm. Sci.* 114 (2018) 199-209.
- [109] H.M. Aldawsari, K.M. Hosny, Solid lipid nanoparticles of vancomycin loaded with Ellagic acid as a tool for overcoming nephrotoxic side effects: Preparation, characterization, and nephrotoxicity evaluation, *J. Drug Del. Sci. Tech.* 45 (2018) 76-80.
- [110] M. Farrokhi Rad, A. Fateh, T. Shahrabi, Electrophoretic deposition of vancomycin loaded halloysite nanotubes-chitosan nanocomposite coatings, *Surf. Coatings Techn.* 349 (2018) 144-156.
- [111] B.D. Loveymi, M. Jelvehgari, P. Zakeri Milani, H. Valizadeh, Design of vancomycin RS-100 nanoparticles in order to increase the intestinal permeability, *Adv. Pharm. Bulletin* 2 (2012) 43.
- [112] B.D. Loveymi, M. Jelvehgari, P. Zakeri Milani, H. Valizadeh, Statistical optimization of oral vancomycin-eudragit rs nanoparticles using response surface methodology, *Iranian J. Pharm. Research: IJPR* 11(4) (2012) 1001.
- [113] S. Bajaj, S. Rajamani, M. Gogia, Stability considerations in the life cycle of generic products, *Methods for Stability Testing of Pharmaceuticals*, Springer 2018, pp. 195-212.
- [114] S. Bajaj, D. Singla, N. Sakhuja, Stability testing of pharmaceutical products, *J. App. Pharm. Sci.* 2 (2012) 129-38.

- [115] L. Qi, Z. Xu, X. Jiang, C. Hu, X. Zou, Preparation and antibacterial activity of chitosan nanoparticles, *Carbohydr. Res.* 339 (2004) 2693-2700.
- [116] B. Jamil, H. Habib, S. Abbasi, H. Nasir, A. Rahman, A. Rehman, H. Bokhari, M. Imran, Cefazolin loaded chitosan nanoparticles to cure multi drug resistant Gram-negative pathogens, *Carbohydr. Polymers* 136 (2016) 682-691.
- [117] S. Ramteke, N. Ganesh, S. Bhattacharya, N.K. Jain, Amoxicillin, clarithromycin, and omeprazole based targeted nanoparticles for the treatment of *H. pylori*, *J. Drug Target.* 17 (2009) 225-234.
- [118] P. Sanpui, A. Murugadoss, P.D. Prasad, S.S. Ghosh, A. Chattopadhyay, The antibacterial properties of a novel chitosan-Ag-nanoparticle composite, *Int. J. Food Microbio.* 124 (2008) 142-146.
- [119] A. Van Holle, M.D. Machado, E.V. Soares, Flocculation in ale brewing strains of *Saccharomyces cerevisiae*: Re-evaluation of the role of cell surface charge and hydrophobicity, *Appl. Microbio. Biotech.* 93 (2012) 1221-1229.
- [120] M. Cristani, M. D'Arrigo, G. Mandalari, F. Castelli, M.G. Sarpietro, D. Micieli, V. Venuti, G. Bisignano, A. Saija, D. Trombetta, Interaction of four monoterpenes contained in essential oils with model membranes: Implications for their antibacterial activity, *J. Agri. Food Chem.* 55 (2007) 6300-6308.
- [121] G. Rukholm, C. Mugabe, A.O. Azghani, A. Omri, Antibacterial activity of liposomal gentamicin against *Pseudomonas aeruginosa*: A time-kill study, *Inter. J. Ant. Agents* 27 (2006) 247-252.
- [122] L.H. Lin, L.W. Lee, S.Y. Sheu, P.Y. Lin, Study on the stevioside analogues of steviolbioside, steviol, and isosteviol 19-alkyl amide dimers: synthesis and cytotoxic and antibacterial activity, *Chem. Pharm. Bulletin* 52 (2004) 1117-1122.
- [123] A. Gajewicz, N. Schaeublin, B. Rasulev, S. Hussain, D. Leszczynska, T. Puzyn, J. Leszczynski, Towards understanding mechanisms governing cytotoxicity of metal oxides nanoparticles: Hints from nano-QSAR studies, *Nanotox.* 9 (2015) 313-325.
- [124] S. Finger, C. Wiegand, H.J. Buschmann, U.C. Hipler, Antimicrobial properties of cyclodextrin-antiseptics-complexes determined by microplate laser nephelometry and ATP bioluminescence assay, *Int. J. Pharm.* 436 (2012) 851-856.
- [125] L. Xu, X. Xu, G. Yuan, Y. Wang, Y. Qu, E. Liu, Mechanism of Azalomycin F5a against Methicillin-Resistant *Staphylococcus aureus*, *BioMed Res. Inter.* 2018 (2018).
- [126] X. Zhao, J. Zhong, C. Wei, C.W. Lin, T. Ding, Current perspectives on viable but non-culturable state in foodborne pathogens, *Front. Microbio.* 8 (2017) 580.

- [127] C. Robben, S. Fister, A.K. Witte, D. Schoder, P. Rossmann, P. Mester, Induction of the viable but non-culturable state in bacterial pathogens by household cleaners and inorganic salts, *Scientific Reports* 8 (2018) 15132.
- [128] J. Keer, L. Birch, Molecular methods for the assessment of bacterial viability, *J. Microbio. Methods* 53 (2003) 175-183.
- [129] P.R. Ingram, D.C. Lye, P.A. Tambyah, W.P. Goh, V.H. Tam, D.A. Fisher, Risk factors for nephrotoxicity associated with continuous vancomycin infusion in outpatient parenteral antibiotic therapy, *J. Anti. Chemoth.* 62 (2008) 168-171.
- [130] B. Yoon, J. Jackman, E. Valle González, N.J. Cho, Antibacterial free fatty acids and monoglycerides: biological activities, experimental testing, and therapeutic applications, *Int. J. Mol. Sci.* 19 (2018) 1114.
- [131] D.K. Joung, S.H. Mun, S.H. Choi, O.H. Kang, S.B. Kim, Y.S. Lee, T. Zhou, R. Kong, J.G. Choi, D.W. Shin, Antibacterial activity of oxyresveratrol against methicillin-resistant *Staphylococcus aureus* and its mechanism, *Exp. Therapeu. Med.* 12 (2016) 1579-1584.
- [132] Y. Pei, M.F. Mohamed, M.N. Seleem, Y. Yeo, Particle engineering for intracellular delivery of vancomycin to methicillin-resistant *Staphylococcus aureus* (MRSA) infected macrophages, *J. Cont. Rel.* 267 (2017) 133-143.

## CHAPTER FOUR: EXPERIMENTAL PAPER THREE

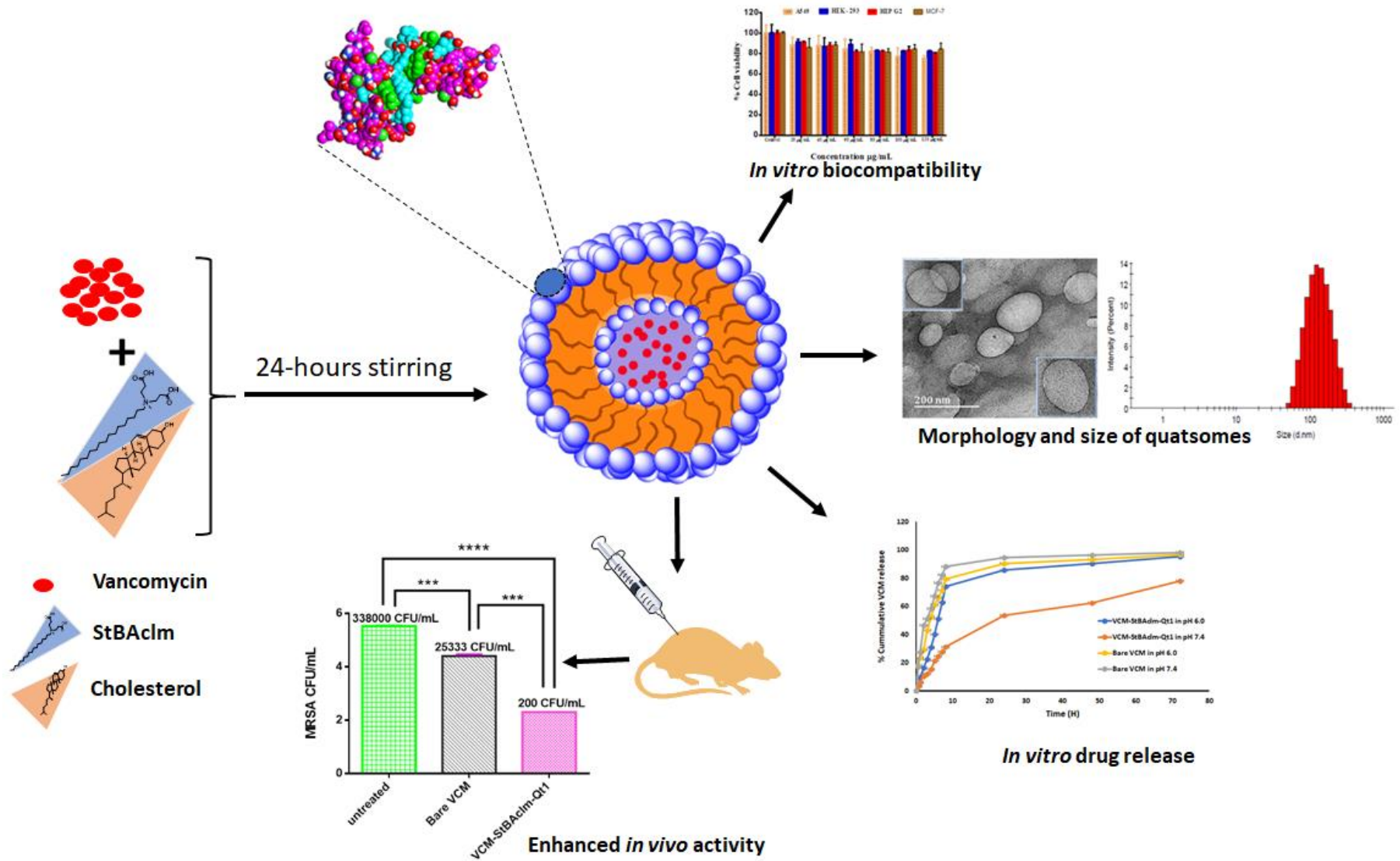
### 4.1 Introduction

This chapter addresses **Aim 3** and **Objectives 1- 6**. It is a first authored experimental article submitted and highlights the formulation and characterisation of pH-responsive quatsomes (VCM-StBAclm-Qt<sub>1</sub>) from the novel quaternary bicephalic surfactant (StBAclm). The quatsomes (VCM-StBAclm-Qt<sub>1</sub>) was evaluated for *in vitro* toxicity, physicochemical properties, morphology, molecular dynamics (MD) simulations, *in vitro* electrical conductivity, protein/DNA concentration quantification, membrane damage, time killing assay, membrane disruption, bacteria-killing percentage, biofilm eradication, *in vitro* and *in vivo* antibacterial properties.

The ethical approval is attached in Appendix II.



## 4.2 Graphical Abstract



### 4.3 Submitted Manuscript

**Quaternary Bicephalic Surfactant (StBAclm) and Cholesterol pH-responsive Quatsomes for Enhanced Activity of Antibiotics against Methicillin-Resistant *Staphylococcus aureus* (MRSA).**

**Daniel Hassan<sup>1</sup>, Calvin A. Omolo<sup>1,2#</sup>, Victoria Oluwaseun Fasiku<sup>1</sup>, Ahmed A Elrashedy<sup>3</sup>, Chunderika Mocktar<sup>1</sup>, Mahmoud E. S. Soliman<sup>3</sup>, Thirumala Govender<sup>1#</sup>**

<sup>1</sup> Discipline of Pharmaceutical Sciences, College of Health Sciences, University of KwaZulu-Natal, Private Bag X54001, Durban, South Africa.

<sup>2</sup> United States International University-Africa, School of Pharmacy and Health Sciences, Department of Pharmaceutics, P. O. Box 14634-00800, Nairobi, Kenya.

<sup>3</sup> Molecular Bio-computation and Drug Design Laboratory School of Health Sciences, University of KwaZulu-Natal, Westville Campus, Durban, 4001, South Africa.

Tel: +27 31 260 7357/8, Fax: +27 31 260 7792

#Corresponding authors.

Email address: govenderth@ukzn.ac.za; comolo@usiu.ac.ke

## Highlights

- A novel surfactant (StBAclm) was synthesized and its structure confirmed.
- Vancomycin-loaded pH-responsive quatsomes (VCM-StBAclm-Qt1) were prepared from StBAclm.
- The *in vitro* drug results showed a faster VCM release from the quatsomes at pH 6.0 compared to pH 7.4 and enhanced *in vitro* antibacterial activity against MRSA as compared to bare VCM.
- There was an enhanced bacterial killing kinetics and high perforation of MRSA membrane cell wall by the quatsomes.
- A higher electrical conductivity, reduced DNA, and protein concentration were achieved by the quatsomes.
- There was an enhanced *in vivo* antibacterial activity of the drug quatsomes against MRSA compared to bare VCM in a mice skin infection model.

## Abbreviation

ATP	Adenosine triphosphatase
A-549	Adenocarcinomic alveolar basal epithelial cells
BCA	Bicinchoninic acid
CDC	Centers for Disease Control and Prevention
CTAB	Cationic hexadecyltrimethylammonium bromide
CFU	<i>Colony-forming unit</i>
CHol	Cholesterol
DCM	Dichloromethane
DLC	Drug loading capacity
DMSO	Dimethyl sulfoxide
DNA	Deoxyribonucleic acids
DSC	Differential scanning calorimetry
DEE	Drug encapsulation efficiency
FT-IR	Fourier transform infrared
HR-MS	High-resolution <i>mass spectrometry</i>
HEK-293	Human embryonic kidney cell lines
Hep-G2	liver hepatocellular carcinoma cell lines
MCF-7	Human breast adenocarcinoma cell lines
MDT	Mean dissolution time
MHA	Mueller-Hinton agar
MHD	Mean hydrodynamic diameter
MHB	Mueller-Hinton Broth
MI	Methyl iodide
MICs	Minimum inhibitory concentrations
MRSA	Methicillin-resistant <i>Staphylococcus aureus</i>
MTT	3-(4,5-dimethylthiazol-2-yl)-2,5-diphenyltetrazolium bromide
NB	Nutrient Broth
OD	Optical density
PDI	Polydispersity index
PI	Propidium iodide
pDNA	Plasmid deoxyribonucleic acid
PBS	Phosphate saline buffer
RMSE	Root mean square error
R <sup>2</sup>	Correlation coefficient
SA	Stearylamine
siRNA	Small interfering ribonucleic acid
<i>t</i> BA	<i>Tert</i> -butyl acrylate
TFA	Trifluoroacetic acid
TIPs	Triisopropylsilane
UVis-Spec	UV Spectrophotometer
VCM	Vancomycin
ζ	Zeta potential
<sup>1</sup> H NMR	Proton nuclear magnetic resonance
<sup>13</sup> C NMR	Carbon 13 nuclear magnetic resonance

## Abstract

Globally, human beings continue to be at high risk of infectious diseases caused by Methicillin-resistant *Staphylococcus aureus* (MRSA) and current treatments are being depleted due to antimicrobial resistance. Therefore, the synthesis and formulation of novel materials are essential for combating antimicrobial resistance. The study aimed to synthesize a quaternary bicephalic surfactant (StBAclm) and formulate pH-responsive vancomycin (VCM) quatsomes to increase the activity of VCM against MRSA and its structure was confirmed using  $^1\text{H}$ ,  $^{13}\text{C}$  NMR, FT-IR, and HRMS. The quatsomes were prepared using a sonication/dispersion method and were characterised using various *in vitro*, *in vivo* and *in silico* techniques. The *in vitro* cell biocompatibility studies of StBAclm and pH-responsive vancomycin-loaded quatsomes (VCM-StBAclm-Qt<sub>1</sub>) revealed cell viability of more than 75%. The VCM-StBAclm-Qt<sub>1</sub> prepared had a mean hydrodynamic diameter (MHD), polydispersity-index (PDI) and drug encapsulation efficiency (DEE) of  $122.9 \pm 3.78\text{nm}$ ,  $0.169 \pm 0.02\text{mV}$  and  $45.61 \pm 0.539\%$ , respectively, with surface charge switching from negative to positive at pH 7.4 and pH 6.0, respectively. HR-TEM characterisation of the VCM-StBAclm-Qt<sub>1</sub> confirmed spherical vesicles with MHD similar to the one obtained from Zeta-sizer. The *in vitro* drug release of VCM from the VCM-StBAclm-Qt<sub>1</sub> was faster at pH 6.0, compared to pH 7.4. The minimum inhibitory concentration (MIC) of the VCM-StBAclm-Qt<sub>1</sub> quatsomes against MRSA was 32-fold and 8-fold lower in pH 6.0 and pH 7.4, respectively, compared to bare VCM, demonstrating the pH-responsiveness of the quatsomes. The VCM-StBAclm-Qt<sub>1</sub> demonstrated higher electrical conductivity and decreases in protein and deoxyribonucleic acid (DNA), which confirmed greater MRSA membrane damage compared to treatment with bare VCM. The flow cytometry study showed that the quatsomes had a similar bactericidal killing effect on MRSA, despite a lower (8-fold) VCM concentration than the bare VCM. The *in silico* studies confirmed the spontaneous formation and interaction of the self-assembled quatsomes in the presence of non-solvent accessible areas. The *in vivo* studies in a skin infection of mice models showed that the quatsomes treated groups had a 13.34-fold decrease in MRSA CFUs when compared to the bare VCM treated groups. This study indicated the potential of pH-responsive quatsomes as an effective delivery system for antibiotics.

Keywords: Quatsomes, pH-responsive, Vancomycin, Methicillin-resistant *Staphylococcus aureus* (MRSA), Quaternary, Surfactant.

## 1.0 Introduction

Despite the progress made in combating infectious diseases, they still continue to pose a significant health challenge, leading to high morbidity and mortality rates [1, 2]. In a review requested by the British government, and chaired by O'Neill in 2016, it was highlighted that global antimicrobial resistance would result in the loss of 10 million lives by 2050 [3]. One of the major bacteria recognised as a serious threat is *Staphylococcus aureus*, which has mutated into a resistant strain: Methicillin-resistant *Staphylococcus aureus* (MRSA), and has been a global problem since its discovery in a London hospital in 1960 [4]. Human beings continue to be at higher risk of infections caused by MRSA, and current antibiotic treatments are being depleted due to antibacterial resistance [5, 6]. This has led to debilitating conditions resulting in longer in-hospital stays, and economic loss due to extended therapy [5, 6]. The Centers for Disease Control and Prevention (CDC) reported that the loss of nearly 11,285 [7], 5,400 [8] and 4,150,000 [9] lives would be recorded in the United States, the European Union Member States, and Africa by 2050, respectively. These figures will continue to rise, and the World Health Organization (WHO) warns of entering into a post-antibiotic era if innovative strategies are not adopted to curb the rise of antimicrobial resistance [10, 11].

Novel drug delivery systems using nanotechnology are an alternative option for solving antimicrobial resistance. Nano-sized drug delivery systems offer greater versatility due to size; composition; stimuli-responsiveness [12]; biocompatibility; biodegradability; reduced side effects [13, 14]; and decreased exposure of antibiotics to healthy sites, when compared to conventional dosage forms [15]. Loading of antibiotics into nano-sized drug delivery systems offers higher drug pharmacokinetic profiles and enhanced antibacterial activity, and protects the drug from enzymatic destruction leading to fewer side effects [16, 17]. These traits tend to address the limitations of conventional dosage forms, which have been used for treating infectious diseases since the introduction of antibiotics [18, 19].

Several nano-drug delivery systems have been involved in the effective delivery of antimicrobials with great success, and currently they are being introduced to the market [20, 21]. Lipidic vesicles are the nanostructures most employed for drug delivery since their serendipitous discovery in 1964 [22]. They can entrap hydrophobic molecules within their bilayers and hydrophilic molecules in their lumen, which makes them excellent as nano-carriers for the delivery of drugs [23, 24]. Despite their desirable traits, their use in drug delivery has been limited by their low degree of structural homogeneity, which is a critical requirement for their enhancement of the pharmacological property of the loaded drugs [24]. Their stability is

also a limiting factor because of their lipid building blocks being insoluble in water [25, 26]. These limitations have prompted research into other vesicles for drug delivery, such as polymersomes from amphiphilic polymers [27], dendrimersomes from dendrimers [28, 29], and peptosomes from self-assembling peptides [30]. However, these vehicles still have limitations due to their structural stability, low entrapment, membrane thickness and area density, which is greatly affected by block length and the size of the polymer, dendrimers, or peptides [31].

Recently, pH-responsive drug delivery systems for antibiotics have been receiving interest since they can respond to the unique acidic site conditions and offer increased drug delivery and receptor binding to improve treatment. The search for superior vehicles for drug delivery has resulted in the development of quatsomes. They are nanoscopic vesicles, composed of sterols and quaternary ammonium surfactants in defined molar ratios [31]. Unlike conventional liposomes, they have been reported to be stable for long storage time, have high vesicle-to-vesicle homogeneity in size and lamellarity and high drug-loading capacity [32]. Furthermore, quatsomes have been shown to offer protection against premature drug degradation and intracellular penetration [33], and are potential platform for site-specific delivery of hydrophilic and lipophilic molecules. However, most of the reported studies on quatsomes aimed at understanding the physical-chemical properties of its membrane [24, 34].

To date, no studies on quatsomes have explored their value in the delivery of drugs. Existing studies in the literature have reported on quatsomes prepared from available quaternary surfactants in the market to improve their toxicity profile [24, 34]. No pH-responsive quatsomes have been reported. In this project, we report on a pH-responsive quaternary bicephalic surfactant (StBAclm) used in combination with cholesterol (CHol) to formulate quatsomes. There is no reports in the literature on the application of this surfactant and its formulation in the delivery of antibiotics or any class of drug. Such a system will broaden the field of drug delivery as novel stimuli-responsive quatsomes will be introduced. We envisage self-assembly to occur due to the electrostatic interactions between the hydrophobic tail of the surfactant and CHol, whilst the pH-responsiveness will be due to the protonation and deprotonation of the bicephalic carboxylic arms of the surfactant. In this study, we report the synthesis of a novel quaternary bicephalic surfactant (StBAclm) which was further employed, together with CHol, to formulate pH-responsive VCM-loaded quatsomes (VCM-StBAclm-Qt). The *in vitro*, *in vivo* and *in-silico* evaluation of this novel quatsomes, are reported in this paper.

## 2.0 Materials and methods

### 2.1 Materials

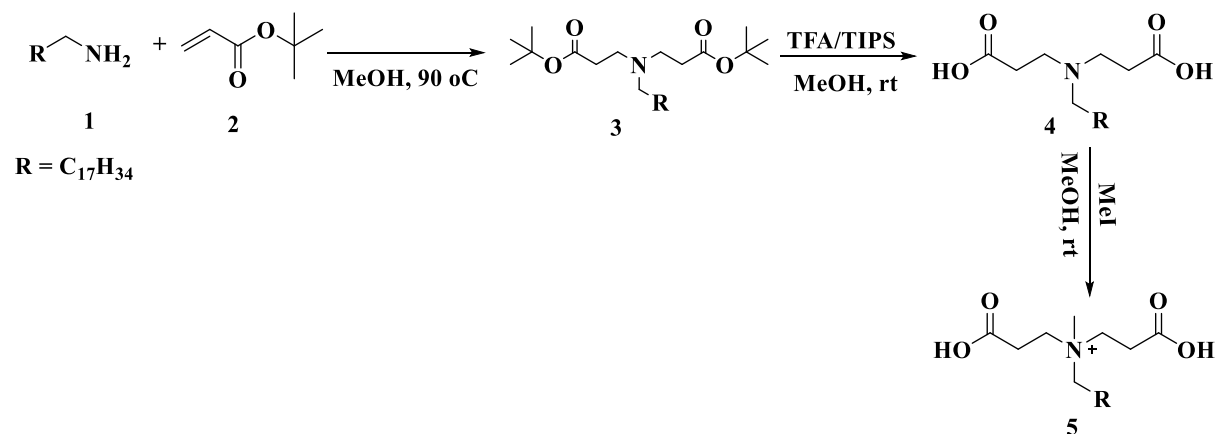
Stearylamine; *tert*-butyl acrylate (tBA); dichloromethane (DCM); trifluoroacetic acid (TFA); triisopropylsilane (TIPS); methyl iodide (MI); cholesterol (CHol) and silica gel were purchased from Sigma-Aldrich (USA). Vancomycin (VCM) and MTT were purchased from Sinobright Import and Export Co., Ltd. (China) and Merck Chemicals (Germany), respectively. NB, MHB, MHA and MRSA (*S. aureus* Rosenbach ATCC BAA 1683) were obtained from Biolab (South Africa). Propidium iodide (PI) and Syto9 dyes Kit were obtained from Thermofisher (USA). Bacteria DNA and BCA Kits were purchased from Zymo Research California, (USA), and Wako Chemicals, Virginia (USA), respectively. Millipore water used during study was purified in the laboratory using the Milli-Q water purification system (Millipore corp., USA). All other chemicals and solvents used were of analytical grade.

### 2.2 Instrumentation (<sup>1</sup>H NMR, <sup>13</sup>C NMR, FT-IR and HR-MS spectra)

<sup>1</sup>H NMR, <sup>13</sup>C NMR and FT-IR spectra were conducted and recorded on a Bruker 400 Ultra shield™ (United Kingdom) NMR spectrometer and a Bruker Alpha-p spectrometer with a diamond ATR (Germany), respectively. HR-MS was accomplished on a Water Micromass LCT Premier TOF-MS (United Kingdom). The system (GPC: TFA) consisted of a water 717 plus auto-sampler, a water 1515 isocratic HPLC pump, a water refractive index detector, and a water 600E system controller. Optical density (OD) was measured (Spectrostarano, Germany).

### 2.3 Synthesis and characterisation of the surfactant.

The bicephalic surfactant was synthesized as per **Scheme 1**: characterisation and structural elucidation is found in the **Supporting Materials S1**.



**Scheme 1.** a). Dichloromethane (DCM), reflux with constant stirring at 80 °C, 24 h, b). DCM, room temperature, 8-hours and c). DCM, room temperature, 12-hours.



#### **2.4 *In vitro* cytotoxicity of StBAclm and VCM-StBAclm-Qt against different cell lines**

The biocompatibility of the novel StBAclm and VCM-StBAclm-Qt quatsomes was evaluated using a modified MTT assay method previously reported [21, 35]. Four different cell lines were used, including: human embryonic kidney (HEK-293), liver hepatocellular carcinoma (Hep-G2), human breast adenocarcinoma (MCF-7), and adenocarcinomic alveolar basal epithelial cells (A-549). All four cell lines were grown exponentially at 37°C in a 5% CO<sub>2</sub> humidified atmosphere. The cell lines containing greater than 80% confluency were trypsinised and seeded into 96-well plates and then incubated for 24-hours. The StBAclm and VCM-StBAclm-Qt quatsomes were prepared and diluted with sterilised Milli-Q water, separately, to final concentrations of 20, 40, 60, 80, 100 and 120µg/mL [21]. Subsequently, the culture medium and the quatsomes were removed after 48-hours and replaced with 100µL of fresh medium followed by the addition of MTT solution (5mg/mL in PBS) in each well. The cells were further incubated for an additional 4-hours, followed by the removal of the solution previously added. Afterwards, solubilisation of the MTT formazan was achieved by the addition of 100µL DMSO into each well. The optical density of each well was measured on a Microplate Spectrophotometer (Spectrostar Nano, Germany) at 540nm. All the experiments were performed in six replicates and percentage cell viability was calculated using Equation 1.

$$\% \text{ Cell viability} = \left( \frac{\text{A540 nm treated cells}}{\text{A540 nm untreated cells}} \right) \times 100 \dots \dots \dots \text{Equation 1}$$

#### **2.5 Formulation of VCM-loaded quatsomes (VCM-StBAclm-Qt)**

The quatsomes were prepared according to a previously reported method with slight modification [32]. Briefly, StBAclm (final StBAclm concentration 0.5, 1, 2.5, 5 and 10mg/mL) and CHol were accurately weighed into beakers keeping the molar ratio of the two excipients constant (1:1). Drug-loaded quatsomes were formulated by the addition of the bicephalic surfactant, VCM, and Chol at different concentrations. This was followed by the addition of 40mL of Milli-Q water, and the mixture was further sonicated for 10, 15, 20 and 30-minutes (30/10 second on/off cycle, 30% amplitude) using a probe-sonicator in an ice bath. The dispersions were further stirred at 500rpm on a magnetic stirring plate for 24-hours at room temperature. Milli-Q water was used as the dispersion medium to avoid changes in the solubility of StBAclm as the presence of electrolytes can adversely affect the formation of the quatsomes [24, 32]. After 24-hours of equilibration, potential aggregates were removed from the blank (StBAclm-Qt) and the drug-loaded VCM-StBAclm-Qt quatsomes by filtration using a syringe/filter (0.45µm pore size).

## 2.6 Characterisation of the VCM-StBAclm-Qt quatsomes

### 2.6.1 Mean hydrodynamic diameter (MHD), polydispersity index (PDI), zeta potential ( $\zeta$ ) and morphology

The MHD, PDI, and  $\zeta$  of VCM-StBAclm-Qt quatsomes were analysed using a zetasizer nano ZS90 (Malvern Instruments Ltd., UK). A cryogenic-HR transmission electron microscopy (Cryo-HR-TEM) on a Jeol, JEM-2100 (Japan) was used to examine VCM-StBAclm-Qt the quatsomes' morphology. Briefly, the drug-loaded quatsomes were diluted accordingly and mounted onto the copper grid surface, and immediately 2% uranyl acetate (UA) solution was added and used to stain. The excess VCM-StBAclm-Qt quatsomes and stain on the grid were removed by blotting off with filter paper and affixed with liquid nitrogen [36]. Before virtualisation of the quatsomes' morphology, the sample grid was kept in liquid nitrogen and transferred into the chamber. The images were captured and obtained at an accelerating voltage of 200kV.

### 2.6.2 Drug entrapment efficiency (DEE%) and drug loading capacity (DLC%)

The VCM-StBAclm-Qt quatsomes were further characterized to determine DEE% and DLC%. The DEE% was determined using an ultrafiltration method, as previously reported [37, 38]. Briefly, exactly, 2mL of the drug-loaded quatsomes was loaded into the Amicon® Ultra-4 centrifugal filter tubes (Millipore Corp., USA), with 10kDa pore size, and centrifuged at 3000rpm for exactly 30-minutes at 25°C. The amount of the untrapped drug in the filtrate was determined spectrophotometrically using Shimadzu UV 1601, Japan at 280nm. The regression equation of the calibration curve ( $y = 0.0038x - 0.0031$ ), with a linear regression coefficient ( $R^2$ ) of 0.9998, was used to determine the unknown drug concentrations values. The experiment was done in triplicate, and the DEE% was calculated using equation 2.

$$DEE\% = \left( \frac{\text{Weight of VCM in quatsomes}}{\text{Weight of VCM added during preparation}} \right) \times 100 \dots \dots \dots \text{Equation 2}$$

The DLC% was determined by freeze-drying the quatsomes, and the weight of VCM was calculated using the equation 3 below.

$$DLC\% = \left( \frac{\text{Weight of VCM in quatsomes}}{\text{Total weight of quatsomes}} \right) \times 100 \dots \dots \dots \text{Equation 3}$$

### **2.6.3 Molecular modelling simulations (MDS)**

#### **2.6.3.1 Vancomycin, CHol and surfactant simulation quatsomes**

To evaluate the self-assembling quatsomes and the encapsulation of VCM, molecular modelling simulations were employed. The VCM, CHol and the surfactant (StBAclm) structures were drawn with ChemDraw professional 17.0. Chimera molecular modelling suite was used to prepare the initial VCM-CHol-surfactant complex [39]. The LEAP module implemented in AMBER 14 was used to combine, neutralise and solvate the system by adding hydrogen atoms, chloride and sodium ions and suspending them in an orthorhombic box of TIP3P water molecules such that all atoms were within 10Å of the box edges [40]. The system contains a total of 2082 water molecules and 1 molecule of VCM, 1 molecule of CHol, and 1 molecule of the surfactant. The system was minimised for 2500 steps with a strong constraint on VCM, CHol and surfactant for 1000 steps (500 steepest descent followed by 500 steps of the conjugate gradient). This was followed by 1000 steps of full minimisation Langevin thermostat, with a collision frequency of 1.0ps<sup>-1</sup> with harmonic restraint of 5kcal/mol Å on the solutes during the gradual heating up of the systems to a temperature of 300.00 K in the canonical ensemble for 50ps. This was followed by 50ps of density equilibration in NPT ensemble and a final 500ps equilibration at 300.00K, 1 bar pressure and coupling constant of 2 ps. MDS production was carried out for 10 ns using classical MDS with a time step of 2fs, with the frame being recorded at every 500 steps of simulation. All the bond lengths involving hydrogen atoms were constrained using the SHAKE algorithm [41].

#### **2.6.3.2 VCM, CHol and surfactant self-assembly complexation simulation**

The Chimera tool was used for random insertion of six complexes of VCM, CHol and the surfactant complex. The system was then minimised for 2500 steps with strong constraint on VCM, cholesterol and surfactant for 1000 steps (500 steepest descent followed by 500 steps of the conjugate gradient), followed by 1000 steps of full minimisation Langevin thermostat, with a collision frequency of 1.0ps<sup>-1</sup> with harmonic restraint of 5kcal/mol Å on the solutes during the gradual heating up of the systems to a temperature of 300.00K in the canonical ensemble for 50ps. This was followed by 50ps of density equilibration in NPT ensemble and a final 500ps equilibration at 300.00K, 1 bar pressure and coupling constant of 2ps. MDS production was carried out for 10ns using classical MDS with a time step of 2fs, with the frame being recorded at every 500 steps of simulation. All the bond lengths involving hydrogen atoms were constrained using the SHAKE algorithm [41]. All the molecular dynamics simulation were carried out using the GPU amber 14 software package [42].

### 2.6.3.3 Post-dynamic analysis and binding free energy calculations

The trajectories generated after MDS simulations were each saved every 1ps, followed by analysis using the CPPTRAJ [43] module employed in the AMBER 14 suit. All plots and visualisations were completed using the Origin data analysis tool [44] and Chimera [39], respectively. Binding free energy calculations is an important endpoint method that elucidates on the mechanism of binding between a ligand and protein, including both enthalpic and entropic contributions [45, 46]. To estimate the binding affinity of the docked systems, the free binding energy was calculated using the Molecular Mechanics/GB Surface Area method (MM/GBSA) [47]. Binding free energy was averaged over 1000 snapshots extracted from the ten ns trajectory. The free binding energy has been computed by this method for each molecular species (complex, ligand and receptor) and can be represented as:

$$\Delta G_{\text{bind}} = G_{\text{complex}} - G_{\text{receptor}} - G_{\text{ligand}} \quad (1)$$

$$\Delta G_{\text{bind}} = E_{\text{gas}} + G_{\text{sol}} - TS \quad (2)$$

$$E_{\text{gas}} = E_{\text{int}} + E_{\text{vdw}} + E_{\text{ele}} \quad (3)$$

$$G_{\text{sol}} = G_{\text{GB}} + G_{\text{SA}} \quad (4)$$

$$G_{\text{SA}} = \gamma \text{SASA} \quad (5)$$

The terms  $E_{\text{gas}}$ ,  $E_{\text{int}}$ ,  $E_{\text{ele}}$ , and  $E_{\text{vdw}}$  symbolise the gas-phase energy, internal energy, Coulomb energy and Van der Waals energy, respectively. The  $E_{\text{gas}}$  was directly assessed from the force field terms. Solvation free energy ( $G_{\text{sol}}$ ), was assessed from the energy involvement from the polar states ( $G_{\text{GB}}$ ), and non-polar states ( $G$ ). The non-polar solvation energy ( $G_{\text{SA}}$ ), was determined from the solvent-accessible surface area (SASA), using a water probe radius of 1.4 Å, while the polar solvation ( $G_{\text{GB}}$ ) contribution was assessed by solving the GB equation. S and T symbolise the total entropy of the solute and temperature, respectively [47].

### 2.8 *In vitro* drug release of VCM from VCM-StBAclm-Qt quatsomes

The drug release of VCM was performed as per previously reported procedures [48, 49]. Two mL of the bare VCM, VCM-StBAclm-Qt and the corresponding blank StBAclm-Qt were loaded into the dialysis bags with a size porosity of 8,000-14,400Da. The dialysis bags containing the bare VCM, drug-loaded quatsomes and the corresponding blank were placed separately in a 40mL receiver compartment of PBS (pH 6.0 and pH 7.4) at 37°C in a shaking incubator at 100rpm. Samples of 3mL were withdrawn at specific time intervals from the receiver compartment solution. Immediately, an equal amount of fresh PBS (pH 6.0 and pH

7.4, respectively) was replaced into the corresponding compartment to keep the initial receiver volume constant. The quantity of VCM released from the dialysis bags in the receiver chamber was measured spectrophotometrically with Shimadzu UV 1601, Japan at 280nm using the regression equation mentioned in **Section 2.5.2**. The release fraction of VCM from VCM-StBAclm-Qt quatsomes and VCM solution was calculated using equation 4 below (n=3), where  $A_t$  is the amount of VCM released from drug-loaded VCM-StBAclm-Qt<sub>1</sub> quatsomes at time t, and  $A_p$  the amount of VCM pre-loaded in the VCM-StBAclm-Qt<sub>1</sub> quatsomes.

$$\% \text{ Cumulative release profile} = \left( \frac{A_t}{A_p} \right) \times 100 \% \dots \dots \dots \text{Equation 4}$$

## **2.9 Evaluation of *in vitro* antibacterial activities on VCM-StBAclm-Qt quatsomes**

### **2.9.1 Minimum inhibitory concentrations (MICs) determination**

The MICs studies were conducted against MRSA, according to the previously reported procedure [50]. The bacteria were cultured and grown in MHB with relevant dilutions achieved at  $5 \times 10^5$  colony-forming units per mL (CFU/mL) [51]. The bare VCM, StBAclm-Qt and VCM-StBAclm-Qt quatsomes were serially diluted in MHB and incubated with bacteria cultures ( $5 \times 10^5$ ) colony-forming units per mL (CFU/mL) for exactly 20-hours in a shaking incubator at 37°C and 100rpm. Precisely 10µL of the serially diluted solutions was spotted on MHA plates and incubated for 24-hours; and the MIC was regarded as the point with no visible bacteria growth.

### **2.9.2 Time killing assays VCM-StBAclm-Qt quatsomes**

An overnight MRSA cultured in nutrient broth (NB) was diluted with phosphate buffer saline (pH 7.4) to a concentration of  $5 \times 10^5$  CFU/mL. Bare VCM, and VCM-StBAclm-Qt quatsomes were added at concentrations equivalent to  $5 \times \text{MIC}$ . For the negative control, sterile deionised water was added into the bacterial MHB alone, and bacterial cell viability was overseen up to 24-hours. Tested materials bare VCM and VCM-StBAclm-Qt quatsomes were removed at designated times, serially diluted in PBS, plated on an MHA plate, and incubated for 24-hours at 37 °C. After 24-hours of incubation, CFU was counted, converted to log<sub>10</sub> values and plotted on a graph [52, 53].

$$\%W = \left( \frac{\text{Population of control bacteria} - \text{population of experimental bacteria}}{\text{Population of control bacteria}} \right) \times 100$$

## 2.10. Molecular and mechanistic studies on VCM-StBAclm-Qt quatsomes

### 2.10.1 Downstream physiological phenomena: electrical conductivity quantification

1% MRSA was inoculated in 10mL MHB with bacteria (control), bare VCM and VCM-StBAclm-Qt quatsomes (100µg/mL) and cultured for 16-hours. Three mL of the cultured samples were centrifuged at 4000rpm for 15-minutes and the supernatant collected in order to determine its electrical conductivity [6]. The electrical conductivity was determined using an electrical conductivity meter (OHAUS USA) and calculated using the equation 5 (n=3), where Q refers to the conductivity change rate, and Qs and Qc are the conductivity of the test groups and the control group, respectively.

$$Q \% = \left( \frac{Q_s - Q_c}{Q_c} \right) \times 100\% \dots \dots \dots \text{Equation 5}$$

### 2.10.2 Determination of DNA and protein quantification

The samples were incubated with the bacteria and centrifuged according to the procedure in **Section 2.10.1**. The DNA concentrations of MRSA treated with bare VCM and VCM-StBAclm-Qt quatsomes were extracted using a DNA Kit (Zymo Research California, USA), and analysed using Nanodrop 1000 Thermo Fisher Scientific, Waltham, MA, USA at 562nm absorbance. The protein concentration of MRSA treated with bare VCM and VCM-StBAclm-Qt quatsomes was determined and analysed using BCA Kits based on the bicinchoninic acid method on a microplates spectrophotometer (Spectrostar Nano, Germany) [6] at an absorbance of 562nm.

### 2.10.3 Bacterial membrane disruption

Suspensions of MRSA with a concentration ( $1.5 \times 10^8$  CFU/mL) in PBS were incubated with VCM-StBAclm-Qt quatsomes containing 153µg/mL of VCM (50:50) ratio and incubated for 4-hours in a sterilised Eppendorf tube. The mixture was diluted properly and mounted onto the surface of a copper grid, according to a previously reported method [54]. The excess sample was withdrawn by blotting off with filter paper and allowed to dry at 25°C before measurement. The images of the samples were obtained using a high-Resolution transmission electron microscope (brightfield, darkfield, TEM- JEOL HR-TEM 2100).

### 2.10.4 Fluorescence-activated cell sorting (FACS) bacterial cell viability

The bacterial cell viability was assessed using a previously reported flow cytometry method [55-58]. Briefly, MHB was used to grow pure MRSA culture overnight at 100rpm in a shaking incubator (Labcon, USA) at 37°C. Serial dilution of the bacteria at final concentrations

CFU/mL of  $5 \times 10^5$  was used; 15 $\mu$ L of the bacteria suspension was pipetted into the 96-well plate containing 135 $\mu$ L of bare VCM at MIC concentrations of 31.25 $\mu$ g/mL, and VCM-StBAclm-Qt quatsomes at MIC concentration of 3.90 $\mu$ g/mL. The mixture was incubated for an additional 6-hours at 37°C and 100rpm. The percentage cell viability was determined after 6-hours of incubation, and untreated MRSA cells were used as the negative control [59]. Exactly 50 $\mu$ L of the bare VCM and VCM-StBAclm-Qt quatsomes broths were appended into the flow cytometry tubes containing 350 $\mu$ L of sheath fluid vortexed and incubated for approximately 5-minutes [59, 60]. The cytometry tubes containing the samples were incubated for another 30-minutes with 5 $\mu$ L of non-cell wall permeant and cell-permeant dye, PI and Syto9, respectively. The PI fluorescence was excited at 455nm laser and gathered between 636nm bandpass filter, while the Syto9 excitation laser was set at 485nm laser and collected at 498nm bandpass filter [55-57]. The bacteria were gated using forward scatter (FSC), with approximately 10,000 cells gathered for individual sample in triplicate. Particles smaller than the bacteria were detected at a threshold of 100 in the SSC analyses to avoid background signals [61]. Data were captured from the flow cytometry and analysed using Kaluza-1.5.20 software (Beckman Coulter USA) [56, 62].

#### **2.10.5 Reduction of MRSA biofilm using fluorescence microscopy**

Biofilm eradication of MRSA by bare VCM and VCM-StBAclm-Qt quatsomes were quantified using fluorescence microscopy according to a previously reported procedure [63]. Briefly, coverslips were placed in a 24-well plate. Exactly 4mL of MBH was added into the 24-well plate, followed by the addition of 2mL of MRSA ( $1.5 \times 10^8$  CFU/mL) suspensions grown in MHB. The solution was incubated for four-days at 37°C to form matured biofilm. Before treatment, the media used to grow the bacteria were removed out of the 24-well plates using a sterilized Pasteur pipette to avoid any contamination. The plate wells were subsequently washed four-times using sterilized water to remove excess and non-adhered bacteria. Exactly 1mL of bare VCM suspension and VCM-StBAclm-Qt1 quatsomes, each containing 125 $\mu$ g/mL of VCM, were added into the appropriate 24-well plates and incubated for an additional 12-hours at 37°C. After incubation, the wells were washed with PBS (pH 7.4) to remove the non-adhered treatments on the biofilms. Coverslips were stained with 30 $\mu$ L of Syto9 and Propidium iodide (PI) dyes in deionised water and left in the dark to incubate for another 30-minutes. The treated and stained 24-well plates were washed for the second time to remove excess dyes used, and the cover plate was carefully glued and inverted on a microscope

glass slide. Biofilm reduction by bare VCM and the VCM-StBAclm-Qt quatsomes was visualised on a fluorescence microscope (Nikon Eclipse 80i FM Japan).

### 2.10.6 *In vivo* antibacterial activity

For proof of enhanced antibacterial activity, an *in vivo* antibacterial activity study of the bare VCM and VCM-StBAclm-Qt quatsomes was conducted. A mice skin infection model was used, following a protocol approved by the University of KwaZulu-Natal's (UKZN) Animal Research Ethics Committee (Approval number: AREC/104/015PD) [64, 65]. The use of animals and humane care followed the guidelines of UKZN AREC and South African National Standard SANS 10386:2008. Male BALB/c mice of approximately 18-20g were obtained from the Biomedical Research Unit (BRU) of UKZN. The mice were then divided into treatment, positive and negative control groups (n = 4). The mice skin, which was the site of administration of the treatments, was shaved and disinfected using 70% ethanol 24-hours before the experiment. The following day, 50µL of MRSA (1.5 x 10<sup>8</sup> CFU/mL), suspended in saline, was injected intradermally. Thirty minutes after bacterial infection, 50µL of the bare VCM, VCM-StBAclm-Qt quatsomes and saline were injected separately at the same site of infection into the various test groups. The mice were kept under observation for 48-hours with normal conditions of twelve-hours of light and twelve-hours of dark at 19-23°C, and 55 ± 10% relative humidity with adequate ventilation. After 48-hours, the mice were euthanised with halothane and the infected areas of the skin were harvested and homogenised in 5mL PBS of pH 7.4. Tissue homogenates were serially diluted in the PBS, 50µL of the homogenised in PBS was spotted on nutrient agar plates and incubated at 37°C for 24-hours. The number of CFU and the CFU/mL were counted and calculated using the equation below:

$$\frac{\text{CFU}}{\text{mL}} = \frac{\text{number of colonies} \times \text{dilution factor}}{\text{volume of a culture plate}} \dots \dots \dots \text{Equation 6}$$

### 2.10.7 Stability studies

To study the stability of the novel drug-loaded quatsomes (VCM-StBAclm-Qt), the samples were sealed in a 50mL vial in the dark after flushing with nitrogen and stored at 4°C and 25 ± 1°C for 30, 60 and 90 days. The stability of the VCM-StBAclm-Qt quatsomes was assessed by observing the MHD, PDI, ζ and DEE % with respect to time.

### 2.11 Statistical analysis of the experiment

The results of the experiments were all determined as mean values standard deviation with statistical analysis performed using GraphPad Prism<sup>®</sup> 6 (GraphPad Software Inc., USA). Data obtained from the MHD, PDI, ζ, DEE %, and the *in vitro* drug release were subjected to one-



way ANOVA and considered statistically significant at  $P$ -value  $< 0.05$  with a 95% significance level.

### 3.0 Results and discussion

#### 3.1 Synthesis and characterisation of StBAclm

The cationic bicephalic pH-responsive surfactant was synthesised in three steps. The first step involved Michael's addition reaction, as described in **Scheme 1**. **Compound 3** was synthesised by drop-wise addition of *tert*-butyl acrylic acid (**Compound 2** to **Compound 1**), and the synthesis was confirmed by  $^1\text{H}$  NMR,  $^{13}\text{C}$  NMR and HR-MS, as shown in **Supplementary material S1**. The appearance of a strong single peak at 1.3711ppm integrating for 18 protons in  $^1\text{H}$  NMR, and the appearance of carbon peaks at  $\delta$  82.1 in  $^{13}\text{C}$  NMR, representing *tert* butylate acrylate, confirmed the formation of **Compound 3**. The second step involved the deprotection of the carboxylic group. Tertiary butyl esters of **Compound 3** were deprotected through cleavage to form StBAclm, using TFA/TIPs (**Supplementary material S2**). The successful synthesis of StBAclm was confirmed by the disappearance of peaks at 1.3711ppm in  $^1\text{H}$  NMR and 82ppm in  $^{13}\text{C}$  NMR. The third step involved the methylation reaction on the amine group. Methyl iodide was added to **Compound 4** to obtain **Compound 5**. The product was confirmed by the appearance of a single peak at 3.2752 ppm  $^1\text{H}$  NMR and 49.8ppm in  $^{13}\text{C}$  NMR and mass spectrometer, respectively (**Supplementary material S3**).

#### 3.2 Cytotoxicity assay

##### 3.2.1 *In vitro* cytotoxicity assay

The determination of cell viability is a significant assay to evaluate the cytotoxicity of biomaterials and nano-systems [66]. The MTT assay is a rapid quantitative procedure based on the transformation of a yellow tetrazolium salt to insoluble purple formazan crystals in the mitochondria of viable cells [58]. **Figures 1A and B** show the bar chart breakdown of the biocompatibility assay of StBAclm and VCM-StBAclm-Qt<sub>1</sub> quatsomes on four different cell lines (A-549, HEK-293, Hep-G2 and MCF-7 cells). The bicephalic surfactant StBAclm demonstrated cell viability of 77.31-95.80%; 78.88-98.05%; 75.93-93.90% and 84.11-92.00% against A-549; HEK-293; Hep-G2 and MCF-7, respectively, across all concentrations from 20 -120 $\mu\text{g}/\text{mL}$ . The VCM-StBAclm-Qt<sub>1</sub> quatsomes demonstrated higher percentage cell viability, from 77.02-88.35% for A-549; 82.25-91.42% for HEK-293; 80.03-91.06% for Hep-G2 and 81.16-85.67% for MCF-7 cell lines across all concentrations of VCM in the quatsomes.

Based on the above results, StBAclm and VCM-StBAclm-Qt<sub>1</sub> quatsomes are considered non-cytotoxic and safe, with greater than 75% cell viability. This result obtained is a preliminary

indication of the non-toxic nature of the novel surfactant and nano-system in all the mammalian cells tested [67]. Therefore, based on these results, the drug-loaded quatsomes (VCM-StBAclm-Qt<sub>1</sub>) could be a suitable vehicle for drug delivery.

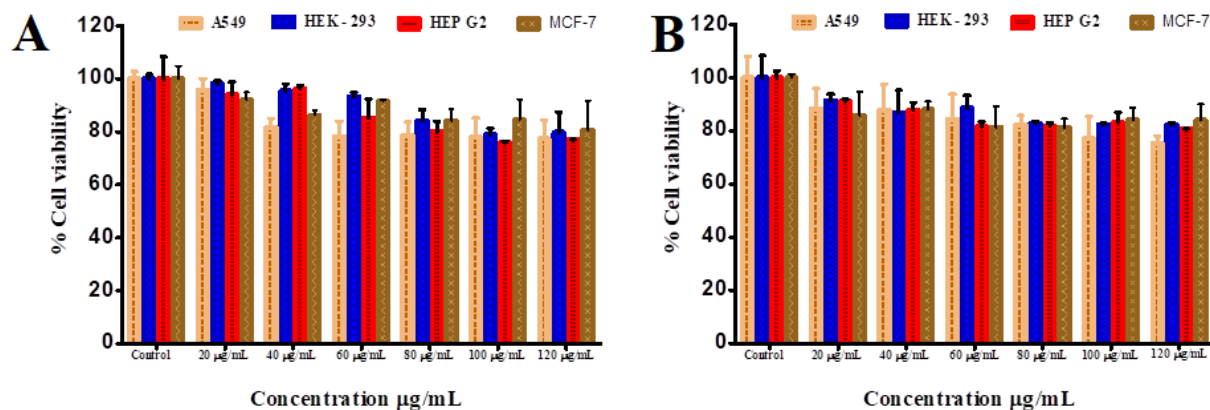


**Figure 1:** A) Percentage cell viability of StBAclm on different cell lines A-549; HEK-293; Hep-G2 and MCF-7; B) Percentage cell viability of VCM-StBAclm-Qt<sub>1</sub> quatsomes on different cell lines A-549; HEK-293; Hep-G2 and MCF-7.

### 3.3 Preparation and characterisation of VCM-StBAclm-Qt<sub>1</sub>

#### 3.3.1 Preparation, characterisation and morphology of VCM-StBAclm-Qt<sub>1</sub> quatsomes

Following the successful synthesis of StBAclm surfactant and the confirmation of its biosafety, its potential to formulate VCM-StBAclm-Qt<sub>1</sub> quatsomes was then investigated. Preliminary studies involving different molar ratios of StBAclm:CHol were screened in order to get an optimal formulation of the quatsomes. The optimised drug-loaded quatsomes (VCM-StBAclm-Qt<sub>1</sub>) had MHD and PDI of  $122.9 \pm 3.78\text{nm}$  and  $0.169 \pm 0.02$ , respectively, at physiological pH 7.4. The MHD values were similar to the sizes of quatsomes that have been previously reported [32, 68]. In contrast, the VCM-StBAclm-Qt<sub>1</sub> quatsomes in the acid environment of pH 6.0 showed an increase in MHD value from  $122.9 \pm 3.78\text{nm}$  to  $145.7 \pm 5.08\text{nm}$ . The VCM-StBAclm-Qt<sub>1</sub> quatsomes demonstrated surface charge switching ( $\zeta$ ) from negative ( $-5.74 \pm 2.57\text{mV}$ ) in physiological pH 7.4 to positive ( $+16.0 \pm 1.59\text{mV}$ ) in acidic environment pH 6.0 (**Supplementary material Table S1**). The DEE% of the VCM-StBAclm-Qt<sub>1</sub> quatsomes was  $45.61 \pm 0.54\%$ , which is higher compared to other previously reported formulated VCM vesicle systems with DEE% of  $28.30 \pm 4.94\%$  [69, 70]. This could be due to the ability of the VCM to partition, both in the lipidic bilayer and aqueous lumen of the quatsomes. Furthermore, the DSC studies showed that the lyophilised quatsomes showed the disappearance of the VCM thermal peak when compared to the physical mixture of the excipients and VCM, thus

indicating a successful encapsulation of VCM (**Supplementary materials S4**). The VCM-StBAclm-Qt<sub>1</sub> quatsomes' morphology, as shown in **Figure 2A**, was observed to be spherical vesicles, containing a thin membrane and an aqueous core, and having a similar MHD size, obtained from dynamic light scattering measurement. This image was similar to other reported quatsomes [24, 71].

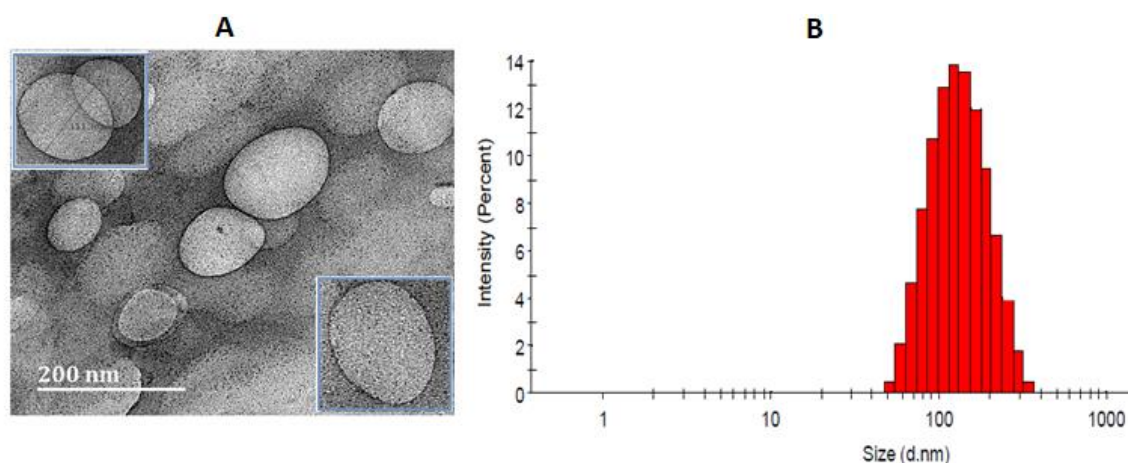


**Figure 2:** A) Morphology of VCM-StBAclm-Qt<sub>1</sub> quatsomes Scale bar: 200nm; B) size distribution of VCM-StBAclm-Qt<sub>1</sub> quatsomes measured using Dynamic Light Scattering (DLS).

### 3.3.2 Effect of change in pH on MHD, and $\zeta$

The effect of pH on size, and surface charge-switching ( $\zeta$ ) was determined at different pHs (7.4, 6.0 and 5.5), as shown in **Figure 3B**. There was an increase in the size of the quatsomes with a decrease in pH. The effect of pH on the  $\zeta$  demonstrated surface charge-switching from negative at physiological pH (pH 7.4) to positive at acidic pH 6.0 and pH 5.5. The charge-switch could be attributed to protonation and deprotonation of the surfactant. At physiological pH, the bicephalic carboxylic groups deprotonated, which neutralised the quaternary charge leaving the surfactant to have an overall negative charge. At acidic pH, the carboxylic groups protonated, gaining a neutral charge; thus, the surfactant gained an overall positive charge due to the positive charge on the quaternary nitrogen. Similar  $\zeta$  was reported for liposomes formulated with stearylamine and dicety phosphate (DCP), a quaternary compound [72].

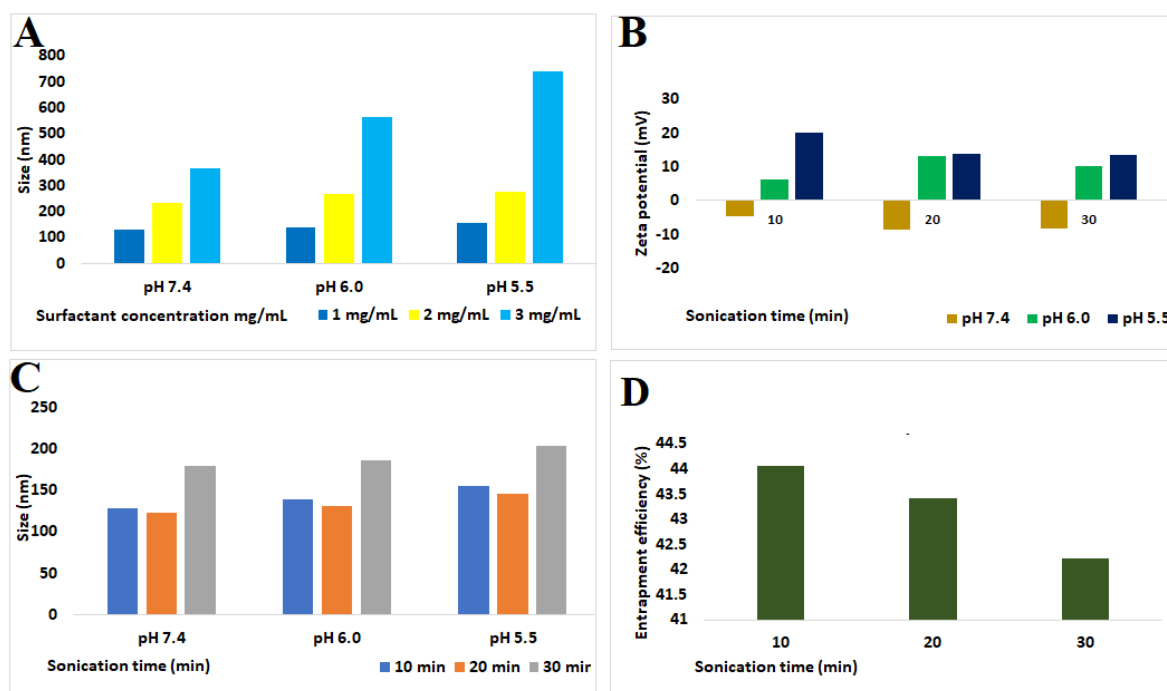


**Figure 3:** Preliminary, optimised characterization of quatsomes. **A)** Effect of novel surfactant (StBAclm) concentration on size at different pHs; **B)** Effect of  $\zeta$  at different pH; demonstrated a notable switch from negative to positive charge with decrease in pH; **C)** Effect of sonication time at different pHs; **D)** Effect of sonication time on DEE%. (n = 3 for all observations).

### 3.3.3 Vancomycin, CHol and StBAclm complex and self-assembly of inserted complexes

The total binding free energy was calculated to gain insight into the binding energetics of vancomycin, cholesterol and surfactant complex. The MM-GBSA program in AMBER was used in calculating the binding free energies by extracting snapshots from the trajectories of the compounds.

**Table 1.** The binding energies (Kcal/mol) for the VCM-CHol-StBAclm computed from the MD trajectories:

Complex	Energy Components (kcal/mol)				
	$\Delta E_{vdW}$	$\Delta E_{elec}$	$\Delta G_{gas}$	$\Delta G_{solv}$	$\Delta G_{bind}$
VCM	-26.44± 0.35	32.98±0.79	6.53 ± 0.76	-26.81± 0.76	-20.27± 0.31
CHol	-15.66± 0.30	-0.91±0.19	-16.58± 0.34	5.02± 0.17	-11.55±0.28
StBAclm	-15.06± 0.50	33.01±0.83	17.94 ±0.99	-30.28± 0.83	-12.33± 0.42

From **Table 1**, it was observed that Van der Waals (VdW) energy played a major role in the binding of the molecules. The last frame (100ns) of the first simulation was taken; the VCM

interacted with CHol and StBAclm complex. This was replicated in order to make six complexes and perform 35ns self-assembly simulations. It was observed that these complexes started to assemble within a few nanoseconds (ns) after simulations (**Figure 4**). Simulation data revealed that at ~15ns three dimers were formed, at 25ns and 35ns two trimers and a hexamer were formed, respectively. There was self-assembling of the complexes throughout the simulation period. At 25ns, two trimers were formed with a hydrophilic component on either side of the trimers (**Figure 4C**). Interestingly, the two trimers fused to form a sort of a bilayer ridge-like structure with hydrophobic portions at the centre forming non-solvent accessible areas, while the hydrophilic groups were seen on the opposite facing water (**Figure 4D**). This could be due to the initial arrangement before assembling into a vesicle. This study indicates the possible steps involved in the formation of the quatsomes.

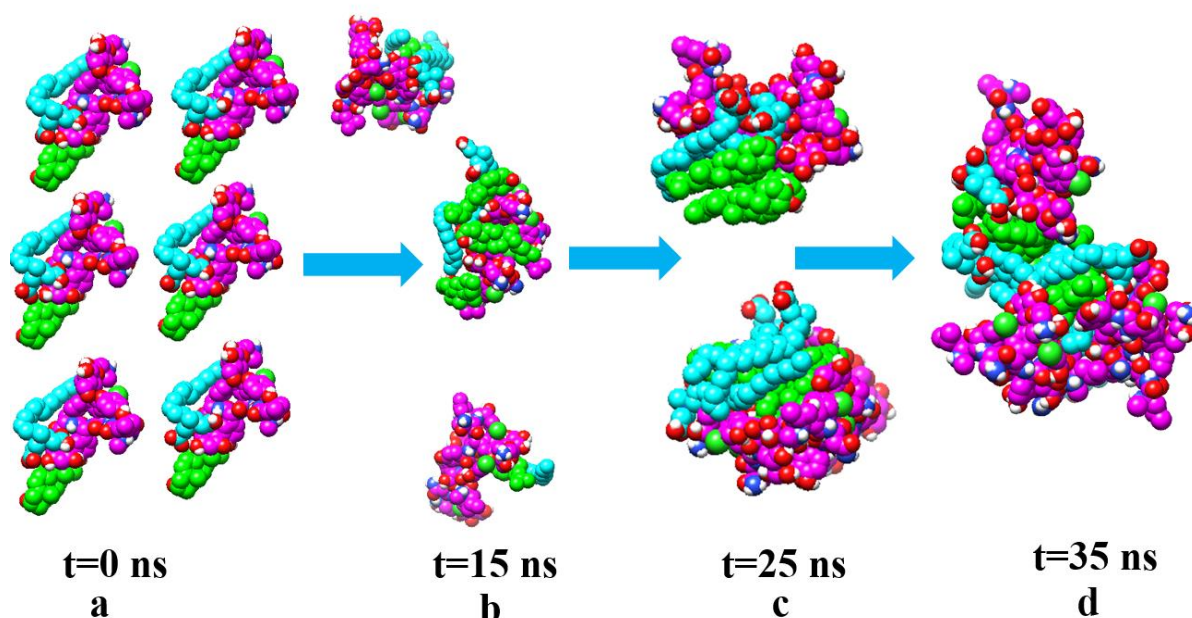


**Figure 4:** Self-assembly simulation at a different time point (a-d). Where purple is VCM, green is CHol and sky blue is StBAclm.

### 3.4 *In vitro* drug release behaviour

The *in vitro* drug release study was carried out in PBS (pH 6.0 and 7.4) at 37°C to investigate the cumulative release profile of VCM from the quatsomes. The cumulative amount of VCM released from VCM-StBAclm-Qt<sub>1</sub> quatsomes was observed to be faster at pH 6.0 compared to pH 7.4 (**Figure 5**). The higher VCM release at pH 6.0 could be due to the protonation and the deprotonation of the amine group in the bicephalic surfactant StBAclm, resulting in the destabilisation of the quatsomes nanosystem [73]. A similar triggered release of methotrexate under acidic conditions was observed for stearylamine-chitosan nanoparticles [74]. The release

profile during this experiment indicated that VCM release from VCM-StBAclm-Qt<sub>1</sub> quatsomes was pH-responsive and showed potential for application in targeting drugs to diseases that thrive in an acidic environment.

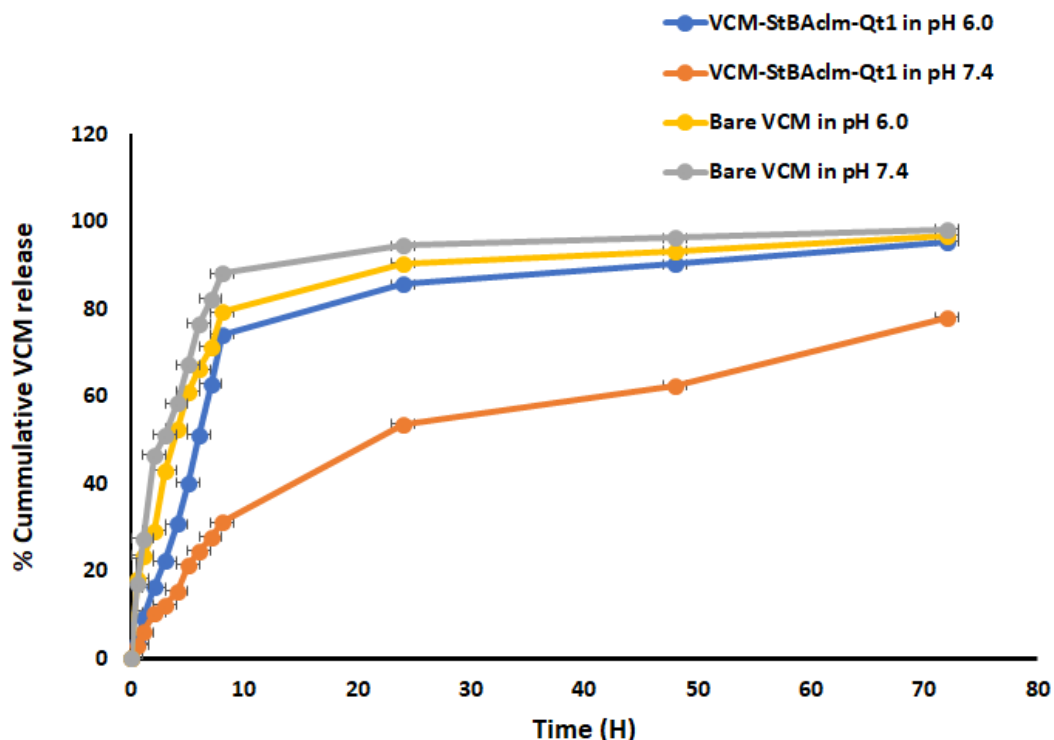


**Figure 5:** Drug release profiles of bare VCM and VCM-StBAclm-Qt<sub>1</sub> quatsomes in different (pH 7.4 and pH 6.0). (Mean  $\pm$  SD, n = 3).

### 3.5 Stability studies

The colloidal stability of the quatsomes indicated no significant change in MHD, PDI,  $\zeta$  and DEE % ( $P > 0.5$ ) over twelve weeks. The results are similar to other reported quatsomes by Ferrer-Tasies *et al.* in 2013, which showed stability with great homogeneity with respect to MHD [24].

**Table 2.** Stability observation on MHD, PDI,  $\zeta$  and DEE% of VCM-StBAclm-Qt<sub>1</sub> quatsomes after twelve weeks of storage.

Time (days)	Room temperature ( $25 \pm 1^\circ\text{C}$ )				$(4 \pm 1^\circ\text{C})$			
	MHD	PDI	$\zeta$ (mV)	DEE%	MHD	PDI	$\zeta$ (mV)	DEE%
0	141.9 $\pm$ 3.78	0.285 $\pm$ 0.04	-5.74 $\pm$ 2.57	52.22 $\pm$ 8.4	141.9 $\pm$ 3.78	0.285 $\pm$ 0.04	-5.74 $\pm$ 2.57	52.22 $\pm$ 8.45
30	145.2 $\pm$ 5.12	0.265 $\pm$ 1.21	-6.12 $\pm$ 1.23	51.24 $\pm$ 5.2	144.3 $\pm$ 2.44	0.242 $\pm$ 0.01	-7.29 $\pm$ 1.45	52.02 $\pm$ 5.21
60	143.4 $\pm$ 6.77	0.275 $\pm$ 2.41	-5.86 $\pm$ 2.41	51.65 $\pm$ 6.4	140.2 $\pm$ 3.21	0.251 $\pm$ 0.03	-6.12 $\pm$ 1.25	51.53 $\pm$ 4.32
90	144.1 $\pm$ 6.92	0.264 $\pm$ 1.03	-5.88 $\pm$ 3.10	52.01 $\pm$ 3.8	142.3 $\pm$ 2.22	0.263 $\pm$ 1.02	-6.12 $\pm$ 1.25	51.24 $\pm$ 3.01

### 3.6 MIC determination

The antimicrobial activity of VCM-StBAclm-Qt<sub>1</sub> quatsomes and bare VCM were studied against MRSA. The minimum inhibitory concentration (MICs) for bare VCM at both pH values was constant against MRSA (31.25 µg/mL). In contrast, VCM-StBAclm-Qt<sub>1</sub> quatsomes showed lower MICs values of 0.97 µg/mL at acidic pH 6.0, compared to the physiological pH 7.4 with 3.90 µg/mL against MRSA, as shown in **Table 3**. The VCM-StBAclm-Qt<sub>1</sub> quatsomes had an 8-fold and 32-fold antimicrobial activity enhancement against MRSA at physiological pH 7.4 and acidic pH 6.0, respectively, when compared to bare VCM. The VCM-StBAclm-Qt<sub>1</sub> quatsomes at pH 6.0 had a 4-fold antibacterial activity enhancement against MRSA compared to VCM-StBAclm-Qt<sub>1</sub> quatsomes at physiological pH 7.4. The enhanced activity at pH 6.0 could be due to the small MHD and pH-responsiveness of the quatsomes. This might have produced an excellent surface-area-to-volume ratio, thus leading to a proper distribution of the quatsomes on the surface of the bacteria [75]. Furthermore, enhanced activity of the quatsomes against MRSA could be due to the quatsomes enhancing the transport of the drug into the thick peptidoglycan layer of MRSA. The ability of the quatsomes to enhance the transport of the drug through the peptidoglycan layer might have prevented VCM ion trapping, which is the main resistance mechanism of MRSA to bare VCM [76-78]. Another proposed reason for the improved antimicrobial activity at acidic pH could be due to the concentrated release of the drug on the bacterial membrane as the system breaks down at acidic pH, thus releasing the drug in lethal concentrations to effectively eliminate the bacteria. These results showed the enhanced efficiency of the novel quatsomes at acidic pH compared to physiological pH conditions, thus indicating its potential for targeting bacteria that thrive in environments with low pH.

**Table 3.** MICs values of bare VCM, StBAclm-Qt<sub>1</sub> and VCM-StBAclm-Qt<sub>1</sub> quatsomes against MRSA at pH 6.0 and pH 7.4.

Time (h)	<i>In vitro</i> antibacterial activity at pH 6.0			pH 7.4		
	24	48	72	24	48	72
	MRSA (MIC µg/mL)			MRSA (MIC µg/mL)		
Bare VCM	31.25	31.25	31.25	31.25	31.25	31.25
StBAclm-Qt	125	125	125	250	250	250
VCM-StBAclm-Qt <sub>1</sub>	0.97	0.97	0.97	3.90	3.90	3.90
<i>All values are expressed as mean ± SD (n = 3)</i>						



### 3.7 Bactericidal time assay of VCM-StBAclm-Qt<sub>1</sub> quatsomes

From the antibacterial studies, it was established that the time of bactericidal effect of VCM-StBAclm-Qt<sub>1</sub> quatsomes could efficiently eliminate MRSA. Therefore, bacterial killing kinetic studies were performed to determine the killing kinetics of bare VCM and VCM-StBAclm-Qt<sub>1</sub> towards MRSA. **Figure 6A** presents time killing rates of bacteria by VCM and VCM-StBAclm-Qt<sub>1</sub> quatsomes when exposed to MRSA at 5 × MIC of each treatment over a period of 24-hours incubation at 37°C. The killing kinetics of bare VCM was similar to reports in the literature [52]. The VCM-StBAclm-Qt<sub>1</sub> quatsomes eliminated almost 100% of MRSA within 8-hours of the procedure. The shorter time taken to reduce the MRSA population by VCM-StBAclm-Qt<sub>1</sub> quatsomes could be an indication that the quatsomes system can be used for a shorter treatment course, compared to bare VCM.

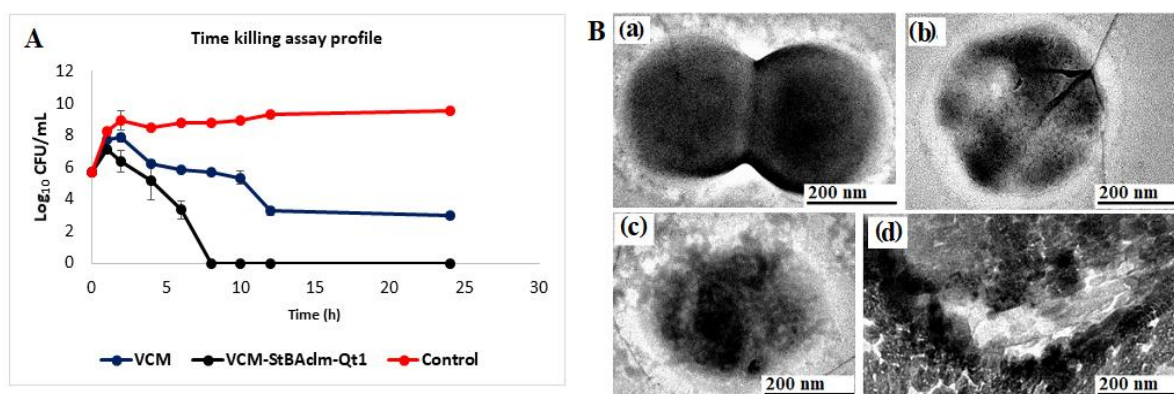


**Figure 6:** **A**) Killing kinetics of MRSA exposed to 5 x MIC of VCM-StBAclm-Qt<sub>1</sub> quatsomes, VCM, bacterial in PBS 7.4 (positive control) and sterile water (negative control) at different time intervals (n = 3); **B**) (a) HR-TEM images of MRSA bacteria exposed to water, (b) HR-TEM images of VM, (c-d) HR-TEM images of MRSA treated with VCM-StBAclm-Qt<sub>1</sub> quatsomes (5× MICs) showing the membrane disruption that occurred after 1-hour incubation, pores on bacterial membrane after treatment and total loss of MRSA cell membrane after 4-hours of VCM-StBAclm-Qt<sub>1</sub> quatsomes treatment. These arrows shows the damaged cytoplasmic membrane exposure to VCM-StBAclm-Qt<sub>1</sub> quatsomes.

### 3.8 Mechanistic studies of VCM-StBAclm-Qt<sub>1</sub> quatsomes

#### 3.8.1 Bacterial membrane disruption

The effect of VCM-StBAclm-Qt<sub>1</sub> quatsomes on the membrane of MRSA was determined by incubating MRSA with our novel VCM-StBAclm-Qt<sub>1</sub> quatsomes for approximately 5-hours. **Figure 6B(c)** shows the perforation of the MRSA cell wall, which demonstrated the effectiveness of the VCM-StBAclm-Qt<sub>1</sub> quatsomes' killing ability **Figure 6B (c and d)**.



Subsequently, after 5-hours of treatment with the VCM-StBAclm-Qt<sub>1</sub> quatsomes, a total loss of bacteria cell wall was observed, demonstrating an effective membrane disruption ability against MRSA, as shown in **Figure 6B (d)**. The interaction of the VCM-StBAclm-Qt<sub>1</sub> quatsomes with the MRSA could be due to the antibacterial activity of quaternary bicephalic surfactant, which resulted in effective delivery of the VCM which led to bacteria membrane disruption. This result correlates with the MICs and killing kinetics studies, which showed effective killing and clearance of bacteria by the VCM-StBAclm-Qt<sub>1</sub> quatsomes. This study revealed the possible mechanism of the quatsomes in the elimination of bacteria.

### **3.8.2 Fluorescence-activated cell sorting (FACS) cell viability**

Cell viability of MRSA was further evaluated by using fluorescence-activated cell sorting (FACS) techniques and MRSA was incubated with bare VCM and VCM-StBAclm-Qt<sub>1</sub> quatsomes at their respective MICs. Under environmental stress conditions, several pathogens enter into a viable but not cultivable state. Thus, a plate-counts method may overestimate viability efficiency by not detecting reversible, viable damaged bacterial cells [79]. The MICs study showed that the VCM-StBAclm-Qt<sub>1</sub> quatsomes reduced the MIC of VCM by 8-fold. The lowering of the MIC could result in vegetative forms of bacteria which could give negative results using the plate-count method [80]. FACS tends to solve this problem by effectively separating the dead cells from viable cells by using cell permeant and non-cell permeant dyes. **Figure 7A** shows the flow cytometry results of bare VCM and VCM-StBAclm-Qt<sub>1</sub> quatsomes. The killing percentage of VCM-StBAclm-Qt<sub>1</sub> quatsomes against MRSA cells after incubation was similar to VCM (**Figure 7A**) at their respective MICs, despite having an 8-fold lower concentration. These results demonstrated that, even with the reduction of the MIC of VCM by incorporation into the quatsomes, the system efficiently killed the bacteria without turning the bacteria into a viable but non-cultivable state. This state has been attributed to the development of resistant strains when the bacteria are exposed to sublethal concentrations. The lowering of the MIC value of VCM shows the translational potential of this system without compromising the therapeutic effect of the loaded drug. This could lead to a reduction in the dose-dependent side effects of VCM, such as nephrotoxicity and Redman syndrome [81].

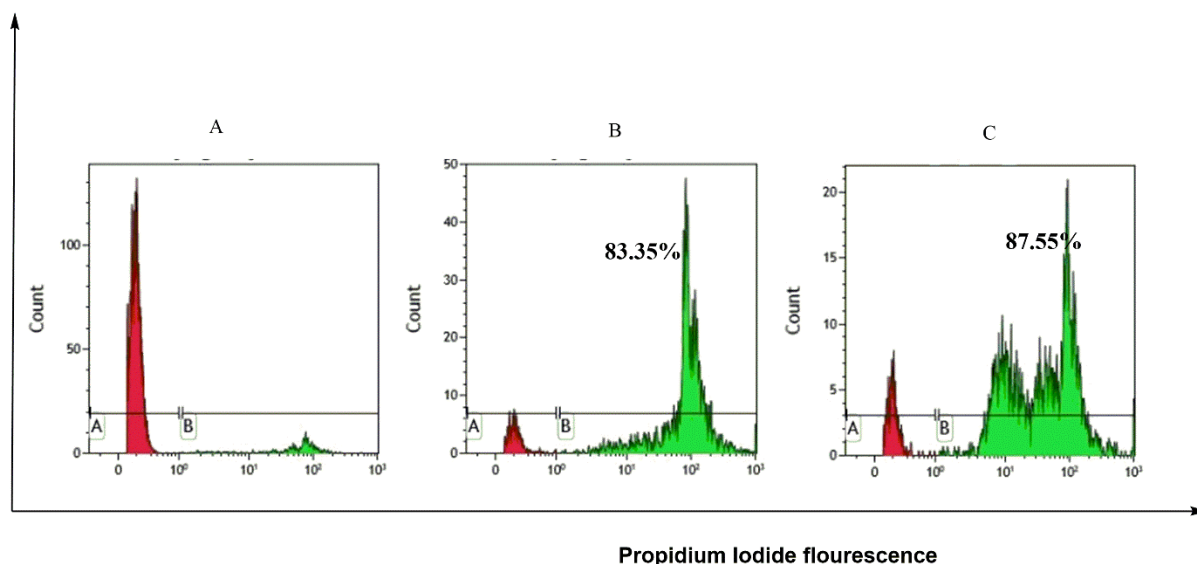


**Figure 7:** Red colour represents the gate for alive MRSA cells while the Green colour represents the gate for dead cells in the population. Flow cytometry PI emission intensity plot) **A)** Histogram plot of the control group showing live MRSA cells; **B)** Histogram plots percentage uptake of dead MRSA cells when treated with bare VCM; **C)** Histogram plot showing percentage uptake of dead MRSA cells when treated VCM-StBAclm-Qt<sub>1</sub> quatsomes.

### 3.8.3 Biofilm eradication of VCM-StBAclm-Qt<sub>1</sub> quatsomes using fluorescence microscopy

Fluorescence microscopy was also used to investigate the quatsomes' ability to eliminate biofilms. Biofilms are microbial communities attached to surfaces and encased in a protective extracellular polymeric substances (EPS) matrix of microbial origin [82, 83]. An EPS matrix acts as a biofilm protective barrier that prevents antimicrobial drugs from penetration, thereby protecting the bacteria cells. A four-days, fully mature MRSA biofilm was grown on a coverslip, treated with bare VCM and VCM-StBAclm-Qt<sub>1</sub> quatsomes and further investigated and analysed using fluorescence microscopy. The biofilms were stained with 1mL of a solution containing 30µL each of PI and Syto9. The samples were kept in the dark for 30-minutes, followed by washing with sterilised water; and then the coverslips were inverted on the glass slides (**Figure 8**). Cell permeating dye (Syto9) revealed high intensity due to the intact membrane of cells on the coverslip of the untreated samples [119, 120]. However, no fluorescence intensity was observed for PI dye as it cannot penetrate intact cell membrane and the EPS matrix (**Figure 8A**). Biofilms treated with bare VCM showed Syto9 intensity and PI fluorescence demonstrating VCM had a level of penetration into the biofilm protective EPS matrix, thus reaching the protected MRSA cells (**Figure 8B**).

When the biofilms were treated with VCM-StBAclm-Qt<sub>1</sub> quatsomes, there was an increased red fluorescence due to PI penetration and interacting with the DNA of the MRSA cells (**Figure**

**8C).** The higher PI fluorescence emittance observed for biofilms treated with VCM-StBAclm-Qt<sub>1</sub> indicated that quatsomes could penetrate or destroy the EPS matrix of the biofilm, thus reaching MRSA cells. Upon reaching the MRSA cells, the membranes of the cells were destroyed, resulting in the intercalation of PI with the DNA, as observed in an increased PI fluorescence. This indicates that VCM-StBAclm-Qt<sub>1</sub> quatsomes disrupted the biofilms and MRSA cell membrane, which led to higher PI penetration and DNA. These results, therefore, demonstrated that VCM-StBAclm-Qt<sub>1</sub> quatsomes is a system with the potential to eliminate bacteria biofilms from devices such as respirators [84]; catheters (central venous, urinary); prosthetic heart valves; orthopaedic devices [85]; and surgical and dental implants [86].

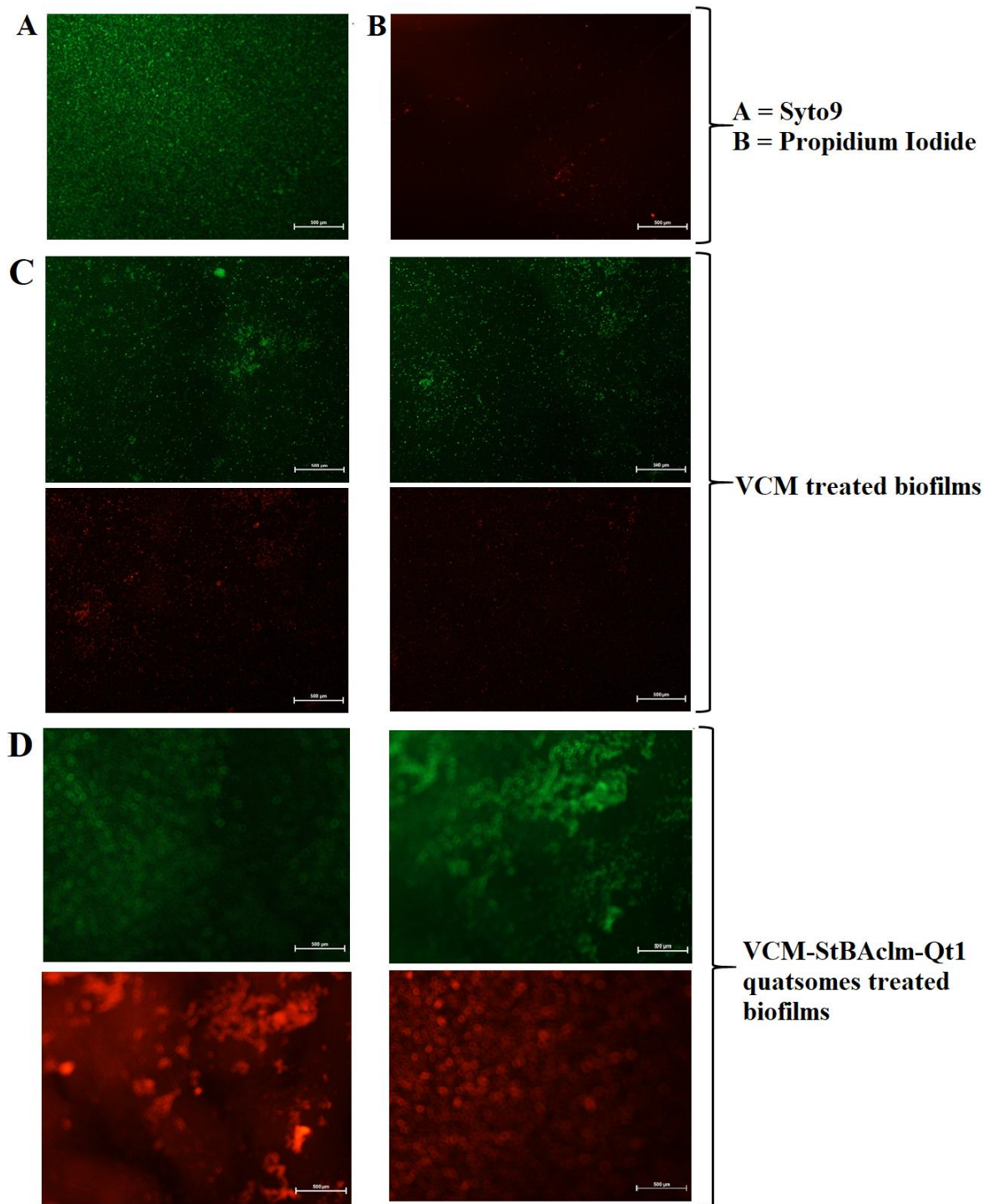


**Figure 8:** Fluorescence microscopy images of MRSA biofilm: **A)** Untreated biofilms stained with Syto9; **B)** Untreated biofilms stained with Syto9 and Propidium Iodide; **C)** VCM treated and **D)** VCM-StBAclm-Qt<sub>1</sub> quatsomes treated showing internalisation in the biofilms. (scale bar = 500µm).

### 3.9 Molecular antibacterial studies

#### 3.9.1 Bacterial cell membrane permeability in terms of relative electric conductivity

MRSA cell membrane is composed of lipids and proteins, and they are important factors in cell membrane integrity, stability, and permeability. Cell membrane disruption causes leakage of cellular substance, which leads to cell death. Disruption of the bacterial cell membrane can also lead to leakage of intracellular electrolytes, leading to increased conductivity [87]. To explore the interactions between the quatsomes and cell membrane, against MRSA cells electrical conductivity was measured to investigate bacterial cell disruption. The results from the electrical conductivity of VCM-StBAclm-Qt<sub>1</sub> quatsomes showed an increase from  $0.357 \pm 0.02$  to  $0.487 \pm 0.01 \text{ mS cm}^{-1}$ , when compared to bare VCM treatment (**Table 4** and **Figure 9A**). This corresponds to a 1.36-fold increment in the electrical conductivity when compared to the bare VCM group ( $P < 0.05$ ). The rise in the electrical conductivity could be due to the displacement of the membrane lipids by quatsomes [88-91]. Maintaining ion homeostasis is paramount to the proper cell function of the bacteria, including solute transport, metabolic regulation, control of turgor pressure, motility of cell and energy creation. Changes in the structural integrity of the cell membrane can affect metabolism and lead to cell death [92, 93]. The increase in conductivity displayed in this study implies that MRSA cell membrane was destroyed. This led to electrolytic leakage, causing an increase in electrical conductivity, thus leading to cell lysis [94].

**Table 4.** The analysis of MRSA cell membrane permeability after treatment with bare VCM and VCM-StBAclm-Qt<sub>1</sub> quatsomes.

Parameters	Control	Bare VCM	VCM-StBAclm-Qt <sub>1</sub> quatsomes
Electrical conductivity ( $\text{mS cm}^{-1}$ )	$0.321 \pm 0.01$	$0.35 \pm 0.02$	$0.487 \pm 0.01$
DNA concentration ( $\mu\text{g} \cdot \text{mL}^{-1}$ )	$17.00 \pm 0.49$	$4.30 \pm 0.08$	$2.08 \pm 0.040$
Protein concentration ( $\mu\text{g} \cdot \text{mL}^{-1}$ )	$158.6 \pm 8.54$	$98.1 \pm 4.88$	$75.94 \pm 4.10$

*Values are expressed as mean  $\pm$  SD.*

#### 3.9.2 Leakage of proteins and VCM-StBAclm-Qt<sub>1</sub> quatsomes analysis

Protein plays an essential role in the physiological metabolism of bacteria. The disruption of the membrane results in the loss of membrane integrity, which leads to the leakage of essential proteins responsible for MRSA cell survival [95]. As shown in **Figure 9B**, the DNA concentration of MRSA treated with VCM-StBAclm-Qt<sub>1</sub> quatsomes was significantly decreased from  $4.3 \pm 0.08 \mu\text{g} \cdot \text{mL}^{-1}$  to  $2.08 \pm 0.040 \mu\text{g} \cdot \text{mL}^{-1}$  (2-fold decrease), compared to bare

VCM. The one-way ANOVA showed significant differences in the protein leakage, with a  $P$  value  $< 0.001$  among all the groups. The VCM-StBAclm-Qt<sub>1</sub> quatsomes might have caused the increase in membrane permeability by destroying the cell membrane, leading to the leakage of cellular substance. This result showed that VCM-StBAclm-Qt<sub>1</sub> quatsomes had a greater impact on the bacterial membrane, which led to DNA leakage [96]. This implies that, even at low concentrations of VCM in the VCM-StBAclm-Qt<sub>1</sub>, it was more effective compared to bare VCM. Thus, this suggests that the quatsomes can potentially serve as a drug delivery system with effective and low therapeutic doses requirement.

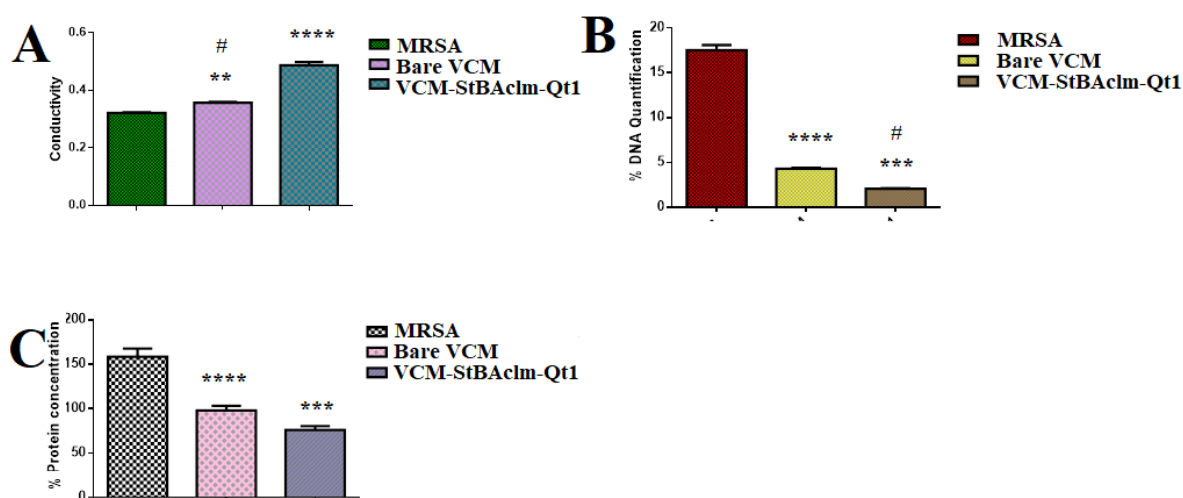


**Figure 9:** **A)** Electrical conductivity of bare VCM and VCM-StBAclm-Qt<sub>1</sub> quatsomes. \*\* denote statistical significance of bare VCM compared to MRSA (control): \*\*\*\* denotes statistical significance of bare VCM compared to VCM-StBAclm-Qt<sub>1</sub> quatsomes, and # denoted when VCM-StBAclm-Qt<sub>1</sub> quatsomes was compared to MRSA (control); **B)** Reduction of DNA quantification of bare VCM and VCM-StBAclm-Qt<sub>1</sub> quatsomes. \*\*\*\* denote statistical significance of bare VCM compared to MRSA (control): \*\*\* denotes statistical significance of bare VCM compared to VCM-StBAclm-Qt<sub>1</sub> quatsomes, and # denoted when VCM-StBAclm-Qt<sub>1</sub> quatsomes was compared to MRSA (control); **C)** Reduction of protein quantification bare VCM and VCM-StBAclm-Qt<sub>1</sub> quatsomes. \*\*\*\* denote statistical significance of bare VCM compared to MRSA (control): \*\*\* denotes statistical significance of bare VCM compared to VCM-StBAclm-Qt<sub>1</sub> quatsomes.

### 3.10 *In vivo* antibacterial activity

As a proof of the efficacy of VCM-StBAclm-Qt<sub>1</sub> quatsomes in animal systems, *in vivo* studies were conducted using BALB/c a mice skin infection model. The colony-forming unit (CFUs)

numbers from each treatment group were evaluated and represented as  $\log_{10}$  (**Figure 10**). The one-way ANOVA showed significant differences in CFUs among all the groups with a *P value* = 0.001. The mean MRSA load ( $\log_{10}$  CFU) obtained from the groups treated with VCM-StBAclm-Qt<sub>1</sub> quatsomes, bare VCM and untreated groups were 2.3010 (200 CFU/mL);  $4.40 \pm 0.05$  ( $25333 \pm 3055$  CFU/mL); and  $5.528 \pm 0.014$  ( $338000 \pm 11135$  CFU/mL), respectively. The mice groups treated with bare VCM had significantly reduced MRSA burden in their skin samples (126.67-fold) when compared to the untreated groups (*P value* = 0.001). On the other hand, VCM-StBAclm-Qt<sub>1</sub> quatsomes significantly decreased the MRSA burden in the skin samples by 1690-fold, when compared to the untreated groups. Furthermore, groups treated with VCM-StBAclm-Qt<sub>1</sub> quatsomes had significantly reduced MRSA burden (13.34-fold) in the mice skin samples when compared to bare VCM treated groups. This result is in agreement with other *in vivo* studies that involved the use of antibiotics such as streptomycin, gentamicin and doxycycline nanoplexes against bacterial infections [97, 98]. The observation from this study revealed the significant potential of VCM quatsomes in combating MRSA infections.

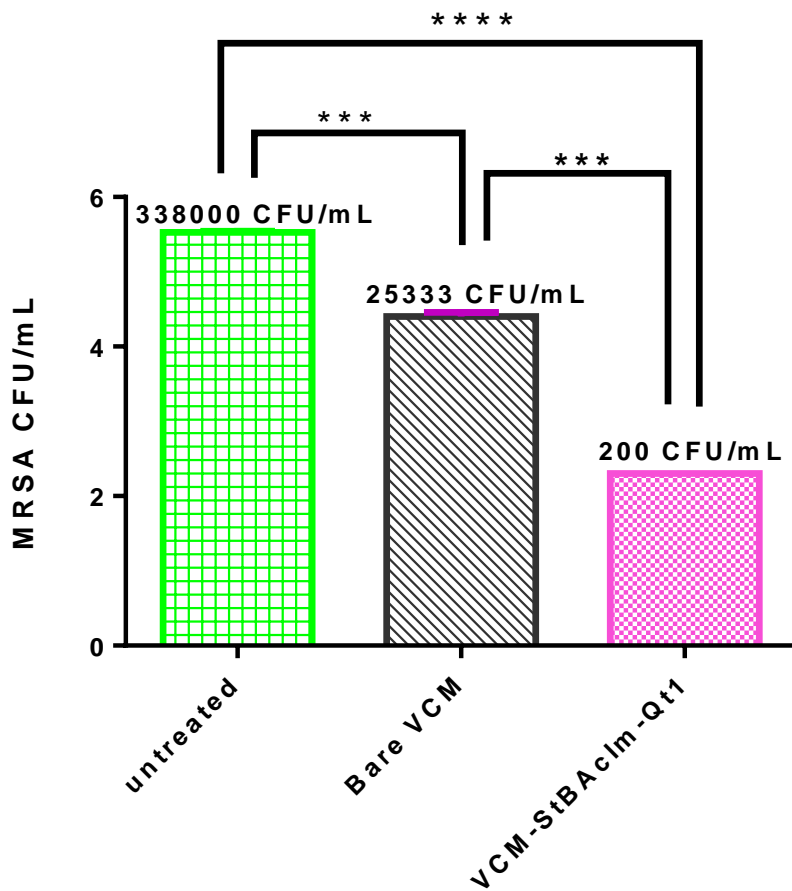


**Figure 10:** MRSA CFU evaluation post 48-hour of treatment (mean  $\pm$  SD) (n=3). \*\*\* denotes the significant difference between the bare VCM vs VCM-StBAclm-Qt<sub>1</sub> quatsomes and VCM vs Untreated groups. \*\*\*\* denotes the significant difference between VCM-StBAclm-Qt<sub>1</sub> quatsomes vs Untreated groups.



#### 4.0 Conclusions

Due to the diminishing antimicrobial activity of VCM against MRSA, effective and efficient treatment is urgently needed to combat the widespread infections globally. In this research, a novel quaternary bicephalic surfactant (StBAclm) was synthesised and used in formulating pH-responsive quatsomes (VCM-StBAclm-Qt<sub>1</sub>) by electrostatic interaction for the delivery and antibacterial enhancement against MRSA. The StBAclm structure, and the biosafety activity were confirmed. The VCM-StBAclm-Qt<sub>1</sub> quatsomes demonstrated smaller MHD, higher DEE and DLC%, as well as a fast and sustained release of VCM at the acidic environment of pH 6.0, compared to physiological pH 7.4. The molecular modelling simulation (MDS) studies demonstrated self-assembly formation of the quatsomes. *In vitro* antibacterial studies of the quatsomes against MRSA revealed the enhanced antimicrobial activity of quatsomes compared to bare VCM. The results from the *in vitro* antimicrobial activity was further confirmed by flow cytometry, time-killing assay and biofilm studies. This further showed a better antimicrobial effect of the quatsomes at 8-fold lower concentrations when compared to bare VCM. The quatsomes also displayed the ability to eliminate MRSA biofilms. The *in vivo* studies using the BALB/c mice-infected model revealed that the treatment of MRSA infections with VCM-StBAclm-Qt<sub>1</sub> quatsomes significantly decreased the MRSA burden compared to the treatment with bare VCM. The pH-responsiveness, biosafety and antimicrobial activity of the novel pH-responsive VCM-StBAclm-Qt<sub>1</sub> quatsomes confirmed its potential for application as a promising novel nano-drug carrier for antibiotics.

**Conflict of interest**

The authors declare no conflict of interest.

**Acknowledgement**

The authors acknowledge the College of Health Sciences, University of KwaZulu-Natal (UKZN), UKZN Nanotechnology Platform, National Research Foundation of South Africa (Grant No. 87790 and 88453) for financial support. The Microscopy and Microanalysis Unit, Biomedical Resource Unit, Department of Human Physiology and Flow Cytometry Research Laboratory at UKZN, CHPC (Cape Town) for supercomputing resources are acknowledged.

## References

- [1] J.R. Rohr, C.B. Barrett, D.J. Civitello, M.E. Craft, B. Delius, G.A. DeLeo, P.J. Hudson, N. Jouanard, K.H. Nguyen, R.S. Ostfeld, Emerging human infectious diseases and the links to global food production, *Nat. Sust.*, 2 (2019) 445-456.
- [2] M. D. Ryckera, B. Baragaña, S.L. Duceb, I.H. Gilberta, Challenges and recent progress in tropical disease drug discovery, *Nature.*, 559 (2018) 498-506.
- [3] S.A. Ahmed, E. Bariş, D.S. Go, H. Lofgren, I. Osorio-Rodarte, K. Thierfelder, Assessing the global poverty effects of antimicrobial resistance, *World Devel.*, 111 (2018) 148-160.
- [4] C.P. Harkins, B. Pichon, M. Doumith, J. Parkhill, H. Westh, A. Tomasz, H. D Lencastre, S.D. Bentley, A.M. Kearns, M.T. Holden, Methicillin-resistant *Staphylococcus aureus* emerged long before the introduction of methicillin into clinical practice, *Gen. Bio.*, 18 (2017) 130-140.
- [5] S.R. Ritchie, K.J. Jayanatha, E.J. Duffy, J. Chancellor, Z. Allport, M.G. Thomas, Previous antibiotic-related adverse drug reactions do not reduce expectations for antibiotic treatment of upper respiratory tract infections, *J. Glo. Ant. Res.*, 10 (2017) 256-260.
- [6] L. Lin, X. Mao, Y. Sun, H. Cui, Antibacterial mechanism of artemisinin/beta-cyclodextrins against Methicillin-resistant *Staphylococcus aureus* (MRSA), *Micro. Path.*, 118 (2018) 66-73.
- [7] N. Andreatos, F. Shehadeh, E.E. Pliakos, E. Mylonakis, The impact of antibiotic prescription rates on the incidence of MRSA bloodstream infections: A county-level, US-wide analysis, *Inter. J. Ant. Agents.*, 52 (2018) 195-200.
- [8] H. Iqbal, N. Ponniah, S. Long, N. Rath, M. Kent, Review of MRSA screening and antibiotics prophylaxis in orthopaedic trauma patients; The risk of surgical site infection with inadequate antibiotic prophylaxis in patients colonized with MRSA, *Injury.*, 48 (2017) 1382-1387.
- [9] K. Govender, S. Sharma, W. Jessee, K. Nagaraju, N.J. Pearse, P. Chhetri, E.M. Bodenstab, P. Yu, S.C. Srinivas, Leadership and Task Shifting to Address the Challenges of Antimicrobial Resistance in South Africa, *Asian J. Pharm. Res. Health Care.*, 10 (2018) 10-20.
- [10] L.J. Shallcross, S.J. Howard, T. Fowler, S.C. Davies, Tackling the threat of antimicrobial resistance: from policy to sustainable action, *Philo. Trans. Royal Soc. B: Bio. Sci.*, 370 (2015) p20140082.
- [11] B. Spellberg, The future of antibiotics, *Crit. Care*, 18 (2014) 228-234.
- [12] S. Ramanavičius, R. Žalnėravičius, G. Niaura, A. Drabavičius, A. Jagminas, Shell-dependent antimicrobial efficiency of cobalt ferrite nanoparticles, *Nano. Stru. Nano Obj.*, 15 (2018) 40-47.

- [13] X. Jiang, J. Li, M. Ding, H. Tan, Q. Ling, Y. Zhong, Q. Fu, Synthesis and degradation of nontoxic biodegradable waterborne polyurethanes elastomer with poly ( $\epsilon$ -caprolactone) and poly (ethylene glycol) as soft segment, *Eur. Polymer J.*, 43 (2007) 1838-1846.
- [14] Y. Wen, S. Pan, X. Luo, X. Zhang, W. Zhang, M. Feng, A biodegradable low molecular weight polyethylenimine derivative as low toxicity and efficient gene vector, *Biocon. Chem.*, 20 (2009) 322-332.
- [15] S. Honary, P. Ebrahimi, R. Hadianamrei, Optimization of particle size and encapsulation efficiency of vancomycin nanoparticles by response surface methodology, *Pharm. Devel. Tech.*, 19 (2014) 987-998.
- [16] G. Tiwari, R. Tiwari, B. Sriwastawa, L. Bhati, S. Pandey, P. Pandey, S.K. Bannerjee, Drug delivery systems: An updated review, *Inter. J. Pharm. Investig.*, 2 (2012) 2-11.
- [17] S. Bamrungsap, Z. Zhao, T. Chen, L. Wang, C. Li, T. Fu, W. Tan, Nanotechnology in therapeutics: A focus on nanoparticles as a drug delivery system, *Nanomed.*, 7 (2012) 1253-1271.
- [18] S.A. Agnihotri, N.N. Mallikarjuna, T.M. Aminabhavi, Recent advances on chitosan-based micro-and nanoparticles in drug delivery, *J. Contr. Rel.*, 100 (2004) 5-28.
- [19] M.H. Xiong, Y. Bao, X.Z. Yang, Y.H. Zhu, J. Wang, Delivery of antibiotics with polymeric particles, *Adv. Drug Delivery Reviews*, 78 (2014) 63-76.
- [20] D. Hassan, C.A. Omolo, R. Gannimani, A.Y. Waddad, C. Mocktar, S. Rambharose, N. Agrawal, T. Govender, Delivery of novel vancomycin nanoplexes for combating methicillin resistant *Staphylococcus aureus* (MRSA) infections, *Inter. J. Pharm.*, 558 (2019) 143-156.
- [21] C.A. Omolo, R.S. Kalhapure, M. Jadhav, S. Rambharose, C. Mocktar, V.M. Ndesendo, T. Govender, Pegylated oleic acid: A promising amphiphilic polymer for nano-antibiotic delivery, *Euro. J. Pharm. Biopharm.*, 112 (2017) 96-108.
- [22] S.M. Barros, S.K. Whitaker, P. Sukthankar, L.A. Avila, S. Gudlur, M. Warner, E.I. Beltrao, J.M. Tomich, A review of solute encapsulating nanoparticles used as delivery systems with emphasis on branched amphipathic peptide capsules, *Arch. Biochem. Biophys.*, 596 (2016) 22-42.
- [23] D.G. Fatouros, D.A. Lamprou, A.J. Urquhart, S.N. Yannopoulos, I.S. Vizirianakis, S. Zhang, S. Koutsopoulos, Lipid-like self-assembling peptide nanovesicles for drug delivery, *ACS Appl. Mat. Inter.*, 6 (2014) 8184-8189.
- [24] L. Ferrer Tasies, E. Moreno Calvo, M. Cano Sarabia, M. Aguilera Arzo, A. Angelova, S. Lesieur, S. Ricart, J. Faraudo, N. Ventosa, J. Veciana, Quatsomes: Vesicles formed by self-assembly of sterols and quaternary ammonium surfactants, *Langmuir.*, 29 (2013) 6519-6528.

- [25] F. Caboi, M. Monduzzi, Didodecyldimethylammonium bromide vesicles and lamellar liquid crystals. A multinuclear NMR and optical microscopy study, *Langmuir.*, 12 (1996) 3548-3556.
- [26] M. Antonietti, S. Förster, Vesicles and liposomes: A self-assembly principle beyond lipids, *Adv. Mat.*, 15 (2003) 1323-1333.
- [27] T. Elkin, S.M. Copp, R.L. Hamblin, J.S. Martinez, G.A. Montaña, R.C. Rocha, Synthesis of terpyridine-terminated amphiphilic block copolymers and their self-assembly into metallo-polymer nanovesicles, *Materials.*, 12 (2019) 601-610.
- [28] S.S. Yadavalli, Q. Xiao, S.E. Sherman, W.D. Hasley, M.L. Klein, M. Goulian, V. Percec, Bioactive cell-like hybrids from dendrimersomes with a human cell membrane and its components, *Proc. Nat. Acad. Sci.*, 116 (2019) 744-752.
- [29] I.O. Lebedeva, E.B. Zhulina, O.V. Borisov, Self-assembly of linear-dendritic and double dendritic block copolymers: From dendromicelles to dendrimersomes, *Macromolecules.*, (2019) 3655-3667.
- [30] J.M. Tomich, E. Wessel, J. Choi, L.A. Avila, Nonviral Gene Therapy: Peptiplexes, in: *Nucl. Acid Nanoth.*, Elsevier, 2019, pp. 247-276.
- [31] Y.L. Lin, H.Y. Chang, Y.J. Sheng, H.K. Tsao, Structural and mechanical properties of polymersomes formed by rod-coil diblock copolymers, *Soft Matter.*, 9 (2013) 4802-4814.
- [32] N. Thomas, D. Dong, K. Richter, M. Ramezanpour, S. Vreugde, B. Thierry, P.J. Wormald, C.A. Prestidge, Quatsomes for the treatment of *Staphylococcus aureus* biofilm, *J. Mat. Chem. B*, 3 (2015) 2770-2777.
- [33] N. Ventosa, I. Cabrera, J. Veciana, H. Santana, E. Martinez, J. Berlanga, Vesicles comprising epidermal growth factor and compositions that contain them, *Cuban Patent Appl. CU*, 112 (2012) 2012.
- [34] B. Gumí Audenis, S. Illa Tuset, N. Grimaldi, L. Pasquina Lemonche, L. Ferrer Tasies, F. Sanz, J. Veciana, I. Ratera, J. Faraudo, N. Ventosa, Insights into the structure and nanomechanics of a quatsome membrane by force spectroscopy measurements and molecular simulations, *Nanoscale*, 10 (2018) 23001-23011.
- [35] R.S. Kalhapure, D.R. Sikwal, S. Rambharose, C. Mocktar, S. Singh, L. Bester, J.K. Oh, J. Renukuntla, T. Govender, Enhancing targeted antibiotic therapy via pH responsive solid lipid nanoparticles from an acid cleavable lipid, *Nano.: Nanotech., Bio. Med.*, 13 (2017) 2067-2077.
- [36] Y. Wang, J. Fang, D. Cheng, Y. Wang, X. Shuai, A pH-sensitive micelle for codelivery of siRNA and doxorubicin to hepatoma cells, *Polymer.*, 55 (2014) 3217-3226.

- [37] Q. Wang, H. Jiang, Y. Li, W. Chen, H. Li, K. Peng, Z. Zhang, X. Sun, Targeting NF- $\kappa$ B signaling with polymeric hybrid micelles that co-deliver siRNA and dexamethasone for arthritis therapy, *Biomater.*, 122 (2017) 10-22.
- [38] N. Liu, J. Han, X. Zhang, Y. Yang, Y. Liu, Y. Wang, G. Wu, pH-responsive zwitterionic polypeptide as a platform for anti-tumor drug delivery, *Coll. Surf. B: Biointer.*, 145 (2016) 401-409.
- [39] E.F. Pettersen, T.D. Goddard, C.C. Huang, G.S. Couch, D.M. Greenblatt, E.C. Meng, T.E. Ferrin, UCSF Chimera-A visualization system for exploratory research and analysis, *J. Comput. Chem.*, 25 (2004) 1605-1612.
- [40] Y. Shao, L.F. Molnar, Y. Jung, J. Kussmann, C. Ochsenfeld, S.T. Brown, A.T. Gilbert, L.V. Slipchenko, S.V. Levchenko, D.P. O'Neill, Advances in methods and algorithms in a modern quantum chemistry program package, *Phy. Chem. Phys.*, 8 (2006) 3172-3191.
- [41] J.P. Ryckaert, G. Ciccotti, H.J. Berendsen, Numerical integration of the cartesian equations of motion of a system with constraints: molecular dynamics of n-alkanes, *J. Comput. Phys.*, 23 (1977) 327-341.
- [42] D.A. Case, T.E. Cheatham III, T. Darden, H. Gohlke, R. Luo, K.M. Merz Jr, A. Onufriev, C. Simmerling, B. Wang, R.J. Woods, The Amber biomolecular simulation programs, *J. Comput. Chem.*, 26 (2005) 1668-1688.
- [43] D.R. Roe, T.E. Cheatham III, PTRAJ and CPPTRAJ: Software for processing and analysis of molecular dynamics trajectory data, *J. Chem. Theory Comput.*, 9 (2013) 3084-3095.
- [44] E. Seifert, Originpro 9.1: Scientific data analysis and graphing software-Software review, in, *J. Chem. Inf. Model*, 2014, pp. 1552-1552.
- [45] K. Raha, K.M. Merz Jr, Calculating binding free energy in protein-ligand interaction, *Ann. Reports Comput. Chem.*, 1 (2005) 113-130.
- [46] M. Ylilauri, O.T. Pentikäinen, MMGBSA as a tool to understand the binding affinities of filamin-peptide interactions, *J. Chem. Inform. Modeling*, 53 (2013) 2626-2633.
- [47] T. Hou, J. Wang, Y. Li, W. Wang, Assessing the performance of the MM/PBSA and MM/GBSA methods. 1. The accuracy of binding free energy calculations based on molecular dynamics simulations, *J. Chem. Inform. Modeling*, 51 (2010) 69-82.
- [48] S.J. Sonawane, R.S. Kalhapure, S. Rambharose, C. Mocktar, S.B. Vepuri, M. Soliman, T. Govender, Ultra-small lipid-dendrimer hybrid nanoparticles as a promising strategy for antibiotic delivery: *In vitro* and *in silico* studies, *Inter. J. Pharm.*, 504 (2016) 1-10.
- [49] X. Cheng, H. Yan, X. Jia, Z. Zhang, Preparation and *in vivo/in vitro* evaluation of formononetin phospholipid/vitamin E TPGS micelles, *J. Drug Target.*, 24 (2016) 161-168.

- [50] J.H. Jorgensen, J.D. Turnidge, Susceptibility test methods: Dilution and disk diffusion methods, in: *Manual Clinical Microbiology*, Eleventh Edition, Ame. Soc. Microbio., 2015, pp. 1253-1273.
- [51] L.B. Reller, M. Weinstein, J.H. Jorgensen, M.J. Ferraro, Antimicrobial susceptibility testing: A review of general principles and contemporary practices, *Clin. Infect. Dis.*, 49 (2009) 1749-1755.
- [52] M.F. Mohamed, M.I. Hamed, A. Panitch, M.N. Seleem, Targeting methicillin-resistant *Staphylococcus aureus* with short salt-resistant synthetic peptides, *Anti. Agents Chemoth.*, 58 (2014) 4113-4122.
- [53] H. Cui, H. Zhou, L. Lin, The specific antibacterial effect of the Salvia oil nanoliposomes against *Staphylococcus aureus* biofilms on milk container, *Food Cont.*, 61 (2016) 92-98.
- [54] N. Chauhan, A.K. Tyagi, P. Kumar, A. Malik, Antibacterial potential of jatropha curcas synthesized silver nanoparticles against food borne pathogens, *Front. Microbio.*, 7 (2016) 1748-1761.
- [55] A. Bexfield, A.E. Bond, E.C. Roberts, E. Dudley, Y. Nigam, S. Thomas, R.P. Newton, N.A. Ratcliffe, The antibacterial activity against MRSA strains and other bacteria of a < 500Da fraction from maggot excretions/secretions of *Lucilia sericata* (Diptera: Calliphoridae), *Microbes Infect.*, 10 (2008) 325-333.
- [56] N.K. Shrestha, N.M. Scalera, D.A. Wilson, G.W. Procop, Rapid differentiation of methicillin-resistant and methicillin-susceptible *Staphylococcus aureus* by flow cytometry after brief antibiotic exposure, *J. Clin. Microbio.*, 49 (2011) 2116-2120.
- [57] D.J. Arndt-Jovin, T.M. Jovin, Fluorescence labeling and microscopy of DNA, *Methods Cell Bio.*, 30 (1989) 417-448.
- [58] A.T. Ogunjimi, S.M. Melo, C.G. Vargas-Rechia, F.S. Emery, R.F. Lopez, Hydrophilic polymeric nanoparticles prepared from Delonix galactomannan with low cytotoxicity for ocular drug delivery, *Carbohydr. Polymers*, 157 (2017) 1065-1075.
- [59] N.M. O'Brien-Simpson, N. Pantarat, T.J. Attard, K.A. Walsh, E.C. Reynolds, A rapid and quantitative flow cytometry method for the analysis of membrane disruptive antimicrobial activity, *PloS One*, 11 (2016) e0151694.
- [60] M. Rüger, G. Bensch, R. Tüngler, U. Reichl, A flow cytometric method for viability assessment of *Staphylococcus aureus* and *Burkholderia cepacia* in mixed culture, *Cytomet. Part A*, 81 (2012) 1055-1066.

- [61] S. Renggli, W. Keck, U. Jenal, D. Ritz, Role of autofluorescence in flow cytometric analysis of *Escherichia coli* treated with bactericidal antibiotics, *J. Bacter.*, 195 (2013) 4067-4073.
- [62] M. Fittipaldi, A. Nocker, F. Codony, Progress in understanding preferential detection of live cells using viability dyes in combination with DNA amplification, *J. Microbio. Methods.*, 91 (2012) 276-289.
- [63] F. Berlutti, A. Frioni, T. Natalizi, F. Pantanella, P. Valenti, Influence of sub-inhibitory antibiotics and flow condition on *Staphylococcus aureus* ATCC 6538 biofilm development and biofilm growth rate: Bio timer assay as a study model, *J. Antibiotics*, 67 (2014) 763.
- [64] E. Kugelberg, T. Norström, T.K. Petersen, T. Duvold, D.I. Andersson, D. Hughes, Establishment of a superficial skin infection model in mice by using *Staphylococcus aureus* and *Streptococcus pyogenes*, *Anti. Agents Chemoth.*, 49 (2005) 3435-3441.
- [65] R.S. Kalhapure, M. Jadhav, S. Rambharose, C. Mocktar, S. Singh, J. Renukuntla, T. Govender, pH-responsive chitosan nanoparticles from a novel twin-chain anionic amphiphile for controlled and targeted delivery of vancomycin, *Coll. Surf. B: Biointer.*, 158 (2017) 650-657.
- [66] Ö.S. Aslantürk, *In vitro* cytotoxicity and cell viability assays: Principles, advantages, and disadvantages, InTech, , 2018.
- [67] N. Gharaati Far, M.R. Tohidkia, A. Dehnad, Y. Omid, Efficiency and cytotoxicity analysis of cationic lipids-mediated gene transfection into AGS gastric cancer cells, *Artif. Cells, Nanomed. Biotechnol.*, 46 (2018) 1001-1008.
- [68] L. Ferrer-Tasies, E. Moreno-Calvo, M. Cano-Sarabia, M. Aguilera-Arzo, A. Angelova, S. Lesieur, S. Ricart, J. Faraudo, N. Ventosa, J. Veciana, Quasomes: vesicles formed by self-assembly of sterols and quaternary ammonium surfactants, *Langmuir*, 29 (2013) 6519-6528.
- [69] J.M. Unagolla, A.C. Jayasuriya, Drug transport mechanisms and *in vitro* release kinetics of vancomycin encapsulated chitosan-alginate polyelectrolyte microparticles as a controlled drug delivery system, *Eur. J. Pharm. Sci.*, 114 (2018) 199-209.
- [70] T. Cerchiara, A. Abruzzo, R.A.Ñ. Palomino, B. Vitali, R. De Rose, G. Chidichimo, L. Ceseracciu, A. Athanassiou, B. Saladini, F. Dalena, Spanish Broom (*Spartium junceum* L.) fibers impregnated with vancomycin-loaded chitosan nanoparticles as new antibacterial wound dressing: Preparation, characterization and antibacterial activity, *Eur. J. Pharm. Sci.*, 99 (2017) 105-112.



- [71] S.J. Sonawane, R.S. Kalhapure, M. Jadhav, S. Rambharose, C. Mocktar, T. Govender, Transforming linoleic acid into a nanoemulsion for enhanced activity against methicillin susceptible and resistant *Staphylococcus aureus*, RSC Adv., 5 (2015) 90482-90492.
- [72] C.D. Kaur, M. Nahar, N.K. Jain, Lymphatic targeting of zidovudine using surface-engineered liposomes, J. Drug Target., 16 (2008) 798-805.
- [73] C. Mao, X. Xie, X. Liu, Z. Cui, X. Yang, K. Yeung, H. Pan, P.K. Chu, S. Wu, The controlled drug release by pH-sensitive molecularly imprinted nanospheres for enhanced antibacterial activity, Mat. Sci. Eng.: C, 77 (2017) 84-91.
- [74] D.R. Nogueira, L. Tavano, M. Mitjans, L. Pérez, M.R. Infante, M.P. Vinardell, *In vitro* antitumor activity of methotrexate via pH-sensitive chitosan nanoparticles, Biomaterials., 34 (2013) 2758-2772.
- [75] C.A. Omolo, R.S. Kalhapure, N. Agrawal, S. Rambharose, C. Mocktar, T. Govender, Formulation and molecular dynamics simulations of a fusidic acid nanosuspension for simultaneously enhancing solubility and antibacterial activity, Mol. Pharm., 15 (2018) 3512-3526.
- [76] I. Gheorghe, M. Popa, L.G. Măruțescu, Molecular features of virulence and resistance mechanisms in nosocomial and community-acquired *Staphylococcus aureus*, in: *Staphylococcus aureus*, IntechOpen, 2018.
- [77] A. de Souza Monteiro, W.R.N. Neto, A.R.S. Mendes, B.L. dos Santos Pinto, L.C.N. da Silva, G.F. Ferreira, Effects of alterations in *Staphylococcus aureus* cell membrane and cell wall in antimicrobial resistance, in: *The Rise of Virulence and Antibiotic Resistance in Staphylococcus aureus*, IntechOpen, 2017.
- [78] C. Kehrenberg, S. Schwarz, L. Jacobsen, L.H. Hansen, B. Vester, A new mechanism for chloramphenicol, florfenicol and clindamycin resistance: methylation of 23S ribosomal RNA at A2503, Mol. Microb., 57 (2005) 1064-1073.
- [79] M. Rosenberg, N.F. Azevedo, A. Ivask, Propidium iodide staining underestimates viability of adherent bacterial cells, Sci. Reports, 9 (2019) 6483.
- [80] X. Zhao, J. Zhong, C. Wei, C.W. Lin, T. Ding, Current perspectives on viable but non-culturable state in foodborne pathogens, Front. Microbio., 8 (2017) 580.
- [81] K. Fukushima, A. Okada, Y. Hayashi, H. Ichikawa, A. Nishimura, N. Shibata, N. Sugioka, Enhanced oral bioavailability of vancomycin in rats treated with long-term parenteral nutrition, SpringerPlus, 4 (2015) 442.
- [82] T.R. Garrett, M. Bhakoo, Z. Zhang, Bacterial adhesion and biofilms on surfaces, Prog. Nat. Sci., 18 (2008) 1049-1056.

- [83] P. Bogino, M. Oliva, F. Sorroche, W. Giordano, The role of bacterial biofilms and surface components in plant-bacterial associations, *Inter. J. Mol. Sci.*, 14 (2013) 15838-15859.
- [84] S. Parasion, M. Kwiatek, R. Gryko, L. Mizak, A. Malm, Bacteriophages as an alternative strategy for fighting biofilm development, *Pol. J. Microbiol.*, 63 (2014) 137-145.
- [85] P. Stoodley, G.D. Ehrlich, P.P. Sedghizadeh, L. Hall Stoodley, M.E. Baratz, D.T. Altman, N.G. Sotereanos, J.W. Costerton, P. DeMeo, Orthopaedic biofilm infections, *Cur. Orthop. Pract.*, 22 (2011) 558.
- [86] M. Alhag, S. Renvert, I. Polyzois, N. Claffey, Re-osseointegration on rough implant surfaces previously coated with bacterial biofilm: An experimental study in the dog, *Cli. Oral Impl. Res.*, 19 (2008) 182-187.
- [87] Z.H. Li, M. Cai, Y.S. Liu, P.L. Sun, S.L. Luo, Antibacterial activity and mechanisms of essential oil from *Citrus medica* L. var. *sarcodactylis*, *Molecules*, 24 (2019) 1577.
- [88] A. Van Holle, M.D. Machado, E.V. Soares, Flocculation in ale brewing strains of *Saccharomyces cerevisiae*: Re-evaluation of the role of cell surface charge and hydrophobicity, *Appl. Microbio. Biotech.*, 93 (2012) 1221-1229.
- [89] M. Cristani, M. D'Arrigo, G. Mandalari, F. Castelli, M.G. Sarpietro, D. Micieli, V. Venuti, G. Bisignano, A. Saija, D. Trombetta, Interaction of four monoterpenes contained in essential oils with model membranes: Implications for their antibacterial activity, *J. Agri. Food Chem.*, 55 (2007) 6300-6308.
- [90] G. Rukholm, C. Mugabe, A.O. Azghani, A. Omri, Antibacterial activity of liposomal gentamicin against *Pseudomonas aeruginosa*: A time-kill study, *Inter. J. Ant. Agents*, 27 (2006) 247-252.
- [91] L.H. Lin, L.W. Lee, S.Y. Sheu, P.Y. Lin, Study on the stevioside analogues of steviolbioside, steviol, and isosteviol 19-alkyl amide dimers: synthesis and cytotoxic and antibacterial activity, *Chem. Pharm. Bulletin*, 52 (2004) 1117-1122.
- [92] M. Sadiq, J. Tarning, T. Aye Cho, A. Anal, Antibacterial activities and possible modes of action of *Acacia nilotica* (L.) Del. against multidrug-resistant *Escherichia coli* and *Salmonella*, *Molecules*, 22 (2017) 47.
- [93] W.R. Diao, Q.-P. Hu, H. Zhang, J.-G. Xu, Chemical composition, antibacterial activity and mechanism of action of essential oil from seeds of fennel (*Foeniculum vulgare* Mill.), *Food Contr.*, 35 (2014) 109-116.
- [94] L. Xu, X. Xu, G. Yuan, Y. Wang, Y. Qu, E. Liu, Mechanism of Azalomycin F5a against Methicillin-Resistant *Staphylococcus aureus*, *BioMed Res. Inter.*, 2018 (2018).

- [95] S. Finger, C. Wiegand, H.J. Buschmann, U.C. Hipler, Antimicrobial properties of cyclodextrin-antiseptics-complexes determined by microplate laser nephelometry and ATP bioluminescence assay, *Int. J. Pharm.*, 436 (2012) 851-856.
- [96] A. Gajewicz, N. Schaeublin, B. Rasulev, S. Hussain, D. Leszczynska, T. Puzyn, J. Leszczynski, Towards understanding mechanisms governing cytotoxicity of metal oxides nanoparticles: Hints from nano-QSAR studies, *Nanotox.*, 9 (2015) 313-325.
- [97] M.N. Seleem, N. Jain, N. Pothayee, A. Ranjan, J. Riffle, N. Sriranganathan, Targeting *Brucella melitensis* with polymeric nanoparticles containing streptomycin and doxycycline, *FEMS Microb. Letters*, 294 (2009) 24-31.
- [98] A. Ranjan, N. Pothayee, M. Seleem, N. Jain, N. Sriranganathan, J. Riffle, R. Kasimanickam, Drug delivery using novel nanoplexes against a *Salmonella* mouse infection model, *J. Nanopar. Res.*, 12 (2010) 905-914.

## CHAPTER FIVE: CONCLUSION

### 5.1 General conclusions

Despite significant progress in antibiotics usage over the past century, infectious diseases remain a major cause of morbidity and mortality in developed and developing countries. Majority of infectious bacterial pathogens have developed multiple resistance to different classes of antibiotics. Hence, the demand for novel materials to deliver and enhance current available antibiotics across bacterial membranes to counteract antimicrobial agents resistance and improve their efficacy through the help of nanotechnology is urgently needed. Therefore, this study aimed to utilise high molecular weight polymer (dextran sulfate sodium salt), design and synthesise novel materials of zwitterionic pH-responsive lipid (OLA) and quaternary bicephalic surfactant (StBAclm) and explore their potential for delivery and enhancement of antibiotics to combat infectious diseases. The research study aims were, therefore to i) explore the potential of delivering antimicrobial drug (vancomycin) through nanoplex formulated with high molecular weight dextran sulfate sodium salt, ii) synthesise a novel zwitterionic pH-responsive lipid (OLA) and explore its potential for the formulation of a novel chitosan-based pH-responsive lipid- polymer hybrid vancomycin nanovesicles (VM-OLA-LPHVs1) for delivery of vancomycin against MRSA, and iii) synthesise a novel quaternary bicephalic surfactant (StBAclm) and explore its potential to the formulate pH-responsive quatsomes (VCM-StBAclm-Qt) for enhanced activity of antibiotic (vancomycin) against Methicillin-Resistant *Staphylococcus aureus* (MRSA).

The main conclusions generated from these research data are summarised below:

#### **Aim 1:**

- A novel vancomycin nanoplex was successfully formulated using high molecular weight dextran sulfate sodium salt.
- Cytotoxicity studies on three different mammalian cell lines. These including adenocarcinoma alveolar basal epithelial cells (A-549), liver hepatocellular carcinoma (Hep-G2), and human embryonic kidney cells 293 (HEK-293) revealed the novel vancomycin nanoplex to be non-cytotoxic.
- The *in silico* simulations showed spontaneous self-aggregation of the VCM-DXT<sub>5</sub> nanoplex in the presence of sodium salt, with interaction energy between the two monomers being  $-146.07 \pm 4.92$  kJ/mol, and Van der Waals interactions playing a major role for the aggregates' stability. The *in silico* experiments explained the

stability of the nanovesicles and the arrangement of VCM-DXT<sub>5</sub> nanoplex that led to the formation of unique ultra-small vesicles.

- The VCM-DXT<sub>5</sub> nanoplex exhibited size, PDI and ZP of  $84.6 \pm 4.24\text{nm}$ ,  $0.449 \pm 0.024$ ,  $-33.0 \pm 4.87\text{mV}$  respectively, with the complexation efficiency being  $90.4 \pm 0.77\%$  and drug loading capacity of  $62.3 \pm 0.23\%$ . The VCM-DXT<sub>5</sub> nanoplex release from the drug-loaded nanovesicles was found to be sustained, with a 65.8% release throughout 48-hours.
- The *in vitro* antibacterial test revealed that the drug-loaded nanovesicles had a 6.24-fold lower minimum inhibitory concentration (MIC) against MRSA compared to the free drug.
- The flow cytometry study showed 67% bactericidal killing effect against MRSA population by the VCM-DXT<sub>5</sub> nanoplex when compared to 32.98% by the bare VCM at drug MIC of  $1.25\mu\text{g/mL}$ .
- The *in vivo* studies using BALB/c mouse skin infection model revealed that nanoplexes reduced MRSA burden by 2.3-folds compared to bare VCM. The novel nanoplexes have the potential to be a promising delivery system to combat MRSA infections for improved treatment of bacterial infections.

## **Aim 2:**

- A novel zwitterionic pH-responsive lipid (OLA) was synthesised and the structure confirmed using <sup>1</sup>H NMR, <sup>13</sup>C NMR, FT-IR, and HR-MS.
- Biocompatibility studies of the novel OLA and the novel chitosan-based pH-responsive vancomycin lipid-polymer hybrid nanovesicles (VM-OLA-LPHVs1) performed using MTT assay on four different cell lines: adenocarcinoma alveolar basal epithelial cells (A-549), liver hepatocellular carcinoma cell-lines (Hep-G2), human embryonic kidney cells 293 (HEK-293), and human breast cancer cell line (MCF-7) confirmed the biocompatibility of OLA and VM-OLA-LPHVs1 nanovesicles.
- The result of the *in vitro* cytotoxicity study revealed cell viability of above 75% in all cell lines when exposed to OLA and VM-OLA-LPHVs1, thus indicating their biosafety.
- The VM-OLA-LPHVs1 had a ( $D_H$ ), polydispersity index (PDI), and EE% of  $198.0 \pm 14.04\text{ nm}$ ,  $0.137 \pm 0.02$ , and  $45.61 \pm 0.54\%$  respectively at physiological pH, with surface-charge ( $\zeta$ ) switching from negative at pH 7.4 to positive at pH

6.0. The encapsulation efficiency and the drug loading capacity were found to be  $45.61 \pm 0.54\%$  and  $8.92 \pm 2.34\%$ , respectively. The *in vitro* VM release of the nanovesicles was faster at acidic pH compared to the physiological pH 7.4. With 97% release after 72-hours demonstrating the pH-responsiveness of the VM-OLA-LPHVs1 nanovesicles.

- The VM release from the VM-OLA-LPHVs1 was faster at pH 6.0 compared to physiological pH, with 97% release after 72-hours. The VM-OLA-LPHVs1 had lower minimum inhibitory concentration (MIC) value of  $0.59\mu\text{g/mL}$  at pH 6.0 compared to  $2.39\mu\text{g/mL}$  at pH 7.4 against MRSA with 52.9-fold antibacterial enhancement.
- The *in vitro* antibacterial studies against Methicillin-resistant *Staphylococcus aureus* (MRSA) showed lower MICs of  $0.59\mu\text{g/mL}$  at pH 6.0 compared to  $2.39\mu\text{g/mL}$  at pH 7.4 with 52.9-fold antibacterial enhancement compared the bare VM.
- The flow cytometry study revealed that VM-OLA-LPHVs1 had higher bactericidal efficacy on MRSA compared to bare VM, despite an 8-fold lower VM concentration in the nanovesicles indicating the eradication of MRSA biofilms.
- Additionally, fluorescence microscopy study showed the ability of the VM-OLA-LPHVs1 to eliminate biofilms. The electrical conductivity, and protein/DNA concentration increased and decreased respectively when compared to treatment with bare VM, which indicated greater MRSA membrane damage.
- The *in vivo* studies in BALB/c mouse infected skin model treated with VM-OLA-LPHVs1 revealed 95-fold lower MRSA burden compared to the group treated with bare VM. These findings suggest that OLA can be used as an effective novel material for complexation with biodegradable polymer chitosan (CHs) to form pH-responsive VM-OLA-LPHVs1 nanovesicles which show greater potential for enhancement and improvement of bacterial infections treatment.

### **Aim 3:**

- A novel quaternary bicephalic surfactant (StBAclm) was synthesised, and the structure was confirmed using  $^1\text{H}$  NMR,  $^{13}\text{C}$  NMR, FT-IR, and HR-MS.
- Biocompatibility studies of the novel quaternary bicephalic surfactant (StBAclm) and the formulated pH-responsive quatsomes (VCM-StBAclm-Qt1) was

performed using MTT assay on four different cell lines: adenocarcinoma alveolar basal epithelial cells (A-549), liver hepatocellular carcinoma (Hep-G2), human embryonic kidney cells (HEK-293) and human breast cancer (MCF-7) cell lines. The results confirmed the biocompatibility and non-cytotoxic nature of the StBAclm and VCM-StBAclm-Qt1 quatsomes.

- The StBAclm was employed in the formulation of the quaternary bicephalic pH-responsive vancomycin-loaded quatsomes. The formulated VCM loaded nanovesicles were found to have a mean hydrodynamic diameter (MHD), and PDI of  $122.9 \pm 3.78$  nm, and  $0.169 \pm 0.02$  at pH 7.4 respectively. The VCM-StBAclm-Qt1 quatsomes revealed to have a surface charge switching from negative to positive at pH 7.4 and pH 6.0, respectively. The observed mean hydrodynamic diameter (MHD) changes and surface charge switching at different pH indicated the pH-responsiveness of the quatsomes and could be considered for effective drug delivery at the acidic environment (pH 6.0). The *in vitro* VCM release from the quatsomes was faster at acidic pH 6.0 compared to the physiological pH 7.4.
- The minimum inhibitory concentration (MIC) of the VCM-StBAclm-Qt1 quatsomes against MRSA was 32-fold and 8-fold lower in pH 6.0 and pH 7.4 respectively compared to bare VCM demonstrating the pH-responsiveness of the quatsomes.
- The VCM-StBAclm-Qt1 demonstrated higher electrical conductivity and decreased protein and deoxyribonucleic acid (DNA) concentration which confirmed greater MRSA membrane damage compared to treatment with bare VCM.
- The flow cytometry study showed that the quatsomes had a similar bactericidal killing effect on MRSA despite a lower (8-fold) VCM concentration when compared to the treatment with bare VCM. Fluorescence microscopy revealed the ability of the VCM-StBAclm-Qt1 to clear MRSA biofilms.
- The *in vivo* studies in a skin infection of the mice model showed that quatsomes treated groups had a 13.34-fold decrease in MRSA CFUs when compared to the bare VCM treated groups. This study indicated the potential of pH-responsive quatsomes as an effective delivery system for antibiotics.

The findings of these studies, therefore, confirmed that the newly synthesised materials are biocompatible for biomedical applications and their potential to develop novel nano-drug delivery systems, which enhanced the antibacterial activity of the antibiotics

against MRSA. Furthermore, the studies also converted vancomycin into a nanoplex suspension, nanovesicles and quatsomes. The nano-drug systems reported in this study include VCM-DXT<sub>5</sub> nanoplex, VM-OLA-LPHVs1 nanovesicles and VCM-StBAclm-Qt1 quatsomes for vancomycin enhancement and treatment of infections caused by MRSA.

## **5.2 Significance of the findings in the study**

The newly designed and synthesised material VCM-DXT<sub>5</sub> nanoplex, chitosan-based pH-responsive vancomycin-loaded lipid-polymer hydride nanovesicles (VM-OLA-LPHVs1) and quaternary bicephalic quatsomes (VCM-StBAclm-Qt1) were successfully formulated. These nano-systems were formulated to address, combat the limitations and antibacterial resistance associated with conventional dosage forms of antibiotics. The significance of the findings in these studies include the following:

**New pharmaceutical products:** Novel materials nanoplexes, OLA and StBAclm, were synthesised. This will expand the pool of available pharmaceutical excipient for preparing novel medicines to combat infectious diseases. These studies introduced three novel pharmaceutical products VCM-DXT<sub>5</sub> nanoplex, chitosan-based pH-responsive lipid polymer hydride nanovesicles (VM-OLA-LPHVs1) and quaternary bicephalic vancomycin-loaded pH-responsive quatsomes (VCM-StBAclm-Qt1) quatsomes. With this, local pharmaceutical industries can be stimulated for cost-effective, superior medicines manufacturing.

**Improved patient therapy and disease treatment:** The newly designed VCM-DXT<sub>5</sub> nanoplex chitosan-based pH-responsive lipid-polymer hydride nanovesicles (VM-OLA-LPHVs1) and quaternary bicephalic vancomycin-loaded pH-responsive quatsomes (VCM-StBAclm-Qt1) were formulated to improve patients' therapy and combat infectious diseases caused by MRSA. The novel nanosystems lowered drug MIC significantly. These could lead to the lowering of treatment doses and dosages without affecting therapeutic outcomes. Therefore, these findings prove the potential of these nanosystems in improving patient therapy and treatment of infectious diseases.

**Creation of new knowledge to the scientific community:** The various nanosystems findings have contributed to the pharmaceutical sciences knowledge database. These include the following:



- New knowledge in the synthesis, characterisation, determination of the biocompatibility and hemolytic profile of the OLA and StBAclm was generated. The properties of the nanoplex and the drug-loaded nanosystem (VM-OLA-LPHVs1 and VCM-StBAclm-Qt1) were utilised using various *in vitro*, *in silico*, and *in vivo* techniques.
- *In silico* studies and the spontaneous binding between the vancomycin and dextran sulfate sodium salt was successfully identified. The effect of chitosan-based pH-responsive lipid-polymer hydride nanovesicles VM-OLA-LPHVs1 and quaternary bicephalic vancomycin-loaded pH-responsive quatsomes VCM-StBAclm-Qt1 binding unto the model bacterial membrane was identified.
- Formulation parameters and processes of VCM-DXT<sub>5</sub> nanoplex, chitosan-based pH-responsive lipid-polymer hydride nanovesicles (VM-OLA-LPHVs1) and quaternary bicephalic vancomycin-loaded pH-responsive quatsomes (VCM-StBAclm-Qt1) were identified using various experimental *in vitro* and *in vivo* techniques.
- The antimicrobial testing from the MIC determination, biocompatibility, time-killing assay, electrical conductivity, flow cytometry, fluorescence microscopy and *in vivo* antibacterial infection models successfully showed the *in vitro* and *in vivo* correlation of the VCM-DXT<sub>5</sub> nanoplex, chitosan-based pH-responsive lipid-polymer hydride nanovesicles VM-OLA-LPHVs1 and quaternary bicephalic vancomycin-loaded pH-responsive VCM-StBAclm-Qt1 quatsomes nano-drug delivery system.

**Stimulation of new research:** The research findings of the studies and the successful development of VCM-DXT<sub>5</sub> nanoplex, chitosan-based pH-responsive lipid-polymer hydride nanovesicles VM-OLA-LPHVs1 and quaternary bicephalic vancomycin-loaded pH-responsive VCM-StBAclm-Qt1 quatsomes holds great prospects in combating antimicrobial resistance and stimulate new research areas, including the following:

- The newly synthesised OLA and StBAclm can be utilised for delivering other classes of drugs to treat various disease conditions, such as urinary tract infection, pneumonia, sexually transmitted disease, HIV/AIDS, cardiovascular diseases, cancers, and other gene therapy-related diseases.

- The successful formulation and *in vitro* and *in vivo* characterisation of the reported nano-drug delivery systems in this study could stimulate research into the formulation of other nano-drug delivery systems for other classes of drugs to treat other diseases.
- The newly designed VCM-DXT<sub>5</sub> nanoplex, due to its ability to enhance the antibacterial activity of vancomycin could lead to the application of this strategy and stimulate research to develop nanosuspensions of nanoplexes for clinical trials.
- The successful elimination of intracellular MRSA with the novel chitosan-based pH-responsive lipid polymer hydride nanovesicles VM-OLA-LPHVs1 and quaternary bicephalic vancomycin-loaded pH-responsive quatsomes VCM-StBAclm-Qt1. These have demonstrated the potential of pH-responsive nanovesicles and quatsomes to eliminate intracellular bacteria and can stimulate research in the synthesis of other pH-responsive lipids and surfactants novel drug delivery systems to treat bacteria infectious concealed inside the cells, thereby acting as reservoirs and a source of resistant strains.

### 5.3 Recommendations for future studies

Although the design of VCM-DXT<sub>5</sub> nanoplex, chitosan-based pH-responsive lipid polymer hydride nanovesicles VM-OLA-LPHVs1 and quaternary bicephalic vancomycin-loaded pH-responsive quatsomes VCM-StBAclm-Qt1 were reported as novel nano-drug delivery systems for the eradication of bacterial resistance. From the three formulations, chitosan-based pH-responsive lipid polymer hydride nanovesicles (VM-OLA-LPHVs1) is the most effective because it has showed higher enhanced *in vitro* and *in vivo* antibacterial activities with 52.9-fold and 95-fold respectively. therefore, this formulation (VM-OLA-LPHVs1) could be as the first choice for optimization. Additional studies are essential to improve their formulations to ensure eventually regulatory approval for patient's use in the alternative for conventional dosage forms of vancomycin. The following studies are proposed:

- In the case of the novel VCM-DXT<sub>5</sub> nanoplex, there is a need for coarse-grain *Molecular dynamics* (MD) simulations to build a system that can completely self-assemble into drug-loaded nanoplexes and to simulate the release of drug from the nanosystem.

- In the case of VCM-DXT<sub>5</sub> nanoplex, the next phase would be to formulate other Biopharmaceutical Classification System (BCS) class III drugs using this simple technique, as well as using other available polymers in the market to further enhance their activity and water solubility.
- The qualitative analysis of the bacterial cell protein degradation performed using SDS-PAGE technique to understand the mechanism of antibacterial action of chitosan-based pH-responsive lipid-polymer hydride nanovesicles VM-OLA-LPHVs1 and quaternary bicephalic vancomycin-loaded pH-responsive quatsomes VCM-StBAclm-Qt1 can be upgraded with a quantitative determination of a specific protein using techniques, such as western blot analysis.
- The successfully developed chitosan-based pH-responsive lipid-polymer hydride nanovesicles VM-OLA-LPHVs1 and quaternary bicephalic vancomycin-loaded pH-responsive quatsomes VCM-StBAclm-Qt1 nanosystem for vancomycin delivery can be loaded with different classes of antibiotics and tested against various bacteria to evaluate its efficacies over different bacteria strains.
- Long-term stability studies using International Conference on Harmonisation (ICH) conditions to determine the physical and chemical stability of optimised formulations is needed to undertake and assess their shelf life.
- *In vivo* IV infection model, bioavailability and pharmacokinetic studies followed by clinical trials on both the developed nano-systems could be performed to achieve approval for market introduction.
- *In vivo* acute, long-term toxicity and study models can be performed to determine the full toxicological profile of the material and the formulations reported in this study for clinical trials.
- A method for high scale production of the nanosystems presented in these studies should be developed to enable their applications for pharmaceutical industries.

## **5.4 Conclusion**

The findings of this study had demonstrated and confirmed the potential of the various newly developed nanosystems for improving the treatment, prevention and treatment of extracellular, intracellular and resistant of bacterial infections. This current research has made a significant contribution to the field of drug delivery by alleviating the challenges associated with current conventional antibiotic therapy. Nanotechnology has advanced and addresses the current global conventional antimicrobial drug therapy by encapsulating different antibiotics moieties into a nano-based drug delivery system. This approach will play a vital role in improving the treatment of diseases associated with bacterial infections, with tremendous impact on public health.

# APPENDIXES

## Appendix I

International Journal of Pharmaceutics 558 (2019) 143–156



Contents lists available at ScienceDirect

International Journal of Pharmaceutics

journal homepage: [www.elsevier.com/locate/ijpharm](http://www.elsevier.com/locate/ijpharm)



### Delivery of novel vancomycin nanoplexes for combating methicillin resistant *Staphylococcus aureus* (MRSA) infections



Daniel Hassan<sup>a</sup>, Calvin A. Omolo<sup>a</sup>, Ramesh Gannamani<sup>a</sup>, Ayman Y. Waddad<sup>a</sup>,  
Chunderika Mocktar<sup>a</sup>, Sanjeev Rambharose<sup>a,b</sup>, Nikhil Agrawal<sup>a</sup>, Thirumala Govender<sup>a,\*</sup>

<sup>a</sup> Discipline of Pharmaceutical Sciences, College of Health Sciences, University of KwaZulu-Natal, Private Bag X54001, Durban, South Africa

<sup>b</sup> Division of Emergency Medicine, Department of Surgery, University of Cape Town, Cape Town, South Africa

#### ARTICLE INFO

##### Keywords:

Vancomycin  
Dextran sulfate sodium salt (DXT)  
Nanoplexes  
Antibacterial  
Methicillin-resistant *Staphylococcus aureus*

#### ABSTRACT

The development of novel antibiotic systems is needed to address the methicillin-resistant *Staphylococcus aureus* (MRSA) infections. The aim of the study was to explore the novel nanoplex delivery method for vancomycin (VCM) against MRSA using dextran sulfate sodium salt (DXT) as a polyelectrolyte complexing agent. Nanoplexes were formulated by the self-assembling amphiphile polyelectrolyte complexation method and characterized. The size, polydispersity index (PDI), and zeta potential (ZP) of the optimized VCM nanoplexes were  $84.6 \pm 4.248$  nm,  $0.449 \pm 0.024$  and  $-33.0 \pm 4.87$  mV respectively, with  $90.4 \pm 0.77\%$  complexation efficiency (CE %) and  $62.3 \pm 0.23\%$  drug loading. The *in vitro* (3-(4,5-dimethylthiazol-2-yl)-2,5-diphenyltetrazolium bromide)tetrazolium (MTT) studies of the nanoplexes were found to be non-toxic against different mammalian cell lines tested and may confirm its biosafety. While the *in vitro* drug release studies demonstrated sustained slower release. The *in silico* study confirmed the spontaneous interaction of VCM with DXT in the presence of sodium chloride. A 6.24-fold enhancement was observed for VCM nanoplexes via *in vitro* antibacterial studies. Flow-cytometric analysis showed effective cell killing of 67% from VCM nanoplexes compared to 32.98% from the bare vancomycin at the minimum inhibitory concentration (MIC) of 1.25  $\mu\text{g}/\text{mL}$ . The *in vivo* studies using BALB/c mouse skin infection model revealed that nanoplexes reduced MRSA burden by 2.3-folds compared to bare VCM. The novel nanoplexes have potential to be a promising delivery system to combat MRSA infections for improved treatment of bacterial infections.

#### 1. Introduction

Infectious diseases caused by methicillin-resistant *Staphylococcus aureus* (MRSA) continues to be a major concern globally. Statistics by the United State Center for Disease Control and Prevention specifically reported approximately 80,000 invasive MRSA infections and 11,285 associated deaths in 2017 (Wijesiri et al., 2017). The effectiveness of conventional antibiotics, such as  $\beta$ -lactam antibiotics (penicillins and cephalosporins) and trimethoprim against MRSA, is compromised due to antibiotic resistance (Lazzarini et al., 2005). Currently, vancomycin

(VCM), a tricyclic glycopeptide, is one of the major drugs widely used to combat MRSA infections (Bal et al., 2017; Ghosh et al., 2014). However, its frequent use and misuse as well as limitations of current dosage forms which include; inadequate drug concentration at disease site (Jain et al., 2008), increased exposure of healthy sites to the drug, higher doses required and side effects, increased frequency of administration and poor patient adherence leads to poor disease treatment outcomes and development of resistance (Chang et al., 2003; Deurenberg et al., 2007; Lodise et al., 2008). Furthermore, vancomycin suffers from several major drawbacks, such as inducement of

**Abbreviations:** ALZ, after lyophilisation; A549, adenocarcinoma human alveolar basal epithelial cells; BLZ, before lyophilisation; CE, complexation efficiency; CFUs, colony forming units; COM, centre of mass; DL, drug loading; DSC, differential scanning calorimetry; DXT, dextran sulfate sodium salt; FACS, fluorescence-activated cell sorting; FT-IR, Fourier transform-infrared; HEK-293, human embryonic kidney cells; Hep G2, human liver hepatocellular carcinoma cell; H&E, hematoxylin and eosin; MHA, Mueller-Hinton Agar; MHB, Mueller-Hinton Broth; MIC, minimum inhibitory concentration; MRSA, methicillin-resistant *Staphylococcus aureus*; MTT, 3-(4,5-dimethylthiazole-2-yl)-2,5-diphenyltetrazolium bromide; NCP, no cryoprotectant; NPT, isobaric-isothermic ensemble; NVT, canonical ensemble; PBS, phosphate buffers saline; PDI, poly dispersity Index; PI, propidium iodide; PME, particle mesh ewald; PS, particles size; PY, percentage yield;  $R_{VCM,DXT}$ , charge ratio of vancomycin to dextran sulfate sodium salt; TEM, transmission electron microscope; UFF, Universal force field; VCM, vancomycin; XRD, X-ray powder diffractometry; ZP, zeta potential

\* Corresponding author.

E-mail address: [govenderth@ukzn.ac.za](mailto:govenderth@ukzn.ac.za) (T. Govender).

<https://doi.org/10.1016/j.ijpharm.2019.01.010>

Received 23 August 2018; Received in revised form 31 December 2018; Accepted 3 January 2019

Available online 12 January 2019

0378-5173/© 2019 Elsevier B.V. All rights reserved.

nephrotoxicity upon on prolonged and persistent usage (Michael and Ian, 2017).

Nano-antibiotic delivery systems can help to overcome the problems associated with vancomycin treatment and reduce MRSA infections by offering several advantages such as, increased localized concentration at the infection sites and decreased exposure of the drug to healthy sites. This results in improved infection treatment, minimized side effects and improved patient compliance (Honary et al., 2014). Vancomycin encapsulation in liposomes (Liu et al., 2015; Yang et al., 2015), solid lipid nanoparticles (Yousry et al., 2016), nanostructured lipid carriers (Lewies et al., 2017), polymersomes (Omolo et al., 2017) and polymeric nano carriers (Xu et al., 2015) have been reported to be an effective method to increase drug accumulation at the site of infection with reduced toxicity and side effects. However, some of these formulations are not feasible due to a number of limitations, such as poor scalability, use of toxic solvents and expensive materials, and high material wastage during preparation (Cheow et al., 2015; Vo et al., 2013).

Amorphous VCM–nanoplexes, which involve drug nanoparticles complexed with an oppositely charged polyelectrolyte, is a good alternative to conventional solid dosage forms and the afore-mentioned nano-formulation strategies (Cheow et al., 2015). The advantages of nanoplexes include easy preparation methods with high drug loading capacities, solvent free conditions, feasibility in scale-up, minimal energy expenses and drug loss or wastage. Recently, Sikwal et al. reported VCM polyacrylic acid nanoplexes with size ranges of  $229.7 \pm 47.76$  nm and complexation efficiency up to 75%, using the anionic polymer polyacrylic acid sodium and VCM hydrochloride (Sikwal et al., 2016). To the best of our knowledge, this is the only nanoplexes formulation of VCM reported in the literature and hence, there is a need to identify other complexing agents to widen their applicability. While other nanoplexes for drugs, such as curcumin (Nguyen et al., 2016), ciprofloxacin (Yu et al., 2016), streptomycin (Seleem et al., 2009), ofloxacin, levofloxacin (Cheow and Hadinoto, 2012a), ibuprofen (Cheow and Hadinoto, 2012a), gentamicin (Ranjan et al., 2010) and doxorubicin (Yousefpour et al., 2011), have been reported, there is no data on VCM–dextran sulfate sodium salt (DXT) nanoplexes. Herein we extend the investigation of VCM nanoplexes to a different anionic polysaccharide polymer dextran sulfate sodium salt (DXT) for improved preparation efficiencies.

DXT is widely used in pharmaceutical formulation applications, due to its biodegradable and biocompatible properties (Heo et al., 2017; Nimesh et al., 2006; Tiyaboonchai et al., 2003). The anionic electrostatic interaction, arising from sulfate-groups, enables dextran sulfate sodium salt to readily undergo electrostatic complexation with oppositely charged drug molecules, while hydrophobic interaction from glucoside rings plays an important role in the formation of nanoplexes with small molecule drugs (Yu and Hadinoto, 2017). DXT has been reported to be a useful agent in nanoplexes preparation and for delivering nucleic acids, antibacterial and anticancer drug molecules (Cheow et al., 2015; Heo et al., 2017; Nimesh et al., 2006; Niu et al., 2017; Tiyaboonchai et al., 2003; Yu and Hadinoto, 2017). The use of natural polysaccharides-based polyelectrolyte architectures could offer VCM nanoplexes desirable pharmaceutical properties for commercial applications.

The aim of this study was to explore the potential of dextran sulfate sodium salt for complexation with vancomycin into a stable nanoplexes formulation. In this study, VCM–DXT binary nanoplexes were successfully formulated and characterized for their physicochemical properties, followed by *in silico*, *in vitro* and *in vivo* antibacterial activity to assess their potential in VCM delivery.

## 2. Materials and methods

### 2.1. Materials

VCM hydrochloride (VCM) was obtained from Sinobright Import and Export Co. Ltd. (China), Dextran sulfate sodium salt (MW = 500,000) was purchased from Millipore/Calbiochem® (Japan). Dialysis tubing of MWCO 14,000 Da (Sigma-Aldrich, USA) was employed for drug release studies and 3-(4,5-dimethylthiazole-2-yl)-2,5-diphenyltetrazolium bromide (MTT) used in cytotoxicity study was obtained from Merck Chemicals (Germany). Mueller-Hinton Agar (MHA), Mueller-Hinton Broth (MHB) and Nutrient Broth used for antibacterial assay were Biolab (South Africa) products. The bacterial culture used was MRSA (Rosenbach ATCC BAA 1683), propidium iodide (PI) and Syto9 cell permeant dye were obtained from ThermoFisher Scientific (USA).

### 2.2. Preparation of VCM–DXT nanoplexes

VCM–DXT nanoplexes were prepared by a previously reported self-assembling amphiphile polyelectrolyte complexation method, with minor modifications (Kutscher et al., 2015). Briefly, 0.45% (w/v) of DXT in 0.1 M sodium chloride solution and 1% (w/v) VCM solution in milli-Q water were prepared separately. Varying amounts of VCM solution of 2.5, 5, 10, 15 and 20 mL were added drop wise to 5 mL of DXT solution (0.45% w/v) under gentle and constant stirring at ambient condition. The mixture was left for one hour under ambient stirring conditions for the formation of VCM–DXT nanoplexes.

The effect of the VCM concentrations on the nanoplexes formation were explored at an initial DXT concentration of 4.5 mg/mL. The VCM concentration in the formulation varied from 3.3 mg/mL to 8 mg/mL, resulting in the VCM–DXT nanoplexes formation with charge ratios ( $R_{VCM/DXT}$ ) ranges from 0.31 to 2.49. The charge ratios were calculated from the molecular weights of VCM and DXT and the number of charged groups per molecule for both VCM and DXT (Supplementary material). The 24-OSO<sub>3</sub><sup>-</sup> groups per DXT molecule, that contribute to charge density of  $4.8 \times 10^{-6}$  mol charge/mg for DXT (Cheow et al., 2014) and two amine groups ( $-NH_3^+$ ) per VCM molecule, resulting in  $1.3 \times 10^{-6}$  mol.charge/mg for VCM (Sikwal et al., 2016) (Supplementary materials).

### 2.3. Physical characterizations of VCM–DXT nanoplexes

#### 2.3.1. Particle size, polydispersity index, zeta potential and morphology

The VCM–DXT nanoplexes, before and after lyophilization were analysed for particles size (PS), polydispersity index (PDI) and zeta potential (ZP) using a zeta sizer (Nano ZS, Malvern Instruments Corp, UK) at 25 °C after diluting the dispersion to an appropriate volume with deionized water. All measurements were done in triplicate. The morphology of VCM–DXT nanoplexes was observed using transmission electron microscope (TEM, Jeol, JEM-1000) at an accelerated voltage of 100 kv. Samples for TEM analysis were prepared by loading a small amount of nanoplex dispersion onto a carbon coated grid and dried for approximately three minutes to ensure the adherence of sample to grid, with the excess dispersion being removed by filter paper.

#### 2.3.2. Complexation efficiency (CE %)

The complexation efficiency (CE %) is characterized as the mass percentage of drug that forms nanoplexes relative to the initial amount of drug added (Cheow and Hadinoto, 2012a). Untrapped drug from the VCM–DXT formulations was separated after centrifuging (Beckman Coulter Optima™ MAX XP Centrifuge) at 1300 ×g for 30 min at 4 °C. The free drug from the supernatant was collected and estimated using UV spectrophotometry (Shimadzu UV 1601, Japan) at 280 nm. The complexation efficiency percentage (CE %) was calculated based on Eq. (1).



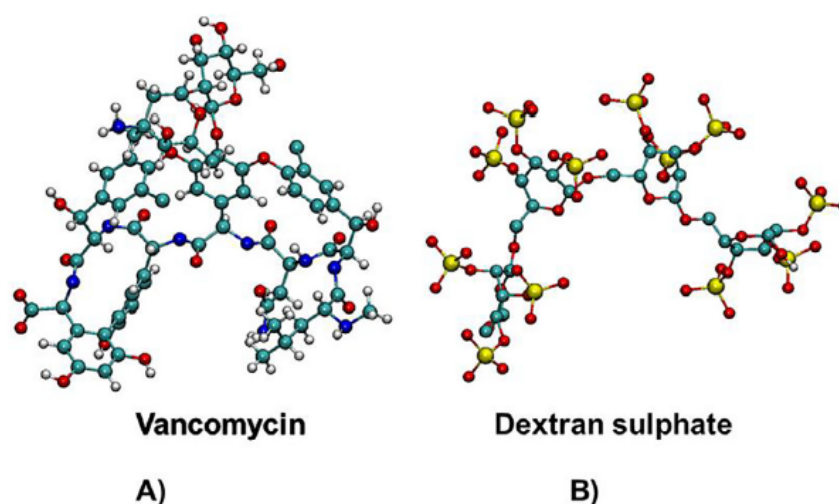


Fig. 1. Structure of A) VCM and B) DXT used in present study.

$$CE \% = \frac{(Total\ amount\ of\ VCM - amount\ of\ VCM\ in\ supernatant)}{Total\ amount\ of\ VCM} \times 100 \quad (1)$$

### 2.3.3. Drug loading (DL)

Drug loading was determined by measuring the amount of drug released when a known amount of nanoplexes was completely dissolved in PBS (Cheow and Hadinoto, 2012a). The freeze dried VCM-DXT nanoplexes concentration was calculated after re-dispersion in the deionized water. The drug percentage loading was determined using UV spectrophotometry (Shimadzu UV 1601, Japan) at 280 nm using Eq. (2).

$$DL = \frac{Weight\ of\ VCM\ in\ nanoplexes}{Weight\ of\ nanoplexes} \times 100 \quad (2)$$

### 2.3.4. Percentage yield

The percentage yield of the total nanoplexes mass produced was determined via method previously reported (Cheow and Hadinoto, 2012a; Nguyen et al., 2015). The VCM-DXT nanoplexes was centrifuged following three washing cycles to remove un-complexed VCM and DXT. The obtained nanoplex dispersion was freeze dried. The resulted amount of nanoplex was weighed, and the percentage yield calculated using Equation (3).

$$Percentage\ yield = \frac{weight\ of\ nanoplexes\ obtained\ after\ freeze\ drying}{Total\ weight\ of\ VCM\ and\ DXT\ added} \times 100 \quad (3)$$

### 2.3.5. Solid state characterisation of nanoplexes

The melting and crystallization behaviour of DXT, VCM, physical mixtures (DXT and VCM) and lyophilized VCM-DXT nanoplexes were determined using differential scanning calorimetry (DSC) (Sikwal et al., 2016). The powder X-ray diffraction (XRD) patterns of DXT, VCM, physical mixture (DXT and VCM) and nanoplexes VCM-DXT were recorded on a Bruker D8 Advance instrument that was equipped with an Anton-Paar XRK 900 reaction chamber and a Cu radiation source with a wavelength of 1.5406 Å at ambient temperature. Fourier Transform Infrared Spectroscopy (FT-IR) was adopted to investigate the structural changes in the VCM-DXT nanoplexes compared to the VCM and DXT using a Bruker Alfa Spectrophotometer (Germany). The spectrum of all samples was recorded within the wave number range of 550–3700  $cm^{-1}$  at an average of 16 scans and resolution of 4  $cm^{-1}$ .

### 2.4. In vitro drug release

An *in vitro* drug release study was performed to understand the drug release pattern by applying sink conditions (Begum et al., 2016). Briefly, a dialysis bag of approximately 10 mm (MWCO 14,000 Da) was filled with 1 mL of nanoplexes dispersion. The dialysis bag was tied at both ends and immersed into 40 mL bottle filled with phosphate buffers saline (PBS) pH 7.4 and placed in a mechanical shaker at 37 °C and 100 rpm. At designated time intervals (0.5, 1, 2, 3, 4, 5, 6, 7, 8, 12, 24, and 48 h), 3 mL of sample solution was withdrawn and substituted with fresh PBS solution (pH 7.4) that had been kept at the same temperature. The VCM concentration from the triplicate samples was quantified at 280 nm using a UV Spectrophotometer using appropriate blanks (Baelo et al., 2015). Thus obtained release data of the bare VCM and VCM-DXT nanoplexes were kinetically studied using several mathematical models, with the correlation coefficient ( $R^2$ ), root mean square error (RMSE) and mean dissolution time (MDT) calculated using excel add-in DDSolver program (China) (Zhang et al., 2010).

### 2.5. Molecular modelling

In order to investigate the interaction between VCM and DXT at different ion concentrations, MD simulations were performed. The structure of Vancomycin (Fig. 1A) was taken from PDB id: 1QD8 (Loll et al., 1999), and the DXT structure was extracted from PDB id: 50CA (Gustafsen et al., 2017). The obtained DXT structure contained two units, which were replicated to four units using the VMD software (Humphrey et al., 1996) (Fig. 1B), with universal Force Field (UFF) (Rappé et al., 1992) parameters being used for VCM and DXT. The UFF parameters were generated using the OBGMX server (Garberoglio, 2012), and the VCM and DXT simulations were performed at two different ion concentrations (12Na<sup>+</sup> and 12Cl<sup>-</sup>, 24Na<sup>+</sup> and 24Cl<sup>-</sup>). The SPC water model was used for solvation, and the system with 12Na<sup>+</sup> and 12Cl<sup>-</sup> contained 3982 water molecules, while the 24Na<sup>+</sup> and 24Cl<sup>-</sup> system contained 3958 water molecules. VCM and DXT were placed at ~30.00 Å centre of mass distance (COM) in the systems, both of which were first energy minimized using the 5000 steps of steepest descent method (Bixon and Lifson, 1967). Two short equilibration simulations were performed using canonical ensemble (NVT), followed by an isobaric-isothermic ensemble (NPT) for 100 ps, each. The production run for both systems was performed using the NPT ensemble for 1 ns each (total 2 ns), at 323K temperature with a velocity-rescale thermostat (Bussi et al., 2007) at 1 atm pressure using the Parrinello-Rahman pressure coupling method (Parrinello and Rahman, 1981). The

pressure coupling time was 2.0 ps while that of the temperature was 0.1 ps. The particle Mesh Ewald (PME) method (Darden et al., 1993) was used for long-range electrostatic interactions, and for both the short-range coulombic and VdW interactions, a 10 Å cut-off was used. The simulations were performed using GROMACS (Abraham et al., 2015), and the COM were calculated between VCM and DXT using in-house Tcl script, while the interaction energies were calculated using a rerun option of the “MDRUN” package of GROMACS.

## 2.6. Stability

The short-term physical stability of the VCM-DXT nanoplexes was evaluated at 4 °C and at room temperature (RT) for 90 days. The evaluation of the formulation's physical appearance, particle sizes, PDI and ZP was performed at the end of 30, 60 and 90 days. This study was performed in triplicate, and the effects of cryoprotectant at 5% was explored on their sizes, PDI and ZP.

## 2.7. In vitro cytotoxicity

The MTT assay was employed to determine the cytotoxicity of the bare VCM and the optimized VCM-DXT nanoplexes with the lower charge ratio using adenocarcinoma human alveolar basal epithelial cells (A549), embryonic kidney cells (HEK-293) and liver hepatocellular carcinoma (Hep G2) cell lines. The cells were cultured and seeded as per previously reported procedure (n = 6) (Omolo et al., 2018). Different concentrations of bare VCM and VCM-DXT nanoplexes (20, 40, 60, 80 and 100 µg/mL) were introduced into the wells seeded with cells (Sikwal et al., 2016). The positive control wells (with culture medium containing cells only) and the negative control (with culture medium without cells) were also included. The sample were incubated for 48 h, there-after sample-laden medium was replaced with 100 µL of fresh culture medium and 20 µL of MTT solution (5 mg/mL in PBS) in each well. Cell viability was determined at absorbance wavelength of 540 nm (Spectrostar Nano, Germany) and percentage cell viability was calculated using Equation (4).

$$\% \text{ Cell Viability} = \frac{(\text{A540 nm treated cells})}{(\text{A540 nm untreated cells})} \times 100 \quad (4)$$

## 2.8. In vitro antibacterial activity

The minimum inhibitory concentration (MIC) of the VCM-DXT nanoplexes and bare VCM were evaluated against methicillin resistant *Staphylococcus aureus* Rosenbach ATCC®BAA-1683 (MRSA) using the broth dilution technique (Omolo et al., 2017). The bacterial cultures were grown in Nutrient Broth (Biolab, South Africa) at 37 °C for 18 h in a shaking incubator set at 100 rpm. The bacterial cultures were adjusted with sterile distilled water to achieve a concentration equivalent to 0.5 McFarland Standard using a DEN-1B McFarland densitometer (Latvia). The bacterial cultures were further diluted (1:150) with sterile distilled water to obtain a final concentration of  $5 \times 10^5$  colony forming units (CFU)/mL. Serial dilutions of the VCM-DXT nanoplexes and VCM were prepared in Mueller-Hinton Broth 2 (MHB) (Sigma-Aldrich, USA) using 96 well plates. These were then inoculated with the diluted bacterial cultures and incubated at 37 °C for 18 h in a shaking incubator set at 100 rpm. After incubation, 10 µL of the VCM-DXT nanoplex and bare VCM were spotted onto the Mueller-Hinton Agar (MHA) (Biolab, South Africa) plates and incubated for a further 18 h at 37 °C. This procedure was repeated daily for three days, and all MIC studies were carried out in triplicate. The blank formulation of dextran was used as a negative control the while bare VCM served as a positive control.

## 2.9. Bacterial cell viability assay

Cell viability is the determination of the number of live cells in a

sample population (Gandhi and Shah, 2015) and was estimated via flow cytometry using different fluorescent dyes (Wilkinson, 2018). Cell viability studies on the MRSA cells were performed using flow cytometry according to previously reported method (Arndt-Jovin and Jovin, 1989; Bexfield et al., 2008; Shrestha et al., 2011). The processing of bacteria and percentage cell viability was determined after six hours of incubation with VCM and VCM-DXT following our previously reported procedure (O'Brien-Simpson et al., 2016). The VCM and VCM-DXT broths (50 µL) were added to the flow cytometry tubes, each containing 350 µL of the sheath fluid, and vortexed for 5 min (O'Brien-Simpson et al., 2016; Rieger et al., 2012). The mixture was incubated for 30 min with 5 µL of the non-cell wall permeant propidium iodide (PI) and the Syto9 cell permeant dye. Thereafter, study and analysis was performed on BD FACSCANTO II (Becton Dickinson, CA, USA) following our previously reported protocol (Omolo et al., 2018).

## 2.10. In vivo antibacterial activity and histological evaluation

A mouse skin infection model was used to determine the *in vivo* antibacterial activity of the VCM-DXT nanoplex (Omolo et al., 2017) with ethical clearance from the University of KwaZulu-Natal's Animal Research Ethics Committee (Approval number: AREC/104/015PD). The guidelines of the AREC of UKZN and the South African National Standard SANS 10386:2008 were followed for humane care and animal use. BALB/c mice weighing 18–20 g were obtained and housed in Biomedical Research Unit, University of KwaZulu-Natal. One day preceding the study, the mice back hair was shaved, and the shaven area was disinfected with 70% ethanol. On the following day, the mice were intradermally infected with 50 µL MRSA of  $1.5 \times 10^8$  CFU/mL then divided into three groups, (negative control, positive control and treatment) (n = 4). Thirty minutes post-infection, 50 µL of bare VCM, DXT and VCM-DXT nanoplexes were injected at the same infection site in all the three groups. The mice were kept under observation for 48 h with normal 12 h light and dark condition at 19–23 °C, and  $55 \pm 10\%$  relative humidity with adequate ventilation.

The mice were euthanized, and the infected skin was harvested and processed to prepare tissue homogenates (Omolo et al., 2017). The obtained homogenates were spotted (20 µL) on nutrient agar plates, incubated at 37 °C for 24 h, before being analysed for number of colonies forming units (CFU). For histological investigations the skin samples were processed and stained following reported procedure (Omolo et al., 2017), then sections were examined and captured with a Leica Microscope DM 500 that was fitted with a Leica ICC50 HD camera (Leica Biosystems, Germany).

## 2.11. Statistical analysis

Statistical analysis of data was performed using one-way analysis of variance (ANOVA), followed by Bonferroni's multiple comparison test using GraphPad Prism® 6 (GraphPad Software Inc., USA). Statistical significance was based on a *P* value < 0.05 and the data was expressed as mean ± standard deviation (SD).

## 3. Results and discussion

### 3.1. Preparation of VCM-DXT nanoplexes

Preparation of VCM-DXT nanoplexes were evaluated as a function of charge ratios  $R_{(VCM/DXT)}$  (0.31, 0.62, 1.24, 1.86 and 2.49) using a solution of DXT in 0.1 M NaCl. For all the tested charge ratios, a complexation efficiency of higher than 90% of the VCM were observed, and the particle size varied with varying concentrations of VCM. The different charge ratios  $R_{(VCM/DXT)}$  of 0.31, 0.62, 1.24, 1.86, and 2.49, which corresponded to the varying concentration of VCM, resulted in nanoplexes with particle sizes of  $84.6 \pm 4.24$ ,  $247.7 \pm 28.0$ ,  $404.0 \pm 13.24$ ,  $429.4 \pm 40.24$  and  $500.6 \pm 0.33$ , respectively



**Table 1**  
Effect of charge ratios on sizes, PDI, ZP and CE % of nanoplexes (n = 3).

Formulation	$R_{(VCM/DXT)}$	Size (nm)	PDI	ZP (mV)	CE %
VCM-DXT <sub>1</sub>	2.49	500.6 ± 0.33	0.29 ± 0.07	-23.1 ± 4.71	95.26 ± 0.18
VCM-DXT <sub>2</sub>	1.86	429.4 ± 40.28	0.24 ± 0.03	-28.0 ± 3.75	96.86 ± 0.29
VCM-DXT <sub>3</sub>	1.24	404.0 ± 13.23	0.22 ± 0.02	-26.3 ± 3.40	98.67 ± 0.14
VCM-DXT <sub>4</sub>	0.62	247.7 ± 28.0	0.45 ± 0.08	-28.4 ± 4.40	95.87 ± 0.20
VCM-DXT <sub>5</sub>	0.31	84.6 ± 4.24	0.45 ± 0.02	-33.0 ± 4.87	90.40 ± 0.77

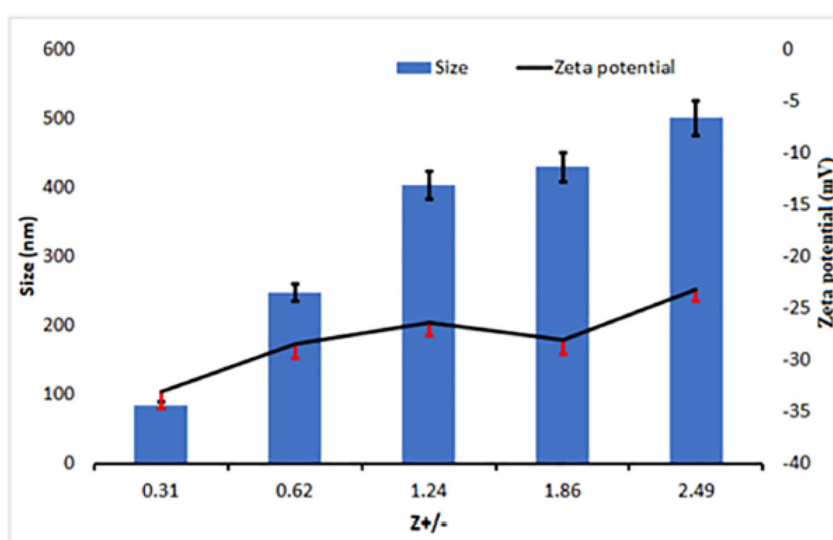


**Fig. 2.** Effect of charge ratio on particle sizes and zeta potential of VCM-DXT. Values are expressed as mean ± SD (n = 3).

(Table 1). The ZP was proportional to the concentration of VCM and varied from  $-33.0 \pm 4.87$  to  $-23.1 \pm 4.71$  mV as the VCM concentration varied. The negative ZP was an indication of the colloidal stability in the aqueous suspension that formed, as shown in Fig. 2. The above studies showed that the VCM-DXT could be successfully prepared at different charge ratios.

The percentage of CEs at the different charge ratio  $R_{(VCM/DXT)}$  were found to be in the range of 90–98% (Table 1). The CE % increased when charge ratio varied from  $R_{(VCM/DXT)}$  of 0.31 to 1.24, after which, as the charge ratio increased, a slight reduction in CE % was observed. At a higher charge ratio the sizes of the VCM-DXT nanoplexes obtained were similar to other studies, where ciprofloxacin was complexed with DXT (Cheow et al., 2015; Kutscher et al., 2015). At higher charge ratio, the amount of DXT being completely utilised in complexation process, does not favour the aggregation of excess VCM added and hence decreasing CE % at higher concentration VCM (Cheow and Hadinoto, 2012a). Thus, the ratio of  $R_{(VCM/DXT)}$  had a significant influence on CE % and ZP. The higher complexation efficiency of the VCM in VCM-DXT nanoplexes was attributed to the higher charge density of the DXT (Cheow and Hadinoto, 2012a). However, the particle sizes were different for various charge ratios, with an increase in the particle sizes being observed with an increase in charge ratio (Table 1).

### 3.2. Characterization of the optimized VCM-DXT<sub>5</sub> nanoplexes formulation

From Table 1, the addition of 2.5 mL of the VCM solution (1% w/v) to 5 mL DXT (0.45% w/v) under magnetic stirring for 1 h, was concluded as optimal nanoplexes preparation method. Thus obtained, VCM-DXT<sub>5</sub> nanoplexes formulation, with particle size of  $84.55 \pm 4.24$  nm, PDI  $0.45 \pm 0.02$ , and ZP of  $-33.0 \pm 4.87$  mV at the lowest charge ratio  $R_{(VCM/DXT)}$  of 0.31, was therefore considered as the optimized formulation due to its lower sizes, higher ZP value and CE

%. In other studies, where polyacrylic acid sodium was complexed with VCM, sizes greater than 220 nm with only ~74 CE % were observed (Sikwal et al., 2016). Thus, the VCM nanoplexes obtained in this study with DXT were found to have better size, stability and CE % compared to previous reports. Similar CE % for other drugs, such as ofloxacin, levofloxacin and ciprofloxacin, using DXT as a polyelectrolyte (Cheow and Hadinoto, 2012a), indicating that DXT could be a suitable complexing agent for antibiotics, with further studies therefore being performed on the optimized formulation.

To prevent aggregation of the VCM-DXT<sub>5</sub> nanoplexes, the formulation was lyophilized in presence of different cryoprotectants i.e 0.5% of mannitol, sucrose, D(+) glucose and D(-) glucose (Kiew et al., 2015; Sikwal et al., 2016). The effect of lyophilisation on its stability of nanoplexes was determined in terms of size, PDI and ZP, after dispersing 10 mg of the freeze-dried formulation in 10 mL of distilled water, with the results being depicted in Table 2. Interestingly, lyophilisation in the presence of cryoprotectant improved the PDI values of nanoplexes formulation, while there were no significant changes in ZP indicating their stability in the dry form. The VCM-DXT<sub>5</sub> nanoplexes in dry form is a great advantage for its pharmaceutical applications as lyophilized solid nano drug delivery systems have been found to be more stable than those is liquid dosage forms (Cheow et al., 2011; Cheow and Hadinoto, 2012a).

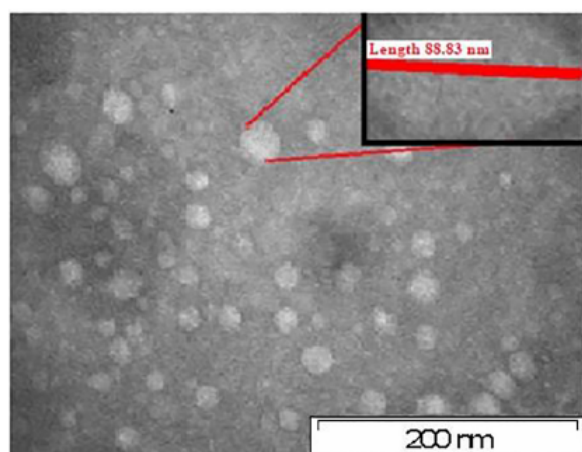
#### 3.2.1. Drug loading (DL)

Drug loading capacity calculated was  $62.27 \pm 0.23\%$ , which was relatively higher than that obtained using polyacrylic acid sodium (PAA) in a previous study (Sikwal et al., 2016). Higher drug loading in the VCM-DXT<sub>5</sub> indicates a stronger affinity between the positively charged amines in the VCM and the negatively charged sulfate groups in the DXT, leading to a stable polyelectrolyte complexation.

**Table 2**Effect of cryoprotectant on sizes, PDI and ZP of VCM-DXT<sub>5</sub> nanoplexes before and after lyophilization (n = 3).

Parameters	BLZ	ALZ (Mannitol)	ALZ (Sucrose)	ALZ (D + glucose)	ALZ (D-glucose)	ALZ NCP
Size (nm)	84.55 ± 4.24	91.33 ± 4.62	91.44 ± 6.08	93.17 ± 13.13	104.8 ± 17.14	97.37 ± 8.10
PDI	0.450 ± 0.02	0.330 ± 0.09	0.320 ± 0.09	0.240 ± 0.16	0.380 ± 0.15	0.220 ± 0.07
ZP (mV)	-33.0 ± 4.87	-34.6 ± 3.13	-33.4 ± 1.36	-33.9 ± 0.46	-33.3 ± 1.23	-32.4 ± 4.26

BLZ = before lyophilisation, ALZ = after lyophilisation, NCP = No cryoprotectant.

**Fig. 3.** Morphology of VCM-DXT<sub>5</sub> nanoplexes scale bar = 200 nm.

### 3.2.2. Percentage yield

The percentage yield of VCM-DXT<sub>5</sub> calculated was found to be  $84.52 \pm 0.31\%$ , this result was similar to other studies where DXT was employed as a polyelectrolyte, further indicating mass efficiency of the technique (Cheow and Hadinoto, 2012; Cheow et al., 2014).

### 3.2.3. Morphology

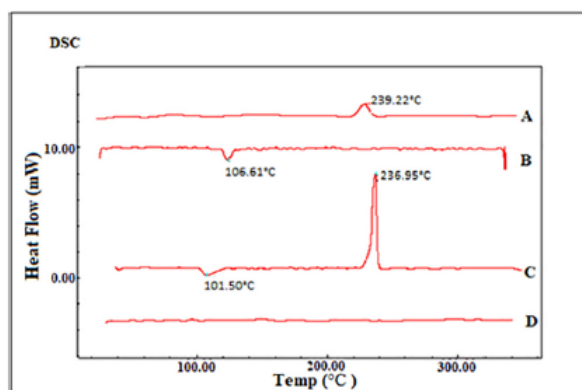
The morphological analysis of the VCM-DXT<sub>5</sub> nanoplexes was performed using TEM. TEM images showed that the VCM-DXT<sub>5</sub> nanoplexes were discrete and homogeneous, with an almost spherical shape (Fig. 3). The images were similar in previous studies (Cheow et al., 2015; Cheow et al., 2014; Kutscher et al., 2015). The sizes were also comparable to that observed in dynamic light scattering studies.

### 3.2.4. Differential scanning calorimetry (DSC)

An overview of the DSC thermograms of DXT, VCM, physical mixture (VCM and DXT) and nanoplexes (VCM-DXT<sub>5</sub>) is shown in Fig. 4. The DSC thermograms of the VCM and DXT contained characteristics peak at 106 °C and 239 °C respectively, with Cevher et al. (2006) observing a similar VCM thermogram profile (Cevher et al., 2006). The profile of the physical mixture revealed no major shifts in the thermal peaks of the DXT, while the VCM had a minor shift. In contrast, no sharp thermal events were observed for the lyophilized nanoplexes, indicating its conversion from crystalline form into amorphous form upon complexation with DXT.

### 3.2.5. X-ray diffraction (XRD)

The inter- and intra-molecular interactions involved during the formation of the nanoplexes affects the crystal properties of both the VCM and DXT, which can be studied by changes in the diffraction pattern. Fig. 5 represents the comparative diffraction pattern of the DXT, VCM, their physical mixture and the nanoplexes. The powder XRD pattern of the DXT contained several sharp peaks indicating its crystalline nature, while the bare VCM did not show any theta values. Similar phenomenon has also been reported in literature (Saidykh

**Fig. 4.** DSC profiles of (A) DXT, (B) VCM, (C) Physical mixture of VCM and DXT, and (D) VCM-DXT<sub>5</sub> nanoplexes.

et al., 2016; Zarif et al., 2012) due to its transformation from crystalline states into amorphous states after complexation in the nanoplexes. The physical mixture of the DXT and VCM contained sharp peaks, indicating that the simple mixing did not result in nanoplexes formation. In liquid state the crystalline nature of the ingredients are broken and free ions are available for complexation, unlike in the solid state where there are no charges to induce electrostatic interactions (Ahmed et al., 2018; Chen et al., 2018; Waltho and Williams, 2007). In contrast, the freeze dried VCM-DXT<sub>5</sub> nanoplexes did not show any noticeable peaks in the spectra, confirming the nanoplexes formation. This is in good agreement with the DSC results, and can be attributed to the amorphous nature of VCM in the VCM-DXT<sub>5</sub>.

### 3.2.6. Fourier transform-infrared (FT-IR) analysis

The FT-IR spectroscopy analysis was performed to confirm the presence of VCM in the nanoplexes formulation and its complexation with DXT, the comparative infrared (IR) spectra being presented in Fig. 6. The IR spectra of dextran sulfate sodium salt contained peaks at 1219, 980, 798 and 574  $\text{cm}^{-1}$ , due to the vibrations of S=O and O-S-O chemical bonds (Cakić et al., 2005). These bands shifted to 1229, 1017, 695 and 578  $\text{cm}^{-1}$ , respectively in the nanoplexes, indicating that the sulfate group interacted with the oppositely charged VCM molecules. In addition, the peak at 1585  $\text{cm}^{-1}$  (aromatic C=C) for VCM shifted to 1587  $\text{cm}^{-1}$ , which could be due to the  $\pi$ - $\pi$  stacking interaction between the aromatic rings of VCM during the self-assembly process. These changes in IR frequencies confirmed the formation of nanoplexes in a polyelectrolyte directed self-assembly process.

### 3.3. In vitro drug release

The *in vitro* release of VCM from the optimized nanoplexes and the nanoplex with high charge ratio which resulted to high particles (VCM-DXT<sub>1</sub>) was studied in PBS (pH 7.4) over 48 h at 37 °C and is shown in Fig. 7. At the end of the first two hours, the cumulative percentage of bare VCM released was  $40.9 \pm 2.77\%$ , whereas for VCM-DXT<sub>5</sub> it was  $20.7 \pm 1.9\%$  and  $20.63 \pm 1.54\%$  for VCM-DXT<sub>1</sub>. The bare VCM reached nearly  $94.9 \pm 2.59\%$  release at the end of eight hours, while

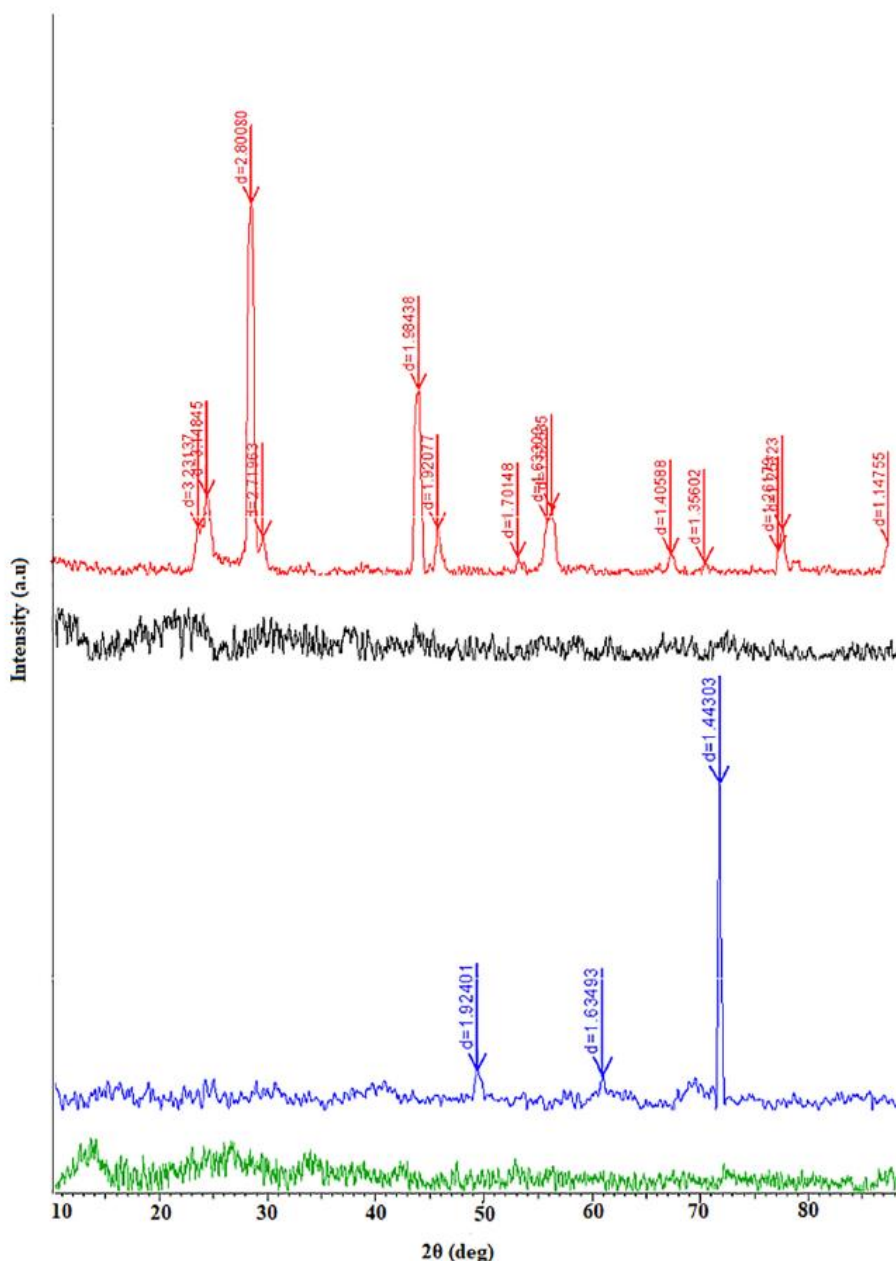


Fig. 5. Diffractograms of (A) DXT, (B) VCM, (C) Physical mixture (DXT and VCM) and (D) VCM-DXT<sub>5</sub> nanoplexes.

only  $60.4 \pm 1.70\%$  was achieved from the optimized VCM-DXT<sub>5</sub> and  $20.63 \pm 1.54\%$  for the nanoplex with higher charge ratio. By the end of the 48 h, approximately 86% and  $39.76 \pm 0.10\%$  of the VCM was released from the VCM-DXT<sub>5</sub> and VCM-DXT<sub>1</sub> respectively. The slower release pattern of VCM from the VCM-DXT<sub>1</sub> nanoplex compared to the optimal formulation VCM-DXT<sub>5</sub> formulation and the bare drug could be due to the high electrostatic force between VCM and DXT and the higher charge ratio. This slower release profile could be beneficial for reducing the dosage frequency of VCM-DXT<sub>5</sub> nanoplexes formulation.

Additionally, the erodibility of DXT, owing to its biodegradability properties, possibly contributed to the release of VCM from VCM-DXT<sub>5</sub> nanoplexes. The high molecular weight of VCM could be an obstacle to its passage through the DXT matrix, while the unique properties of DXT to swell and erode provided the sustained release pattern of the VCM-

DXT<sub>5</sub> nanoplexes over the 48 h compared to 12 h and 15 min in similar studies (Kutscher et al., 2015; Sikwal et al., 2016). The slower release profile displayed by the VCM-DXT<sub>5</sub> nanoplexes compared to the bare drug could provide an effective drug delivery system that reduces the frequency of administration and increases patient adherence, which could lead to better patient treatment outcomes.

#### 3.4. Stability study

The novel VCM-DXT<sub>5</sub> nanoplexes formulation was studied for its stability for three months at both room temperature (RT) and 4 °C. The stability of the formulation was assessed in terms of the PS, PDI and ZP, with the results being presented in Table 3. The VCM-DXT<sub>5</sub> were stable for the period of three months at 4 °C (*P* value > 0.05), as no change in



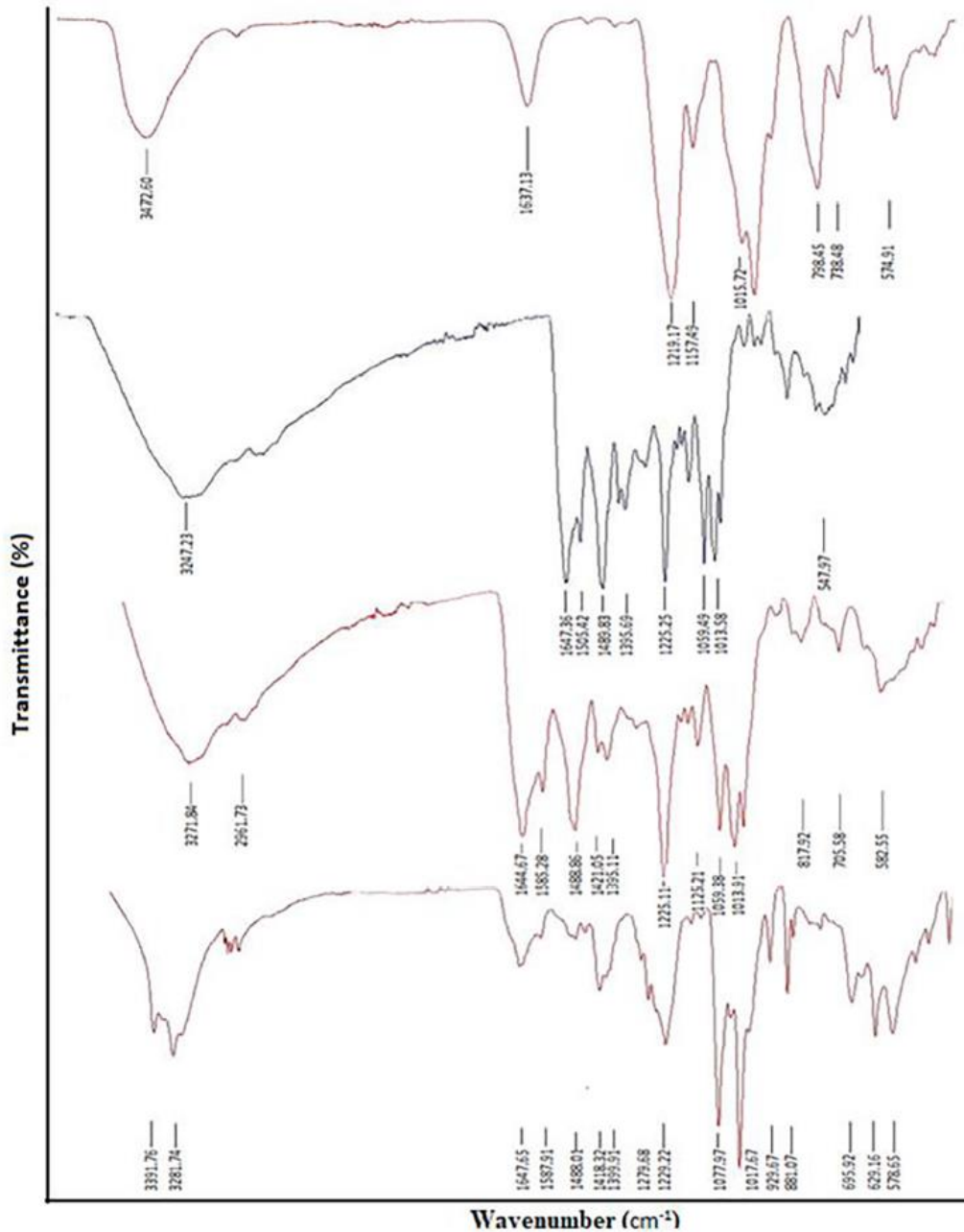


Fig. 6. FT-IR spectra for (A) DXT, (B) VCM, (C) Physical mixture of VCM and DXT, and (D) VCM-DXT<sub>5</sub> nanoplexes.

physical appearance of the formulation was observed. At room temperature (RT), change in size and zeta potential was observed after the second month of the study (*P* value < 0.05), indicating that the physical stability was achieved only for the first month. The instability of the VCM-DXT<sub>5</sub> nanoplexes at room temperature could be associated with the structural changes and relaxation behaviour of the DXT due to the swelling process in the aqueous medium (Florence and Attwood, 1988).

### 3.5. In vitro cytotoxicity

Biosafety is an essential criterion to establish the non-toxic dosages of formulation for biomedical applications. The MTT assay based

cytotoxicity study was employed to evaluate and quantify the cytotoxicity of the bare VCM and newly derived nanoplexes formulation (Sonawane et al., 2015). The viability of cells after exposure to the bare VCM and the VCM-DXT<sub>5</sub> nanoplexes were assessed by quantifying crystalline blue formazan formation [51]. Fig. 8 shows the bar chart breakdown of the cytotoxicity assay of the VCM-DXT<sub>5</sub> against the A549, HEK 293 and HEP G2 cells. The bare VCM demonstrated cell viability from 77.05 to 93.71% for A549, 77.31 to 95.18% for HEK-293 and 76.37 to 91.48% for HEP G2 cell across all concentration (Supplementary Material 2: Fig. S1). These results indicate a high percentage cell viability, from 77.9 to 90.6% for A549 cells, 78.1 to 85.6% for HEK 293, and 76.0 to 92.6% for HEP G2 cell for all

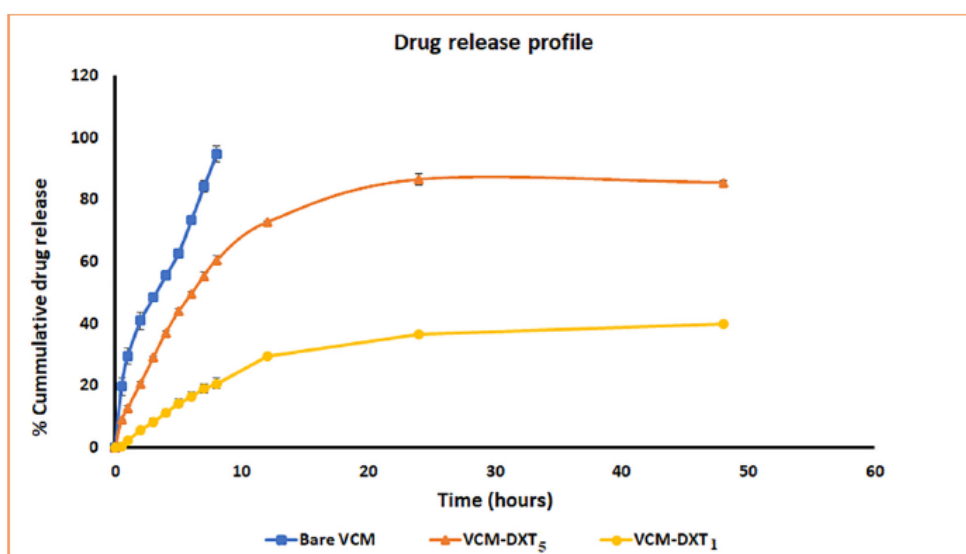


Fig. 7. Drug release profile of bare VCM, VCM-DXT<sub>5</sub> and VCM-DXT<sub>5</sub> nanoplexes. The values are expressed as mean  $\pm$  SD, n = 3.

concentrations of nanoplexes tested. This indicates the non-cytotoxic nature of the VCM-DXT<sub>5</sub> nanoplexes as with greater than 75% cell viability denotes non-toxicity of the material to the mammalian cells (Sikwal et al., 2016). Based on these results, the VCM-DXT<sub>5</sub> can therefore be considered as a non-toxic and safe drug delivery system.

### 3.6. Molecular modelling (spontaneous interaction between VCM and DXT)

In the experiments, conducted as shown in Fig. 1, it was observed that spontaneous interaction between the VCM and DXT to form nanoplexes occurred only in the presence of a higher concentration of ions. To investigate the interaction between VCM and DXT at different ion concentrations MD simulations were performed. In the system with 12Na<sup>+</sup> and 12Cl<sup>-</sup> ions, there was no noticeable interaction between the VCM and the DXT unit at the end of the simulations (Fig. 9). However, in the system with 24Na<sup>+</sup> and 24Cl<sup>-</sup> ions, the VCM and DXT formed a spontaneous interaction during equilibration simulation, which was further strengthened during the production run, with both molecules remained bound to each other until the end of the simulation time (Fig. 10A and C). The interaction energy between VCM and DXT was  $\sim -80$  kJ/mol in the presence of 24Na<sup>+</sup> and 24Cl<sup>-</sup> ions (Fig. 10B). Thus, the simulation data corroborated to the experimental data.

Previous *in silico* studies indicated that VCM complexation could have been through the  $\pi$ - $\pi$  stacking and alkyl-alkyl hydrophobic interactions (Sikwal et al., 2016). A balance between the attractive and repulsive forces could be the reason for the salt-induced spontaneous interaction between VCM and DXT. The <sup>-</sup>OSO<sub>4</sub> functional group of DXT being negatively charged in presence of sodium salt, might have complexed with ammonium groups (NH<sub>3</sub><sup>+</sup>) positively charged groups of VCM (Caram-Lelham et al., 1997). Thus, the anionic DXT might have

neutralized the positive charge on the VCM molecules and reducing the repulsive forces between them (Cheow et al., 2015). The ionic concentration could have enhanced the mutual inter molecular interaction between the hydrophobic VCM counter ions by reducing their aqueous solubility (Ozbas et al., 2004), thus supporting antibiotic formation of the nanoplexes with polyelectrolyte DXT. The electrostatic charge shielding function of the sodium salt also might have helped to reduce the inter-molecular repulsions between the like-charges of the DXT chains, and promoting the conformational arrangements to the favoured nanoplexes formation (Caram-Lelham et al., 1997; Cheow and Hadinoto, 2012b). Thus, a series of salt driven mechanism might have led to nanoplexes formation.

### 3.7. In vitro antibacterial activity

The *in vitro* antibacterial activity of the bare VCM, the DXT, VCM-DXT<sub>1</sub> and the VCM-DXT<sub>5</sub> was determined by using the 96 well plate-broth dilution technique to confirm and compare the potency and enhancement of VCM upon its transformation into a nanoplexes formation (Table 4). The DXT alone did not show any activity, even at the highest concentration tested. After 24 h, the MIC values for bare VCM, VCM-DXT<sub>1</sub> and VCM-DXT<sub>5</sub> against MRSA at physiological pH 7.4 were 7.8  $\mu$ g/mL, 62.5  $\mu$ g/mL and 1.25  $\mu$ g/mL respectively, indicating 0.14-fold and 6.24-fold increase in activity of VCM-DXT<sub>1</sub> and VCM-DXT<sub>5</sub> when compared to the bare VCM. Although, VCM-DXT<sub>1</sub> demonstrated slower sustained release compared to VCM-DXT<sub>5</sub>, its MIC was shown to be higher. We could not fully explain this result however, this could be attributed to very slow release of the drug limiting the amount of drug available to kill the bacteria due to retarded release however, more studies are needed to explain this phenomenon. The complexation of the VCM with DXT therefore did not adversely affect the antimicrobial

Table 3

Effect of storage conditions on physicochemical characteristics of VCM-DXT<sub>5</sub> nanoplexes. The values are expressed as mean  $\pm$  SD, n = 3.

Time (days)	Particle sizes		PDI		ZP	
	4 °C	RT	4 °C	RT	4 °C	RT
0	84.53 $\pm$ 4.24	84.55 $\pm$ 4.24	0.449 $\pm$ 0.02	0.449 $\pm$ 0.02	-33.0 $\pm$ 4.87	-33.0 $\pm$ 4.87
30	84.90 $\pm$ 6.01	88.13 $\pm$ 6.23	0.448 $\pm$ 0.03	0.456 $\pm$ 0.08	-29.0 $\pm$ 3.19	-23.9 $\pm$ 2.34
60	87.33 $\pm$ 1.77	89.51 $\pm$ 2.30	0.433 $\pm$ 0.09	0.459 $\pm$ 0.01	-22.0 $\pm$ 3.47	-22.2 $\pm$ 6.27
90	88.92 $\pm$ 1.46	90.20 $\pm$ 1.43	0.457 $\pm$ 0.01	0.455 $\pm$ 0.01	-35.2 $\pm$ 1.52	-22.21 $\pm$ 2.2

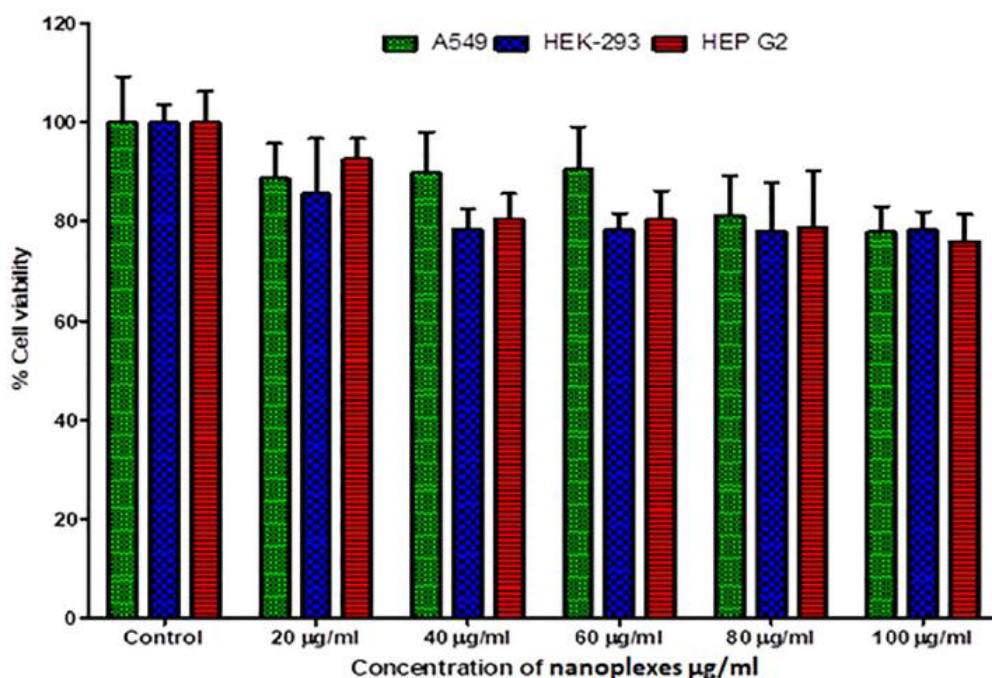


Fig. 8. Percentage cell viabilities of A549, HEK-293 and HEP G2 cells, after being exposed to different concentration of VCM-DXT<sub>5</sub> nanoplexes. Results are presented as mean ± SD (n = 6).

activity of the VCM. The results were in good agreement with previous studies, which reported no adverse changes in the antibacterial activity of ofloxacin and levofloxacin after complexation with DXT (Cheow and Hadinoto, 2012a; Cheow et al., 2015). For the VCM nanoplexes derived from the polyacrylic acid sodium (PAA) (Sikwal et al., 2016), and for those involving other antibiotics (ofloxacin and ciprofloxacin) with DXT (Cheow and Hadinoto, 2012a; Cheow et al., 2015), the activity

remained the same as for the free drug, with no enhancement. Interestingly, an enhancement by 6.24-folds was observed for VCM-DXT nanoplexes, which could be attributed to a smaller size, high CE % sustained release resulting in the continuous delivery of lethal concentration of the antibiotics to the bacteria for long periods of time thus resulting to complete elimination of the bacteria (Ionita et al., 2017). The improved antibacterial activity could also be attributed to the small

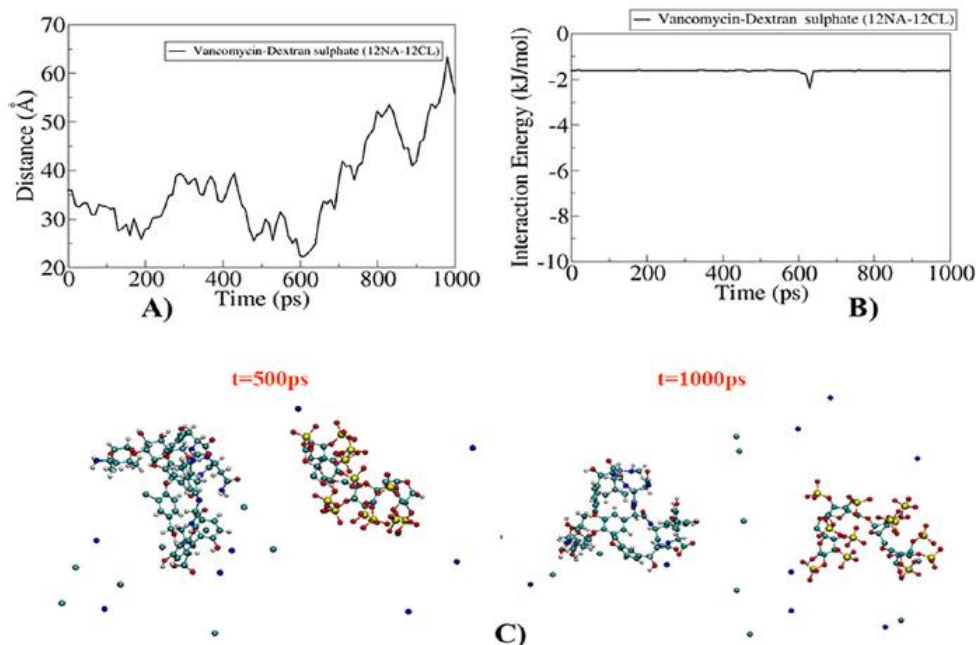


Fig. 9. A) Shows time evolution of COM distance between VCM and DXT; B) Shows time evolution of interaction energy between VCM and DXT; C) Shows two representative images from the simulations at two different time points in presence of 12Na<sup>+</sup> and 12Cl<sup>-</sup>.



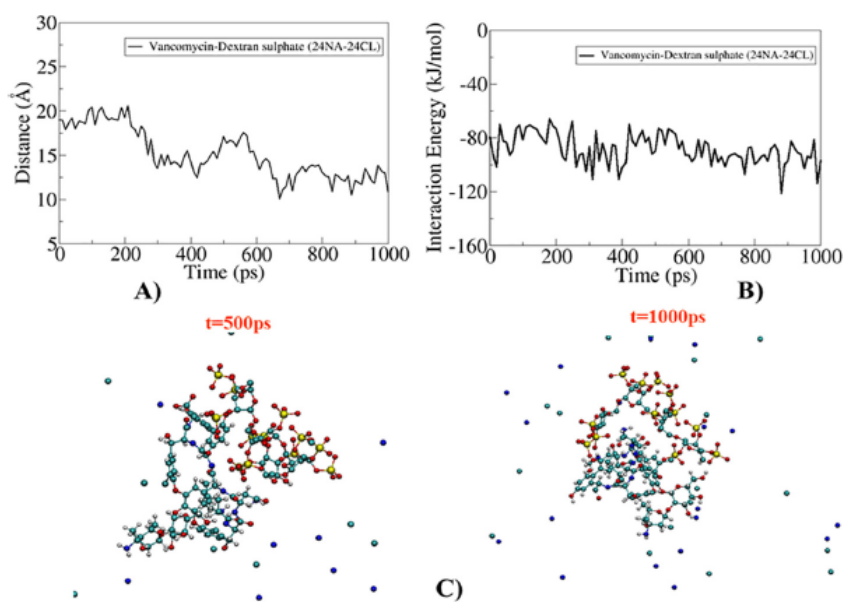


Fig. 10. A) Shows time evolution of COM distance between VCM and DXT; B) Shows time evolution of interaction energy between VCM and DXT; C) Shows two representative images from the simulations at two different time points in presence of 24Na<sup>+</sup> and 24Cl<sup>-</sup>.

**Table 4**  
*In vitro* antibacterial activity of the formulations (VCM-DXT<sub>5</sub>) and (VCM-DXT<sub>1</sub>) against MRSA at PBS pH 7.4. The values are expressed as mean ± SD, n = 3.

	(MIC µg/mL) after 24 hrs.	(MIC µg/mL) after 48 hrs.	(MIC µg/mL) after 72 hrs.
Bare VCM	7.8	7.8	7.8
DXT	NA	NA	NA
VCM-DXT <sub>5</sub> nanoplexes	1.25	1.25	1.25
VCM-DXT <sub>1</sub> nanoplexes	62.5	62.5	62.5

NA = No activity.

sizes of VCM-DXT<sub>5</sub> nanoplex which could lead to an increase in the surface area to volumes ratio. This could also affect drug adsorption efficiency which led to higher penetration and uptake. Thus, the *in vitro* studies confirmed the ability of the VCM-DXT<sub>5</sub> to enhance the activity of VCM against MRSA upon its complexation with DXT.

### 3.8. Bacterial cell viability assay

Percentage bacterial cell death after exposure to the bare VCM and VCM-DXT<sub>5</sub> nanoplexes at their respective MICs (7.8 µg/mL and

1.25 µg/mL VCM concentrations respectively) were quantified as shown in Fig. 11. The results showed that the bare VCM and VCM-DXT<sub>5</sub> nanoplexes at the MIC of formulation 1.25 µg/mL had a killing percentage of 32.98 ± 1.49% (Fig. 11C) and 66.24 ± 0.56% (Fig. 11D) respectively. This indicates a 2-fold higher killing activity of VCM-DXT<sub>5</sub> compared to bare VCM at similar concentrations. When the MRSA cells were incubated with the VCM-DXT<sub>5</sub> nanoplex and bare VCM at their respective MIC of 1.25 µg/mL and 7.8 µg/mL, they showed similar results of 66.24 ± 0.56% (Fig. 11D) and 65.27 ± 1.3% (Fig. 11B). Although the VCM concentration in the VCM-DXT<sub>5</sub> (MIC of 1.25 µg/mL) was 6.24-folds lower than that of the bare VCM treatment, it was still able to achieve a similar killing percent as that of the bare VCM (MIC of 7.8 µg/mL). This result indicated that the VCM-DXT<sub>5</sub> nanoplexes can be used at lower drug concentrations for treatment without affecting the desired therapeutic outcomes. Moreover, lower doses of treatment could be achieved using the VCM-DXT<sub>5</sub> nanoplexes could which lead to an avoidance of a dose dependent nephrotoxicity of VCM (Ingram et al., 2008). This further confirmed the ability of the VCM-DXT<sub>5</sub> nanoplexes to retain their potency and enhance the antibacterial activity of VCM.

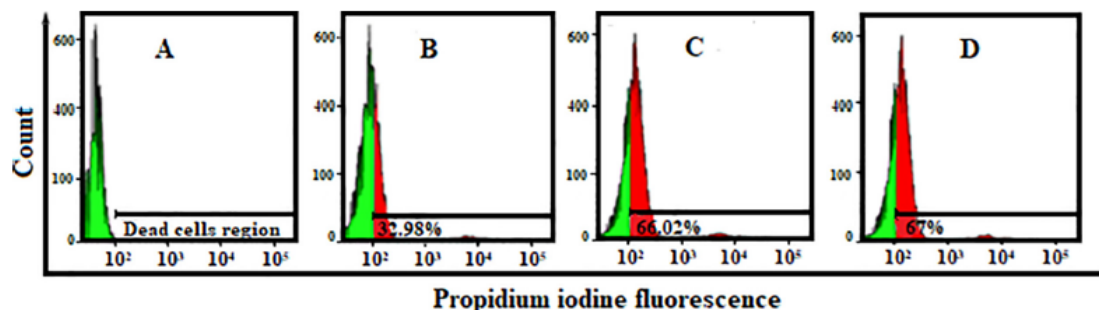


Fig. 11. *In vitro* antibacterial activity of MRSA cells determined by flow cytometry analysis. A) Cell fluorescence of untreated MRSA; B) Overlay of fluorescence of treated MRSA cells with bare VCM at its MIC; C) Overlay of fluorescence of MRSA cells treated with bare VCM at the MIC value of VCM-DXT<sub>5</sub> nanoplexes; D) Overlay of percentage fluorescence of MRSA cells treated with VCM-DXT<sub>5</sub> at its MIC values.

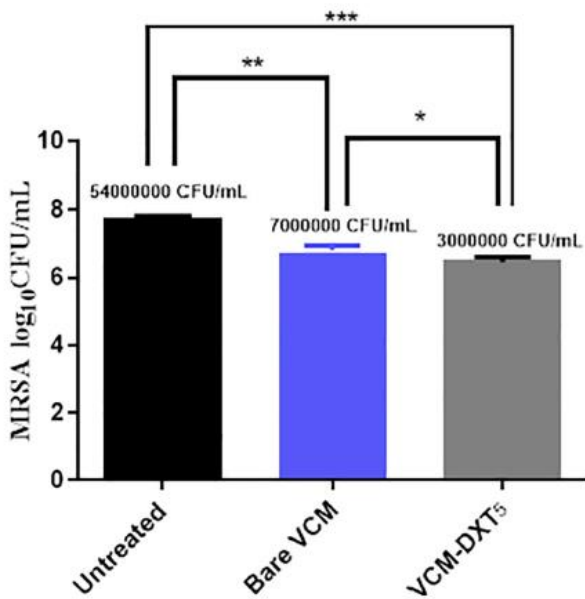


Fig. 12. MRSA CFUs quantification post 48 h of treatment, the data represent the mean ± SD (n = 3). \*\*\*Denotes significant differences when compared untreated with VCM-DXT<sub>5</sub> nanoplexes. \*\*Denotes untreated when compared to bare VCM, and \* denotes significant difference between the bare VCM and VCM-DXT<sub>5</sub> nanoplexes.

3.9. In vivo antibacterial activity

The *in vivo* studies were determined using a BALB/c mice skin infection model to confirm the antimicrobial activity of VCM-DXT<sub>5</sub> nanoplexes. The number of colony-forming units (CFUs) from each treatment group were quantified and represented as log<sub>10</sub>, shown in Fig. 12. The mean MRSA load (log<sub>10</sub> CFU) retrieved from the VCM-DXT<sub>5</sub> and bare VCM treatments, and untreated skin samples were 6.46 ± 0.15 (3,000,000 CFU/mL), 6.83 ± 0.13 (7,000,000 CFU/mL) and 7.72 ± 0.11 (54,000,000 CFU/mL), respectively. The results showed that the bare VCM had a 7.7-fold lower CFUs when compared to the untreated group. However, when VCM-DXT<sub>5</sub> nanoplexes treatment group was compared to the untreated group, the VCM-DXT<sub>5</sub> nanoplexes had an 18-fold reduction in CFUs with *P* = 0.001. When CFUs from the bare VCM treatment group were compared to the VCM-DXT<sub>5</sub>

nanoplexes, the latter had lowered CFUs of up to 2.3-fold, with a *P* value = 0.0324.

The one-way ANOVA showed significant differences in CFUs, with a *P* value = 0.001 among all the groups. The groups treated with VCM-DXT<sub>5</sub> nanoplexes significantly decreased the MRSA load in the skin samples by 2.5-fold compared to the bare VCM treated groups. This was in agreement with other *in vivo* results, for example: streptomycin, doxycycline and gentamicin nanoplexes against bacterial infections (Ranjan et al., 2010; Seleem et al., 2009). As the DXT on its own does not demonstrate antibacterial activity, the experiment showcased the degree of VCM binding to the DXT, with the subsequent improved targeting by nanoplexes possibly having led to the enhanced activities (Burygin et al., 2009). Therefore, the VCM-DXT<sub>5</sub> nanoplexes formulated in this study demonstrated the potential for combating MRSA infections.

The skin samples collected from all the groups were assessed for histomorphological changes that occurred on the experimental groups after infection and treatment, with the samples being stained with hematoxylin and eosin (H&E) and observed under a light microscope. The results indicated that the untreated skin samples showed tissue inflammation and abscess formation, as shown in Fig. 13A. The signs of swelling and abscess formation were observed for bare VCM treated group (Fig. 13B), but to a lesser extent than the untreated group (Fig. 13A). However, the VCM-DXT<sub>5</sub> nanoplexes displayed minimal signs of tissue inflammation and abscess formation (Fig. 13C). The extensive quantities of white blood cells (WBC) at the infection site were present for the untreated and bare VCM groups. Nevertheless, lower WBCs were displayed for the group treated with VCM-DXT<sub>5</sub> nanoplexes, as shown in Fig. 13C. The histomorphology analysis was found to correlate with the CFU/mL calculated in the *in vivo* antibacterial study. The absence of abscess formation and reduced immune response mechanisms (lesser extent of inflammation and reduced number of white blood cells) at infection site for the skin samples of VCM-DXT<sub>5</sub> treated group, when compared to that of untreated and VCM treated group, confirmed the antimicrobial potency of the VCM-DXT<sub>5</sub> nanoplexes.

4. Conclusion

With increasing rates of antimicrobial resistance, novel drug delivery systems, such as nanoplexes, which protect and enhance current antibiotics in the market are required. In this study, a novel VCM-DXT nanoplex was successfully formulated by polyelectrolyte complexation of VCM and DXT for the bio-safe delivery of vancomycin against MRSA. Complexation efficiency of greater than 90% was achieved for the drug

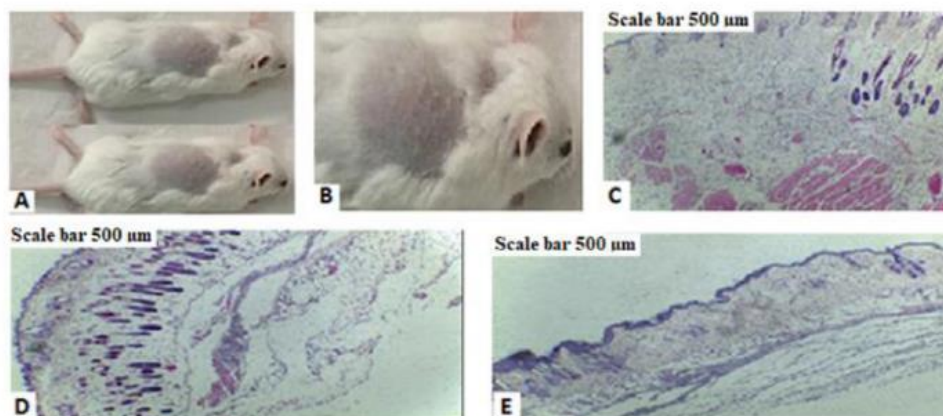


Fig. 13. Photomicrographs of the skin lesions at the site of injection; A) control and B) treated mice. Histomorphology of controls and treated (Scale bar = 500 μm): C) control/untreated, D) Bare VCM treated, E) VCM-DXT<sub>5</sub> nanoplexes treated scale bar = 500 μm.



VCM, with the drug release from nanoplexes occurring in a sustained manner. The molecular modelling studies proved that the presence of salt concentration is a pre-requisite for nanoplex formation. *In vitro* antibacterial studies of the nanoplexes against MRSA showed enhanced activity for nanoplexes over bare VCM. The results were further confirmed by flow cytometry, where the VCM-DXT<sub>5</sub>-nanoplexes had a better percentage killing compared to the bare VCM at similar applied concentrations. The *in vivo* BALB/c mouse, skin infection model revealed that treatment with the VCM-DXT<sub>5</sub>-nanoplexes significantly reduced the MRSA burden compared to the bare VCM. The superior antimicrobial activity and non-toxicity/biosafety of the VCM-DXT nanoplexes formulation upholds its applicability as a promising novel nano-carrier for antibiotic delivery.

#### Conflict of interest

The authors declare no conflict of interest.

#### Acknowledgements

The authors acknowledge the College of Health Sciences, University of KwaZulu-Natal (UKZN), UKZN Nanotechnology Platform, National Research Foundation of South Africa (Grant No. 87790 and 88453) for financial support. The Microscopy and Microanalysis Unit, Biomedical Research Unit, Department of Human Physiology and Flow Cytometry Research Laboratory at UKZN, CHPC (Cape Town) for supercomputing resources are acknowledged.

#### Data availability

The raw/processed data if required to reproduce these findings can be shared at any time.

#### Appendix A. Supplementary data

Supplementary data to this article can be found online at <https://doi.org/10.1016/j.ijpharm.2019.01.010>.

#### References

Abraham, M.J., Murtola, T., Schulz, R., Páll, S., Smith, J.C., Hess, B., Lindahl, E., 2015. GROMACS: high performance molecular simulations through multi-level parallelism from laptops to supercomputers. *SoftwareX* 1, 19–25.

Ahmed, S., Vepuri, S.B., Jadhav, M., Kalhapure, R.S., Govender, T., 2018. Identifying the interaction of vancomycin with novel pH-responsive lipids as antibacterial biomaterials via accelerated molecular dynamics and binding free energy calculations. *Cell Biochem. Biophys.* 76, 147–159.

Ardnt-Jovin, D.J., Jovin, T.M., 1989. Fluorescence labeling and microscopy of DNA. *Methods Cell Biol.* 30, 417–448.

Baelo, A., Levato, R., Julián, E., Crespo, A., Astola, J., Gavaldà, J., Engel, E., Mateos-Timoneda, M.A., Torrents, E., 2015. Disassembling bacterial extracellular matrix with DNase-coated nanoparticles to enhance antibiotic delivery in biofilm infections. *J. Controlled Release* 209, 150–158.

Bal, A., David, M., Garau, J., Gottlieb, T., Mazzei, T., Scaglione, F., Tattevin, P., Gould, I., 2017. Future trends in the treatment of methicillin-resistant *Staphylococcus aureus* (MRSA) infection: an in-depth review of newer antibiotics active against an enduring pathogen. *J. Glob. Antimicrob. Resist.* 10, 295–303.

Begum, G., Reddy, T.N., Kumar, K.P., Dhevendar, K., Singh, S., Amamath, M., Misra, S., Rangari, V.K., Rana, R.K., 2016. *In situ* strategy to encapsulate antibiotics in a bioinspired CaCO<sub>3</sub> structure enabling pH-sensitive drug release Apt for therapeutic and imaging applications. *ACS Appl. Mater. Interfaces* 8, 22056–22063.

Bexfield, A., Bond, A.E., Roberts, E.C., Dudley, E., Nigam, Y., Thomas, S., Newton, R.P., Ratcliffe, N.A., 2008. The antibacterial activity against MRSA strains and other bacteria of a < 500 Da fraction from maggot excretions/secretions of *Lucilia sericata* (Diptera: Calliphoridae). *Microbes Infect.* 10, 325–333.

Bixon, M., Lifson, S., 1967. Potential functions and conformations in cycloalkanes. *Tetrahedron* 23, 769–784.

Burygin, G., Khlebtsov, B., Shantrokha, A., Dykman, L., Bogatyrev, V., Khlebtsov, N., 2009. On the enhanced antibacterial activity of antibiotics mixed with gold nanoparticles. *Nanoscale Res. Lett.* 4, 794.

Bussi, G., Donadio, D., Parrinello, M., 2007. Canonical sampling through velocity rescaling. *J. Chem. Phys.* 126, 014101.

Cakić, M., Nikolić, G., Ilić, L., Stanković, S., 2005. Synthesis and FTIR characterization of

some dextran sulphates. *Chem. Ind. Chem. Eng. Q.* 11, 74–78.

Caram-Lelham, N., Hed, F., Sundelöf, L.O., 1997. Adsorption of charged amphiphiles to oppositely charged polysaccharides—a study of the influence of polysaccharide structure and hydrophobicity of the amphiphile molecule. *Biopolymers* 41, 765–772.

Cevher, E., Orhan, Z., Mülazımoğlu, L., Şensoy, D., Alper, M., Yıldız, A., Özsoy, Y., 2006. Characterization of biodegradable chitosan microspheres containing vancomycin and treatment of experimental osteomyelitis caused by methicillin-resistant *Staphylococcus aureus* with prepared microspheres. *Int. J. Pharm.* 317, 127–135.

Chang, S., Sievert, D.M., Hageman, J.C., Boulton, M.L., Tenover, F.C., Downes, F.P., Shah, S., Rudrik, J.T., Pupp, G.R., Brown, W.J., 2003. Infection with vancomycin-resistant *Staphylococcus aureus* containing the vanA resistance gene. *N. Engl. J. Med.* 348, 1342–1347.

Chen, C.-H., Lin, Y.-S., Wu, S.-J., Mi, F.-L., 2018. Multifunctional nanoparticles prepared from arginine-modified chitosan and thiolated fucoidan for oral delivery of hydrophobic and hydrophilic drugs. *Carbohydr. Polym.* 193, 163–172.

Cheow, W.S., Chang, M.W., Hadinoto, K., 2011. The roles of lipid in anti-biofilm efficacy of lipid-polymer hybrid nanoparticles encapsulating antibiotics. *Colloids Surf., A* 389, 158–165.

Cheow, W.S., Hadinoto, K., 2012a. Green preparation of antibiotic nanoparticle complex as potential anti-biofilm therapeutics via self-assembly amphiphile-polyelectrolyte complexation with dextran sulfate. *Colloids Surf., B* 92, 55–63.

Cheow, W.S., Hadinoto, K., 2012b. Self-assembled amorphous drug-polyelectrolyte nanoparticle complex with enhanced dissolution rate and saturation solubility. *J. Colloid Interface Sci.* 367, 518–526.

Cheow, W.S., Kiew, T.Y., Hadinoto, K., 2015. Amorphous nanodrugs prepared by complexation with polysaccharides: Carrageenan versus dextran sulfate. *Carbohydr. Polym.* 117, 549–558.

Cheow, W.S., Kiew, T.Y., Yang, Y., Hadinoto, K., 2014. Amorphization strategy affects the stability and supersaturation profile of amorphous drug nanoparticles. *Mol. Pharm.* 11, 1611–1620.

Darden, T., York, D., Pedersen, L., 1993. Particle mesh Ewald: An N-log(N) method for Ewald sums in large systems. *J. Chem. Phys.* 98, 10089–10092.

Deurenberg, R., Vink, C., Kalenic, S., Friedrich, A., Bruggeman, C., Stobberingh, E., 2007. The molecular evolution of methicillin-resistant *Staphylococcus aureus*. *Clin. Microbiol. Infect.* 13, 222–235.

Florence, A.T., Attwood, D., 1988. *Physicochemical Principles of Pharmacy*, 2nd ed. Chapman and Hall, New York, NY.

Gandhi, A., Shah, N.P., 2015. Effect of salt on cell viability and membrane integrity of *Lactobacillus acidophilus*, *Lactobacillus casei* and *Bifidobacterium longum* as observed by flow cytometry. *Food Microbiol.* 49, 197–202.

Garberoglio, G., 2012. OBGMX: a web-based generator of GROMACS topologies for molecular and periodic systems using the universal force field. *J. Comput. Chem.* 33, 2204–2208.

Ghosh, N., Chavada, R., Maley, M., van Hal, S., 2014. Impact of source of infection and vancomycin AUC<sub>0–24</sub>/MIC<sub>BMD</sub> targets on treatment failure in patients with methicillin-resistant *Staphylococcus aureus* bacteraemia. *Clin. Microbiol. Infect.* 20, O1098–O1105.

Gustafsen, C., Olsen, D., Vilstrup, J., Lund, S., Reinhardt, A., Welner, N., Larsen, T., Andersen, C.B., Weyer, K., Li, J.-P., 2017. Heparan sulfate proteoglycans present PCSK9 to the LDL receptor. *Nat. Commun.* 8, 503.

Heo, R., You, D.G., Um, W., Choi, K.Y., Jeon, S., Park, J.-S., Choi, Y., Kwon, S., Kim, K., Kwon, I.C., 2017. Dextran sulfate nanoparticles as a theranostic nanomedicine for rheumatoid arthritis. *Biomaterials* 131, 15–26.

Honary, S., Ebrahimi, P., Hadianamrei, R., 2014. Optimization of particle size and encapsulation efficiency of vancomycin nanoparticles by response surface methodology. *Pharm. Dev. Technol.* 19, 987–998.

Humphrey, W., Dalke, A., Schulten, K., 1996. VMD: visual molecular dynamics. *J. Mol. Graph.* 14, 33–38.

Ingram, P.R., Lye, D.C., Tambyah, P.A., Goh, W.P., Tam, V.H., Fisher, D.A., 2008. Risk factors for nephrotoxicity associated with continuous vancomycin infusion in out-patient parenteral antibiotic therapy. *J. Antimicrob. Chemother.* 62, 168–171.

Ionita, D., Bajenaru-Georgescu, D., Totea, G., Mazare, A., Schmuki, P., Demetrescu, I., 2017. Activity of vancomycin release from bioinspired coatings of hydroxyapatite or TiO<sub>2</sub> nanotubes. *Int. J. Pharm.* 517, 296–302.

Jain, N., Jain, G.K., Javed, S., Iqbal, Z., Talegaonkar, S., Ahmad, F.J., Khar, R.K., 2008. Recent approaches for the treatment of periodontitis. *Drug Discovery Today* 13, 932–943.

Kiew, T.Y., Cheow, W.S., Hadinoto, K., 2015. Preserving the supersaturation generation capability of amorphous drug-polysaccharide nanoparticle complex after freeze drying. *Int. J. Pharm.* 484, 115–123.

Kutscher, M., Cheow, W.S., Werner, V., Lorenz, U., Ohlsen, K., Meinel, L., Hadinoto, K., Gernershaus, O., 2015. Influence of salt type and ionic strength on self-assembly of dextran sulfate-ciprofloxacin nanoplexes. *Int. J. Pharm.* 486, 21–29.

Lazzarini, L., Lipsky, B.A., Mader, J.T., 2005. Antibiotic treatment of osteomyelitis: what have we learned from 30 years of clinical trials? *Int. J. Infect. Dis.* 9, 127–138.

Lewies, A., Wentzel, J.F., Jordaan, A., Bezuidenhout, C., Du Plessis, L.H., 2017. Interactions of the antimicrobial peptide nisin Z with conventional antibiotics and the use of nanostructured lipid carriers to enhance antimicrobial activity. *Int. J. Pharm.* 526, 244–253.

Liu, J., Wang, Z., Li, F., Gao, J., Wang, L., Huang, G., 2015. Liposomes for systematic delivery of vancomycin hydrochloride to decrease nephrotoxicity: characterization and evaluation. *Asian J. Pharm. Sci.* 10, 212–222.

Lodise, T., Miller, C., Graves, J., Evans, A., Graffunder, E., Helmecke, M., Stellrecht, K., 2008. Predictors of high vancomycin MIC values among patients with methicillin-resistant *Staphylococcus aureus* bacteraemia. *J. Antimicrob. Chemother.* 62, 1138–1141.

- Loll, P.J., Kaplan, J., Selinsky, B.S., Axelsen, P.H., 1999. Vancomycin binding to low-affinity ligands: delineating a minimum set of interactions necessary for high-affinity binding. *J. Med. Chem.* 42, 4714–4719.
- Michael, Z., Ian, M., 2017. Recently approved antibacterials for MRSA and other gram-positive pathogens: the shock of the new. *Int. J. Antimicrob. Agents.*
- Nguyen, M.-H., Tran, T.-T., Hadinoto, K., 2016. Controlling the burst release of amorphous drug–polysaccharide nanoparticle complex via crosslinking of the polysaccharide chains. *Eur. J. Pharm. Biopharm.* 104, 156–163.
- Nguyen, M.H., Yu, H., Kiew, T.Y., Hadinoto, K., 2015. Cost-effective alternative to nanoencapsulation: amorphous curcumin–chitosan nanoparticle complex exhibiting high payload and supersaturation generation. *Eur. J. Pharm. Biopharm.* 96, 1–10.
- Nimesh, S., Kumar, R., Chandra, R., 2006. Novel polyallylamine–dextran sulfate–DNA nanoplexes: highly efficient non-viral vector for gene delivery. *Int. J. Pharm.* 320, 143–149.
- Niu, X., Zhang, Z., Zhong, Y., 2017. Hydrogel loaded with self-assembled dextran sulfate–doxorubicin complexes as a delivery system for chemotherapy. *Mater. Sci. Eng., C* 77, 888–894.
- O'Brien-Simpson, N.M., Pantarat, N., Attard, T.J., Walsh, K.A., Reynolds, E.C., 2016. A rapid and quantitative flow cytometry method for the analysis of membrane disruptive antimicrobial activity. *PLoS One* 11, e0151694.
- Omolo, C.A., Kalhapure, R.S., Agrawal, N., Rambharose, S., Mocktar, C., Govender, T., 2018. Formulation and molecular dynamics simulations of a fusidic acid nanosuspension for simultaneously enhancing solubility and antibacterial activity. *Mol. Pharm.*
- Omolo, C.A., Kalhapure, R.S., Jadhav, M., Rambharose, S., Mocktar, C., Ndesendo, V.M., Govender, T., 2017. Pegylated oleic acid: a promising amphiphilic polymer for nanoantibiotic delivery. *Eur. J. Pharm. Biopharm.* 112, 96–108.
- Ozbas, B., Kretsinger, J., Rajagopal, K., Schneider, J.P., Pochan, D.J., 2004. Salt-triggered peptide folding and consequent self-assembly into hydrogels with tunable modulus. *Macromolecules* 37, 7331–7337.
- Parrinello, M., Rahman, A., 1981. Polymorphic transitions in single crystals: a new molecular dynamics method. *J. Appl. Phys.* 52, 7182–7190.
- Ranjana, A., Pothayee, N., Seleem, M., Jain, N., Sriranganathan, N., Riffle, J., Kasimanickam, R., 2010. Drug delivery using novel nanoplexes against a Salmonella mouse infection model. *J. Nanopart. Res.* 12, 905–914.
- Rappé, A.K., Casewit, C.J., Colwell, K., Goddard III, W., Skiff, W., 1992. UFF, a full periodic table force field for molecular mechanics and molecular dynamics simulations. *J. Am. Chem. Soc.* 114, 10024–10035.
- Rüger, M., Bensch, G., Tüngler, R., Reichl, U., 2012. A flow cytometric method for viability assessment of *Staphylococcus aureus* and *Burkholderia cepacia* in mixed culture. *Cytometry Part A* 81, 1055–1066.
- Saidykhan, L., Bakar, M.Z.B.A., Rukayadi, Y., Kura, A.U., Latifah, S.Y., 2016. Development of nanoantibiotic delivery system using cockle shell-derived aragonite nanoparticles for treatment of osteomyelitis. *Int. J. Nanomed.* 11, 661.
- Seleem, M.N., Jain, N., Pothayee, N., Ranjana, A., Riffle, J., Sriranganathan, N., 2009. Targeting *Brucella melitensis* with polymeric nanoparticles containing streptomycin and doxycycline. *FEMS Microbiol. Lett.* 294, 24–31.
- Shrestha, N.K., Scalera, N.M., Wilson, D.A., Procop, G.W., 2011. Rapid differentiation of methicillin-resistant and methicillin-susceptible *Staphylococcus aureus* by flow cytometry after brief antibiotic exposure. *J. Clin. Microbiol.* 49, 2116–2120.
- Sikwal, D.R., Kalhapure, R.S., Rambharose, S., Vepuri, S., Soliman, M., Mocktar, C., Govender, T., 2016. Polyelectrolyte complex of vancomycin as a nanoantibiotic: preparation, in vitro and in silico studies. *Mater. Sci. Eng., C* 63, 489–498.
- Sonawane, S.J., Kalhapure, R.S., Jadhav, M., Rambharose, S., Mocktar, C., Govender, T., 2015. Transforming linoleic acid into a nanoemulsion for enhanced activity against methicillin susceptible and resistant *Staphylococcus aureus*. *RSC Adv.* 5, 90482–90492.
- Tiyaboonchai, W., Woiszwill, J., Middaugh, C.R., 2003. Formulation and characterization of DNA–polyethylenimine–dextran sulfate nanoparticles. *Eur. J. Pharm. Sci.* 19, 191–202.
- Vo, C.L.-N., Park, C., Lee, B.-J., 2013. Current trends and future perspectives of solid dispersions containing poorly water-soluble drugs. *Eur. J. Pharm. Biopharm.* 85, 799–813.
- Waltho, J.P., Williams, D.H., 2007. The natural design of vancomycin family antibiotics to bind their target peptides, Ciba Foundation Symposium 158–Host-Guest Molecular Interactions: From Chemistry to Biology: Host-Guest Molecular Interactions: From Chemistry to Biology: Ciba Foundation Symposium 158. Wiley Online Lib. 73–97.
- Wijesiri, N., Ozkaya-Ahmadov, T., Wang, P., Zhang, J., Tang, H., Yu, X., Ayres, N., Zhang, P., 2017. Photodynamic inactivation of multidrug-resistant *Staphylococcus aureus* using hybrid photosensitizers based on amphiphilic block copolymer-functionalized gold nanoparticles. *ACS Omega* 2, 5364–5369.
- Wilkinson, M.G., 2018. Flow cytometry as a potential method of measuring bacterial viability in probiotic products: a review. *Trends Food Sci. Technol.*
- Xu, J., Xu, B., Shou, D., Xia, X., Hu, Y., 2015. Preparation and evaluation of vancomycin-loaded N-trimethyl chitosan nanoparticles. *Polymers* 7, 1850–1870.
- Yang, Z., Liu, J., Gao, J., Chen, S., Huang, G., 2015. Chitosan coated vancomycin hydrochloride liposomes: characterizations and evaluation. *Int. J. Pharm.* 495, 508–515.
- Yousefpour, P., Atyabi, F., Farahani, E.V., Sakhtianchi, R., Dinarvand, R., 2011. Polymeric carbohydrate doxorubicin–dextran nanocomplex as a delivery system for anticancer drugs: in vitro analysis and evaluations. *Int. J. Nanomed.* 6, 1487.
- Yousry, C., Fahmy, R.H., Essam, T., El-Laithy, H.M., Elkhesheh, S.A., 2016. Nanoparticles as tool for enhanced ophthalmic delivery of vancomycin: a multidistrict-based microbiological study, solid lipid nanoparticles formulation and evaluation. *Drug Dev. Ind. Pharm.* 42, 1752–1762.
- Yu, H., Hadinoto, K., 2017. Impacts of dextran sulfate's chain length on the characteristics of its self-assembled colloidal complex formed with amphiphilic small-molecule drug. *Int. J. Biol. Macromol.* 103, 493–500.
- Yu, H., Teo, J., Chew, J.W., Hadinoto, K., 2016. Dry powder inhaler formulation of high-payload antibiotic nanoparticle complex intended for bronchiectasis therapy: spray drying versus spray freeze drying preparation. *Int. J. Pharm.* 499, 38–46.
- Zarif, M., Afidah, A., Abdullah, J., Shariza, A., 2012. Physicochemical characterization of vancomycin and its complexes with  $\beta$ -cyclodextrin. *Biomed. Res.* 23.
- Zhang, Y., Huo, M., Zhou, J., Zou, A., Li, W., Yao, C., Xie, S., 2010. DDSolver: an add-in program for modeling and comparison of drug dissolution profiles. *AAPS J.* 12, 263–271.

## Appendix II



06 November 2017

Dr Rahul Kalhapure (38560)  
School of Health Sciences  
Westville Campus

Dear Dr Kalhapure,

**Protocol reference number: AREC/104/015PD**

**Project title: *In vivo* antibacterial activity of Antimicrobial based nanoantibiotic formulations in BALB/c mice**

**Full Approval – Renewal Application**

With regards to your renewal application received on 10 October 2017. The documents submitted have been accepted by the Animal Research Ethics Committee and **FULL APPROVAL** for the renewal has **been** granted.

**Please note: Any Veterinary and Para-Veterinary procedures must be conducted by a SAVC registered VET or SAVC authorized person.**

**Any alteration/s to the approved research protocol, i.e Title of Project, Location of the Study, Research Approach and Methods must be reviewed and approved through the amendment/modification prior to its implementation. In case you have further queries, please quote the above reference number.**

Please note: Research data should be securely stored in the discipline/department for a period of 5 years.

**The ethical clearance certificate is only valid for a period of one year from the date of issue. Renewal for the study must be applied for before 06 November 2018.**

**Attached to the Approval letter is a template of the Progress Report that is required at the end of the study, or when applying for Renewal (whichever comes first). An Adverse Event Reporting form has also been attached in the event of any unanticipated event involving the animals' health / wellbeing.**

I take this opportunity of wishing you everything of the best with your study.

Yours faithfully

.....  
Prof S Islam, PhD

Chair: Animal Research Ethics Committee

/ms

Cc Supervisor: Professor Thirumala Govender  
Cc Academic Leader Research: Professor J van Heerden  
Cc Registrar: Mr Simon Mokoena  
Cc NSPCA: Ms Erihia Veruiel  
Cc BRU – Dr Linda Bester  
Cc School Administrator: Ms Phindile Nene

---

Animal Research Ethics Committee (AREC)

Ms Mariette Snyman (Administrator)

Westville Campus, Govan Mbeki Building

Postal Address: Private Bag X54001, Durban 4000

Telephone: +27 (0) 31 260 8350 Facsimile: +27 (0) 31 260 4609 Email: [animalethics@ukzn.ac.za](mailto:animalethics@ukzn.ac.za)

Website: <http://research.ukzn.ac.za/Research-Ethics/Animal-Ethics.aspx>



100 YEARS OF ACADEMIC EXCELLENCE

Founding Campuses: Edgewood Howard College Medical School Pietermaritzburg Westville



## Appendix III



15 April 2019

**Dr Ayman Waddad (60072)**  
School of Health Sciences  
Westville Campus

Dear Dr Waddad,

**Protocol reference number: AREC/104/015PD**

**Project title:** *In vivo* antibacterial activity of antimicrobial based nanoantibiotic formulations in BALB/c mice

### Full Approval – Renewal Application

With regards to your renewal application received on 05 November 2018 and your response on 20 March 2019 to our letter of 05 November 2019. The documents submitted have been accepted by the Animal Research Ethics Committee and **FULL APPROVAL** for the protocol has been granted with the following conditions:

**Please note: Any Veterinary and Para-Veterinary procedures must be conducted by a SAVC registered VET or SAVC authorized person.**

**Any alteration/s to the approved research protocol, i.e Title of Project, Location of the Study, Research Approach and Methods must be reviewed and approved through the amendment/modification prior to its implementation. In case you have further queries, please quote the above reference number.**

Please note: Research data should be securely stored in the discipline/department for a period of 5 years.

**The ethical clearance certificate is only valid for a period of one year from the date of issue. Renewal for the study must be applied for before 15 April 2020.**

**Attached to the Approval letter is a template of the Progress Report that is required at the end of the study, or when applying for Renewal (whichever comes first). An Adverse Event Reporting form has also been attached in the event of any unanticipated event involving the animals' health / wellbeing.**

I take this opportunity of wishing you everything of the best with your study.

Yours faithfully

.....  
**Dr Sanil D. Singh, PhD**  
Acting Chair: Animal Research Ethics Committee

/ms

cc Supervisor: Professor Thirumala Govender  
Cc Academic Leader Research: Dr Brenda de Gama  
Cc Registrar: Mr Simon Mokoena

Cc BRU – Dr Linda Bester

---

**Animal Research Ethics Committee (AREC)**

**Ms Mariette Snyman (Administrator)**

**Westville Campus, Govan Mbeki Building**

**Postal Address: Private Bag X54001, Durban 4000**

**Telephone: +27 (0) 31 260 8350 Facsimile: +27 (0) 31 260 4809 Email: [animalet hics@ukzn.ac.za](mailto:animalet hics@ukzn.ac.za)**


**Website: <http://research.ukzn.ac.za/Research-Ethics/Animal-Ethics.aspx>**



**100 YEARS OF ACADEMIC EXCELLENCE**

Founding Campuses: ■ Edgewood ■ Howard College ■ Medical School ■ Pietermaritzburg ■ Westville

## Appendix IV




UNIVERSITY OF  
KWAZULU-NATAL  
INVUVESI  
YAKWAZULU-NATALI

### DELIVERY OF NOVEL VANCOMYCIN NANOPLEXES FOR COMBATING METHICILLIN RESISTANT *STAPHYLOCOCCUS AUREUS* (MRSA) INFECTIONS

Daniel Hassan<sup>1</sup>, Ayman Y. Waddad<sup>1</sup>, Calvin A. Omolo<sup>1</sup>, Ramesh Gannamani<sup>1</sup>, Sanjeev Rambharose<sup>1</sup>, Chunderika Mocktar<sup>1</sup>, Nikhil Agrawal<sup>1</sup>, and Thirumala Govender<sup>1\*</sup>

<sup>1</sup>Discipline of Pharmaceutical Sciences, College of Health Sciences, University of KwaZulu-Natal, Private Bag X54001, Durban, South Africa



asm  
microbe  
2018  
JUNE 7-11 ATLANTA

---

### INTRODUCTION AND AIMS

- ❖ Infectious diseases caused by methicillin-resistant *Staphylococcus aureus* (MRSA) continues to be a major concern globally [1].
- ❖ The effectiveness of current antibiotics such as vancomycin (VCM),  $\beta$ -lactam antibiotics (penicillins and cephalosporins) and trimethoprim against MRSA is compromised due to antibiotic resistance [2].
- ❖ VCM nanoplexes, which involve drug nanoparticles complexed with an oppositely charged polyelectrolyte, can be a good alternate to conventional dosage forms to evade antibiotic resistance.
- ❖ The aim of this study was to explore the potential of dextran sulfate sodium salt (DXT) for complexation with VCM to deliver novel VCM nanoplexes for combating MRSA infections.

### METHODS

#### Preparation of Nanoplexes

- ❖ Nanoplexes were prepared by a self-assembling amphiphile polyelectrolyte complexation method, with minor modifications [3].
- ❖ Briefly, 0.45 % (w/v) of DXT in 0.1 M sodium chloride solution and 1 % (w/v) VCM solution in milli-Q water were prepared separately. Varying amounts of VCM solution of 2.5, 5, 10, 15 and 20 mL were then added drop wise to 5 mL of DXT solution (0.45 % w/v) under gentle and constant stirring for one hour at ambient condition for the formation of VCM-DXT nanoplexes.

#### Characterization

##### Size, polydispersity index (PDI) and zeta potential (ZP)

- ❖ The nanoplexes was characterized for size, PDI and ZP using a Zetasizer Nano ZS90 (Malvern Instrument Ltd., UK)

##### Complexation efficiency (% CE)

- ❖ Complexation efficiency was calculated using a UV Spectrophotometer at 280.4 nm wavelength.

##### In-vitro cytotoxicity

- ❖ The cytotoxicity of the VCM-DXT<sub>5</sub> nanoplexes was determined using the MTT assay and measured on a microplate spectrophotometer (Spectrostar Nano, Germany) at a wavelength of 540 nm.

##### Molecular modelling

- ❖ Molecular modelling techniques were performed using GROMACS and the centre for mass distance between VCM and DXT was calculated using in-house Tcl script.

##### In vitro drug release

- ❖ Drug release was performed in PBS (pH 7.4) at 37°C using a dialysis bag and analysed using a UV spectrophotometer at 280.4 nm wavelength.

##### In vitro antibacterial activity

- ❖ The minimum inhibitory concentration (MIC) values for VCM-DXT<sub>5</sub> nanoplexes were determined against MRSA at pH 7.4 using a broth dilution method.

##### Bacterial cell viability assay

- ❖ Cell viability studies were performed using a flow cytometry BD FACSCANTO II (Becton Dickinson, CA, USA) instrument and the data was captured using a flow cytometer software (BD FACSDIVA V8.0.1 software [USA]), and analysed using Kaluza-1.5.20 (Beckman Coulter USA) flow cytometer software.

##### In-vivo antibacterial activity and histological evaluation

- ❖ The *in vivo* antibacterial activity was evaluated against MRSA using BALB/c mice (Protocol approval number. AREC/104/015PD).

### RESULTS AND DISCUSSION

Formulation	Z <sub>eta</sub>	Size (nm)	PDI	ZP (mV)	% CE
VCM-DXT <sub>5</sub>	0.31	84.55 ± 4.24	0.45 ± 0.02	-33.0 ± 4.87	90.40 ± 0.77

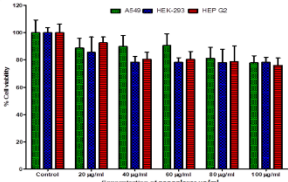


Fig. 1: *In vitro* cytotoxicity profile of VCM-DXT<sub>5</sub> nanoplexes (n = 3).

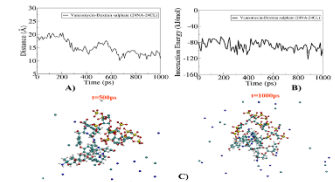


Fig. 2: Simulations at two different time points in presence of 24 Na<sup>+</sup> and 24 Cl<sup>-</sup>.

Antibacterial activity	(MIC µg/mL) Day 1	(MIC µg/mL) Day 2	(MIC µg/mL) Day 3
Bare VCM	7.8	7.8	7.8
DXT	NA	NA	NA
VCM-DXT <sub>5</sub>	1.25	1.25	1.25

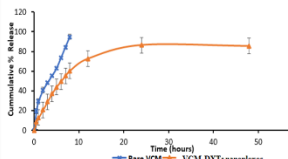


Fig. 3: *In vitro* release profile of VCM-DXT<sub>5</sub> nanoplexes from PBS pH 7.4 (n = 3).

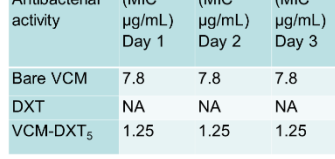


Fig. 4: *In vitro* antibacterial activity of VCM-DXT<sub>5</sub> nanoplexes against MRSA at PBS pH 7.

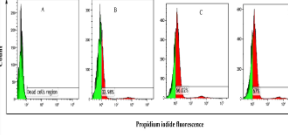


Fig. 5: *In vitro* bacterial cell viability assay profile of VCM-DXT<sub>5</sub> nanoplexes (n = 3).

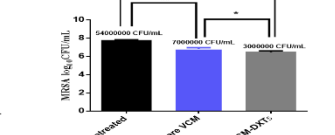


Fig. 6: Colony-forming units (CFUs) represented as log<sub>10</sub> for each treatment group

---

### REFERENCES & ACKNOWLEDGMENT

#### References

1. Wijesiri, Ozkaya-Ahmadov., *et al.*, *ACS Omega*, 2017, pp5364-5369.
2. Lazzarini & Mader, *International Journal of Infectious diseases*. 2005, pp127-138.
3. Kutschern, Cheow, *et al.*, *International Journal of Pharmaceutics*. 2015, pp21-29.

#### Acknowledgment

College of Health Sciences, UKZN Nanotechnology Platform and National Research Foundation of South Africa.

### CONCLUSION

- ❖ DXT can be used to formulate VCM nanoplexes with smaller particles sizes, high complexation efficiency, sustained release, higher percentage bacterial killing and enhanced antibacterial activity.
- ❖ Hence, VCM nanoplexes could be a superior alternative as a novel nano-carrier for antibiotic delivery to combat MRSA burden.

# Appendix V



## Novel pH-responsive zwitterionic vancomycin-chitosan nanovesicles: *In vitro* Antimicrobial activity against *Staphylococcus aureus* (SA) and Methicillin-resistance *Staphylococcus aureus* (MRSA).

Daniel Hassan<sup>1</sup>, Calvin A. Omolo<sup>1</sup>, Chunderika Mocktar<sup>1</sup>, Thirumala Govender<sup>1</sup>

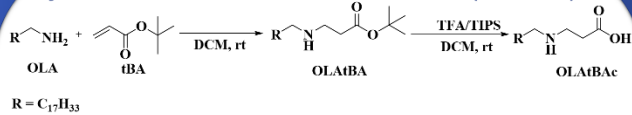
<sup>1</sup>Discipline of Pharmaceutical Sciences, College of Health Sciences, University of KwaZulu-Natal, Private Bag X54001, Durban, South Africa

### INTRODUCTION AND AIMS

- Infectious diseases caused by Methicillin resistant *Staphylococcus aureus* (MRSA) resistance is a serious global concern [Medina et al 2018]. The disadvantages of current conventional dosage forms have contributed to the antimicrobial resistance crisis [Huh & Kwon 2011].
- Recently, pH-responsive nanovesicles are reported to address antibiotics resistance challenges by maximizing targeted delivery of antibiotics against MRSA at the infection site characterized by acidic conditions [Kalhapure et al 2017].
- Developing a novel pH-responsive material is essential for efficient delivery of antibiotics to the site of infection at a required concentration while minimizing the exposure to the healthy sites. Therefore, reduces the development of resistance.
- The aim of the study was to synthesize a novel pH-responsive zwitterionic lipid (OLA<sub>t</sub>BAC) from oleylamine and formulate vancomycin (VM) chitosan nanovesicles for effective delivery, targeting and combating of SA and MRSA infections.

### METHODS

#### Synthesis and characterization of the novel (OLA<sub>t</sub>BAC)



#### Preparation of pH-responsive Nanovesicles

- The novel pH-responsive vancomycin nanovesicles (VM-OLA<sub>t</sub>BAC-NVs) were prepared by using a modified version of an ionic gelation method. Briefly, 60 mg of the novel lipid (OLA<sub>t</sub>BAC) was dissolved in water containing 10 mg of VM and 10 mL of 0.1 % TPP was added. The premixed solution was added dropwise to 50 mL of 0.1 % w/v chitosan (CH) and sonicated resulting in spontaneous formation of the nanovesicles.

#### Characterization

##### Size, polydispersity index (PDI), zeta potential (ZP) and morphology

- The novel vancomycin pH-responsive nanovesicles (VM-OLA<sub>t</sub>BAC-NVs) were characterized for size, PDI and ZP using a Zetasizer Nano ZS90 (Malvern Instrument Ltd., UK) and Cyro-High-resolution Transmission Electron Microscope JEOL, HR-TEM-2100, (Japan) at accelerated voltage of 200 kV.

##### Encapsulation efficiency (% EE)

- Encapsulation efficiency was calculated using a UV Spectrophotometer (Shimadzu UV 1601, Japan) at a wavelength of 280.4 nm.

##### In vitro biocompatibility study

- The biocompatibility of the VM-OLA<sub>t</sub>BAC-NVs was determined using a MTT assay and measured on a microplate spectrophotometer (Spectrostar Nano, Germany) at a wavelength of 540 nm.

##### In vitro drug release

- Drug release study was performed in PBS (pH 7.4 and 6.0) at 37°C using a dialysis bag and analysed using a UV spectrophotometer (Shimadzu UV 1601, Japan) at a wavelength of 280.4 nm.

##### In vitro antibacterial activity

- The minimum inhibitory concentration (MIC) values for novel pH-responsive vancomycin nanovesicles (VM-OLA<sub>t</sub>BAC-NVs) were determined against SA and MRSA at pH (7.4 and 6.0) using a broth dilution method.

### RESULTS AND DISCUSSION

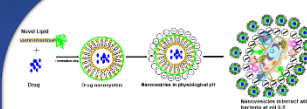


Fig. 1: Schematic representation of VM-OLA<sub>t</sub>BAC-NVs1 formation and interacting with bacteria.

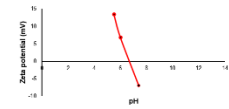


Fig. 2: pH-responsiveness of VM-OLA<sub>t</sub>BAC-NVs1 at pH 7.4, 6.0 and 5.5 (n = 3).

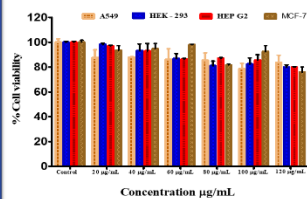


Fig. 3: In vitro cytotoxicity profile of the novel pH-responsive VM-OLA<sub>t</sub>BAC-NVs1 (n = 3).

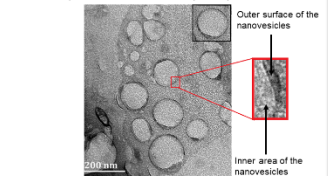


Fig. 4: Morphology of the VM-OLA<sub>t</sub>BAC-NVs1 showing the outer surface and the inner layer.

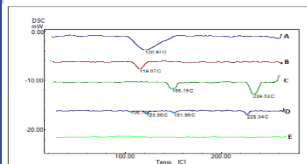


Fig. 5: Thermal profile of VM, OLA<sub>t</sub>BAC, CH, physical mixture (VM, OLA<sub>t</sub>BAC and CH) and lyophilized VM-OLA<sub>t</sub>BAC-NVs1 nanovesicles.

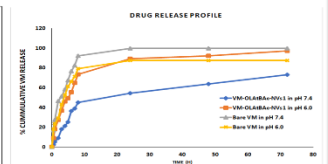


Fig. 6: In vitro drug release profile of the VM-OLA<sub>t</sub>BAC-NVs1 nanovesicles in different pH (7.4 and 6.0) (n = 3).

Table 1. *In vitro* antibacterial activity of bare VM, OLA<sub>t</sub>BAC-NVs and VM-OLA<sub>t</sub>BAC-NVs1 nanovesicles showing MICs against SA and MRSA at pH 7.4 and pH 6.0.

In vitro antibacterial activity at pH 7.4						
Time (h)	24	48	72	24	48	72
	SA (MIC µg/mL)			MRSA (MIC µg/mL)		
Bare VM	1.950	1.950	1.950	31.25	31.25	31.25
VM-OLA <sub>t</sub> BAC-NVs1	0.290	1.190	1.190	2.390	4.780	4.780
In vitro antibacterial activity at pH 6.0						
Time (h)	24	48	72	24	48	72
	SA (MIC µg/mL)			MRSA (MIC µg/mL)		
Bare VM	1.950	1.950	1.950	31.25	31.25	31.25
VM-OLA <sub>t</sub> BAC-NVs1	0.290	1.190	1.190	0.590	0.590	1.190

All experimental result values are expressed as mean ± SD (n=3)

- The *in vitro* biocompatibility study for the OLA<sub>t</sub>BAC and the formulation (VM-OLA<sub>t</sub>BAC-NVs1) confirmed their nontoxic nature to mammalian cells.
- There was a change in size and PDI with respect to decrease in pH from 7.4 to 6.0 (198.5.0 ± 6.69 to 207.0 ± 6.69 nm respectively). Surface charge switching was found to be from -6.95 ± 6.50 to +13.3 ± 1.75 mV as pH decreased from 7.4 to 6.0 respectively. The encapsulation efficiency and drug loading capacity were found to be 44.62 ± 0.34 % and 18.92 ± 2.34 % w<sub>w</sub>, respectively.
- The thermal profile demonstrated and confirmed the formation of the nanovesicles and the successful encapsulation of VM into the bilayered nanovesicles.
- The *in vitro* drug release profile from the (VM-OLA<sub>t</sub>BAC-NVs1) nanovesicles was found to be slower and sustained in pH 7.4 compared to the faster and sustained release in pH 6.0 which was supported by the *in vitro* antibacterial activity.
- The *in vitro* antibacterial activity of the VM-OLA<sub>t</sub>BAC-NVs1 nanovesicles against MRSA showed a 13.07-fold enhancement activity of in pH 7.4 and 52.9-folds in pH 6.0 when compared to bare VM.

### REFERENCES & ACKNOWLEDGMENT

- References
- Medina et al (2018) Journal of Biomedical Materials Research Part A, 106:1400-412.
  - Huh & Kwon (2011) Journal of Controlled Release, 156:128-145.
  - Kalhapure et al (2017) Colloids Surf B Biointerfaces, 158:650-657.

#### Acknowledgment

College of Health Sciences, UKZN Nanotechnology Platform, National Research Foundation of South Africa, Medical Research Council of South Africa and UKZN Microscopy and Microanalysis Unit.

### CONCLUSION

- These findings confirmed that the novel lipid (OLA<sub>t</sub>BAC) can be used as an effective material for complexation with biodegradable CH to form encapsulated VM pH-responsive nanovesicles to enhance its antibacterial activity, thereby showing potential for the treatment of infections diseases.



## Appendix VI



AAR-659  
6/23/2019

# Novel Delivery of pH-responsive Vancomycin Nanovesicles against Superbug (MRSA) Infections

Daniel Hassan<sup>1</sup>, Calvin A. Omolo<sup>1,2</sup>, Chunderika Mocktar<sup>1</sup>, Thirumala Govender<sup>1</sup>

<sup>1</sup>Discipline of Pharmaceutical Sciences, College of Health Sciences, University of KwaZulu-Natal, Private Bag X54001, Durban, South Africa  
<sup>2</sup>United States International University-Africa, School of Pharmacy and Health Sci., Department of Pharmaceutics, P. O. Box 14634-00800, Nairobi Kenya



University of KwaZulu-Natal  
+27 827 366 721  
danielhassanuk1@yahoo.com

### INTRODUCTION AND AIM

- Infectious diseases caused by Methicillin-resistant *Staphylococcus aureus* (MRSA) resistance is a serious global trend that affects more than two million people every year [1]; and conventional antibiotics dosage forms have contributed to the antimicrobial resistance crisis [2].
- Recently, pH-responsive nanovesicles are reported to address antibiotics resistance challenges by maximizing targeted delivery of antibiotics against MRSA at the infection site characterized by acidic conditions [3].
- The aim of the study was to synthesize a novel pH-responsive lipid (OLAtBac) and formulate vancomycin (VM) chitosan nanovesicles to enhance the treatment of MRSA infections.

### METHODS

#### Preparation of pH-responsive Nanovesicles

- The novel pH-responsive vancomycin nanovesicles (VM-OLAtBac-NVs) were prepared by using a modified version of an ionic gelation method. Briefly, a solution of TPP and OLAtBac was prepared while, for the drug loaded, VM was included in the solution. Chitosan (0.1 % w/v) was dissolved in acetic acid (1 % v/v) and the pH was adjusted to 5.5 using 1 M NaOH.

#### Characterization of the novel nanovesicles

- *In vitro* biocompatibility and hemolytic analysis of the OLAtBac (MTT assay and Spectrostar Nano, Germany).
- *In vitro* drug release (dialysis bag and UV spectrophotometer, Japan), *in vitro* antibacterial activity (broth dilution method), *in vitro* downstream physiological phenomena (electrical conductivity meter and UV Spectrophotometer Japan), *in vitro* percentage cell death (Beckman Coulter USA), *in vitro* time killing assay and *in vitro* fluorescence intensity (Fluorescence microscope, Nikon Eclipse 80i FM Japan).
- *In vivo* (CFU) in infected skin mice model (UKZN, Animal Research Ethics Committee; AREC/104/015PD).

### RESULTS AND DISCUSSION

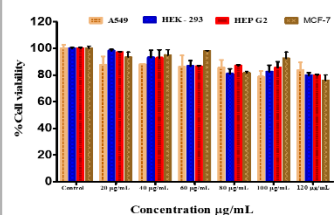


Fig. 1: *In vitro* cytotoxicity of the OLAtBac (n = 3).

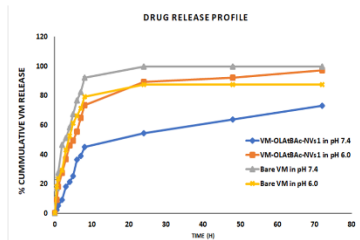


Fig. 3: *In vitro* drug release profile of the VM-OLAtBac-NVs1 nanovesicles in pH 7.4 and 6.0

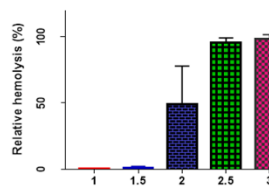


Fig. 4: *In vitro* electrical conductivity, protein and DNA quantifications

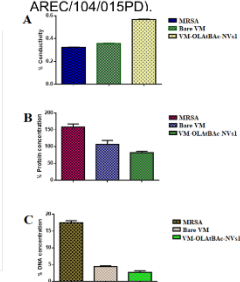


Fig. 5: *In vitro* flow cytometry of the MRSA, bare VM and VM-OLAIBac-NVs1

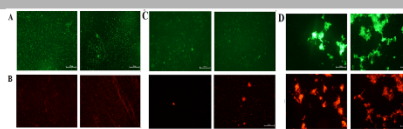


Fig. 6: *In vitro* antibacterial activity of bare Syto9, PI, VM and VM-OLAtBac-NVs1 against MRSA.

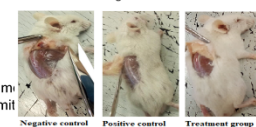


Fig. 8: Photomicrographs of the skin lesions at the site of injection.

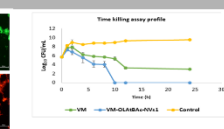


Fig. 7: *In vitro* time killing assay of MRSA, VM and VM-OLAIBac-NVs1 nanovesicles

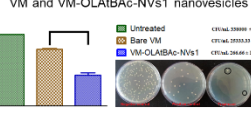


Fig. 9: *In vivo* antibacterial activity of bare VM and VM-OLAIBac-NVs1 against MRSA

- The *in vitro* biocompatibility and the hemolytic studies of the OLAtBac confirmed its nontoxic nature to mammalian cells and non hemolytic activity respectively.
- The *in vitro* drug release profile from the VM-OLAtBac-NVs1 nanovesicles was found to be slower and sustained in pH 6.0 compared to the fast and sustained release in pH 7.4 which was supported by the 52.9-fold enhancement in *in vitro* antibacterial activity.
- The VM-OLAtBac-NVs1 nanovesicles revealed a 62.96% increased in electrical conductivity which revealed higher membrane destruction. While, protein and DNA revealed 76.94% and 61.62% concentration decrease respectively demonstrated protein and DNA leakage ability in membrane in external solution.
- The flow cytometry of bare VM and the VM-OLAtBac-NVs1 nanovesicles demonstrated 35.09% and 98.86% killing percentage, respectively which demonstrated higher killing ability of the VM-OLAtBac-NVs1 nanovesicles.
- The VM-OLAtBac-NVs1 nanovesicles demonstrated spontaneous bacterial elimination with nearly 97.4% clearance of MRSA in 24-hours which shown lost of membrane while the fluorescence revealed decreased in Syto9 fluorescence intensity which demonstrated lower living cells of the biofilms.
- The *in vivo* studies in BALB/c mouse infected skin model revealed CFU/mL of MRSA burden decreased by 95-folds verses the treatment with bare VM.

### CONCLUSION

These findings confirmed that the novel lipid (OLAtBac) can be used as an effective material for complexation with biodegradable chitosan to form a pH-responsive VM nanovesicles which enhance its antibacterial activity, thereby showing potential for the treatment of infectious diseases.

### REFERENCES

- [1] Medina *et al.*, (2018) Journal of Biomedical Materials Research Part A, 106:1400-1412. [2] Souza *et al.*, (2019) Applications of Targeted Nano Drugs and Delivery Systems 327-342. [3] Nogueira *et al.*, (2013) Biomaterials, 34:2758-2772.

### ACKNOWLEDGMENT

College of Health Sciences, UKZN Nanotechnology Platform, National Research Foundation of South Africa, Medical Research Council of South Africa and UKZN Microscopy and Microanalysis Unit

## Appendix VII



### Quaternary two-arm pH-responsive quatsomes for delivery and enhancement of Vancomycin activity against Methicillin-resistant *Staphylococcus Aureus*

Daniel Hassan<sup>1</sup>, Calvin A. Omolo<sup>1,2</sup>, Victoria Fasiku<sup>1</sup>, Chunderika Mocktar<sup>1</sup>, Thirumala Govender<sup>1</sup>

<sup>1</sup>Discipline of Pharmaceutical Sciences, College of Health Sciences, University of KwaZulu-Natal, Private Bag X54001, Durban, South Africa  
<sup>2</sup>United States International University-Africa, School of Pharmacy and Health Sci., Department of Pharmaceutics, P. O. Box 14634-00800, Nairobi Kenya



+27 82 736 6721

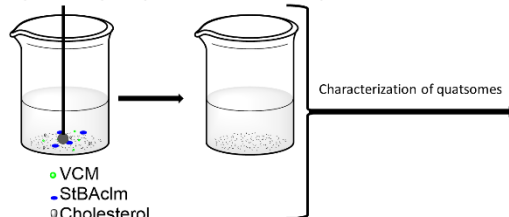
daniel4hassanuk1@yahoo.com

#### INTRODUCTION AND AIM

- Globally, human beings continue to be at high risk of infectious diseases caused by Methicillin-resistant *Staphylococcus aureus* (MRSA), and current treatments are depleted due to bacterial resistance [1].
- Conventional dosage forms of antibiotics have contributed to antibacterial resistance demanding novel nano-drug delivery systems with intrinsic antibacterial activity to combat drug resistance [2-3].
- Therefore, synthesizing novel materials and formulating nano-drug delivery systems are essential to combat antimicrobial resistance and improve drug pharmacokinetic profiles, enhance activity, protect the drug from enzymatic destruction and lower side effects.
- The study aimed to synthesize a novel two-arm hydrophilic quaternary lipid (StBAclm) and explore its potential to formulate pH-responsive vancomycin quatsomes (VCM-StBAclm-Qt) for enhancing antimicrobial activity against MRSA.

#### METHODS

##### Preparation of pH-responsive VCM-StBAclm-Qt quatsomes



- In vitro* cytotoxicity of the StBAclm (MTT assay, Spectrostar Nano, Germany)
- Size, polydispersity index and surface charge (Zetasizer Nano ZS90, Malvern Instruments Ltd., UK)
- Morphology (Cryogenic-HR Transmission Electron Microscopy, Jeol, JEM-2100, Japan)
- In vitro* drug release (dialysis bag, UV Spectrophotometry, Japan)
- In vitro* biofilm inhibition (Fluorescence Microscopy, Nikon Eclipse 80i FM, Japan).
- In vitro* time killing assay (broth dilution)
- In vivo* antibacterial activity (mice skin infection model - AREC/104/015PD)

#### RESULTS AND DISCUSSION

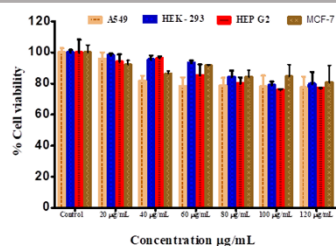


Fig. 1: *In vitro* cytotoxicity of the StBAclm (n = 3).

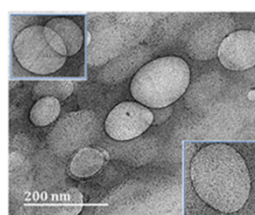


Fig. 2: Morphology of the VCM-StBAclm-Qt1 quatsomes

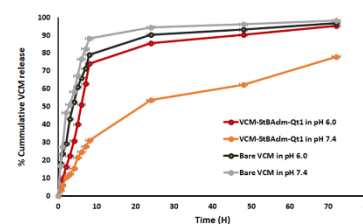


Fig. 3: *In vitro* drug release profile of bare VCM and VCM-StBAclm-Qt1 quatsomes in pH 7.4 and 6.0 (n = 3)

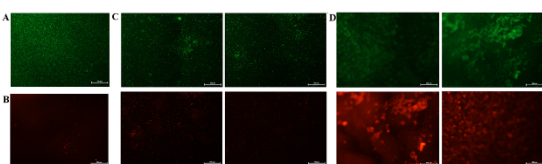


Fig. 4: *In vitro* biofilm inhibition A) Syto9, B)PI, C) bare VCM and D) VCM-StBAclm-Qt1 against MRSA.

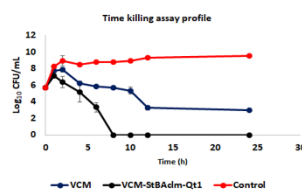


Fig. 5: *In vitro* time killing assay of MRSA, bare VCM and VCM-StBAclm-Qt1 quatsomes

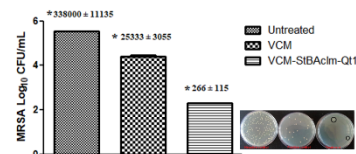


Fig. 6: *In vivo* antibacterial activity of untreated, bare VCM and VCM-StBAclm-Qt1 quatsomes against MRSA (CFU n = 3)

- The *in vitro* cytotoxicity study of the StBAclm synthesized revealed the lipid to be nontoxic in mammalian cell lines (Fig. 1) and can be used to formulate a nano-drug system.
- The size, and polydispersity index were  $122.9 \pm 3.78$  nm and  $0.169 \pm 0.02$  mV respectively with surface charge switching from negative in physiological pH 7.4 to positive in acidic environment pH 6.0.
- The quatsomes morphology was observed to be spherical in shape, containing a thin membrane and an aqueous core (Fig. 2).
- The *in vitro* drug release of VCM from VCM-StBAclm-Qt1 quatsomes was faster in pH 6.0 compared to pH 7.4, confirming pH responsiveness of the VCM-StBAclm-Qt1 quatsomes (Fig. 3).
- The VCM-StBAclm-Qt1 quatsomes exposed to MRSA biofilms exhibited higher fluorescence intensity when compared to bare VCM, thus indicating a higher decrease in biofilm population (Fig. 4).
- The VCM-StBAclm-Qt1 demonstrated spontaneous bacterial elimination with nearly 100% clearance within 8-hours of the study, indicating a shorter treatment course compared to bare VCM (Fig. 5).
- The VCM-StBAclm-Qt1 quatsomes showed a 95-fold higher reduction in MRSA burden (CFU) compared to bare VCM treatment in mice skin infection model (Fig. 6).

#### CONCLUSION

The two-arm hydrophilic quaternary pH-responsive lipid (StBAclm) is a promising material for complexation with VCM to form a biodegradable pH-responsive VCM-StBAclm-Qt1 quatsomes which enhanced its antimicrobial activity, thereby showing potential for the treatment of infectious diseases caused by MRSA.

#### REFERENCES

- Zhang W, Zhuo S, He L, Cheng C, Zhu B, Lu Y, Wu Q, Shang W, Ge W, Shi Li. International Immunopharmacology. 2019. 195-203
- Kumar M, Curtis A, Hoskins C. Pharmaceutics. 2018. 11-28
- Nicky T, Dong D, Katharina R, Mahnaz R, Sarah V, Benjamin T, Peter-John W, Clive AP. Journal of Materials Chemistry B. 2015. 2770-2777

#### ACKNOWLEDGMENT

College of Health Sciences, UKZN Nanotechnology Platform, National Research Foundation of South Africa, Medical Research Council of South Africa, UKZN Microscopy and Microanalysis Unit, and Royal Society of Chemistry (Material Chemistry Division).



## Appendix VIII

OLA-HBA 1 in chloroform

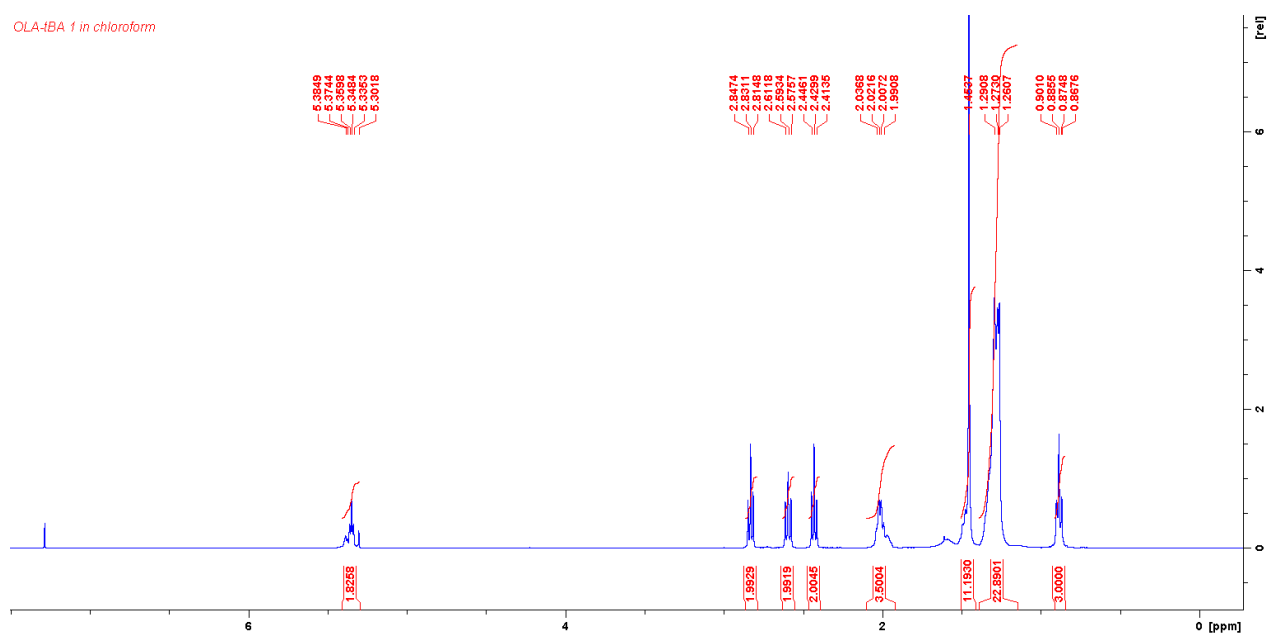


Figure S1:  $^1\text{H}$  NMR of OL (tert-butyl (Z)-3-(octadec-9-en-1-ylamino)propanoate)

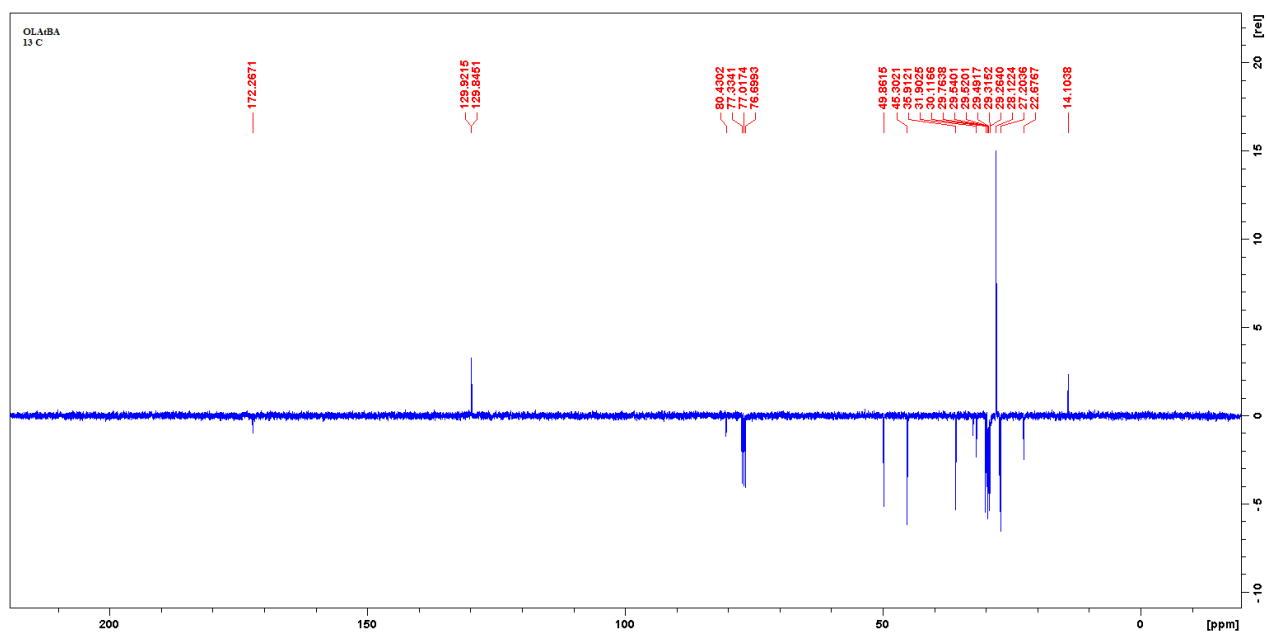
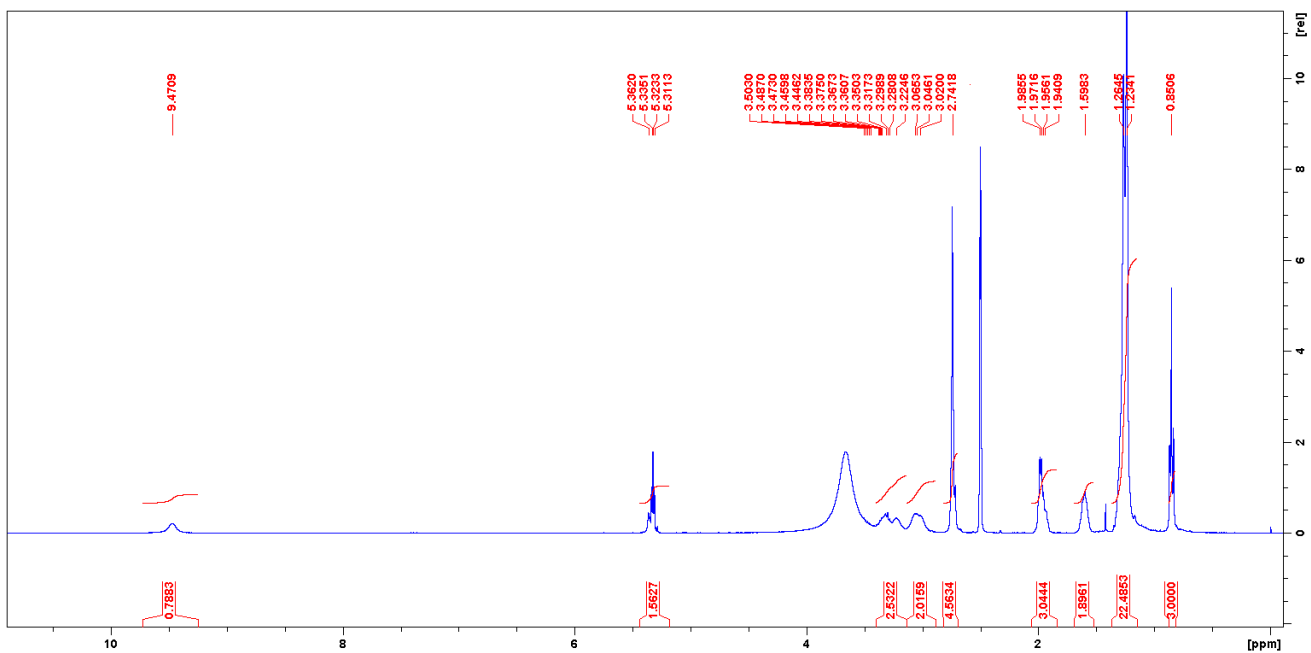
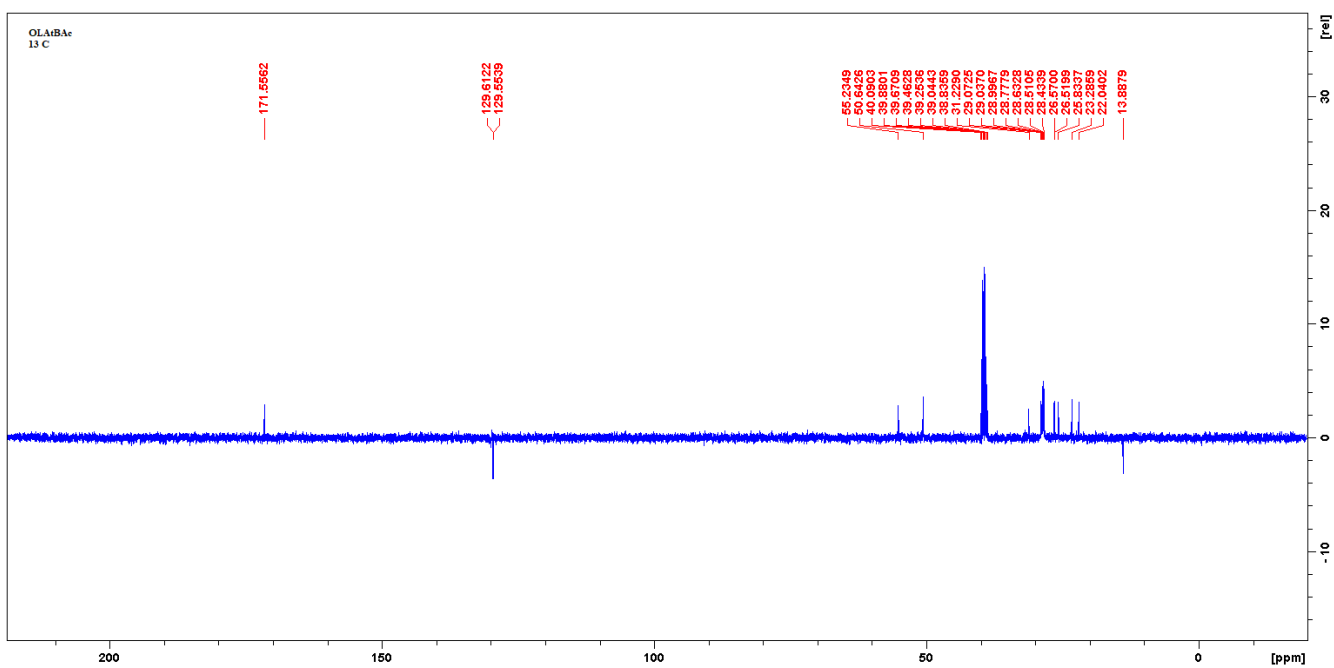


Figure S2:  $^{13}\text{C}$  NMR of OL (tert-butyl (Z)-3-(octadec-9-en-1-ylamino)propanoate)



**Figure S3:**  $^1\text{H}$  NMR of OLA ((Z)-3-(octadec-9-en-1-ylamino)propanoic acid)

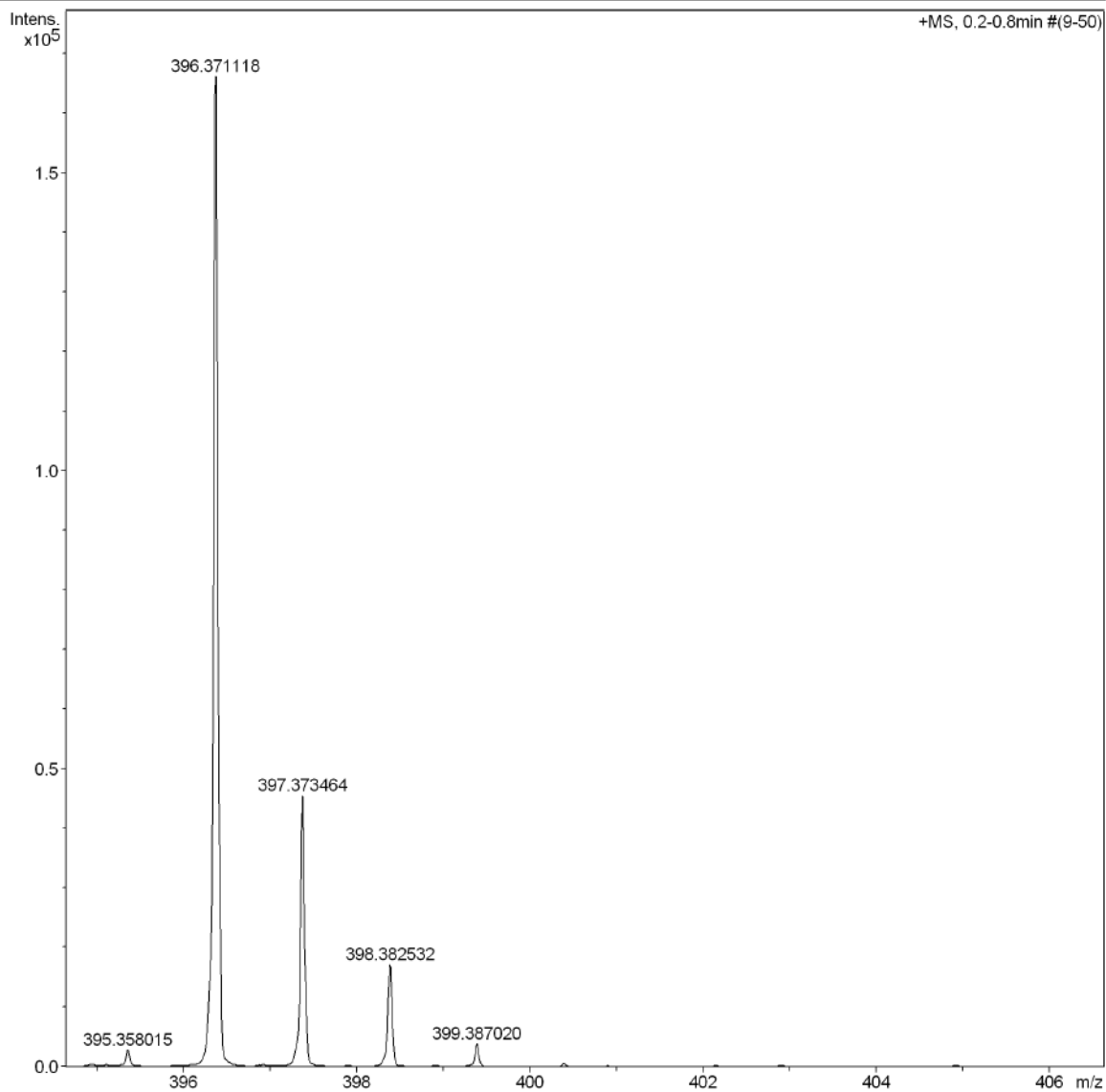


**Figure S4:**  $^{13}\text{C}$  NMR of OLA ((Z)-3-(octadec-9-en-1-ylamino)propanoic acid)

## Appendix IX

### Acquisition Parameter

Source Type	ESI	Ion Polarity	Positive	Set Nebulizer	1.5 Bar
Focus	Not active	Set Capillary	5500 V	Set Dry Heater	220 °C
Scan Begin	150 m/z	Set End Plate Offset	-500 V	Set Dry Gas	8.0 l/min
Scan End	3000 m/z	Set Collision Cell RF	400.0 Vpp	Set Divert Valve	Source



Bruker Compass DataAnalysis 4.0

printed: 2/19/2019 8:30:16 AM

Page 1 of 1

**Figure S5:** HR-MS (ES-TOF):  $[M + H]^+$  of OL (tert-butyl (Z)-3-(octadec-9-en-1-ylamino)propanoate)

**Acquisition Parameter**

Source Type	ESI	Ion Polarity	Positive	Set Nebulizer	1.5 Bar
Focus	Not active	Set Capillary	5500 V	Set Dry Heater	220 °C
Scan Begin	150 m/z	Set End Plate Offset	-500 V	Set Dry Gas	8.0 l/min
Scan End	3000 m/z	Set Collision Cell RF	400.0 Vpp	Set Divert Valve	Source

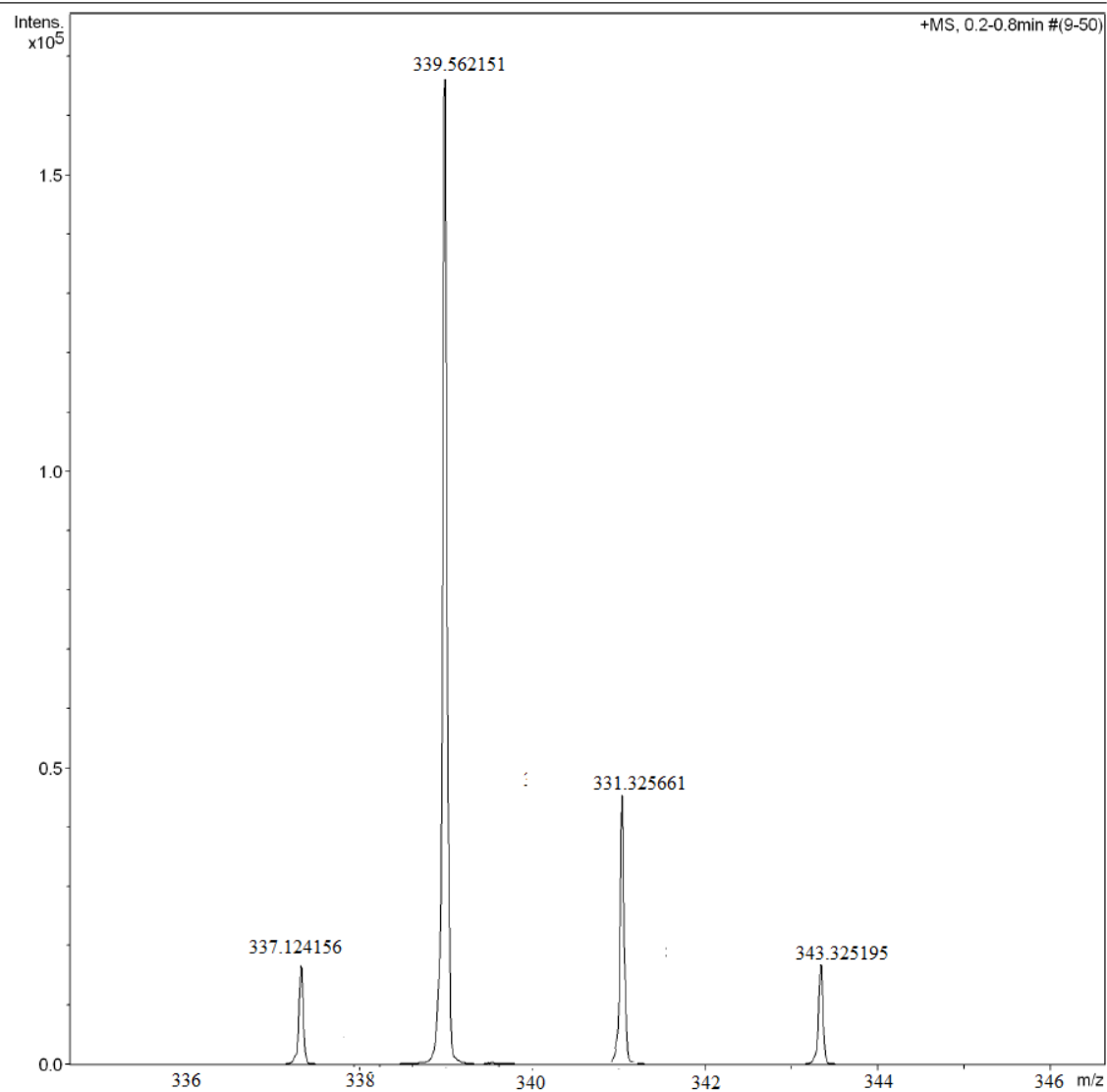


**Figure S6:** HR-MS (ES-TOF):  $[M + H]^+$  of OLA ((Z)-3-(octadec-9-en-1-ylamino)propanoic acid)

## Appendix X

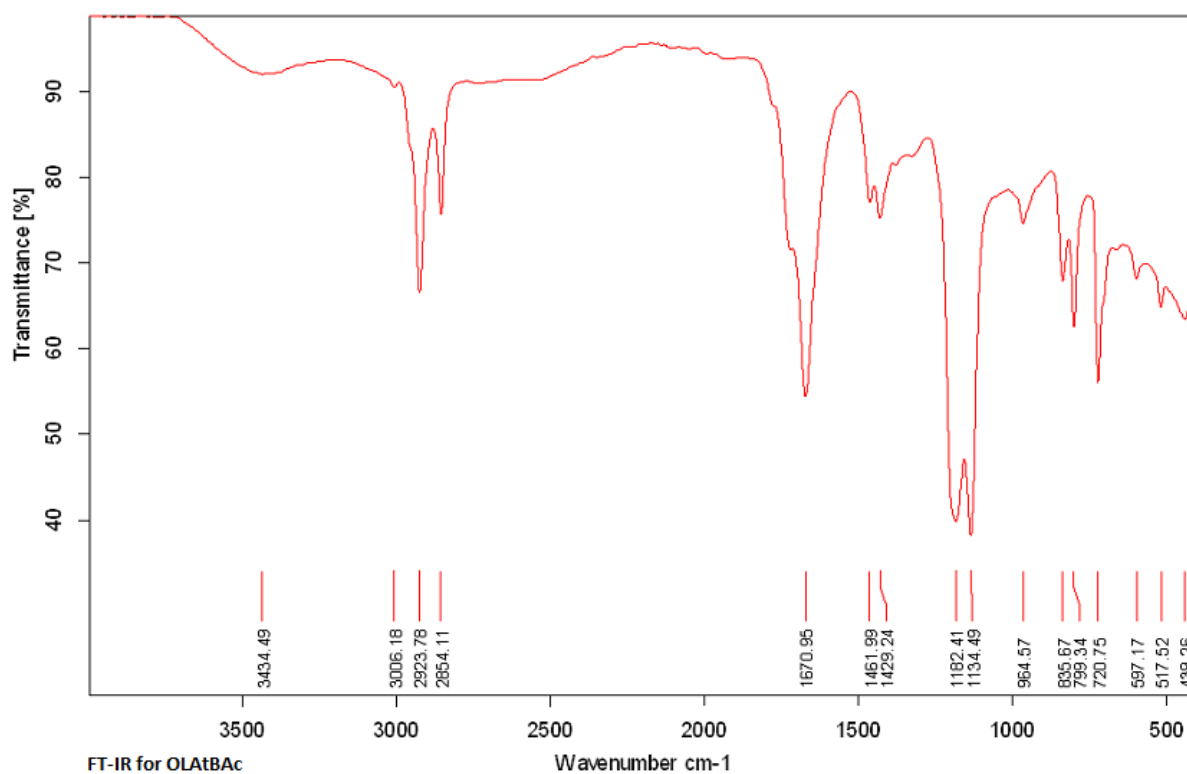


**Figure S7:** FT-IR of OL (tert-butyl (Z)-3-(octadec-9-en-1-ylamino)propanoate)

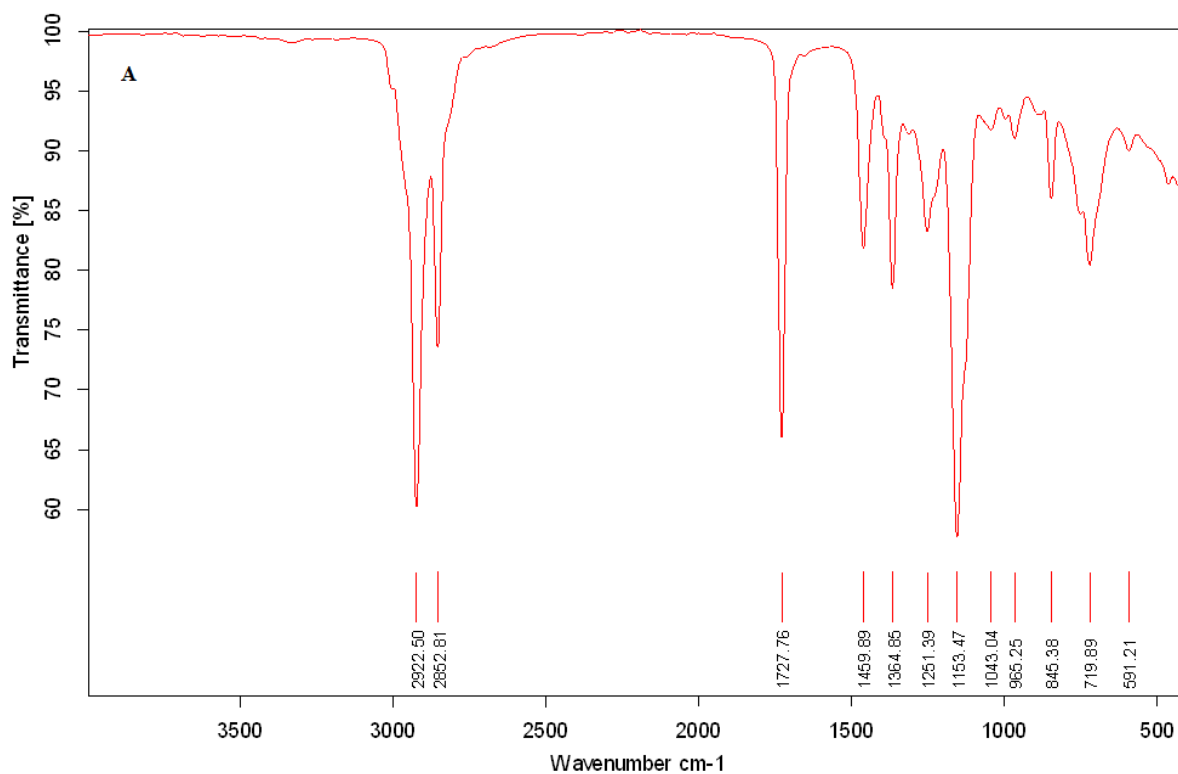


**Figure S8:** FT-IR of OLA ((Z)-3-(octadec-9-en-1-ylamino)propanoic acid)

## Appendix XI

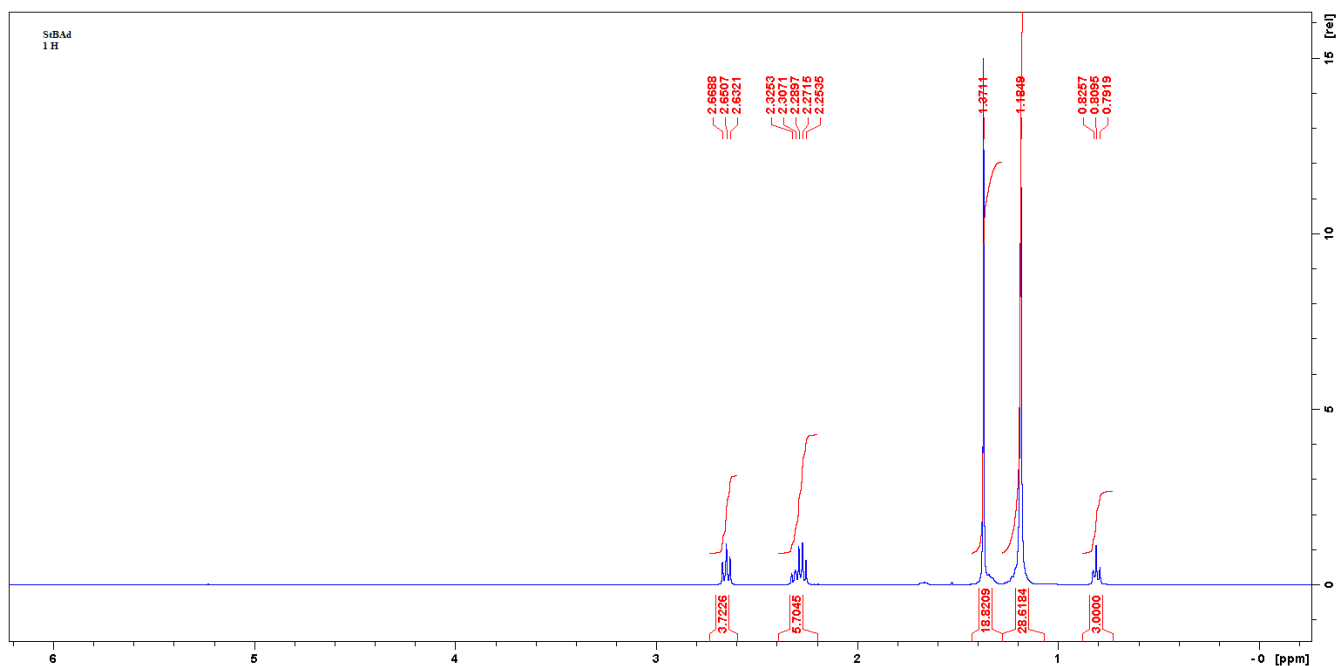


**Figure S9:**  $^1\text{H}$  NMR of StBA (di-tert-butyl 3,3'-(octadecylazanediyl)dipropionate)

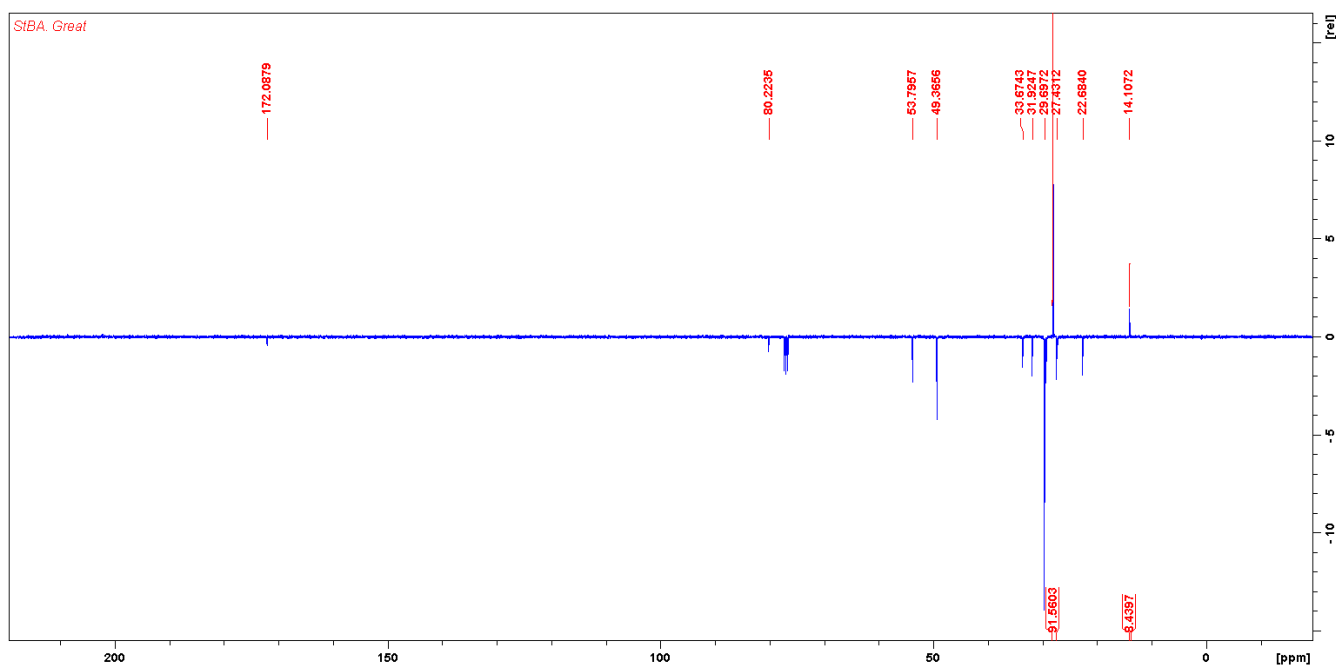


**Figure S10:**  $^{13}\text{C}$  NMR of StBA (di-tert-butyl 3,3'-(octadecylazanediyl)dipropionate)

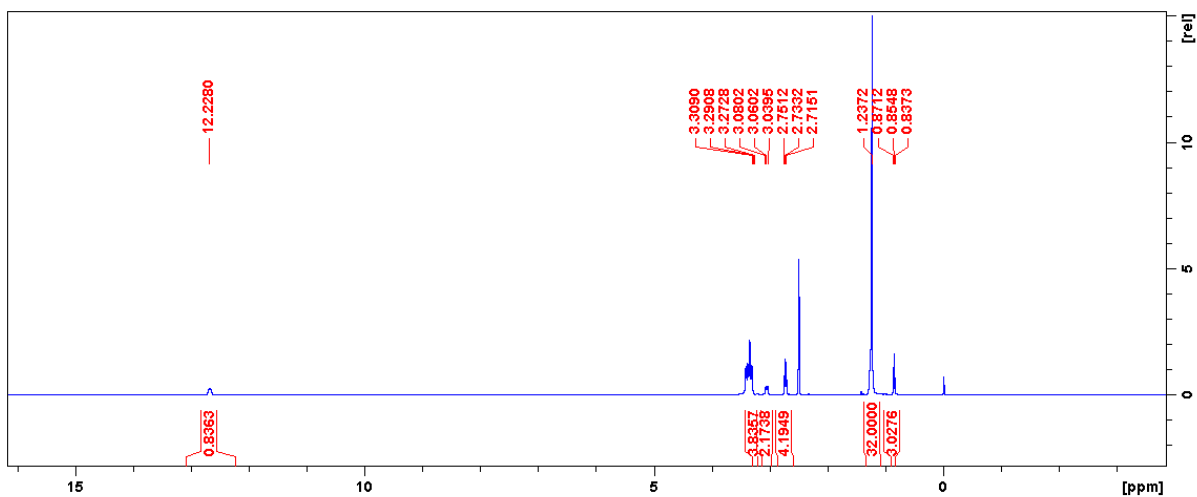


**Figure S11:**  $^1\text{H}$  NMR of StBAcl (3,3'-(octadecylazanediyl)dipropionic acid)

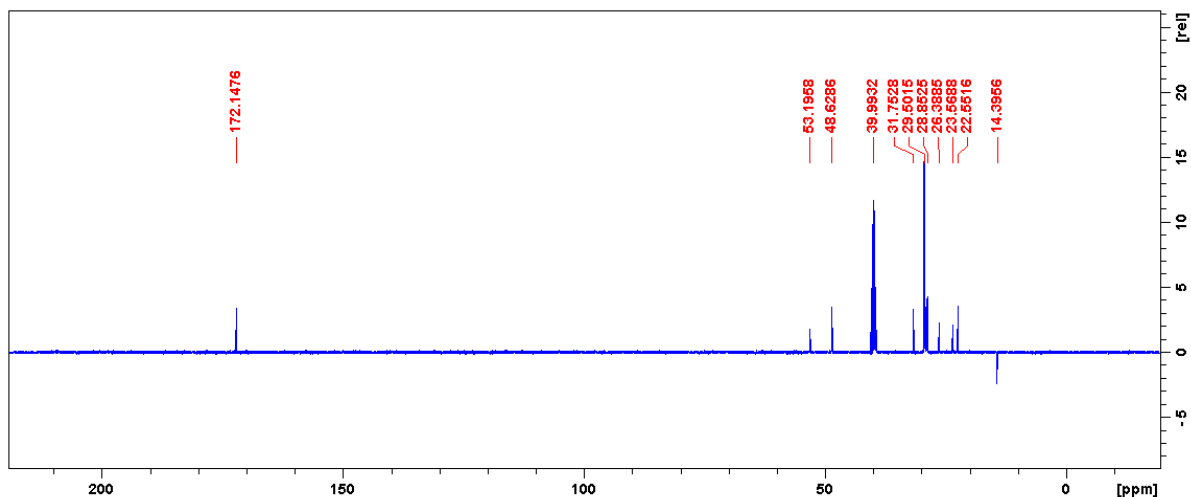


**Figure S12:**  $^{13}\text{C}$  NMR of StBAcl (3,3'-(octadecylazanediyl)dipropionic acid)

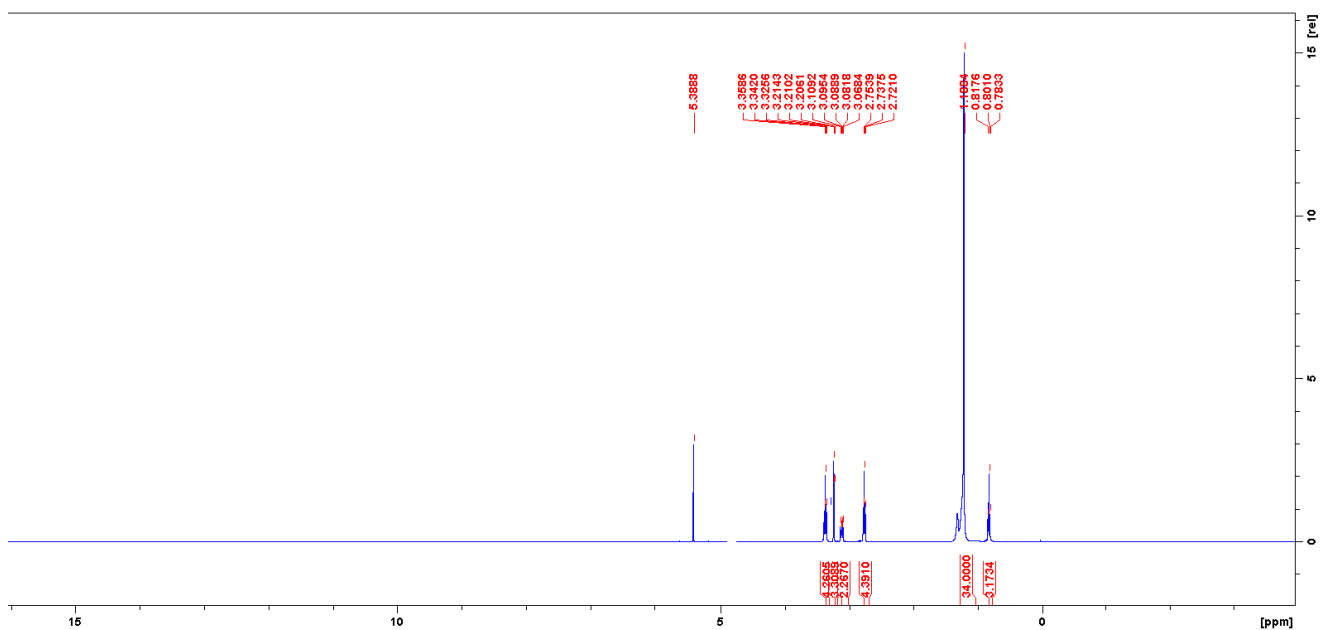


**Figure S13:**  $^1\text{H}$  NMR of StBAclm (*N,N*-bis(2-carboxyethyl)-*N*-methyloctadecan-1-aminium)

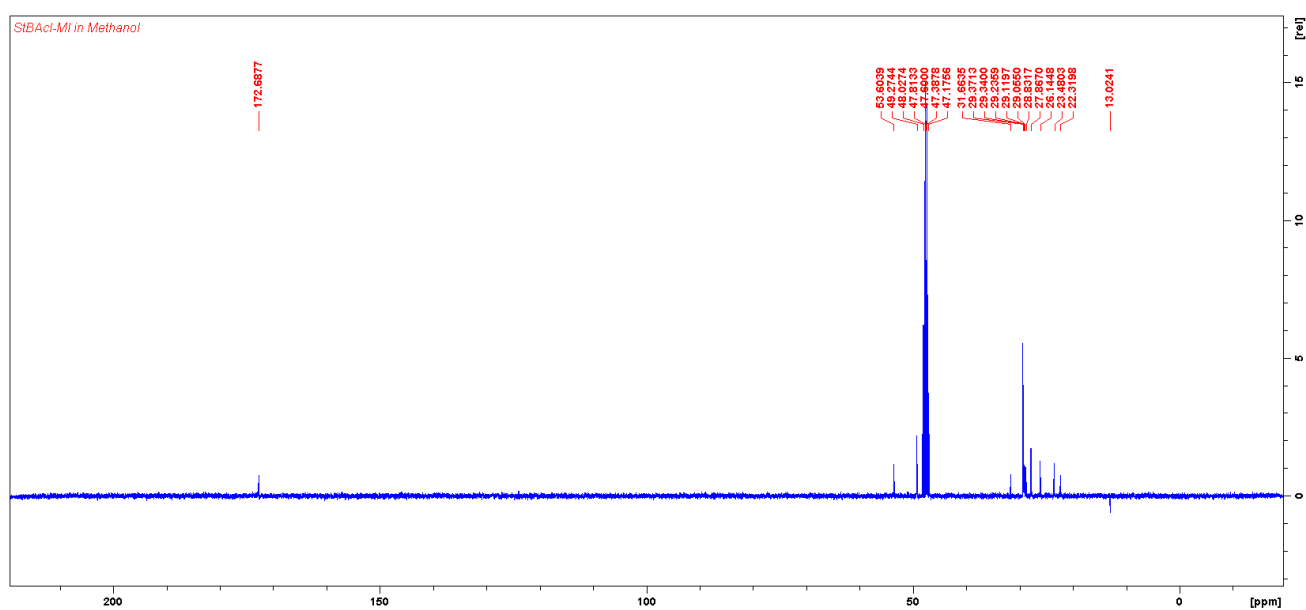


**Figure S14:**  $^{13}\text{C}$  NMR of StBAclm (*N,N*-bis(2-carboxyethyl)-*N*-methyloctadecan-1-aminium))



## Appendix XII

### Display Report

<b>Analysis Info</b>		Acquisition Date	2/15/2019 9:19:41 AM
Analysis Name	D:\Data\sooraj\3_64_01_12775.d	Operator	BDAL@DE
Method	fia_test.m	Instrument	micrOTOF-Q 10139
Sample Name	StBA		
Comment			

<b>Acquisition Parameter</b>					
Source Type	ESI	Ion Polarity	Positive	Set Nebulizer	1.5 Bar
Focus	Not active	Set Capillary	5500 V	Set Dry Heater	220 °C
Scan Begin	150 m/z	Set End Plate Offset	-500 V	Set Dry Gas	8.0 l/min
Scan End	3000 m/z	Set Collision Cell RF	400.0 Vpp	Set Divert Valve	Source

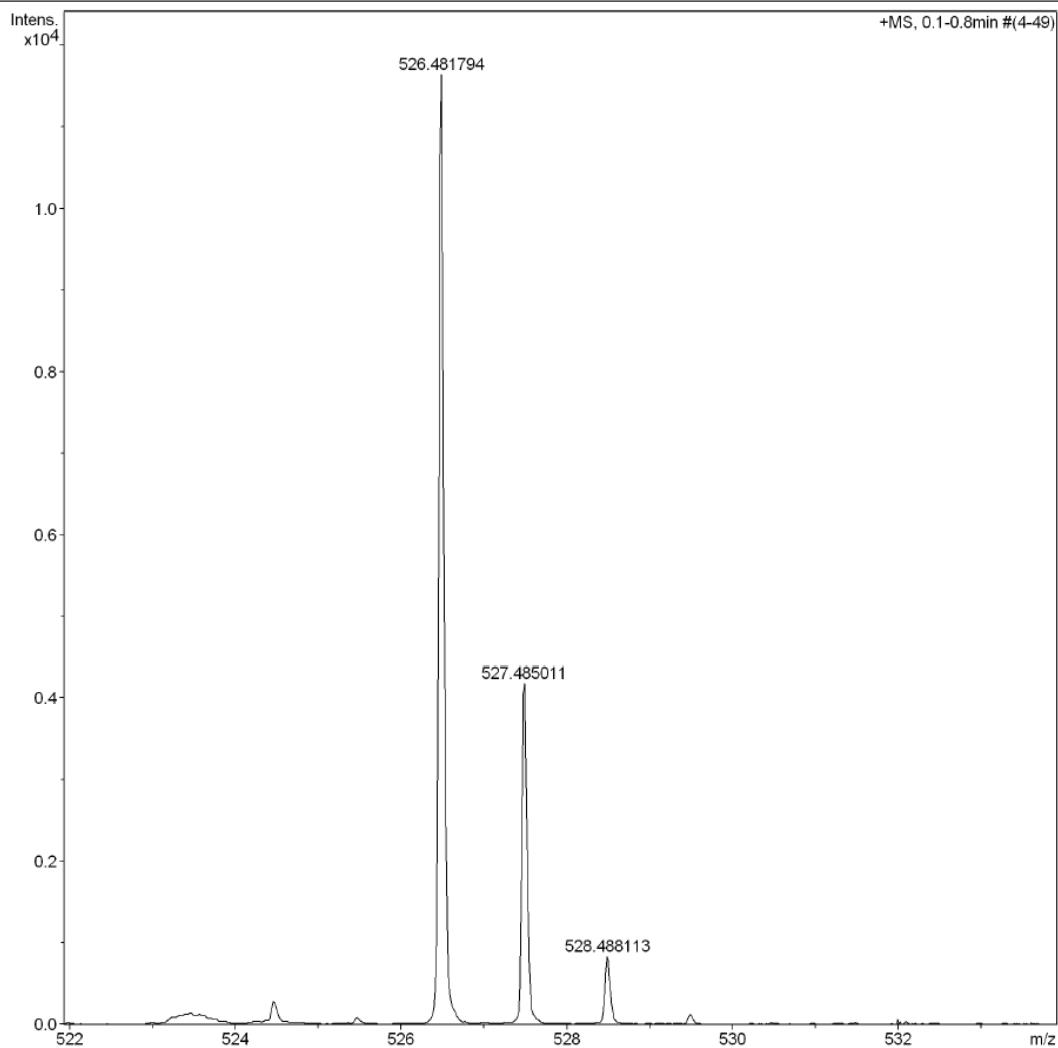


**Figure S15:** HR-MS (ES-TOF):  $[M + H]^+$  for StBA (di-tert-butyl 3,3'-(octadecylazanediyldipropionate)

## Display Report

### Analysis Info

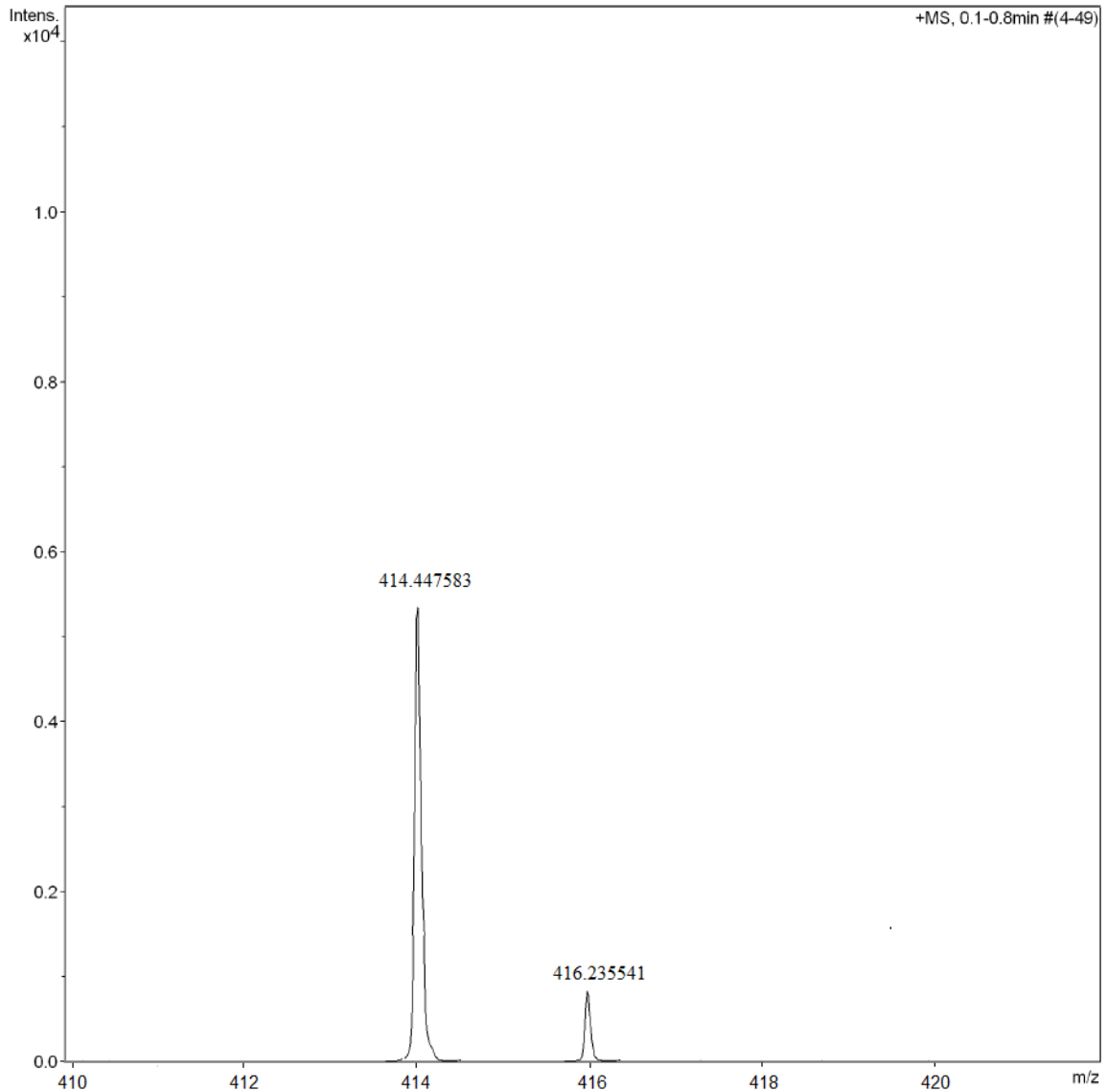
Analysis Name D:\Data\sooraj\3\_64\_01\_12886.d  
Method fia\_test.m  
Sample Name StBAcl  
Comment

Acquisition Date 2/15/2019 9:45:32 AM

Operator BDAL@DE  
Instrument micrOTOF-Q 10140

### Acquisition Parameter

Source Type	ESI	Ion Polarity	Positive	Set Nebulizer	1.5 Bar
Focus	Not active	Set Capillary	5500 V	Set Dry Heater	220 °C
Scan Begin	150 m/z	Set End Plate Offset	-500 V	Set Dry Gas	8.0 l/min
Scan End	3000 m/z	Set Collision Cell RF	400.0 Vpp	Set Divert Valve	Source



Bruker Compass DataAnalysis 4.0

Printed 2/19/2019 9:45:32 AM

Page 1 of 2

**Figure S16:** HR-MS (ES-TOF):  $[M + H]^+$  for StBAcl (3,3'-(octadecylazanediyl)dipropionic acid)

## Display Report

### Analysis Info

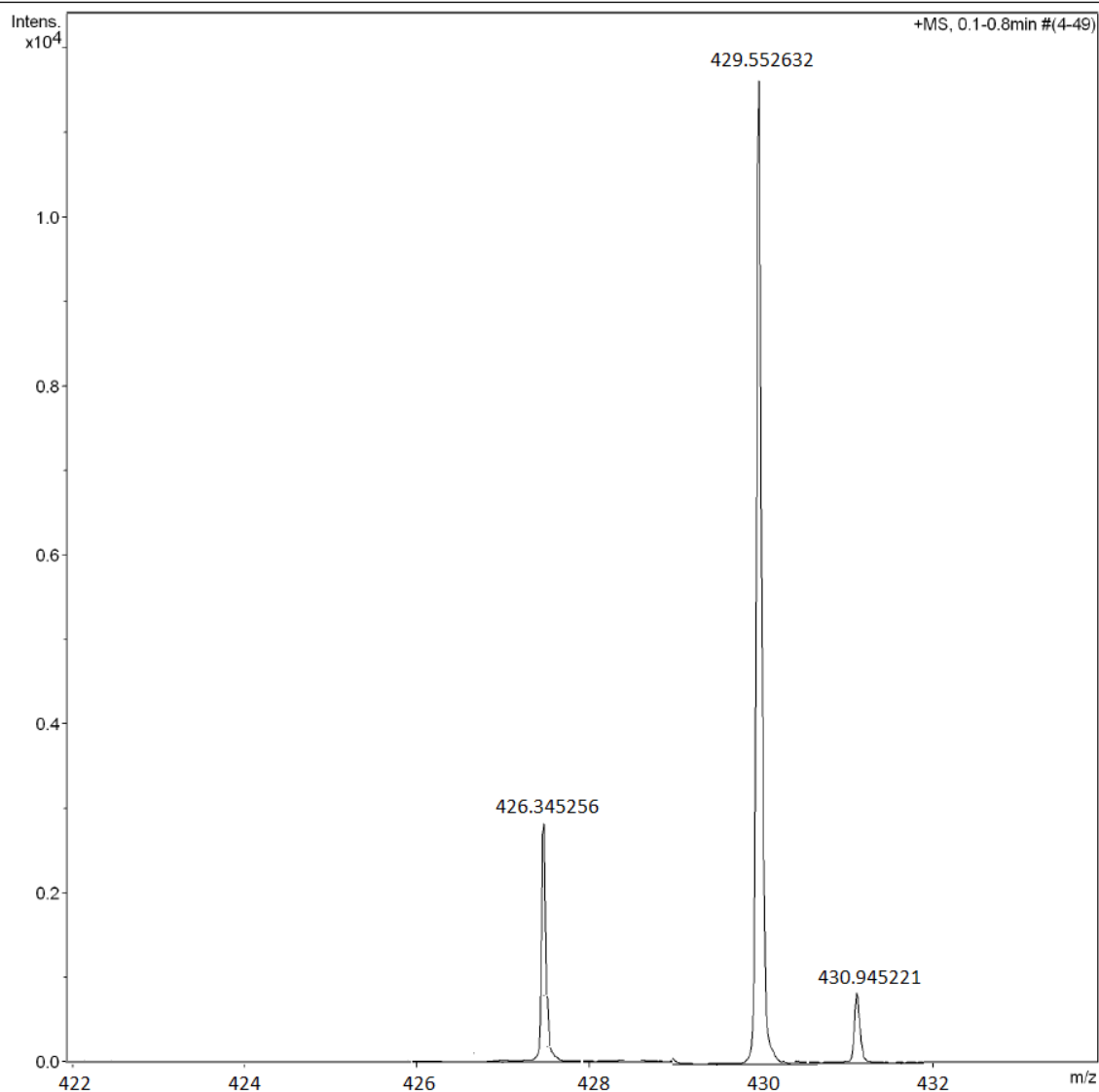
Analysis Name D:\Data\sooraj\3\_64\_01\_13564.d  
Method fia test.m  
Sample Name StBAclm  
Comment

Acquisition Date 2/15/2019 11:32:45 AM

Operator BDAL@DE  
Instrument micrOTOF-Q 10140

### Acquisition Parameter

Source Type	ESI	Ion Polarity	Positive	Set Nebulizer	1.5 Bar
Focus	Not active	Set Capillary	5500 V	Set Dry Heater	220 °C
Scan Begin	150 m/z	Set End Plate Offset	-500 V	Set Dry Gas	8.0 l/min
Scan End	3000 m/z	Set Collision Cell RF	400.0 Vpp	Set Divert Valve	Source



Bruker Compass DataAnalysis 4.0

Printed 2/19/2019 11:32:45 AM

Page 1 of 3

**Figure S17:** HR-MS (ES-TOF):  $[M + H]^+$  for StBAclm (*N,N*-bis(2-carboxyethyl)-*N*-methyloctadecan-1-aminium)

### Appendix XIII

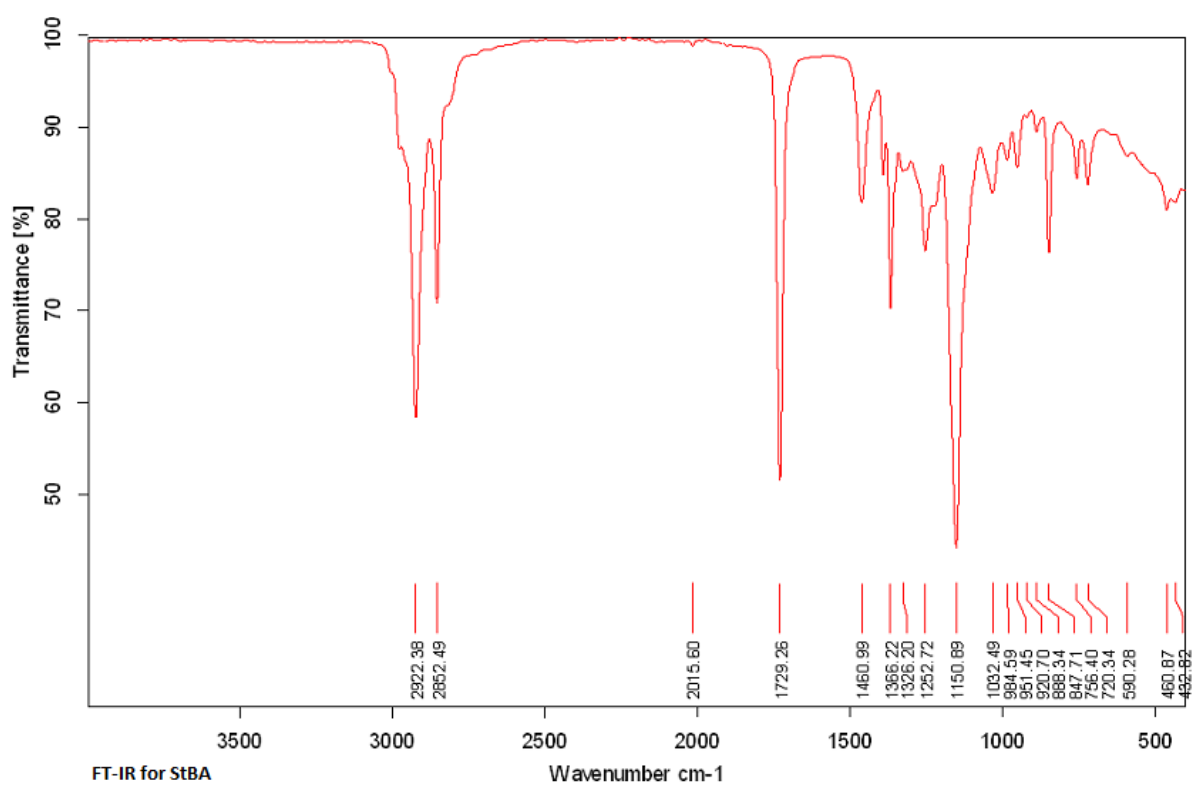


**Figure S18:** FT-IR of StBA (di-tert-butyl 3,3'-(octadecylazanediyl)dipropionate)

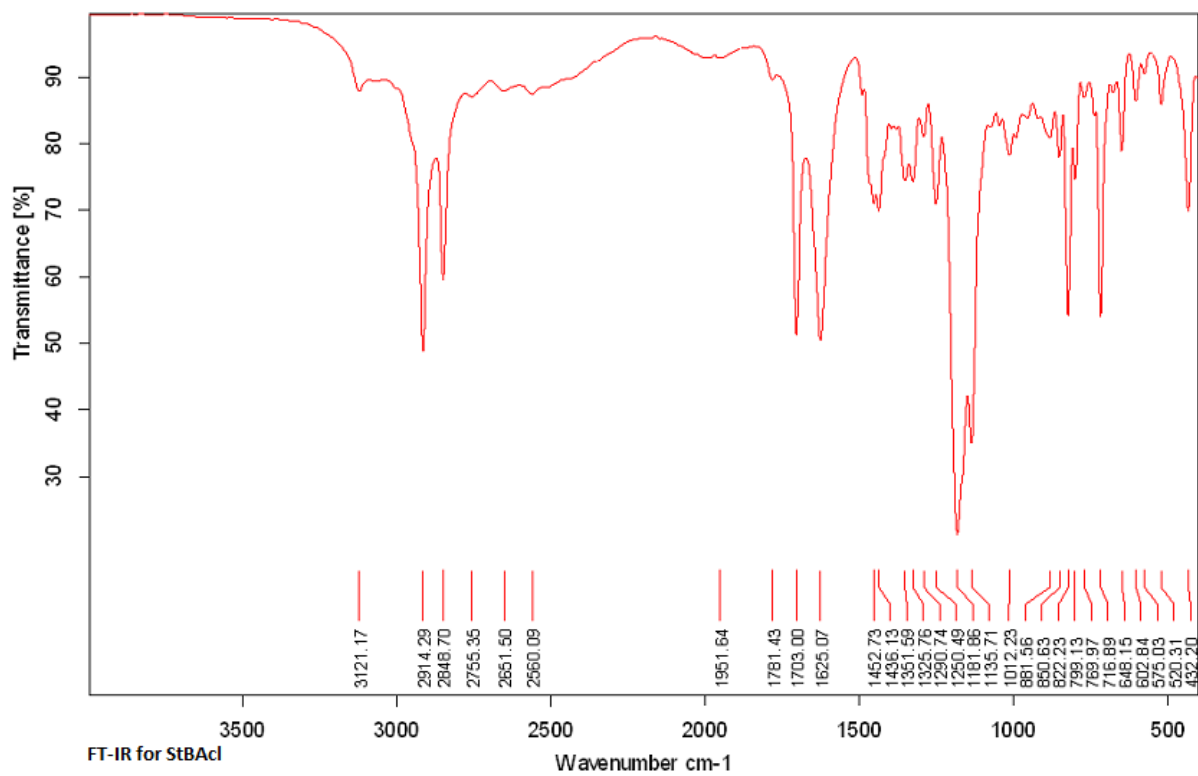


**Figure S19:** FT-IR of StBAcl (3,3'-(octadecylazanediyl)dipropionic acid)

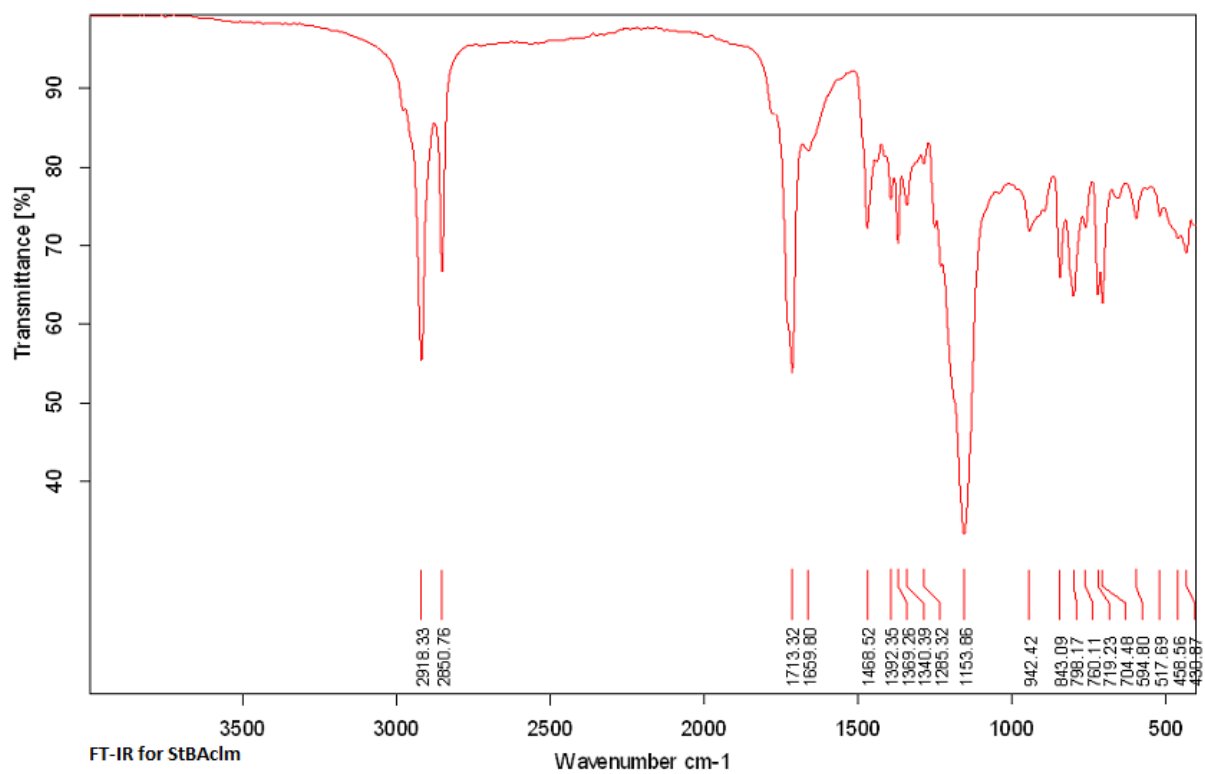


**Figure S20:** FT- IR of StBAclm (*N,N*-bis(2-carboxyethyl)-*N*-methyloctadecan-1-aminium)